THE UNIVERSITY *of* EDINBURGH

Incorporating left-hand cuts into finite-volume scattering formalism

André Baião Raposo

Doctor of Philosophy
The University of Edinburgh
August 2024

Abstract

Obtaining rigorous predictions from Quantum Chromodynamics (QCD), the theory of the strong interaction, is crucial for understanding hadronic and nuclear physics at a fundamental level and for the search for physics beyond the Standard Model. However, because the theory exhibits confinement at low energies, perturbative methods are not applicable in this regime. Lattice QCD currently provides the only reliable nonperturbative tool for *ab-initio* calculations from QCD at these energies. Such calculations necessarily use a finite discretised Euclidean spacetime, requiring additional procedures to extract the infinite-volume continuum physical observables of interest.

This thesis focuses on the formalism that permits the extraction of two-particle elastic scattering observables from the finite-volume spectrum, originally developed by M. Lüscher. Recent lattice calculations have shown limitations in this standard method, specifically when applied to systems where the partial-wave-projected scattering amplitudes contain left-hand branch cuts below the elastic threshold. These cuts arise when the two scattering particles can exchange lighter mesons, two relevant examples being NN and DD^* scattering, which receive contributions from single-pion exchanges. The presence of these cuts has so far been ignored in derivations of the formalism, leading to inconsistencies when it is applied to finite-volume energies that lie near to or on the cuts.

We address this issue by explicitly incorporating the effects of the left-hand cut into the formalism. Alternative quantisation conditions are presented that extend the standard result by Lüscher and are applicable near to and on the cut, both for the case of identical particles (of arbitrary spin) and non-degenerate particles. These conditions allow the determination of intermediate infinite-volume quantities (K-matrices) from the finite-volume energy levels, which can then be used to obtain scattering amplitudes by solving integral equations also derived in this work.

Lay Summary

Quantum Chromodynamics (QCD) is the modern theory of the strong force, the fundamental interaction of nature responsible for holding protons and neutrons together in atomic nuclei. It is also responsible for the existence of those protons and neutrons in the first place, forming them by binding together smaller constituents, the *quarks* and *gluons*. Obtaining predictions from QCD is crucial for advancing our understanding of this interaction and the insights provided are relevant for numerous areas of physics, from nuclear physics to cosmology.

However, extracting theoretical predictions from QCD is especially challenging at low energies due to the property of *confinement* exhibited by the strong interaction, which forbids quarks and gluons from being observed in isolation. Instead, these always appear bound together into composite particles called *hadrons*, of which protons and neutrons are the most well-known examples. At present, Lattice QCD is the only known framework for obtaining numerical results from QCD in this regime. This method employs a four-dimensional spacetime grid to simulate the theory and obtain numerical estimates of observables.

Hadron scattering processes (e.g. a proton-proton collision) cannot be studied directly via Lattice QCD simulations because, among other factors, these are necessarily performed in a finite spacetime. As such, the results obtained are distorted by the effects arising from the finite volume. A class of indirect approaches used to study scattering on the lattice are broadly called finite-volume methods, as they profit from the volume dependence of lattice results to extract infinite-volume scattering information. The Lüscher formalism is the most well-known and widely used among these, applying to two-to-two elastic processes.

Recent lattice calculations have encountered limitations of the standard Lüscher formalism due to the presence of a so-called *left-hand branch cut*. This issue

appears in systems where the scattering particles can exchange a much lighter particle. In practice, this prevents us from applying the usual method to some of the data obtained on the lattice, as doing so produces inconsistent results. The work described in this thesis seeks to solve this problem, extending the standard Lüscher formalism so that it is applicable in systems containing the left-hand cut.

Declaration

I declare that this thesis was composed by myself, that the work contained herein is my own except where explicitly stated otherwise in the text, and that this work has not been submitted for any other degree or professional qualification except as specified.

Parts of this work have appeared in [1, 2] and are included in this thesis with the consent of the co-author.

(*André Baião Raposo, August 2024*)

Acknowledgements

I dedicate this work to my parents – pai e mãe – and my grandparents, who have supported me unconditionally throughout this and other long journeys. The distance never mattered, nor did the fact that they did not quite understand what I was up to with my crazy mathematical squiggles.

I'm very grateful to Max Hansen, for taking me on as his student, guiding me throughout my PhD and introducing me to the lattice QCD community. I was not always the easiest student and I'm thankful to him for always staying positive and patient throughout.

I want to thank all the people who have made my time in Edinburgh an amazing experience, as well as my friends from back home, you'll always have a place in my heart. And to Alex, who has been by my side through bad things and many many more good things, and whose smile is enough to light up my day, thank you. Maite zaitut.

Contents

List of Figures

List of Tables

Introduction

The non-perturbative nature of Quantum Chromodynamics (QCD) in the low-energy regime makes the extraction of predictions from the theory extremely challenging. Such predictions are essential for a first-principles understanding of hadronic and nuclear physics. Lattice QCD is currently the only known approach to QCD which allows calculations directly from the theory. This method employs Monte-Carlo importance sampling to numerically evaluate the QCD path integral in a finite discretised Euclidean spacetime so that correlation functions can be computed. Since lattice data is necessarily obtained in this finite discretised Euclidean spacetime, additional procedures are required to relate it to infinite-volume continuum physical observables of interest.

An important example of quantities extracted in lattice QCD is the energy levels that make up the finite-volume spectrum, which is discretised by the use of a periodic finite spatial volume. These energies will carry a dependence on the total spatial momentum in the finite-volume frame and on the volume itself. This dependence contains information about the underlying interactions in the channel with the quantum numbers considered. As shown by the work of Lüscher [3] (and many later developments [4–14]) for the case of two-hadron systems, we can profit from it to constrain the corresponding hadron-hadron elastic scattering amplitudes in infinite volume.

These relations between finite-volume energies and amplitudes (or related infinite-volume quantities) are expressed mathematically through so-called *quantisation conditions*. These conditions will have specified kinematic regions of validity, centred on the elastic scattering region and often extending below the two-particle threshold. An example is given by the original work of Lüscher and its extensions to moving frames of refs. [4, 6, 7], which are concerned with pion-pion elastic scattering. The

relations provided there hold for

$$0 < E_n(L, \boldsymbol{P})^2 - \boldsymbol{P}^2 < (4M_\pi)^2 \,, \tag{1}$$

where $\boldsymbol{P}$ is the finite-volume frame momentum, $E_n(L, \boldsymbol{P})$ are the finite-volume levels (indexed by $n = 0, 1, ...$), and M_π is the (infinite-volume) pion mass. The upper bound corresponds to the lowest inelastic threshold, the four-pion threshold, since G-parity forbids coupling between even- and odd-number multi-pion states. The lower bound, on the other hand, can be attributed to several reasons. The most relevant for this thesis is that there is a left-hand branch cut due to two-pion t- and u-channel exchanges, with branch point at Mandelstam $s = E^2 - \boldsymbol{P}^2 = 0$.

The lower bound is irrelevant in lattice calculations of pion-pion scattering, as the lowest finite-volume energy level is typically well above $s = 0$. This will be near and above $2M_\pi$ for a scattering state or near a bound state mass. However, if we attempt to use the formalism for systems of two heavier particles where a much lighter particle can be exchanged, this might not be the case. For example, in the extension to nucleon-nucleon (NN) systems [14], the bounds of eq. (1) are modified to

$$(2M_N)^2 - M_\pi^2 < E_n(L, \boldsymbol{P})^2 - \boldsymbol{P}^2 < (2M_N + M_\pi)^2 \,, \tag{2}$$

where M_N is the nucleon mass. The upper bound is again the lowest-lying inelastic threshold, above which a three-particle branch cut opens, associated with $NN\pi$ production. The lower bound is restricted by the left-hand cut arising from single-pion exchanges, such as the t-channel exchange shown in figure 1(a). These lead to t- and u-channel poles in the amplitude, which are converted to a branch cut, that we call the *left-hand cut*, with branch point at $s = (2M_N)^2 - M_\pi^2$ when we project to definite angular momentum. The branch point is positioned quite close to the two-particle threshold since $M_\pi \ll M_N$.

The lower bound restriction of (2) comes about because the exchange is not taken into account in derivations of the Lüscher formalism, and thus the standard quantisation condition is expected to break down at energies near to or on the cut. This has been seen explicitly in recent lattice calculations [15], where finite-volume energies were extracted on top of the cut. For these energies, the standard formalism predicts a real amplitude, although we know that the partial-wave amplitudes must in fact be complex in order to reproduce the exchange poles in the full unprojected amplitude.

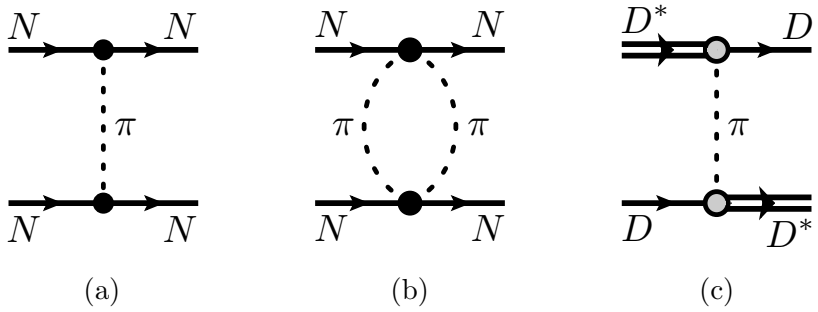

Figure 1 *Examples of pion exchanges leading to left-hand cuts for various processes: (a) single-pion exchange in $NN \to NN$, leading to the branch cut in angular-momentum projected $NN \to NN$ amplitudes treated in this work, (b) two-pion exchange, leading to a branch cut starting at $s = 4M_N^2 - 4M_\pi^2$,* not *treated in this work, (c) single-pion exchange in $DD^* \to DD^*$.*

A similar issue has since been pointed out in the context of DD^* scattering. This process has received increased interest due to its relevance for the study of the doubly-charmed tetraquark $T_{cc}(3875)^+$, recently discovered at LHCb [16, 17]. A lattice QCD calculation for this system was presented in [18] at heavier-than-physical pion mass $M_\pi \approx 280\,\text{MeV}$, for which the D^* is a stable particle. Subsequently, ref. [19] highlighted the impact of the left-hand cut, arising from the pion exchange shown in figure 1(c), in the result and the dangers of ignoring its presence.

The work in this thesis focused on extending the regime of validity of the formalism below the restriction shown above, such that it can be applied on the single-exchange left-hand cut and down to the next-nearest cut, arising from multi-particle exchanges. The main results presented include the derivation of quantisation conditions with this extended range of validity for two-to-two systems with identical particles of arbitrary spin, relevant for $NN \to NN$ and similar processes, and a subsequent generalisation to non-degenerate scalar particles, a big step towards applications such as $DD^* \to DD^*$. Such quantisation conditions allow the determination of intermediate K-matrices, volume-independent quantities, from the two-hadron finite-volume spectrum. These are then related to the physical scattering amplitude using integral equations, in a similar procedure to that employed by the relativistic three-body scattering formalism [20, 21].

This thesis is organised as follows: Chapter 1 reviews fundamental aspects of QCD,

with emphasis on the low-energy non-perturbative regime, Chapter 2 then describes the Lüscher formalism in its modern form, including its derivation and applications. Chapter 4 focuses on the extension of the formalism to the left-hand cut in the case of identical particles, while Chapter 3 discusses the case of non-degenerate scatterers. Finally, Chapter 5 discusses the extraction of scattering amplitudes from intermediate infinite-volume quantities (K-matrices) via integral equations, followed by a conclusion and outlook.

Chapter 1

Quantum Chromodynamics and its non-perturbative regime

The *Standard Model* (SM) of particle physics is the most successful theoretical description of the known subatomic particles and their behaviour under three fundamental interactions of nature – *electromagnetism*, the *strong interaction* and the *weak interaction*. It is a relativistic quantum field theory based on the gauge group $\mathrm{SU}(3)_c \times \mathrm{SU}(2)_L \times \mathrm{U}(1)_Y$, where the $\mathrm{SU}(3)_c$ component corresponds to the strong interaction, while $\mathrm{SU}(2)_L \times \mathrm{U}(1)_Y$ corresponds to the electroweak sector, which describes electromagnetism and the weak interaction.

The particles of the theory include spin-$\frac{1}{2}$ fermions, the *quarks* and *leptons*, each organised into three groups, known as *generations*. These fermions form the building blocks of regular matter. Alongside these, we have spin-1 *gauge bosons* which mediate the interactions: the *photon*, the *gluon*, and the $W^{\pm}$ and Z^0 *bosons*. Finally, there is also the spin-0 *Higgs boson*. The quarks interact via all SM forces, whereas the leptons interact only through electromagnetism and the weak interaction. The Higgs field has a non-zero vacuum expectation value, leading to the spontaneous breaking of electroweak $\mathrm{SU}(2)_L \times \mathrm{U}(1)_Y$ symmetry to a $\mathrm{U}(1)_Q$ symmetry. This causes the $W^{\pm}$ and the Z^0 to acquire large masses (around 80 GeV and 91 GeV respectively, very large compared to other masses such as the proton with ~ 1 GeV [22]), while the photon and gluon remain massless. The masses of the quarks and charged leptons are dynamically generated from their interactions with the Higgs field, as is the case for the Higgs boson itself.

Despite its unmatched success in describing the behaviour of subatomic particles, the SM still falls short of a complete description of nature. The absence of gravity from the framework is perhaps the clearest indicator of this, but many other issues exist. Examples include the neutrino masses, not accounted for in the SM as the mechanism by which they originate is unclear, the nature of dark matter, which does not fit any of the known particles in the SM, and baryogenesis, the origin of matter-antimatter imbalance in the observed universe.

The work done in this thesis focuses on the theory of the strong interactions, *Quantum Chromodynamics* (QCD). This is the gauge theory based on the $\mathrm{SU}(3)_c$ subgroup of the SM gauge group and includes the SM fields charged under this symmetry, the quarks and gluons. The c label in $\mathrm{SU}(3)_c$ stands for *color*, the conserved charge associated with this symmetry. In the next sections, we give a brief description of QCD and some of its relevant properties, with a special focus on the challenging low-energy regime of the theory. This is followed by a discussion of two approaches used to extract predictions from the theory in this regime, namely *chiral perturbation theory* and *lattice QCD*.

1.1 Quantum Chromodynamics

1.1.1 Quarks, color and the rise of QCD

In the first half of the 20th century, the discovery of protons and neutrons, collectively known as *nucleons*, made it clear that an interaction distinct from electromagnetism had to be present to bind nucleons together into atomic nuclei. This interaction had to be powerful enough to overcome the enormous electromagnetic repulsion between the tightly-packed protons and was thus named the *strong interaction*.

Starting in the 1950s, the advent of powerful particle accelerators led to the discovery of a wide variety of strongly interacting particles. These were called *hadrons*, meaning large or massive, due to their relatively large masses compared to the known leptons at the time. The number of newly-discovered hadrons increased dramatically into the 1960s, with the list of known particles growing into a so-called "particle zoo". The large masses and diversity of the hadrons caused many

to believe that they could not all be elementary particles, and must instead be composites formed from other hadrons or more fundamental constituents.

After many classification proposals, the *quark model* was eventually introduced independently by M. Gell-Mann [23] and G. Zweig [24] in 1964. In this approach, the hadrons are built from *quarks* (in Gell-Mann's terminology), from which they inherit their quantum numbers. Fermionic hadrons, called *baryons*, such as the nucleons, are made up of three quarks, while their antiparticles, the *antibaryons*, are made up of three antiquarks. Bosonic hadrons, the *mesons*, are made up of quark-antiquark pairs.

Three quark *flavours* – up, down and strange – and the corresponding antiquarks seemed to be enough to explain the known hadrons at the time. To produce the observed hadron spins, quarks must also be spin-$\frac{1}{2}$ fermions. This, however, raised an issue, as some spin-$\frac{3}{2}$ baryons would require three quarks of the same flavor and with parallel spins, such as the Δ^{++} (three up quarks) or the Ω^{-} (three strange quarks). This would seemingly violate the Pauli exclusion principle, since all three quarks would have the same quantum numbers. To avoid this, the existence of a hidden quantum number, *color*, was proposed [25]. It would take three distinct values, *red*, *green* and *blue*, to maintain the Fermi statistics of the quarks. Moreover, the sum of the three values must equal zero (i.e. *white*) to produce colorless baryons and maintain the unobserved color degree of freedom hidden. Conversely, antiquarks would take the values *anti-red*, *anti-green* and *anti-blue*, which cancel the corresponding quark colors to produce colorless mesons.

The color degree of freedom must then be accompanied by a symmetry under certain rotations of the internal color space, since different permutations of the quark colors should produce the same colorless hadronic states. The symmetry group associated with these transformations is SU(3). In this group-theoretical language, the quarks can be written as three-vectors in color space, which live in the three-dimensional fundamental representation of the group. Antiquarks, on the other hand, live in the anti-fundamental representation.

These insights paved the way for the development of QCD in the early 1970s, a gauge theory in which color symmetry plays the central role as the origin of the strong interaction. Key experimental evidence contributing to the theory's acceptance came from deep inelastic scattering of electrons and nucleons, which showed the nucleons have internal structures composed of three point-like constituents,

generation	flavor	mass	charge
first	u	$2.16^{+0.49}_{-0.26}$ MeV	$+2/3$
	d	$4.67^{+0.48}_{-0.17}$ MeV	$-1/3$
second	s	$93.4^{+8.6}_{-3.4}$ MeV	$-1/3$
	c	1.27 ± 0.02 GeV	$+2/3$
third	b	$4.18^{+0.03}_{-0.02}$ GeV	$-1/3$
	t	172.69 ± 0.3 GeV	$+2/3$

Table 1.1 *Masses and electric charges of the six quark flavors in the SM. The charges are given in units of the elementary charge e and the masses are those given by the Particle Data Group (PDG) [22]. The masses of all except the t quark are obtained in the* $\overline{\text{MS}}$ *renormalisation scheme, at scale* $\mu = 2$ *GeV for* u, d, s *and at the* $\overline{\text{MS}}$ *masses for* c, b*. The t quark mass is extracted from direct measurements of t decays.*

providing evidence for quarks. Subsequent results from three-jet events provided direct evidence for gluons, the mediator particles in QCD. The successful predictions of perturbative QCD at high energies further solidified this picture. More recently, this has been reinforced by numerical results from lattice QCD, which have shown that the theory provides highly accurate, sub-percent level descriptions even in the low-energy regime.

1.1.2 The Lagrangian of QCD

In this section, we discuss the full Lagrangian of QCD, starting from the Lagrangian for free quarks and imposing local gauge symmetry. Quarks are now known to come in six flavors: up (u), down (d), strange (s), charm (c), top (t) and bottom (b). Their masses and electric charges are summarised in Table 1.1. There are, of course, six corresponding antiquarks, with the same masses and opposite electric charges. The gluons are the mediators of the strong interaction and arise when gauging the $\text{SU}(3)_c$ symmetry, as we discuss below.

Consider quark fields q_f, where f labels the flavor. These are three-vectors with components $q_{f,i}$ where $i = 1, 2, 3$ is the color index and each $q_{f,i}$ is a four-component Dirac spinor (spinor indices are omitted here). In the absence of interactions, the

Lagrangian density for the free quarks is given by

$$\mathcal{L}_{\text{free}} = \sum_f \overline{q}_f (i\partial\!\!\!/ - m_f)\, q_f \,, \tag{1.1}$$

where m_f is the mass of the quark flavor f. The sum over the flavor index f runs over the quark flavors we include in the theory. This can be all six flavors, but often we may neglect the heaviest quarks and sum over the lightest flavors only. We have also introduced the operator $\partial\!\!\!/ \equiv \gamma^\mu \partial_\mu$ and the Dirac adjoint $\overline{q}_f \equiv q_f^\dagger \gamma^0$, with the γ^μ being the usual Dirac matrices which obey the appropriate Clifford algebra $\{\gamma^\mu, \gamma^\nu\} = 2\eta^{\mu\nu}$, with Minkowski metric $\eta^{\mu\nu} = \text{diag}(1, -1, -1, -1)$.

It is straightforward to show that the free Lagrangian is invariant under global $\text{SU}(3)_c$ transformations. Such a transformation acts on the quark fields as a unitary 3×3 matrix Ω with unit determinant:

$$q_f(x) \longrightarrow q'_f(x) = \Omega\, q_f(x) = \exp(it^a \theta^a)\, q_f(x) \,. \tag{1.2}$$

The second equality follows from the fact that Ω can be written in terms of the generators of the Lie algebra of SU(3) in the fundamental representation, labelled t^a here. There are eight generators in total and thus a is implicitly summed from 1 to 8. The t^a follow the usual Lie algebra relations:

$$[t^a, t^b] = i f^{abc} t^c \,, \tag{1.3}$$

with f^{abc} being the structure constants, and are normalised such that $\text{Tr}(t^a t^b) = \delta_{ab}/2$. A usual choice for the generators is $t^a = \lambda^a/2$, where the λ^a are the Gell-Mann matrices. Lastly, the θ^a are real parameters which specify the transformation.

We now impose local gauge invariance by changing an SU(3) global transformation to a local one, done by promoting the transformation parameters to functions of the spacetime coordinates $\theta^i \to \theta^i(x)$, such that (1.2) becomes:

$$q_f(x) \longrightarrow q'_f(x) = \Omega(x) q_f(x) = \exp(it^a \theta^a(x))\, q_f(x) \,. \tag{1.4}$$

To preserve the invariance of the Lagrangian under this gauge transformation, we introduce a vector field $A_\mu \equiv A_\mu^a t^a$, which transforms as

$$A_\mu \longrightarrow A'_\mu = \Omega A_\mu \Omega^\dagger + \frac{i}{g} (\partial_\mu \Omega)\, \Omega^\dagger \,. \tag{1.5}$$

The new fields A^a_μ ($i = 1, 2, ..., 8$, one for each generator) are called *gluons* and are spin-1 bosons. Under the gauge group SU(3), the A^a_μ transform in the eight-dimensional adjoint representation. Gluons couple minimally to the quarks via the gauge-covariant derivative:

$$D_\mu \equiv \partial_\mu + igA_\mu = \partial_\mu + igA^a_\mu t^a \,, \tag{1.6}$$

which replaces the partial derivative in the free Lagrangian. The strong coupling g quantifies the strength of the interaction.

The final piece of the QCD Lagrangian is the pure glue or *Yang-Mills* term [26], which must be constructed to respect gauge invariance. It can be shown that the simplest CP-invariant choice is

$$\mathcal{L}_{\rm YM} = -\frac{1}{4} \,{\rm Tr}\, F^{\mu\nu} F_{\mu\nu} \,, \tag{1.7}$$

where $F^{\mu\nu}$ is the *gluon field strength tensor*, defined as

$$F_{\mu\nu} \equiv \frac{1}{ig}[D_\mu, D_\nu] \,, \tag{1.8}$$

$$= \partial_\mu A_\nu - \partial_\nu A_\mu + ig[A_\mu, A_\nu] \tag{1.9}$$

in analogy with the electromagnetic field strength tensor. The trace in (1.7) is performed over the color indices of $F^{\mu\nu}F_{\mu\nu}$. The derivative terms in (1.9) lead to the expected kinetic terms for massless gluons, as for photons in QED. Note that $SU(3)_c$ is non-Abelian and the commutator in (1.9) does not vanish. This gives rise to gluon self-interaction terms, specifically three- and four-gluon vertices. Thus, gluons are themselves charged under the strong interaction.

The most general formulation of the Yang-Mills Lagrangian includes also another gauge-invariant term constructed by contracting the field strength tensor with its dual. This term, sometimes called *θ-term*, breaks CP symmetry and is generally dropped since CP violation has not been experimentally observed in the strong interaction. [1]

Putting together the different contributions discussed, we obtain the full Lagrangian

[1] The question of why the θ term seems to be suppressed in nature and therefore why QCD respects CP symmetry is known as the strong CP problem and has not yet been satisfactorily answered.

of QCD [27]:

$$\mathcal{L}_{\text{QCD}} = \sum_f \bar{q}_f (i \not{D} - m_f) q_f - \frac{1}{4} \operatorname{Tr} F^{\mu\nu} F_{\mu\nu} \tag{1.10}$$

(using the shorthand $\not{D} \equiv \gamma^\mu D_\mu$), which captures all known features of the strong interaction. Note that all quark flavors and colors couple in the same way to the gluon fields, and that the gluon self-couplings are dictated by the quark-gluon coupling, leaving g as the only coupling in the theory. The only other parameters of the Lagrangian are the quark masses.

With (1.10) in hand, we can attempt to calculate correlators and compute observables from the theory. Time-ordered correlators of operators $\hat{\mathcal{O}}_1(x_1) \dots \hat{\mathcal{O}}_n(x_n)$ are formally given by the path integral

$$\langle 0 | \, T \, \hat{\mathcal{O}}_1(x_1) \dots \hat{\mathcal{O}}_n(x_n) | 0 \rangle = \frac{1}{\mathcal{Z}} \int \mathcal{D}[A, q, \bar{q}] \, e^{iS[A,q,\bar{q}]} \; \hat{\mathcal{O}}_1(x_1) \dots \hat{\mathcal{O}}_n(x_n) \,, \tag{1.11}$$

where T denotes time ordering, $S[A, q, \bar{q}] = \int d^4x \, \mathcal{L}_{\text{QCD}}$ is the action functional and $\mathcal{Z}$ is the partition function:

$$\mathcal{Z} \equiv \int \mathcal{D}[A, q, \bar{q}] \, e^{iS[A,q,\bar{q}]} \,. \tag{1.12}$$

A way to make use of these definitions is to apply the machinery of perturbation theory, using Feynman diagrams and Feynman rules to compute observables such as scattering cross sections and decay rates, as is done in the electroweak sector of the SM. This leads to the framework of *perturbative QCD*, which has been particularly successful in understanding the phenomenology of the theory in high-energy collisions. However, this method fails when applied to low-energy observables. To explain this situation in detail, we consider two key properties of QCD – asymptotic freedom and confinement – which describe the drastically different behaviours of the theory at high and low energies.

We have already touched on *confinement* when introducing the color degree of freedom of hadrons. It is simply the property that the color-charged fundamental particles of QCD – the quarks and gluons – are not asymptotic states of the theory at low energies, and can therefore not be observed in isolation. Instead, they are bound into color-neutral hadrons, which comprise the effective degrees of freedom of the theory in this regime. On the other hand, in the high-energy regime we

have *asymptotic freedom*, describing the fact that the strong interaction becomes asymptotically weaker with increasing energy. This is discussed further in the following section.

1.1.3 Perturbation theory and asymptotic freedom

In perturbation theory, we express an observable as an expansion in the coupling $\alpha_s \equiv g^2/4\pi$ (analogous to the fine-structure constant of QED) and perform calculations up to a given order in this coupling. To do this, one must regularise the ultraviolet (UV) divergences that arise from Feynman loop integrals when working at higher orders in the expansion and reabsorb these divergences into the bare parameters of the theory – the coupling and quark masses – defining renormalised parameters.

Regularisation and renormalisation introduce a new energy scale μ. Physical observables cannot depend on this arbitrary scale, an observation that leads to the well-known renormalisation group equations. It follows that the renormalised coupling will itself depend on the energy scale, with its behaviour being encoded in the so-called *β-function*:

$$\beta(\alpha_s) \equiv \mu^2 \frac{d}{d\mu^2} \alpha_s(\mu) \,. \tag{1.13}$$

At the one-loop level in the perturbative expansion, the β-function is given explicitly by:

$$\beta(\alpha_s) = -\beta_0 \, \alpha_s(\mu)^2 + \mathcal{O}\left(\alpha_s(\mu)^3\right) \,, \tag{1.14}$$

with $\beta_0 \equiv \frac{1}{12\pi}(33 - 2N_f) > 0$, where $N_f \leq 6$ is the number of flavors included in the theory. Neglecting higher-order corrections, we can solve eq. (1.13) to get the running of the coupling with the energy:

$$\alpha_s(\mu) = \frac{\alpha_s(\mu_0)}{1 + \beta_0 \, \alpha_s(\mu_0) \log\left(\frac{\mu^2}{\mu_0^2}\right)} \,, \tag{1.15}$$

where μ_0 is some reference scale arising from integration. The negative sign of the β-function causes the coupling to decrease and vanish asymptotically as $\mu \to \infty$. This is known as *asymptotic freedom* [28, 29] and tells us the strong interaction becomes weaker at large energies.

If we instead lower the energy, we see that the coupling increases rapidly and ultimately diverges at some finite scale Λ_{QCD}, called the *QCD scale*. This happens when $1 + \beta_0\,\alpha_s(\mu_0)\log\left(\Lambda^2_{\mathrm{QCD}}/\mu_0^2\right) = 0$, which we can use to rewrite eq. (1.15) as

$$\alpha_s(\mu) = \frac{1}{\beta_0 \log\left(\frac{\mu^2}{\Lambda^2_{\mathrm{QCD}}}\right)}\,. \tag{1.16}$$

The coupling becomes arbitrarily large as $\mu \to \Lambda_{\mathrm{QCD}}$, causing the breakdown of the perturbative expansion. Consequently, perturbation theory is only valid for energies $\mu \gg \Lambda_{\mathrm{QCD}}$. Current estimates for the QCD scale are around 200 MeV [30]. The failure of perturbative methods at low energies can be understood as the onset of confinement.

1.1.4 Symmetries of the QCD Lagrangian

The Lagrangian of QCD exhibits several exact and approximate symmetries in addition to the $\mathrm{SU}(3)_c$ gauge symmetry. Understanding these symmetries proves quite relevant for explaining certain aspects of the observed phenomenology of the strong interaction. This is motivated by Noether's theorem [31], which tells us continuous symmetries of the Lagrangian lead to conserved charges in the classical theory. These conservation laws are often carried over to the quantum theory, although some may be broken upon quantisation due to the so-called anomalies.

As a relativistic quantum field theory, QCD respects the usual Poincaré symmetry. Moreover, in the absence of a CP-breaking θ-term, the discrete CPT symmetries are individually respected: *charge conjugation* C, which interchanges particles with the respective antiparticles, *parity inversion* P, which flips the sign of spatial coordinates, and *time reversal* T, which flips the sign of the time coordinate.

The quark fields can be decomposed into their left- and right-handed components:

$$q_{f,L} \equiv \frac{1-\gamma_5}{2}\,q_f\,, \tag{1.17}$$

$$q_{f,R} \equiv \frac{1+\gamma_5}{2}\,q_f\,, \tag{1.18}$$

where $\gamma_5 \equiv i\gamma^0\gamma^1\gamma^2\gamma^3$. If we first consider the Lagrangian in the *chiral limit*, in

which the quark masses are set to zero, we can show that

$$\mathcal{L}_{\text{QCD}} = \sum_f \left(\bar{q}_{f,L}\, i\not{D}\, q_{f,L} + \bar{q}_{f,R}\, i\not{D}\, q_{f,R} \right) - \frac{1}{4} \operatorname{Tr} F^{\mu\nu} F_{\mu\nu} \,. \tag{1.19}$$

Here, we observe that the dynamics of left- and right-handed quarks decouple. As a result, the Lagrangian in this limit is invariant under independent global phase transformations of the two chiralities: $q_{f,L} \to e^{i\phi_L} q_{f,L}$ and $q_{f,R} \to e^{i\phi_R} q_{f,R}$, with $e^{i\phi_L} \in \mathrm{U}(1)_L$ and $e^{i\phi_R} \in \mathrm{U}(1)_R$. In addition, it is also invariant under transformations which mix the N_f quark flavors of each chirality. Writing the quark fields as N_f-component vectors in flavor space, these transformations act as $q_L \to L\, q_L$ and $q_R \to R\, q_R$, where $L \in \mathrm{SU}(N_f)_L$ and $R \in \mathrm{SU}(N_f)_R$. This gives an overall exact $\mathrm{U}(1)_L \times \mathrm{U}(1)_R \times \mathrm{SU}(N_f)_L \times \mathrm{SU}(N_f)_R$ chiral symmetry of the Lagrangian in the chiral limit.

The $\mathrm{U}(1)_L \times \mathrm{U}(1)_R$ transformations can equivalently be written as $\mathrm{U}(1)_V \times \mathrm{U}(1)_A$, corresponding to *vector transformations*, which modify the quark field phases equally for both chiralities, and *axial transformations*, which modify the phases in opposite directions. Importantly, $\mathrm{U}(1)_A$ turns out not to be a symmetry of the QCD path integral measure and thus does not survive in the quantum theory, a fact known as the *chiral anomaly* [32–34].

Moreover, the $\mathrm{SU}(N_f)_L \times \mathrm{SU}(N_f)_R$ symmetry is spontaneously broken by the vacuum, due the formation of a non-vanishing *chiral condensate* Σ:

$$\langle 0 | \bar{q}_f\, q_{f'} | 0 \rangle = \langle 0 | \bar{q}_{f,R}\, q_{f',L} | 0 \rangle + \langle 0 | \bar{q}_{f,L}\, q_{f',R} | 0 \rangle = \Sigma\, \delta_{ff'} \,, \tag{1.20}$$

where $\Sigma \approx -(250\,\text{MeV})^3$ [35]. The matrix elements which mix left- and right-handed fields are not invariant under transformations $L \in \mathrm{SU}(N_f)_L$, $R \in \mathrm{SU}(N_f)_R$ unless $L = R$. Thus the vacuum state does not respect chiral symmetry and is invariant only under the subgroup $\mathrm{SU}(N_f)_V$ of vector transformations (i.e. those for which both chiralities transform identically).

We can now consider the effect of non-zero quark masses on these symmetries. Dirac mass terms induce mixing of left- and right-handed fields: $m_f\, \bar{q}_f\, q_f = m_f\, \bar{q}_{f,R}\, q_{f,L} + m_f\, \bar{q}_{f,L}\, q_{f,R}$, which explicitly breaks axial symmetry. Additionally, non-degenerate quark masses further violate the residual vector $\mathrm{SU}(N_f)_V$ symmetry of the massless case explicitly.

Because the masses of the u and d quarks are nearly degenerate, as shown in Table 1.1, and are much lower than the chiral symmetry breaking scale, we can still say QCD has an approximate $\mathrm{SU}(2)_V$ symmetry. This is known as *isospin symmetry* and the corresponding conserved quantum numbers are total isospin I and the isospin component I_3. This concept can be extended to include also the strange quark, which is heavier but sufficiently light compared to the symmetry-breaking scale, giving an approximate $\mathrm{SU}(3)_V$ symmetry. The heavy quarks c, b, t are considerably more massive and thus $\mathrm{SU}(N_f)_V$ is no longer a good approximate symmetry of QCD for $N_f > 3$.

Finally, the exact vector $\mathrm{U}(1)_V$ symmetry is preserved by the QCD with massive quarks. A similar notion applies to each flavor individually, as the Lagrangian is invariant under phase transformations $q_f \to e^{i\phi_f} q_f$ with independent parameters ϕ_f for each flavor f. These are $\mathrm{U}(1)_f$ symmetries and result in the conservation of individual flavor quantum numbers, such as strangeness S and charm C. These can be seen as the residual symmetries of $\mathrm{SU}(N_f)_V$ for non-zero and non-degenerate quark masses, specifically the subgroup of diagonal elements which remains an exact symmetry.

1.1.5 Symmetries and the light hadron spectrum

In the low-energy regime, we know QCD is confining and the spectrum is composed only of color-neutral hadronic states. A full study of hadrons from first principles in QCD requires non-perturbative methods, but many of their properties can be understood and inferred from the underlying symmetries of the theory.

Poincaré symmetry tells us particle mass and total angular momentum J are good quantum numbers. In addition, parity invariance means the parity operator eigenvalue $P = \pm 1$ also provides a good quantum number. Hadronic states can thus be classified using their J and P values, usually written J^P, and their mass. Flavorless hadrons, i.e. those which have all flavor quantum numbers (I_3, S, etc.) equal to zero, have an extra conserved quantum number, C-parity $C = \pm 1$, the eigenvalue of the charge conjugation operation, written as an extra label: J^{PC}.

Next, we consider color symmetry. As colorless states, hadrons must transform in the singlet representation $\mathbf{1}$ of the gauge group $\mathrm{SU}(3)_c$. According to the quark model [23], such color singlets can be mesons, formed from quark-antiquark pairs,

or baryons, formed from three quarks. By multiplying the corresponding color group representations, we check that we do indeed obtain singlets:

$$\mathbf{3} \otimes \overline{\mathbf{3}} = \boxed{\mathbf{1}} \oplus \mathbf{8}\,, \quad \mathbf{3} \otimes \mathbf{3} \otimes \mathbf{3} = \boxed{\mathbf{1}} \oplus \mathbf{8} \oplus \mathbf{8} \oplus \mathbf{10}\,, \tag{1.21}$$

where $\mathbf{3}$ and $\overline{\mathbf{3}}$ are the fundamental and antifundamental representations of $\mathrm{SU}(3)_c$, corresponding to quarks and antiquarks, respectively. In the modern QCD perspective, hadrons are composed of both quarks and gluons. Thus, aside from the minimum quark content required to produce the observed quantum numbers, the *valence quarks*, baryons and mesons must also include corrections arising from virtual quark-antiquark pairs, the *sea quarks*, and from virtual gluons. Nevertheless, the quark model is still useful for classifying hadrons based on their valence quark content.

QCD introduces also the possibility of constructing more exotic singlet states beyond the scope of the original quark model. Examples include objects with more than three valence quarks, such as *tetraquarks* or *pentaquarks*, but also objects which include valence gluons, such as *glueballs* (valence gluons only) and *hybrids* (valence quarks and gluons). There is increasing evidence supporting the existence of exotic states, but their identification and classification within the categories listed above is still debated. In the following, we focus mostly on the lightest conventional meson and baryon states.

In addition to color, we need to consider the approximate flavor symmetry of QCD. In the limit of exact $\mathrm{SU}(N_f)_V$ flavor symmetry (i.e. equal quark masses), one should expect hadrons to appear as multiplet representations of $\mathrm{SU}(N_f)_V$ in each J^P channel, with multiplet members having the same mass and interacting identically under the strong force. As discussed in the previous section, the two- and three-flavor cases are the most relevant, since flavor is only a good approximate symmetry in nature for the light quarks u, d, s.

For three flavors, quarks and antiquarks transform in the $\mathbf{3}$ and $\overline{\mathbf{3}}$ representations of $\mathrm{SU}(3)_V$, respectively. The possible meson and baryon multiplets can be found from the decompositions:

$$\mathbf{3} \otimes \overline{\mathbf{3}} = \mathbf{1} \oplus \mathbf{8}\,, \quad \mathbf{3} \otimes \mathbf{3} \otimes \mathbf{3} = \mathbf{1} \oplus \mathbf{8} \oplus \mathbf{8} \oplus \mathbf{10}\,, \tag{1.22}$$

which are, of course, the same we saw for color $\mathrm{SU}(3)_c$ but without the restriction

to singlet states. From this, we see that mesons come in a singlet and an octuplet, while baryons can come in a singlet, octet or decuplet. States within multiplets are usually arranged according to their isospin component I_3 and strangeness S. Both are additive quantum numbers, with $I_3 = +\frac{1}{2}, -\frac{1}{2}, 0$ for the u, d, s quarks, respectively, while $S = -1$ for the s quark and 0 for the other flavors. The sign of these assignments is reversed for the corresponding antiquarks.[2] Examples of the meson and baryon multiplets are shown in Figure 1.1.

The exact $\mathrm{U}(1)_V$ symmetry corresponds to the conservation of *baryon number*, an additive quantum number defined as $B = +\frac{1}{3}$ for quarks and $B = -\frac{1}{3}$ for antiquarks. As such, baryons have $B = +1$, antibaryons have $B = -1$ and mesons have $B = 0$.

In short, baryons and mesons can be arranged according to their J^P values, with each J^P channel containing flavor multiplets. Quark-antiquark pairs have a total spin magnitude of 0 or 1 and, by adding orbital angular momentum ℓ, we can obtain mesons with $J^P = 0^\pm, 1^\pm, 2^\pm, ...$ Similarly, we can get baryons with $J^P = \frac{1}{2}^\pm, \frac{3}{2}^\pm, \frac{5}{2}^\pm, ...$ Within each J^P channel, it is possible to have radial excitations, which differ from the ground state multiplet states by their mass. The states with higher angular momenta can often be interpreted as excited states, or resonances, of the lower angular momentum states with the same flavor quantum numbers.

A list of the pseudoscalar ($J^P = 0^-$) and vector ($J^P = 1^-$) mesons is given in Table 1.2 below. We can contrast this with the experimentally determined spectrum in these channels, shown in Figure 1.2.[3]

The breaking of $\mathrm{SU}(3)_V$ flavor symmetry is immediately apparent in the spectrum from the non-degenerate masses of the octet states. As expected, $\mathrm{SU}(2)_V$ isospin symmetry does considerably better, as the strangeless π and ρ mesons are nearly mass-degenerate. Another consequence of $\mathrm{SU}(3)_V$ breaking is that states with the same I_3 and S can mix between different multiplets of the same J^P channel. As a result, the physical states η, η' are in fact superpositions of η_8, η_1 (with a small admixture of π_0), η consisting predominantly of η_8 and η' consisting predominantly of η_1. Similarly, the ω and ϕ mesons are superpositions of ψ_1, ψ_8. However, in this

[2]Note that I_3 and S are still good quantum numbers even for an approximate flavor symmetry, unlike the Casimirs which label the different multiplets (e.g. the isospin magnitude I for flavor $\mathrm{SU}(2)_V$).

[3]Note that observed hadron masses are affected also by electromagnetic effects, which we neglect here because QCD gives the dominant contributions.

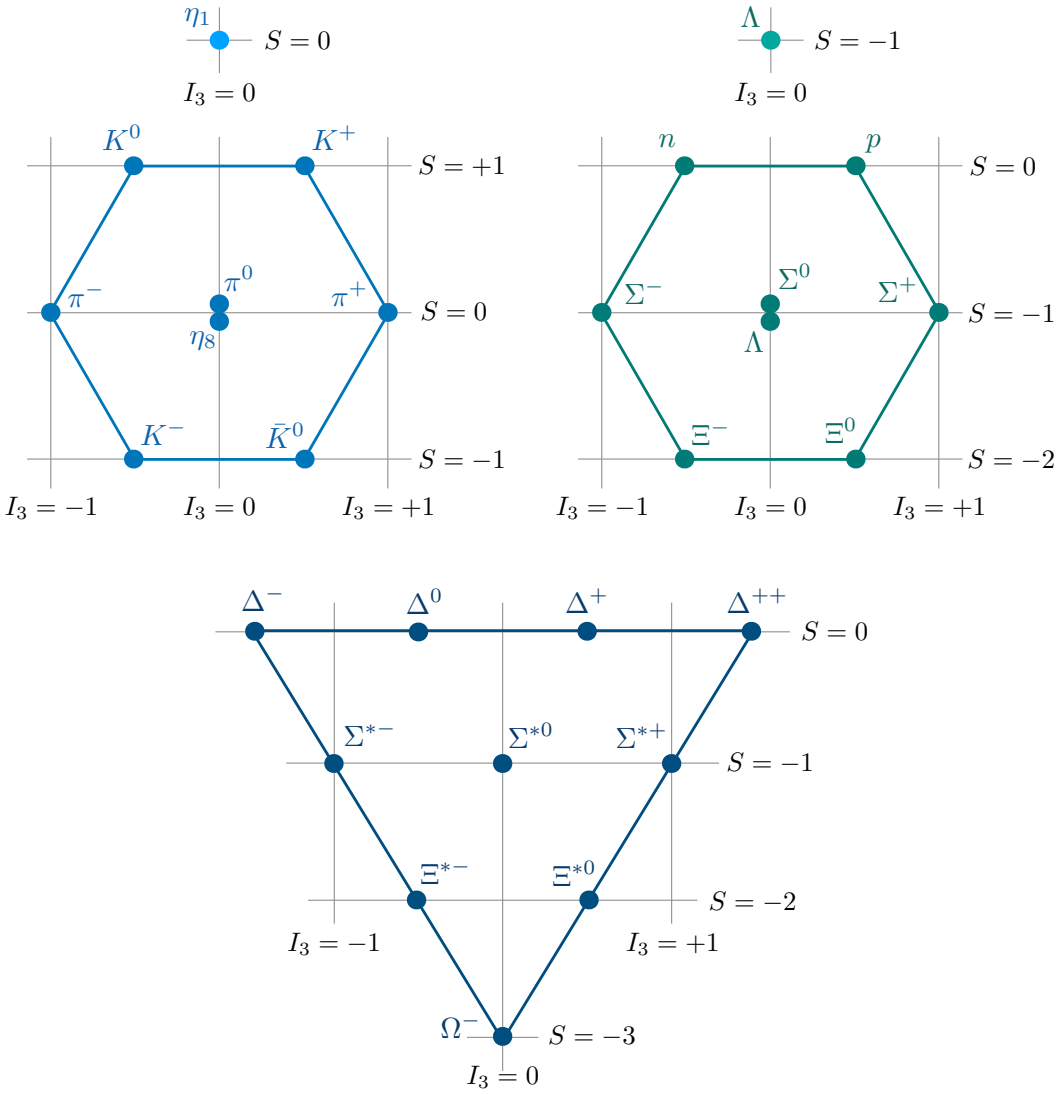

Figure 1.1 *Examples of* SU(3) *meson and baryon multiplets. On the top left, we have the pseudoscalar ($J^P = 0^-$) meson singlet and octet. On the top right, we have the $J^P = \frac{1}{2}^+$ baryon singlet and octet. The $J^P = \frac{3}{2}^+$ baryon decuplet is shown below.*

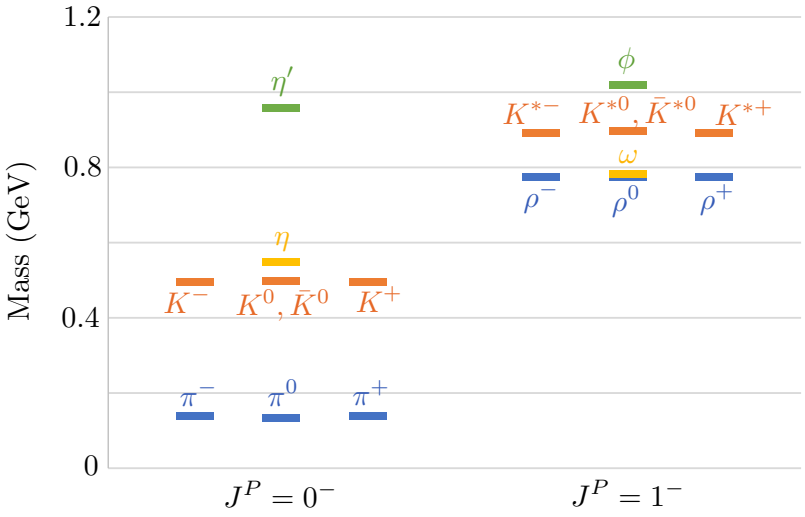

Figure 1.2 *Experimentally determined ground state masses in the $J^P = 0^-, 1^-$ channels. The values are the central values given in [22] and the experimental uncertainties are omitted.*

$J^P = 0^-$	$J^P = 1^-$	I	I_3	S	flavor wf.
π^-	ρ^-	1	-1	0	$d\bar{u}$
π^0	ρ^0	1	0	0	$\frac{1}{\sqrt{2}}(u\bar{u} - d\bar{d})$
π^+	ρ^+	1	$+1$	0	$u\bar{d}$
K^0	K^{*0}	1/2	$-1/2$	$+1$	$d\bar{s}$
K^+	K^{*+}	1/2	$+1/2$	$+1$	$u\bar{s}$
K^-	K^{*-}	1/2	$-1/2$	-1	$s\bar{u}$
$\bar{K}^0$	$\bar{K}^{*0}$	1/2	$+1/2$	-1	$s\bar{d}$
η_8	ω_8	0	0	0	$\frac{1}{\sqrt{3}}(u\bar{u} + d\bar{d} - 2s\bar{s})$
η_1	ω_1	0	0	0	$\frac{1}{\sqrt{3}}(u\bar{u} + d\bar{d} + s\bar{s})$

Table 1.2 *List of the octet and singlet pseudoscalar ($J^P = 0^-$) and vector ($J^P = 1^-$) mesons, labelled by isospin I, third isospin component I_3 and strangeness S, together with the corresponding flavor wavefunctions.*

case, ω is essentially a symmetric $u\bar{u}$-$d\bar{d}$ superposition, while ϕ is almost exclusively $s\bar{s}$.

The mass hierarchy of the vector mesons is naïvely what one might expect from their quark content, given quark masses $m_s \gg m_u \approx m_d$: the ω and ρ mesons have nearly the same mass and the gaps between these, the K^* mesons and the ϕ masses are approximately the same and are roughly attributable to the strange quark mass. The same logic does not seem to hold for the pseudoscalar mesons, as the η' meson is heavier than the η meson, and both are heavier than the remaining pseudoscalars. Moreover, the pseudoscalar octet states are the lightest in the hadron spectrum, seeming almost unnaturally light, especially in the case of the pions π, compared to other hadronic masses.

Another, seemingly unrelated, feature of the meson spectrum is the discrepancy between the masses of the pseudoscalar and vector mesons and the corresponding opposite parity states, the scalars ($J^P = 0^+$) and axial vectors ($J^P = 1^+$) respectively (not shown in Figure 1.2). For example, the π^0 meson ($J^{PC} = 0^{-+}$) has a mass of 139 MeV, while its scalar counterpart a^0 ($J^{PC} = 0^{++}$) has a mass around 980 MeV [22].

Interestingly, these and other characteristics of the hadronic spectrum are well explained through chiral symmetry and its breaking. If this symmetry were respected, hadrons would necessarily appear in identical pairs with opposite parities (parity doublets). Thus, the mass discrepancy between pseudoscalar and scalar mesons described above is a consequence of a broken chiral symmetry.

Recall also that axial $\mathrm{U}(1)_A$ is explicitly broken upon quantisation due to the chiral anomaly, while axial $\mathrm{SU}(N_f)_A$ is spontaneously broken in the chiral limit. According to *Goldstone's Theorem* [36, 37], spontaneous breaking of an exact axial $\mathrm{SU}(N_f)_A$ symmetry will generate $N_f^2 - 1$ massless pseudoscalar *Nambu-Goldstone bosons* (NGBs), one for each broken generator of the axial symmetry. For physical quark masses, however, chiral symmetry is only approximate for the three light flavors. Thus, we should expect to see traces of $3^2 - 1 = 8$ *pseudo-Nambu-Goldstone bosons* (pNGBs) in the spectrum, so-called because they are no longer massless, but are protected by the approximate symmetry keeping them relatively light.[4]

[4]Note that the prefix "pseudo-" does not refer to the fact that the pseudo-Nambu-Goldstone bosons are pseudoscalars, meaning instead that they arise from an approximate symmetry and are therefore not massless. Their pseudoscalar nature here results from the fact that the broken symmetry is an axial symmetry.

This description fits the pseudoscalar octet mesons, the lightest states in the spectrum, quite well. Indeed, we see that the pions are, relatively speaking, almost massless. This would indicate spontaneous symmetry breaking of near-exact isospin $\mathrm{SU}(2)_A$ symmetry, the two-flavor subgroup of $\mathrm{SU}(3)_A$, as expected. Octet mesons which include strange valence quarks, namely the kaons K and the eta η, should feel the $\mathrm{SU}(3)_A$ symmetry breaking more strongly and acquire a larger mass, also seen in the spectrum. The interpretation of the pseudoscalar octet mesons as pNGBs is central to chiral perturbation theory (χPT), discussed in more detail in the next section.

If $\mathrm{U}(1)_A$ were also spontaneously broken in the chiral limit and not explicitly broken, we would expect a ninth pNGB, which would naturally correspond to the remaining pseudoscalar state in the spectrum, η'. However, we observe this meson, made up predominantly of the singlet η_1, to be significantly more massive than the octet states, including the η (predominantly η_8), thereby showing that it cannot result from a spontaneous breaking mechanism. The origin of the heavier η' mass is explained more rigorously through the Witten-Veneziano mechanism [38–40], which clarifies its connection to the chiral anomaly and the non-trivial topology of the Yang-Mills vacuum in the large N_c (number of colors) limit.

Although effective in describing the pseudoscalar states, the quark model fails to convincingly explain the spectrum of the scalar mesons. These present an unexpected mass hierarchy, and some, such as the σ (or $f_0(500)$), are very broad resonances (see e.g. review on scalar mesons in [30]). These and other arguments have supported the view that such states might not correspond to quark-antiquark pairs and may have a more exotic make-up, such as tetraquark states. The same could be true for other meson states with quantum numbers not predicted by the quark model, such as the $\pi_1(1400)$ or $\pi_1(1600)$ ($J^{PC} = 1^{-+}$) [22], which can arise from hybrids.

Let us now turn to the baryons. The lowest-lying baryon states in the experimental spectrum have $J^P = \frac{1}{2}^+, \frac{3}{2}^+$. The ground states in these channels are shown in Figure 1.3. We can compare this to the list of singlet, octet and decuplet baryon states expected from the quark model, given in Table 1.3. Again, because $\mathrm{SU}(3)_V$ is not exact for non-vanishing quark masses, states with the same J^P, I_3 and S quantum numbers in different multiplets can mix. This is more relevant for the states containing strange quarks, the Λ, Σ and Ξ baryons (the *hyperons*), which

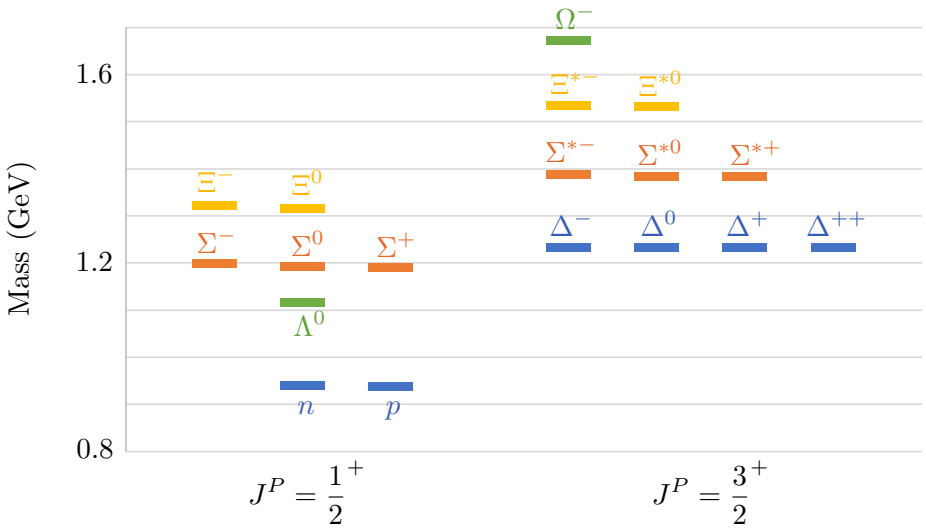

Figure 1.3 *Experimentally determined ground states in the $J^P = \frac{1}{2}^+, \frac{3}{2}^+$ channels. The masses plotted are the PDG central values [22], with experimental uncertainties omitted.*

feel $\mathrm{SU}(3)_V$ breaking more strongly. We see that these predictions agree with the observed ground states quite well.

Beyond the ground states, however, the quark model does not fare as well and it is often difficult to match observed excited states with quark contents. A notable example is the *Roper resonance* $N(1440)$ [41], the lowest nucleon radial excitation, which has a lower mass than expected from its quark content and parity. These features can only be explained by means of more complicated mechanisms, in which contributions from multiquark states play a crucial role [42].

To end this section, let us briefly consider the inclusion of the fourth flavor, charm, into the meson framework outlined above. The flavor symmetry group $\mathrm{SU}(4)_V$ would produce the meson flavor multiplets

$$\mathbf{4} \otimes \overline{\mathbf{4}} = \mathbf{1} \oplus \mathbf{15}\,, \tag{1.23}$$

where $\mathbf{4}$ is the fundamental representation of $\mathrm{SU}(4)$. Multiplet members are arranged by their isospin component I_3, strangeness S and charm C quantum numbers. Charm is an additive quantum number defined as $C = +1$ for the c quark and $C = -1$ for the $\bar{c}$ antiquark.

The much higher mass of the charm quark c means $\mathrm{SU}(4)_V$ breaking effects are

$J^P = \frac{1}{2}^+$	I	I_3	S	flavor
n	$1/2$	$-1/2$	0	udd
p	$1/2$	$+1/2$	0	uud
Σ^-	1	-1	-1	dds
Σ^0	1	0	-1	uds
Σ^+	1	$+1$	-1	uus
Ξ^-	$1/2$	$-1/2$	-2	dss
Ξ^0	$1/2$	$+1/2$	-2	uss
Λ^0	0	0	-1	uds

$J^P = \frac{3}{2}^+$	I	I_3	S	flavor
Δ^-	$3/2$	$-3/2$	0	ddd
Δ^0	$3/2$	$-1/2$	0	udd
Δ^+	$3/2$	$+1/2$	0	uud
Δ^{++}	$3/2$	$+3/2$	0	uuu
Σ^{*-}	1	-1	-1	dds
Σ^{*0}	1	0	-1	uds
Σ^{*+}	1	$+1$	-1	uus
Ξ^{*-}	$1/2$	$-1/2$	-2	dss
Ξ^{*0}	$1/2$	$+1/2$	-2	uss
Ω^-	0	0	-3	sss

Table 1.3 *Quantum numbers and flavor content of the* SU(3) *baryon multiplet elements:* $J^P = \frac{1}{2}^+$ *octet and singlet at the top and* $J^P = \frac{3}{2}^+$ *decuplet below. Note that the singlet and central octet states* ($I_3 = 0$, $S = -1$) *mix to give the* Λ^0 *baryon.*

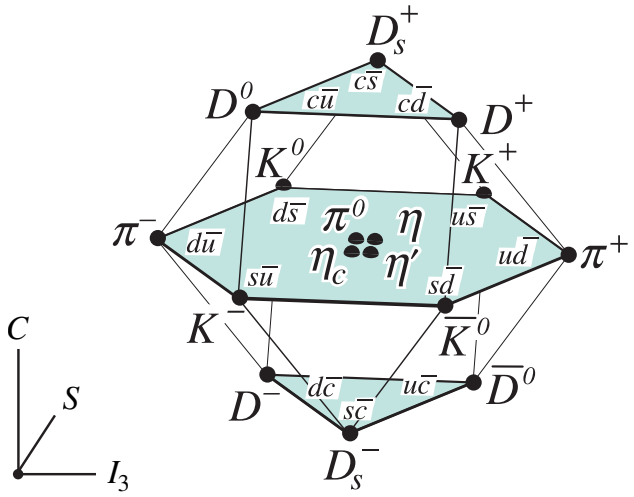

Figure 1.4 *Diagram of the pseudoscalar meson* SU(4) *multiple. This figure was adapted from the review on the quark model in [43].*

$J^P = 0^-$	$J^P = 1^-$	I	I_3	S	C	flavor wf.
D^-	D^{*-}	$1/2$	$-1/2$	0	-1	$d\bar{c}$
D^0	D^{*0}	$1/2$	$-1/2$	0	$+1$	$c\bar{u}$
$\bar{D}^0$	$\bar{D}^{*0}$	$1/2$	$+1/2$	0	-1	$u\bar{c}$
D^+	D^{*+}	$1/2$	$+1/2$	0	$+1$	$c\bar{d}$
D_s^-	D_s^{*-}	0	0	-1	-1	$s\bar{c}$
D_s^+	D_s^{*+}	0	0	$+1$	$+1$	$c\bar{s}$

Table 1.4 *Quantum numbers and flavor wavefunctions of the D and D^* mesons.*

quite severe. Despite this, the quantum numbers I_3, S and C are still conserved and mixing occurs between states in different multiplets with the same values of these quantum numbers. The pseudoscalar singlet and 15-plet, which work effectively as a 16-plet due to intermixing of the central states, are shown in Figure 1.4. Beyond the light pseudoscalar states we have already encountered, the heavy-light *D mesons* and their vector counterparts, the *D^* mesons*, are of particular interest for work done in this thesis. Their quark contents are summarised below in Table 1.4.

The spectrum of the charmed mesons has proved to be prime hunting ground for exotic states. The *charmonium* ($c\bar{c}$) sector, for example, contains a large number of states not explained by the quark-antiquark pair picture, the so-called *XYZ states* [44]. Another example is the recently discovered doubly-charmed tetraquark $T_{cc}(3875)^+$ [16, 17], with minimal quark content $cc\bar{u}\bar{d}$. The structure of these exotic states is still heavily debated. One proposal is that they might in fact be molecules of two heavy-light mesons, owing to their proximity to the respective decay thresholds.

As we have seen in this section, the underlying symmetries of QCD and the quark model go a long way towards explaining the observed low-energy spectrum of the theory. However, it is clear that we quickly reach the limitations of such an approach when we try to tackle higher excitations and exotic states or probe their inner structure. To study the dynamics of hadrons and their properties, we need different methods and techniques that build on and extend the quark model. We discuss two such approaches – chiral perturbation theory and lattice QCD – in the remainder of this chapter.

1.2 Chiral perturbation theory

Chiral perturbation theory is an example of an *effective field theory* (EFT). An EFT is an approximate description of an underlying field theory which captures its relevant features at specified energy or length scales, typically the low-energy regime. This is based on the principle of separation of scales, the assumption that the physics at low energy scales is largely independent from the details at high energy scales. As such, one can construct an EFT that models the low-energy behaviour of a given field theory, valid up to some cut-off scale, while assuming no detailed knowledge of its high-energy behaviour.

The construction of an EFT is generally guided by the known symmetries of the system and makes use of only the relevant degrees of freedom at the chosen energy scales. The usual strategy is to follow *Weinberg's "theorem"* [45]: using the appropriate degrees of freedom, one should write down the most general Lagrangian compatible with all known (or assumed) symmetries. To keep the potentially infinite number of possible terms in the Lagrangian under control, one should also identify a suitable *expansion parameter*. This is a small quantity that controls the size of neglected contributions, allowing us to keep only finitely many dominant terms in a calculation, in a similar way to the role of the coupling in a perturbative expansion.

EFTs are very useful theoretical tools in the absence of an underlying theory valid at all energy scales. They can also be employed when such a theory is known but extracting predictions from it can be quite challenging. The latter case is precisely what we encounter in the low-energy regime of QCD, where confinement forbids the use of perturbative methods. Unsurprisingly, EFTs are a popular method in the study of hadron interactions.

Chiral perturbation theory (χPT), a framework originally developed by Weinberg [45, 46], Gasser and Leutwyler [47], is perhaps the most well-known low-energy EFT of QCD. It is reviewed extensively in [48–50] and we will give only a short description here.

The aim of χPT is to describe the interactions of the lightest hadrons at low momenta by leveraging the approximate chiral symmetry of the strong force. In its simplest form, it deals only with the multiplet pseudoscalar mesons, which are interpreted, in the chiral limit, as the NGBs generated by the spontaneous breaking of chiral

symmetry. These massless excitations can be parameterised by the field $U(x) \in \mathrm{SU}(N_f)$[5], which transforms as

$$U \to RUL^\dagger \tag{1.24}$$

under chiral transformations $(L, R) \in \mathrm{SU}(N_f)_L \times \mathrm{SU}(N_f)_R$. The field $U(x)$ can be written as

$$U(x) = \exp\left(\frac{i}{F}\,\pi(x)\right), \qquad \pi(x) \equiv 2\pi^a(x)t^a\,, \tag{1.25}$$

where the field $\pi(x)$ is valued in the Lie algebra of $\mathrm{SU}(N_f)$, with t^a denoting the corresponding generators (normalised such that $\mathrm{Tr}(t^a t^b) = \delta^{ab}/2$), and F is a constant with dimensions of energy.

The components $\pi^a(x)$ can be related to the pseudoscalar multiplet mesons. Focusing on the two-flavor case, $\pi(x)$ may be written in terms of the pion isospin triplet $\{\pi^-, \pi^0, \pi^+\}$, a common choice being

$$\pi(x) \equiv \begin{pmatrix} \pi^0 & \sqrt{2}\pi^+ \\ \sqrt{2}\pi^- & -\pi^0 \end{pmatrix}. \tag{1.26}$$

To build a Lagrangian for the pion fields, we must include all terms that are compatible with $\mathrm{SU}(2)_L \times \mathrm{SU}(2)_R$ chiral symmetry, according to Weinberg's "theorem". The simplest term we can write down using the field U is $\mathrm{Tr}(U^\dagger U)$, which produces a constant ($U^\dagger U = 1$, by definition) and can thus be ruled out. We turn then to terms containing spacetime derivatives, which correspond to powers of momentum in momentum space. Since we are looking at low-energy dynamics, we can build the Lagrangian order by order as a low-momentum expansion by counting the number of derivatives. The non-vanishing term with the fewest derivatives turns out to be $\mathrm{Tr}(\partial^\mu U^\dagger \partial_\mu U)$, giving a leading order effective Lagrangian

$$\mathcal{L}_\chi^{(2)} = \frac{F^2}{4}\,\mathrm{Tr}(\partial^\mu U^\dagger \partial_\mu U)\,, \tag{1.27}$$

where F is the only unknown constant, which can be matched to experiment, taking the value $F \approx 93$ MeV [30].

The above Lagrangian assumes exact $\mathrm{SU}(2)_L \times \mathrm{SU}(2)_R$ and holds for massless pions. To account for explicit chiral symmetry breaking due to non-zero quark masses, we

[5]Chiral symmetry $G = \mathrm{SU}(N_f)_L \times \mathrm{SU}(N_f)_R$ is broken to the subgroup $H = \mathrm{SU}(N_f)_V$ and the Goldstone bosons live in the resulting coset group, $G/H = \mathrm{SU}(N_f)$.

introduce a new field

$$M \equiv \begin{pmatrix} m_u & 0 \\ 0 & m_d \end{pmatrix}, \tag{1.28}$$

where m_u, m_d are the u and d quark masses, and allow this field to couple to U. Although M is in actuality a constant, we promote now it to a dynamical field – a *spurion* – and impose on it the same transformation law under chiral transformations as U, cf. eq. (1.24). The spurion field serves, in effect, to parameterise the amount of chiral symmetry breaking.

We can now construct chirally-invariant Lagrangians that depend on U and M, which we will then expand in powers of M. At leading order, eq. (1.27) becomes

$$\mathcal{L}_\chi^{(2)} = \frac{F^2}{4} \operatorname{Tr}(\partial^\mu U^\dagger \partial_\mu U) + \frac{BF^2}{2} \operatorname{Tr}(U^\dagger M + M^\dagger U)\,. \tag{1.29}$$

This Lagrangian includes two parameters: F can be identified with the pion weak decay constant in the chiral limit, while B is related to the quark condensate Σ. By further expanding $U(x) = \exp(i\pi(x)/F)$, we can write the Lagrangian explicitly in terms of the pion fields. To second order, we obtain the kinetic and mass terms for the pions:

$$\begin{aligned} \mathcal{L}_\chi^{(2)} &= \partial^\mu \pi^+ \partial_\mu \pi^- - 2B(m_u + m_d)\pi^+\pi^- \\ &\quad + \frac{1}{2}\partial^\mu \pi^0 \partial_\mu \pi^0 - B(m_u + m_d)\pi^0\pi^0 + \mathcal{O}(\pi^4)\,. \end{aligned} \tag{1.30}$$

Importantly, we see that the square of the pion mass is linear in the quark masses at leading order, with B as the proportionality constant: $M_\pi^2 = 2B(m_u + m_d) + \mathcal{O}(m_u^2, m_d^2)$. Keeping a few more higher-order terms in the pion fields, one can already write down Feynman rules and obtain amplitudes for processes such as $\pi\pi$ scattering at tree level.

The pNGB Lagrangian of eq. (1.29) is systematically improvable by the addition of terms of higher order in powers of momentum (increasing number of derivatives) and the quark masses (or, alternatively, the pion mass). Although there are infinitely many terms which satisfy chiral symmetry, we are effectively considering an expansion in the parameters p/Λ_χ and M_π/Λ_χ, where p is a typical momentum scale and Λ_χ is the chiral symmetry breaking scale.[6] By keeping the expansion

[6] Λ_χ is often taken to be of the order of the lightest non-pNGB hadron mass, the ρ meson, at ~ 1 GeV.

parameters small, we can neglect all but the lowest-order terms and reduce an infinite number of coefficients to a small set, the *low-energy constants* (LECs), which can be determined from experimental results. A power-counting scheme is required to organise the terms in the expansion. Lorentz invariance dictates that derivatives must appear in even numbers, while each insertion of M carries a factor of M_π^2, as seen above, and can therefore be counted as order two. Consequently, there will only be even orders contributing to the Lagrangian in this scheme:

$$\mathcal{L}_\chi = \mathcal{L}_\chi^{(2)} + \mathcal{L}_\chi^{(4)} + \mathcal{L}_\chi^{(6)} + \cdots , \tag{1.31}$$

with $\mathcal{L}_\chi^{(2)}$ being given by eq. (1.29). The next term $\mathcal{L}_\chi^{(4)}$ will include a total of eight independent chirally invariant operators in SU(2) χPT, e.g. $\left(\mathrm{Tr}(\partial^\mu U^\dagger \partial_\mu U)\right)^2$, $\mathrm{Tr}(\partial^\mu U^\dagger \partial_\mu U)\,\mathrm{Tr}(U^\dagger M + M^\dagger U)$.

When performing calculations at higher order in χPT, one must also take into account the loop contributions arising from terms at lower orders. As usual, loops can produce divergences, which need to be removed by renormalisation. Although χPT is not renormalisable in general due to the infinite number of parameters of the full Lagrangian, it is renormalisable order by order in the power-counting scheme introduced above. Loop integrals can be assigned an order in the power counting and their divergences absorbed by a renormalisation of the LECs at that order. For example, the divergences arising in one-loop contributions from $\mathcal{L}_\chi^{(2)}$ can be removed by a redefinition of the LECs at the next order, $\mathcal{L}_\chi^{(4)}$.

The χPT framework can be extended quite straightforwardly to three flavors, incorporating the strange quark. The matrix $\pi(x)$ is then given in terms of the pseudoscalar octet mesons:

$$\pi(x) = \begin{pmatrix} \pi^0 + \frac{1}{\sqrt{3}}\eta & \sqrt{2}\pi^+ & \sqrt{2}K^+ \\ \sqrt{2}\pi^- & -\pi^0 + \frac{1}{\sqrt{3}}\eta & \sqrt{2}K^0 \\ \sqrt{2}K^- & \sqrt{2}\bar{K}^0 & -\frac{2}{\sqrt{3}}\eta \end{pmatrix} . \tag{1.32}$$

Because the mass of the charm quark exceeds the chiral symmetry breaking scale, an extension of χPT to four or more flavors is no longer useful for studying the pseudoscalar mesons with heavy quark content at physical quark masses. Other EFTs, such as *heavy quark effective theory* (HQET) [51–53], are more suitable in this context.

An important extension of the chiral Lagrangian is the inclusion of a *Wess-Zumino-Witten term* (WZW term) [39, 54], accounting for the effect of the chiral anomaly. This allows the chiral Lagrangian to describe processes which change intrinsic parity, e.g. $K^+K^- \to \pi^+\pi^-\pi^0$. Another natural modification is to allow coupling to external fields, achieved through the the introduction of appropriate covariant derivatives into the Lagrangian of eq. (1.29). For example, coupling to the electromagnetic field and including a WZW term [55, 56] allows us to treat the neutral pion decay $\pi^0 \to \gamma\gamma$ which proceeds through the chiral anomaly.

The inclusion of the lightest baryons into χPT is also possible, although this creates a few complications. Let us briefly discuss the two-flavor case, assuming exact isospin symmetry ($m_u = m_d$) for simplicity. The lightest baryons are the nucleons (the proton p and neutron n), which come in an isospin doublet $N \equiv \begin{pmatrix} p \\ n \end{pmatrix}$. The pNGB nature of the pseudoscalar mesons fixes their their chiral transformation properties, but we do not have the same constraints for the baryons. As such, we must instead stipulate a convenient transformation law for the nucleon doublet. The usual procedure consists of introducing a field u, defined as the square root of U, which transforms as

$$u = \sqrt{U} \to u' = \sqrt{U'} = \sqrt{L\,U\,R^\dagger} \equiv R\,u\,K^{-1}\,, \tag{1.33}$$

for chiral transformations $(L, R) \in \mathrm{SU}(2)_L \times \mathrm{SU}(2)_R$. Here, we have also defined $K \in \mathrm{SU}(2)$, which depends on L, R and U and that we can solve for explicitly:

$$K = \sqrt{L\,U\,R^\dagger}^{-1} R \sqrt{U}\,. \tag{1.34}$$

The nucleon doublet will thus transform as

$$N \to N' = K N\,. \tag{1.35}$$

We can now start to build a Lagrangian compatible with this transformation. For free nucleons, we should expect it to reduce to the usual Dirac Lagrangian $\overline{N}(i\partial\!\!\!/ - M_N)N$, where M_N is the nucleon mass in the chiral limit. For this to be invariant under the transformation of eq. (1.35), the partial derivative must be promoted to a covariant derivative $D_\mu = \partial_\mu + v_\mu$. A choice of connection which fulfils this

requirement is the vector field given by

$$v_\mu \equiv \frac{1}{2}\left(u^\dagger \partial_\mu u + u\,\partial_\mu u^\dagger\right) . \tag{1.36}$$

There is another type of term which respects the symmetry that we can construct, in which the nucleons couple to an axial vector

$$a_\mu \equiv \frac{i}{2}\left(u^\dagger \partial_\mu u - u\,\partial_\mu u^\dagger\right) . \tag{1.37}$$

We can write the leading-order chiral Lagrangian for the nucleons as [49, 57]

$$\mathcal{L}^{(1)}_{\chi,\pi N} = \overline{N}\left(i\not{D} - M_N + g_A\gamma^\mu\gamma^5 a_\mu\right) N\,, \tag{1.38}$$

where the axial vector coupling g_A is the only new LEC. Note that additional terms can be added to v_μ and a_μ to accommodate couplings to external fields.

For three flavors, the spin-$\frac{1}{2}$ baryon octet can be arranged into the matrix

$$B = \begin{pmatrix} \frac{1}{\sqrt{2}}\Sigma^0 + \frac{1}{\sqrt{6}}\Lambda & \Sigma^+ & p \\ \Sigma^- & -\frac{1}{\sqrt{2}}\Sigma^0 + \frac{1}{\sqrt{6}}\Lambda & n \\ \Xi^- & \Xi^0 & -\frac{2}{\sqrt{6}}\Lambda \end{pmatrix} , \tag{1.39}$$

which transforms under as $B \to KBK^\dagger$ under $(L, R) \in \mathrm{SU}(3)_L \times \mathrm{SU}(3)_R$, with K defined as in eq. (1.34). The chiral Lagrangian can then be built from B and u [58]. We will not go into more detail here, but a detailed review of SU(3) χPT with baryons can be found in [50].

A major issue arising from the expansion of χPT to nucleons and other octet baryons is the failure of the power-counting scheme used in the mesonic sector. This is because we have introduced a new heavy mass scale, the nucleon mass $M_N \sim 1$ GeV, which is comparable in magnitude to the chiral breaking scale Λ_χ. As a result, loop diagrams involving nucleons can contribute at the same order as tree-level diagrams, and an expansion in the parameter $M_N/\Lambda_\chi \sim \mathcal{O}(1)$ is not viable.

This problem is addressed in *heavy-baryon* χPT (HBχPT) [59, 60]. In this EFT, one decomposes the nucleon four-momentum into a large mass contribution and a much smaller residual momentum contribution ($p_\mu = M_N v_\mu + l_\mu$, where v_μ is the nucleon four-velocity) and considers the heavy-field limit, expanding in powers of

$1/M_N$. It is then possible to construct a systematic power-counting scheme based on a two-fold expansion in p/Λ_χ and p/M_N. This framework allows one to determine corrections to nucleon mass or to study $N\pi$ scattering, as discussed in some detail in [50].

After this short review of key aspects of χPT, we now move on to a review of lattice QCD in the following section.

1.3 Lattice QCD

A well-established non-perturbative approach to QCD is provided by *lattice QCD*. In this framework, the theory is formulated on a discretised spacetime consisting of a four-dimensional lattice of points and Monte-Carlo techniques are employed to numerically evaluate the path integral and hence compute expectation values of observables. Such calculations are very computationally demanding and thus rely on high-performance computing resources and advanced algorithms. These have seen remarkable developments and improvements since the initial proposal of lattice QCD by K. Wilson [61] in the 1970s.

Lattice QCD is currently the only rigorous non-perturbative method available for performing first-principles numerical calculations in the low-energy regime of QCD. It also allows for the numerical exploration of QCD and other non-Abelian gauge theories beyond what is experimentally accessible, such as by using unphysical quark masses or changing the number of colors and flavors in the theory. Note that, while the EFT-based alternatives discussed in the previous section can provide systematically improvable analytic results for many low-energy hadronic observables, such approaches require additional inputs, namely the values of the LECs, to give numerical predictions. Because the LECs are not fixed by chiral symmetry and cannot easily be calculated from QCD, they must instead be determined from fits to experimental data or computed in lattice QCD.

Recall that, in a quantum field theory containing fields $\{\phi\}$, the expectation value of an operator $\hat{\mathcal{O}}[\phi]$ is formally given by

$$\langle\hat{\mathcal{O}}\rangle = \frac{1}{\mathcal{Z}}\int \mathcal{D}[\phi]\, e^{iS[\phi]}\,\hat{\mathcal{O}}[\phi]\,, \qquad \mathcal{Z} \equiv \int \mathcal{D}[\phi]\, e^{iS[\phi]}\,, \tag{1.40}$$

in the path integral formulation, where $\mathcal{Z}$ is the partition function and $S[\phi]$ denotes the action of the theory. In practice, there is no reason to expect that these integrals should be well-defined since the integration is performed over an infinite number of degrees of freedom.

Even if the path integrals were rigorously defined from the start, their numerical evaluation is not necessarily straightforward. Firstly, the oscillatory behaviour of the complex exponential factor $e^{iS[\phi]}$ will lead to a sign problem when performing numerical integration. To avoid this, we work instead in a *Euclidean spacetime*, reached from usual Minkowski spacetime by a *Wick rotation* of the time coordinate $t \to -it$. This transformation effectively replaces the Minkowski metric with a Euclidean metric, $\eta_{\mu\nu} \to -\delta_{\mu\nu}$. As a result, the expressions of eq. (1.40) can be written in terms of a real *Euclidean action* $S^E[\phi]$:

$$\langle \hat{\mathcal{O}} \rangle = \frac{1}{\mathcal{Z}} \int \mathcal{D}[\phi]\, e^{-S^E[\phi]}\, \hat{\mathcal{O}}[\phi]\,, \qquad \mathcal{Z} \equiv \int \mathcal{D}[\phi]\, e^{-S^E[\phi]}\,. \tag{1.41}$$

Crucially, the factor $e^{-S^E[\phi]}/\mathcal{Z}$ can be interpreted as a probability density on the space of field configurations.

This probabilistic view of the path integral suggests the following computational strategy: by sampling a large number N of field configurations ϕ_i $(i = 1, ..., N)$ according to this probability distribution using Monte-Carlo techniques, one can approximate the expectation value of eq. (1.41) by averaging over the ϕ_i:

$$\langle \hat{\mathcal{O}} \rangle \approx \frac{1}{N} \sum_{i=1}^{N} \hat{\mathcal{O}}[\phi_i] + \mathcal{O}\left(\frac{1}{\sqrt{N}}\right)\,, \tag{1.42}$$

which converges to the exact value as $N \to \infty$ with a $\mathcal{O}\left(\frac{1}{\sqrt{N}}\right)$ statistical error. Naturally, it is impossible to sample field configurations which take a value at every point of an infinite continuous spacetime. To make this possible in practice, we need to discretise and truncate spacetime, thus making the number of degrees of freedom finite.

As mentioned already, in lattice QCD (and lattice field theory more generally), we discretise Euclidean spacetime into a four-dimensional lattice of points $a\mathbb{Z}^4$. The points are called the *lattice sites* and a is called the *lattice spacing*. We further truncate this infinite four-dimensional grid to have finite temporal extent

T and spatial extent L, corresponding to T/a and L/a sites along these directions, respectively. Anisotropic lattices in which the three spatial directions have different extents or where the lattice spacing differs between temporal and spatial directions can also be considered, but we will not discuss these in the following. In a finite lattice, we need also to impose boundary conditions. Although other choices are possible, we consider only the case of periodic boundary conditions here.

The above procedure naturally regulates the theory. Discretisation creates an ultraviolet (UV) cutoff by restricting momentum components to the interval $(-\frac{\pi}{a}, +\frac{\pi}{a}]$, a restriction which is lifted in the *continuum limit* $a \to 0$. Truncation, in turn, compactifies spacetime and regulates the infrared (IR) physics, discretising the momentum components to integer multiples of $2\pi/L$ and $2\pi/T$ in the spatial and temporal directions, respectively.

We need a version of QCD, in the form of a discretised action, that can be implemented in this spacetime geometry and reproduces the continuum QCD action in the continuum limit. The choice of a lattice action is not unique, as different choices can lead to the same continuum limit. Therefore, one typically picks an option that has some advantages over the alternatives, such as faster convergence to the continuum or lower computational complexity.

1.3.1 Discretisation of the QCD action

Before discussing QCD, let us look first at the simpler case of free real scalars. In the continuum, the Euclidean action for the real scalar field $\phi(x)$ is given by

$$S_{s,\,\mathrm{cont.}}[\phi] = \int d^4x \, \frac{1}{2}\left(\sum_{\mu=0}^{3} \left(\partial_\mu \phi(x)\right)^2 + m^2 \phi(x)^2 \right). \tag{1.43}$$

To construct the lattice action, we need to find suitable discretised replacements for the integral and derivatives above. The derivatives are discretised using *forward* and *backward finite differences*:

$$\delta_\mu \phi(x) \equiv \frac{\phi(x + a\hat{\mu}) - \phi(x)}{a} = \partial_\mu \phi(x) + \frac{1}{2} a\, \partial_\mu^2 \phi(x) + \mathcal{O}(a^2)\,, \tag{1.44}$$

$$\delta_\mu^* \phi(x) \equiv \frac{\phi(x) - \phi(x - a\hat{\mu})}{a} = \partial_\mu \phi(x) - \frac{1}{2} a\, \partial_\mu^2 \phi(x) + \mathcal{O}(a^2)\,, \tag{1.45}$$

where the $\hat{\mu}$ denotes a unit vector in the μ direction. The second equalities in each line follow from expanding about the continuum limit $a \to 0$, showing that these finite differences do indeed converge to the continuum derivative but carry $\mathcal{O}(a)$ discretisation effects. Often, it is more desirable to use instead a symmetric combination $\bar{\delta}_\mu \equiv \frac{1}{2}(\delta_\mu + \delta_\mu^*)$, as this leads to $\mathcal{O}(a^2)$ effects and, therefore, to faster convergence to the continuum result. Second derivatives can be constructed the finite differences above, a usual choice being the combination

$$\delta_\mu \delta_\mu^* \phi(x) = \frac{\phi(x + a\hat{\mu}) - 2\phi(x) + \phi(x - a\hat{\mu})}{a^2}\,, \tag{1.46}$$

which converges to the continuum result as $\mathcal{O}(a^2)$. Note that the repeated indices here are not summed. The integration over spacetime may be replaced with a Riemann sum:

$$\int d^4x \;\longrightarrow\; a^4 \sum_x\,, \tag{1.47}$$

which runs over all lattice sites x and should converge to the integral as $a \to 0$.

Given these ingredients, a natural choice of lattice action for the scalar field is

$$S_s[\phi] = a^4 \sum_x \left(\frac{1}{2} \sum_{\mu=0}^{4} \left(\delta_\mu \phi(x)\right)^2 + \frac{1}{2} m^2 \phi(x)^2 \right)\,, \tag{1.48}$$

which can be shown to be equivalent to

$$S_s[\phi] = a^4 \sum_x \frac{1}{2}\, \phi(x) \left(-\delta^2 + m^2\right) \phi(x)\,, \tag{1.49}$$

where $\delta^2 \equiv \sum_\mu \delta_\mu \delta_\mu^*$ is a discrete Laplacian operator. The two-point function in the free theory $\langle \phi(x)\phi(y)\rangle_0$ can be obtained from this action by diagonalising the operator $(-\delta^2 + m^2)$ in momentum space, from which we obtain

$$\langle \phi(x)\phi(y)\rangle_0 = \int_{-\frac{\pi}{a}}^{\frac{\pi}{a}} \frac{d^4k}{(2\pi)^4} \frac{e^{ik\cdot(x-y)}}{\hat{k}^2 + m^2}\,, \tag{1.50}$$

where the integral runs over the first Brillouin zone $k^\mu \in (-\frac{\pi}{a}, \frac{\pi}{a}]$ and

$$\hat{k}_\mu \equiv \frac{2}{a} \sin\left(\frac{a}{2} k_\mu\right)\,, \qquad \hat{k}^2 = \sum_\mu \hat{k}_\mu^2\,. \tag{1.51}$$

It is easy to see that the familiar result for the free propagator in the continuum

theory is obtained when we take $a \to 0$. The factor $\left(\hat{k}^2 + m^2\right)^{-1}$ here is simply the momentum-space propagator, whose poles correspond to the one-particle states of the theory. For three-momenta $\boldsymbol{k}$, we can find two poles in k_0 with a real part within the first Brillouin zone:

$$k_0 = \pm i\omega(\boldsymbol{k})\,, \qquad \text{with} \quad \omega(\boldsymbol{k}) \equiv \frac{2}{a}\sinh^{-1}\left(\frac{a}{2}\sqrt{\hat{\boldsymbol{k}}^2 + m^2}\right)\,, \tag{1.52}$$

where $\omega(\boldsymbol{k})$ is the single-particle energy. An expansion in the lattice spacing then shows that the usual dispersion relation is recovered in the continuum limit:

$$\omega(\boldsymbol{k}) = \sqrt{\boldsymbol{k}^2 + m^2} + \mathcal{O}(a^2)\,. \tag{1.53}$$

Given the above result for the free propagator, n-point functions can constructed using Wick's theorem, as done in the continuum theory.

Let us move on now to the less straightforward discretisation of fermions. The continuum Dirac action is

$$S_{f,\,\text{cont.}}[\psi, \bar{\psi}] = \int d^4x\ \bar{\psi}(x)(\partial\!\!\!/ + m)\psi(x)\,, \tag{1.54}$$

with $\partial\!\!\!/ \equiv \sum_\mu \gamma_\mu \partial_\mu$. The naïve approach to discretising this action is to simply replace the integral and derivative with discretised alternatives, as done for the scalar case above:

$$S_{f,\,\text{naïve}}[\psi, \bar{\psi}] = a^4 \sum_x \bar{\psi}(x)(\bar{\partial\!\!\!/} + m)\psi(x)\,. \tag{1.55}$$

Here $\bar{\partial\!\!\!/} \equiv \sum_\mu \gamma_\mu \bar{\delta}_\mu$ and $\bar{\delta}_\mu$ is the symmetric finite difference operator introduced above. The Dirac operator $D \equiv (\bar{\partial\!\!\!/} + m)$ can be diagonalised in momentum space to obtain the two-point function

$$\langle \psi(x)\bar{\psi}(y)\rangle_0 = \int_{-\frac{\pi}{a}}^{\frac{\pi}{a}} \frac{d^4k}{(2\pi)^4}\ e^{ik\cdot(x-y)}\,\frac{-i\bar{k}\!\!\!/ + m}{\bar{k}^2 + m^2}\,, \tag{1.56}$$

with

$$\bar{k}_\mu \equiv \frac{1}{a}\sin\left(ak_\mu\right)\,, \qquad \bar{k}\!\!\!/ \equiv \sum_\mu \gamma_\mu \bar{k}_\mu\,. \tag{1.57}$$

Again, the correct continuum result for the Dirac propagator is retrieved as $a \to 0$. However, there is an important difference relative to the scalar case, which arises

due to the different periodicity of the momentum function $\bar{k}_\mu$ (cf. $\hat{k}_\mu$ in the scalar case). For fixed three-momentum $\boldsymbol{k}$, instead of finding the expected two (fermion and antifermion) poles in k_0, we now find four:

$$k_0 = \pm i\omega(\boldsymbol{k}),\, \pm i\omega(\boldsymbol{k}) + \frac{\pi}{a}\,, \tag{1.58}$$

where

$$\omega(\boldsymbol{k}) \equiv \frac{1}{a}\sinh^{-1}\left(a\sqrt{\bar{\boldsymbol{k}}^2 + m^2}\right)\,. \tag{1.59}$$

Adding a shift of $\pm\pi/a$ to $\boldsymbol{k}$ in any of the spatial directions yields the same value of the energy $\omega(\boldsymbol{k})$. This doubles the number of poles within the Brioullin zone for each spatial direction, resulting in a total of 32 propagator poles. The naïve discretised action of eq. (1.55) thus describes 16 mass-degenerate fermions, instead of the single fermion of the continuum Dirac action of eq. (1.54). The issue does not go away in the continuum limit because, while the extra poles in k_0 move away from the origin as $a \to 0$, the extra states remain coupled. This predicament is known as *fermion doubling*, as the number of fermions is doubled for each dimension of Euclidean spacetime.

An early proposal to avoid the presence of doublers was due to Wilson [61], who suggested adding an extra term to the naïve fermion action:

$$S_f[\psi,\bar{\psi}] \equiv S_{f,\,\text{naïve}}[\psi,\bar{\psi}] - \frac{a^5}{2}\sum_x \bar{\psi}(x)\delta^2\psi(x)\,, \tag{1.60}$$

now called the *Wilson term*. This results in a modified two-point function, which reads

$$\langle\psi(x)\bar{\psi}(y)\rangle_0 = \int_{-\frac{\pi}{a}}^{\frac{\pi}{a}} \frac{d^4k}{(2\pi)^4}\; e^{ik\cdot(x-y)}\,\frac{-i\bar{\not{k}} + m + \frac{a}{2}\hat{k}^2}{\bar{k}^2 + (m + \frac{a}{2}\hat{k}^2)^2}\,, \tag{1.61}$$

with $\bar{k}_\mu$ and $\hat{k}_\mu$ as defined above. The additional terms give the fermions an effective momentum-dependent mass

$$\widetilde{m}(k) \equiv m + \frac{a}{2}\hat{k}^2 = m + \frac{1}{a}\sum_\mu \left[1 - \cos(ak_\mu)\right]\,. \tag{1.62}$$

The extra contribution yields the correct continuum limit for a pole near the origin but diverges as $\mathcal{O}(a^{-1})$ for a pole near the edge of the Brillouin zone. This results in the doublers acquiring an infinite mass as $a \to 0$ and decoupling from the theory, while the two poles near the origin remain, as required. Although this proposal solves

the issue of doubling, it does so by introducing a term which explicitly violates chiral symmetry. As a consequence, the action now receives $\mathcal{O}(a)$ discretisation effects, as opposed to the $\mathcal{O}(a^2)$ effects of the naïve action. The fermion masses will now also require an additive renormalisation on top of multiplicative renormalisation.

The relation between fermion doubling and chiral symmetry is clarified by the result known as the *Nielsen-Ninomiya no-go theorem* [62, 63]. It tells us the following four properties cannot be satisfied simultaneously: (i) locality of the action, (ii) correct continuum limit, (iii) absence of doublers, and (iv) chiral symmetry respected. Arguably, all of these are desirable in a discretised action, but we are forced to sacrifice at least one of them when placing fermions on the lattice. The naïve action of eq. (1.55), one gives up (iii) and keeps the remaining properties. In the action of eq. (1.60), including Wilson's term sacrifices (iv) instead, keeping (i)-(iii).

Over the years, a few creative strategies have been devised to circumvent some of the limitations imposed by the Nielsen-Ninomiya theorem. *Staggered fermions* [64], for example, sacrifice locality to reduce the number of doublers. Others, such as *overlap fermions* [65], violate chiral symmetry explicitly but recover it in the continuum limit.

Let us now move on to the discretisation of the gauge fields. As seen in section 1.1.2, these are usually described by the vector field $A_\mu(x)$, valued in the Lie algebra of the gauge group. In Wilson's formulation of lattice gauge theory [61], one instead employs fields $U_\mu(x)$ valued in the gauge group itself. These are called *gauge links* and are defined as

$$U_\mu(x) \equiv e^{iagA_\mu(x)}\,, \tag{1.63}$$

where g is the coupling. Because the links are valued in a compact space, unlike the fields $A_\mu(x)$, gauge fixing is not necessary to remove the redundant degrees of freedom originating from the gauge symmetry.

In contrast to the scalar and fermion fields considered so far, which live at the lattice sites, the links are assigned to the grid lines connecting adjacent sites. More concretely, $U_\mu(x)$ corresponds to the line going from x to $x + a\hat{\mu}$, with $\hat{\mu}$ again denoting the unit vector in the μ direction. Its conjugate $U_\mu(x)^\dagger$ simply goes in the opposite direction, from $x + a\hat{\mu}$ to x.

Under a gauge transformation $\Omega(x)$, the field $U_\mu(x)$ transforms as

$$U_\mu(x) \to \Omega(x) U_\mu(x) \Omega(x + a\hat{\mu})^\dagger\,. \tag{1.64}$$

To build an action for the gauge fields, we need to find a combination of links that is gauge invariant. The simplest non-trivial gauge-invariant combination is the trace of the *plaquette* $U_{\mu\nu}(x)$, the smallest closed loop one can construct using the gauge links:

$$U_{\mu\nu}(x) \equiv U_\mu(x) U_\nu(x + a\hat{\mu}) U_\mu(x + a\hat{\nu})^\dagger U_\nu(x)^\dagger \,. \tag{1.65}$$

The Wilson formulation of the gauge action sums over the traces of all possible plaquettes:

$$S_g[U] = \frac{\beta}{N_c} \sum_x \sum_{\mu>\nu} \mathrm{Re}\,\mathrm{Tr}\left[1 - U_{\mu\nu}(x)\right] \,, \tag{1.66}$$

where β is a coupling constant and N_c is the number of colors (i.e. the degree of the gauge group $\mathrm{SU}(N_c)$). Setting $\beta = 2N_c/g^2$ and expanding in a, we can in fact recover the pure Yang-Mills Lagrangian of eq. (1.7) with $\mathcal{O}(a^2)$ effects.

Fermions $\psi(x)$ in the fundamental representation transform as $\psi(x) \to \Omega(x)\psi(x)$. Their coupling to the gauge links can be achieved through covariant versions of the forward and backward finite differences:

$$\Delta_\mu \psi(x) \equiv \frac{1}{a}\left[U_\mu(x)\psi(x + a\hat{\mu}) - \psi(x)\right] \,, \tag{1.67}$$

$$\Delta^*_\mu \psi(x) \equiv \frac{1}{a}\left[\psi(x) - U_\mu(x - a\hat{\mu})^\dagger \psi(x - a\hat{\mu})\right] \,, \tag{1.68}$$

which play the role of the covariant derivative in the continuum. A central difference is again obtained via the symmetric combination $\frac{1}{2}(\Delta_\mu + \Delta^*_\mu)$.

The Wilson formulation [61] of the full lattice QCD action in terms of $\mathrm{SU}(3)_c$ gauge links $U_\mu(x)$ and quark fields $q(x)$ is given by

$$S_{\mathrm{QCD}}[U, q, \bar{q}] = S_g[U] + a^4 \sum_x \bar{q}(x) D\, q(x) \,. \tag{1.69}$$

The first term is the plaquette action given in (1.66) and the second term is the discretised Dirac action with Wilson fermions (1.60), including also the coupling to the gauge fields. The quark fields $q(x)$ have been written as column vectors in flavor space and the Dirac operator D is defined as

$$D \equiv \sum_\mu \left(\gamma_\mu \frac{\Delta_\mu + \Delta^*_\mu}{2} - \frac{a}{2}\Delta_\mu \Delta^*_\mu\right) + M \,. \tag{1.70}$$

The second term corresponds to Wilson's term and $M \equiv \mathrm{diag}(m_u, m_d, m_s)$ is the

quark mass matrix.

As already discussed, this action breaks chiral symmetry and suffers from $\mathcal{O}(a)$ discretisation effects. Since the work of Wilson, considerable work has since been put into reducing these effects, through the so-called Symanzik improvement programme [66–69], leading to $\mathcal{O}(a)$-improved actions such as the Wilson-clover action.

1.3.2 Monte-Carlo estimation of the path integral

With an appropriate discretised lattice QCD action, we can write operator expectation values using the Euclidean path integral

$$\langle \hat{\mathcal{O}} \rangle = \frac{1}{\mathcal{Z}} \int \mathcal{D}[U, q, \bar{q}] \; e^{-S_{\mathrm{QCD}}[U,q,\bar{q}]} \, \hat{\mathcal{O}}[U, q, \bar{q}] \,, \tag{1.71}$$

with partition function

$$\mathcal{Z} \equiv \int \mathcal{D}[U, q, \bar{q}] \; e^{-S_{\mathrm{QCD}}[U,q,\bar{q}]} \,. \tag{1.72}$$

The fermion action is bilinear in the fermion fields and we can perform the integration over the quark fields analytically, leading to the following expression for the partition function:

$$\mathcal{Z} = \int \mathcal{D}U \; e^{-S_g[U]} \det D[U] \,, \tag{1.73}$$

where $D[U]$ is the matrix form of the Dirac operator in position space. For the path integral itself, we can use Wick's theorem to obtain

$$\langle \hat{\mathcal{O}} \rangle = \frac{1}{\mathcal{Z}} \int \mathcal{D}U \; e^{-S_g[U]} \det D[U] \, \hat{\mathcal{O}}_{\mathrm{Wick}}[U] \,. \tag{1.74}$$

Here, $\hat{\mathcal{O}}_{\mathrm{Wick}}[U]$ is derived from $\hat{\mathcal{O}}[U, q, \bar{q}]$ by performing the Wick contractions of the quark fields, with each $\bar{q}q$ contraction being replaced by the quark "propagator" $D[U]^{-1}$. This simplification helpfully removes the fermionic fields, which are Grassmann variables and would complicate the numerical integration process further.

The functional $\frac{1}{\mathcal{Z}} e^{-S_g[U]} \det D[U]$ can then be interpreted as the probability density on the space of gauge field configurations, allowing the estimation of the path integral

using Monte Carlo importance sampling. If we draw N configurations $U_\mu^{(i)}$ according to this probability distribution, we have

$$\langle \hat{\mathcal{O}} \rangle \approx \frac{1}{N} \sum_{i=1}^{N} \hat{\mathcal{O}}_{\text{Wick}} \left[U^{(i)} \right] + \mathcal{O}\left(\frac{1}{\sqrt{N}} \right) . \tag{1.75}$$

In modern lattice calculations, the generation of gauge field configurations is done through the *Hybrid Monte Carlo* algorithm [70]. This method creates a sequence of configurations via an ergodic Markov chain, whose distribution converges to the target distribution above. To generate the next configuration in the sequence, the gauge field is evolved using the molecular dynamics (MD) algorithm, with the result being accepted into the sequence or rejected by a Metropolis step.

For a gauge field configuration U_μ, the Dirac matrix $D[U]$ is very large and often quite ill-conditioned for physical light quark masses. This, of course, makes the evaluation of the determinant $\det D[U]$ and the inversions necessary to calculate $\hat{\mathcal{O}}_{\text{Wick}}[U]$ computationally intensive. In the first few decades of the development of lattice QCD, calculations were only possible using heavier-than-physical quarks and by making drastic approximations, such as the *quenched approximation*, where $\det D[U]$ is set to unity and all sea quark effects are ignored. Remarkable improvements in algorithms and supercomputing over the last decades have gradually lifted these restrictions and many calculations are now performed at physical quark masses and using dynamical (unquenched) quarks.

1.3.3 Euclidean correlation functions

The framework outlined above allows us to evaluate Euclidean correlation functions, which contain all physical information of the theory. We focus now on quantities that are typically extracted in lattice calculations, namely masses and finite-volume energies, leaving the issue of their interpretation and the impact of discretisation and finite-volume effects to the following subsection.

Let us start by considering a two-point function of the form

$$C(t, \boldsymbol{P}) \equiv a^3 \sum_{\boldsymbol{x}} e^{-i\boldsymbol{P}\cdot\boldsymbol{x}} \langle \hat{\mathcal{A}}(x) \hat{\mathcal{A}}(0)^\dagger \rangle \, , \tag{1.76}$$

which has been projected to total spatial momentum $\boldsymbol{P}$ through a discrete Fourier transform. Here, $\hat{\mathcal{A}}(x)$ is an operator made up of elementary fields, t is Euclidean time and the sum is performed over all lattice sites $\boldsymbol{x}$ at time slice t.

For the moment, suppose that the temporal extent of the lattice is large $T \to \infty$. By inserting a complete set of Hamiltonian eigenstates, we can derive a spectral representation for this correlator:

$$C(t, \boldsymbol{P}) = L^3 \sum_n \left|\langle 0|\hat{\mathcal{A}}(0)|n\rangle\right|^2 e^{-E_n t}\,, \tag{1.77}$$

where $|n\rangle$ denotes the n-th eigenstate, with corresponding energy eigenvalue E_n and normalisation $\langle n'|n\rangle = \delta_{nn'}$. For large Euclidean time $t \gg 0$, the lowest-lying state with the same quantum numbers as $\hat{\mathcal{A}}$ (the ground state) will dominate the sum:

$$C(t, \boldsymbol{P}) \xrightarrow{t\gg 0} L^3 \left|\langle 0|\hat{\mathcal{A}}(0)|n_0\rangle\right|^2 e^{-E_{n_0} t}\,, \tag{1.78}$$

where n_0 labels the ground state and E_{n_0} is its energy.

Choosing an appropriate operator $\hat{\mathcal{A}}$ and taking zero spatial momentum $\boldsymbol{P} = \boldsymbol{0}$, the ground state energy simply reduces to the mass of the lightest hadron with the given quantum numbers, which can then be extracted by performing a fit of the lattice correlator data. For a concrete example, consider the operator $\hat{\pi}^+(x) \equiv \bar{d}(x)\gamma_5 u(x)$. As the notation suggests, this has the quantum numbers of a positive pion (charge $Q = +1$, isospin $I = 1$ with component $I_3 = +1$, parity $P = -1$ and angular momentum $J = 0$) and a pion at rest $|\pi^+, \boldsymbol{0}\rangle$ is the lightest hadron coupling to this operator. Following the discussion above, we get

$$C_{\pi^+}(t, \boldsymbol{0}) \equiv a^3 \sum_{\boldsymbol{x}} \langle \hat{\pi}^+(x)\hat{\pi}^+(0)^\dagger\rangle \xrightarrow{t\gg 0} L^3 \left|\langle 0|\hat{\pi}^+(0)|\pi^+, \boldsymbol{0}\rangle\right|^2 e^{-M_\pi t}\,. \tag{1.79}$$

In an actual lattice calculation, one must consider a finite temporal extent T with periodic boundary conditions. This generates extra contributions arising from particles propagating backwards in time. To reflect this, the spectral representation (1.77) is changed to

$$C(t, \boldsymbol{P}) = L^3 \frac{1}{Z_T} \sum_{m,n} \left|\langle m|\hat{\mathcal{A}}(0)|n\rangle\right|^2 e^{-E_m(T-t)} e^{-E_n t}\,, \tag{1.80}$$

with $Z_T \equiv \sum_n e^{-E_n T}$. At zero spatial momentum and away from the lattice boundaries $0 \ll t \ll T$, the leading contributions now come the forward- and backward-propagating ground states. For the case of the pion two-point function in eq. (1.79), the result now becomes

$$C_{\pi^+}(t, \mathbf{0}) \xrightarrow{0 \ll t \ll T} L^3 \left| \langle 0 | \hat{\pi}^+(0) | \pi^+, \mathbf{0} \rangle \right|^2 \left(e^{-M_\pi t} + e^{-M_\pi (T-t)} \right) . \tag{1.81}$$

The pion mass can then be extracted from a fit of the lattice correlator data using the two-parameter exponential model $A \left(e^{-M_\pi t} + e^{-M_\pi (T-t)} \right)$ (or an equivalent cosh model).

The procedure sketched out above works fine if one is only interested in extracting the masses and ground state energies for particular quantum numbers. To extract also excited state energies, one could potentially attempt to fit the correlator data to a sum of several exponentials, seeking to capture the sub-leading fall-off of the lowest-lying excited states. However, the uncertainty in lattice data makes this unworkable and we must look for more reliable alternatives.

A popular approach in the literature uses a method of *variational analysis* [71, 72]. By choosing an operator basis $\{\hat{\mathcal{A}}_1, ..., \hat{\mathcal{A}}_N\}$, where all operators have the desired quantum numbers, one can construct a matrix $C(t, \boldsymbol{P})$ of correlators with elements

$$C_{ij}(t) \equiv a^3 \sum_{\boldsymbol{x}} e^{-i \boldsymbol{P} \cdot \boldsymbol{x}} \langle \hat{\mathcal{A}}_i(x) \hat{\mathcal{A}}_j(0)^\dagger \rangle \, , \tag{1.82}$$

$$= L^3 \sum_n \langle 0 | \hat{\mathcal{A}}_i(0) | n \rangle \langle n | \hat{\mathcal{A}}_j(0)^\dagger | 0 \rangle e^{-E_n t} \, . \tag{1.83}$$

The second line here follows from a spectral decomposition (assuming large T), as done above. Provided that the basis operators have different overlaps with each of the spectrum states $|n\rangle$, it can be shown that certain linear combinations of operators $\sum_i v_i^{(n)} \hat{\mathcal{A}}_i$ target each particular state $|n\rangle$ optimally, disentangling it, as much as possible, from the rest. The corresponding weights $v_i^{(n)}$ can, in fact, be obtained by solving the *generalised eigenvalue problem* (GEVP) equation [71]

$$C(t) \, v^{(n)}(t, t_0) = \lambda^{(n)}(t, t_0) \, C(t_0) \, v^{(n)}(t, t_0) \, , \tag{1.84}$$

where $\lambda^{(n)}(t, t_0)$ is the corresponding eigenvalue and $t_0 < t$ is a reference Euclidean time, chosen such that the contributions from higher excited states are suppressed and we pick up only the N lowest states. We can show that the eigenvalues have

$\lambda^{(n)}(t, t_0) \sim e^{-E_n(t-t_0)}$, from which we can extract the energy levels E_n.

We should note that the operators discussed in this subsection are not directly used in the the Monte-Carlo estimation of the path integral, as we first need to Wick-contract the quark fields. Looking again at the example of the pion operator $\hat{\pi}^+(x) = \bar{d}(x)\gamma_5 u(x)$, we would have

$$\hat{\mathcal{O}} = \hat{\pi}^+(x)\hat{\pi}^+(0)^\dagger = \bar{d}(x)\gamma_5 u(x)\bar{u}(0)\gamma_5 d(0)\,, \tag{1.85}$$

$$\longrightarrow \quad \hat{\mathcal{O}}_{\text{Wick}} = \text{Tr}\left[\gamma_5 S_u(x,0)\gamma_5 S_d(0,x)\right]\,, \tag{1.86}$$

where the trace is over the spinor and color indices and $S_f(x, y)$ is the quark propagator (i.e. the inverted Dirac operator) for flavor f. One would then use $\hat{\mathcal{O}}_{\text{Wick}}$ in the evaluation of the path integral. Since the quark propagators depend on the gauge fields, they need to be recomputed for each gauge configuration.

1.3.4 Recovering physical observables

As mentioned, working in a finite-volume, discretised spacetime affects observables obtained from lattice QCD calculations. Thus, we should not expect quantities computed on the lattice, such as masses and energy levels, to correspond to their infinite-volume and continuum values. Historically, calculations were mostly performed at heavier-than-physical quark masses, making it also necessary to extrapolate down to physical masses. However, most major collaborations now use physical masses in their calculations, so that this extrapolation is no longer needed.

Discretisation effects are generally addressed by repeating a calculation at multiple values of lattice spacing, allowing an extrapolation to the continuum limit to be performed. A similar strategy applies to the extrapolation to physical quark masses, guided and constrained by analytic χPT relations.

For finite-volume effects, we must rely on an analytic understanding of of how lattice observables depend on the volume. Regarding particle masses, it can be shown (as originally done by M. Lüscher [3] in the case of massive scalars) that a particle placed in a finite volume receives exponentially suppressed corrections to its infinite-volume mass. These decay exponentially with the volume at a rate determined by the mass of the lightest particle in the theory – corresponding to the pion in QCD. As a result, one can mostly avoid these effects by choosing a large enough lattice extent:

$T, L \gg M_\pi^{-1}$. Qualitatively, this can be understood by noting that, in a smaller lattice, particles may interact with themselves across the periodic boundary via pion exchanges, an effect that is attenuated in a larger volume.

Some observables, however, remain inaccessible directly on the lattice due to the use of a Euclidean metric. Lattice correlators, which are functions of Euclidean time, must be analytically continued in order to recover Minkowski correlators. Since lattice results are available only at discrete lattice sites and carry uncertainties, this is a highly challenging task. Consequently, direct computation of scattering amplitudes and other scattering parameters – generally obtained from Minkowski correlation functions through the LSZ formalism [73] – has not been possible in practice. The development of the Lüscher scattering formalism and its modern extensions has provided a way to circumvent this limitation by making use of the finite-volume spectrum. A full description of this method will be the given in the next chapter. It should also be pointed out that recent theoretical advances may make the direct extraction of scattering information from lattice correlators viable and this is very much an active area of research [74–78].

Chapter 2

Two-particle scattering from a finite volume

The study of scattering processes plays an essential role in particle physics, enabling the determination of particle properties and the investigation of their interactions. This is particularly relevant in hadronic physics, as only the lightest hadrons are stable under the strong interaction. Most hadronic states appear instead as short-lived resonances, observable only as peaks in the cross-sections of scattering of light hadrons.

Because lattice QCD is the only known method for performing systematically improvable *ab-initio* calculations of low-energy hadronic observables, it is of great importance to have a theoretical framework in place that allows the extraction of scattering observables from lattice-determined quantities. As discussed in the previous chapter, this is a challenging problem because of the Euclidean nature of the lattice correlation functions, which hinders any direct calculations of amplitudes. Even if possible to circumvent the sign problem and work directly with a Minkowski spacetime, it would be impossible to define asymptotically free states due to boundary effects, forbidding the use of standard infinite-volume scattering theory.

The key development came in the 1980s when M. Lüscher first derived a mathematical relation between the energy levels of a two-particle system in a finite volume and the corresponding two-particle elastic scattering amplitude in infinite volume, for the case of massive scalars. This result, known as the *Lüscher quantisation condition*, has since been generalised to increasingly complex systems, including

moving frames, particles with arbitrary spin, coupled-channel scattering [4–14, 79] and, more recently, three-particle scattering [20, 21, 80–113].

The finite-volume energy spectrum, which is discretised due to the periodic boundary conditions, can be obtained on the lattice via the method outlined in section 1.3.3. The quantisation condition constrains the value of the scattering amplitude at the given finite-volume energies, allowing a fit to be performed.

In this chapter, we begin by discussing some fundamental concepts of infinite-volume scattering theory, followed by a short derivation of Lüscher's quantisation condition and practical considerations regarding its application. We take the opportunity to introduce the notation used in the next chapters, closely following that of [2].

2.1 Infinite-volume scattering

The central object of interest is the *scattering matrix* or *S-matrix*, an operator that connects the initial and final states in a scattering event. More concretely, consider an n-particle initial state $|p_1, p_2, ..., p_n; \text{in}\rangle$, with the p_i denoting the particle momenta, and an n'-particle final state $|p'_1, p'_2, ..., p'_n; \text{out}\rangle$. These are defined as asymptotically free states infinitely far in the past ($t = -\infty$) and the future ($t = +\infty$) respectively. The S-matrix is defined such that its matrix elements

$$S_{fi} = \langle p'_1, p'_2, ..., p'_n; \text{out}| \, \hat{S} \, |p_1, p_2, ..., p_n; \text{in}\rangle \tag{2.1}$$

give the probability amplitude for the transition between the given initial and final states. To ensure the conservation of probability, $\hat{S}$ must be unitary: $\hat{S}\hat{S}^\dagger = 1$.

The S-matrix can be decomposed into a non-interacting contribution, given by the identity operator, and an interacting term given in terms of a *scattering amplitude* $\mathcal{M}$:

$$S_{fi} = \delta_{fi} + (2\pi)^4 \, \delta^4(P_f - P_i) \, i\mathcal{M}_{fi} \, , \tag{2.2}$$

where the delta function in the second term ensures the conservation of total four-momentum $P_i = P_f$. The amplitude $\mathcal{M}$ contains all physical information of the theory and is the quantity we are usually interested in calculating. Through it, we can then compute scattering cross-sections and decay rates.

Let us focus now specifically on elastic scattering of two spinless particles ϕ_1 and ϕ_2, with physical masses M_1 and M_2, respectively. We label the incoming and outgoing ϕ_1 momenta $p = (p^0, \boldsymbol{p})$ and $p' = (p'^0, \boldsymbol{p}')$, respectively. Given a total four-momentum $P = (E, \boldsymbol{P})$, the incoming and outgoing ϕ_2 momenta are simply $P - p$ and $P - p'$. The amplitude $\mathcal{M}(P, p, p')$ for the process $\phi_1\phi_2 \to \phi_1\phi_2$ can alternatively be written in terms of the *Mandelstam variables*

$$s \equiv P^2 = E^2 - \boldsymbol{P}^2 \,, \tag{2.3}$$

$$t \equiv (p' - p)^2 \,, \tag{2.4}$$

$$u \equiv (P - p' - p)^2 \,, \tag{2.5}$$

which are Lorentz invariant.

The physical amplitude has all momentum arguments on their mass shell, that is $p^2 = p'^2 = M_1^2$ and $(P - p)^2 = (P - p')^2 = M_2^2$. Combined, these equations yield the two-particle on-shell condition $E = \omega_1(\boldsymbol{p}) + \omega_2(\boldsymbol{P} - \boldsymbol{p})$ or, equivalently, $\sqrt{s} = \omega_1(\boldsymbol{p}^\star) + \omega_2(\boldsymbol{p}^\star)$, where $\star$ labels quantities that have been boosted to the centre-of-mass (CM) frame. For example, $\boldsymbol{p}^\star$ is the spatial momentum obtained by boosting $p = (\omega_1(\boldsymbol{p}), \boldsymbol{p})$ with boost velocity $\boldsymbol{\beta} = -\boldsymbol{P}/E$:

$$\begin{pmatrix} \omega_1(\boldsymbol{p}^\star) \\ \boldsymbol{p}^\star \end{pmatrix} = \Lambda(\boldsymbol{\beta}) \begin{pmatrix} \omega_1(\boldsymbol{p}) \\ \boldsymbol{p} \end{pmatrix} \,, \tag{2.6}$$

where $\Lambda(\boldsymbol{\beta})$ is a standard Lorentz boost matrix. The same conditions hold for $\boldsymbol{p}'$. As a result of these, the magnitudes of $\boldsymbol{p}^\star$ and $\boldsymbol{p}'^\star$ are constrained to be

$$|\boldsymbol{p}^\star| = |\boldsymbol{p}'^\star| = k^\star_{\rm os} \equiv \frac{1}{2}\sqrt{s - 2(M_1^2 + M_2^2) + (M_1^2 - M_2^2)^2/s} \,, \tag{2.7}$$

where the subscript os stands for "on shell". Their directions, represented by the unit vectors $\hat{\boldsymbol{p}}^\star$ and $\hat{\boldsymbol{p}}'^\star$, remain arbitrary and can be used to define the *scattering angle* $\theta^\star$, through $\cos\theta^\star \equiv \hat{\boldsymbol{p}}^\star \cdot \hat{\boldsymbol{p}}'^\star$.

Another consequence of having all momenta on their madss shell is that $s + t + u = 2M_1^2 + 2M_2^2$, leaving only two independent Mandelstam invariants. The amplitude $\mathcal{M}$ can thus be expressed as a function of s and t (or equivalently u), or of s and the CM *scattering angle* $\theta^\star$. We can perform a partial-wave expansion to strip away the angular dependence and obtain amplitudes with definite angular momentum

quantum number ℓ:

$$\mathcal{M}(s,\theta^\star) = \sum_{\ell=0}^{\infty}(2\ell+1)P_\ell(\cos\theta^\star)\mathcal{M}^{(\ell)}(s)\,, \tag{2.8}$$

where the P_ℓ are Legendre polynomials and the $\mathcal{M}^{(\ell)}(s)$ are the *partial-wave amplitudes*. These are obtained via the integral

$$\mathcal{M}^{(\ell)}(s) \equiv \frac{1}{2}\int_{-1}^{1} d(\cos\theta^\star)P_\ell(\cos\theta^\star)\mathcal{M}(s,\theta^\star)\,. \tag{2.9}$$

From S-matrix unitarity, we can show that the partial-wave amplitudes must obey

$$\operatorname{Im}\mathcal{M}^{(\ell)}(s) = \rho(s)\,|\mathcal{M}^{(\ell)}(s)|^2 \tag{2.10}$$

in the elastic scattering regime. This is the region above the two-particle threshold at $s = (M_1 + M_2)^2$ and below the lowest-lying inelastic threshold, above which final states other than $\phi_1\phi_2$ can be produced. The *phase space factor* $\rho(s)$ is purely kinematic and is given by

$$\rho(s) \equiv \sigma\frac{k^\star_{\text{os}}}{8\pi\sqrt{s}}\,, \tag{2.11}$$

where σ is a symmetry factor, set to $1/2$ for identical scatterers ($\phi_1 = \phi_2$) and to 1 otherwise. A solution to eq. (2.10) is provided by introducing a *K-matrix*, which in effect parameterises the unconstrained real part of the partial-wave amplitudes:

$$\mathcal{M}^{(\ell)}(s) = \frac{1}{\mathcal{K}^{(\ell)}(s)^{-1} - i\rho(s)}\,. \tag{2.12}$$

Angular momentum is a good quantum number in a scattering process, meaning that the S-matrix does not mix incoming and outgoing states with different values of ℓ. For two-particle elastic scattering, the S-matrix element for each angular momentum channel takes the form $e^{2i\delta_\ell(k^\star_{\text{os}})}$ due to unitarity, where $\delta_\ell(k^\star_{\text{os}})$ is called the *scattering phase shift*. The K-matrix element $\mathcal{K}^{(\ell)}(s)$ is related to the corresponding phase shift by

$$\mathcal{K}^{(\ell)}(s)^{-1} = \sigma\frac{k^\star_{\text{os}}\cot\delta_\ell(k^\star_{\text{os}})}{8\pi\sqrt{s}}\,, \tag{2.13}$$

yielding also the well-known expressions for the partial-wave amplitudes:

$$\mathcal{M}^{(\ell)}(s) = \frac{8\pi\sqrt{s}}{2i\sigma k^\star_{\text{os}}}\left(e^{2i\delta_\ell(k^\star_{\text{os}})} - 1\right) = \frac{8\pi\sqrt{s}}{\sigma}\frac{1}{k^\star_{\text{os}}\cot\delta_\ell(k^\star_{\text{os}}) - ik^\star_{\text{os}}}\,. \tag{2.14}$$

The scattering amplitude must be an analytic function on the complex energy (or Mandelstam s) plane, aside from specified branch cuts and pole singularities. Because $\rho(s)$ includes a factor of the on-shell momentum magnitude $k^\star_{\text{os}}$ (defined in eq. (2.7)), it contains a square root cut, which is inherited by the partial-wave amplitudes $\mathcal{M}^{(\ell)}(s)$ and by the full amplitude $\mathcal{M}(s,\theta^*)$, as seen by the unitarity relation eq. (2.10). The branch point occurs at the two-particle threshold $s = (M_1 + M_2)^2$ and the cut, which we call the *two-particle* or *right-hand cut*, is typically routed along the positive real axis towards $s = +\infty$. There are two Riemann sheets, called the *physical sheet*, with $\operatorname{Im} k^\star_{\text{os}} > 0$, and the *unphysical sheet*, with $\operatorname{Im} k^\star_{\text{os}} < 0$. Elastic scattering happens on the physical sheet, just above the cut at $s + i\epsilon$ with $\epsilon \to 0^+$.

Other right-hand branch cuts appear as we analytically continue the amplitude in the complex s-plane towards higher $\operatorname{Re} s$. These lie along the real line and are associated with inelastic thresholds, signalling that these states can go on shell and propagate physically. We will not discuss these further in this work. Going in the other direction, towards lower $\operatorname{Re} s < (M_1 + M_2)^2$, we can encounter another type of branch cuts running down along the real s line, which we generically refer to as *left-hand cuts*. These are central to the work done in this thesis and will be examined in more detail in Chapters 3 and 4.

Besides branch cuts, the amplitude may also contain pole singularities. Their location in the complex-s plane is restricted by unitarity and determines their physical interpretation. Poles can occur on the real axis if below the two-particle threshold. These correspond to *bound states* if on the physical sheet, or *virtual bound states* if on the unphysical sheet. Poles can also appear off the real axis, but only on the unphysical sheet. Those on the lower half-plane usually correspond to *resonances* and are parameterised by $\sqrt{s_r} = M_r - i\Gamma_r/2$, where M_r and Γ_r are the resonance mass and width, respectively. Resonances and bound state poles are in fact interconnected: a resonance can become a (virtual) bound state and vice-versa if we modify particle masses or the strength of the interactions.

In the context of QCD, bound state poles correspond to stable hadrons, which cannot

decay because they are below the respective decay threshold. Resonances are instead unstable hadron states, which give rise to enhancements in the physical amplitude due to their proximity to the physical scattering region, just above the two-particle cut at $s + i\epsilon$ ($\epsilon \to 0^+$). Since all hadrons have specific angular momentum quantum numbers, they will couple only to the corresponding partial-wave amplitude.

For $\mathrm{Re}\, s$ higher than any potential left-hand cuts, the K-matrix elements $\mathcal{K}_\ell(s)$ are expected to be meromorphic functions of s, containing only isolated poles. Consequently, we can expand the function $k^\star_{\mathrm{os}} \cot \delta_\ell(k^\star_{\mathrm{os}})$ as a power series in $(k^\star_{\mathrm{os}})^2$ and include also potential pole contributions:

$$k^\star_{\mathrm{os}} \cot \delta_\ell(k^\star_{\mathrm{os}}) = \left[-\frac{1}{a_\ell k^{2\ell}} \left(1 + \sum_{j=1}^{\infty} c_j k^{2j} \right) + \sum_i \sum_{j=0}^{\infty} \frac{A_{i,j}\, k^j}{k^2 - C_i} \right]_{k=k^\star_{\mathrm{os}}} . \tag{2.15}$$

In the absence of the second term, this is known as an *effective range expansion* (ERE) and its truncation is frequently used to provide a practical parameterisation of the K-matrix at low momenta.

2.1.1 Bethe-Salpeter kernel and diagrammatic representations

We have so far made no assumptions regarding the field theory governing the dynamics of the spinless fields ϕ_1 and ϕ_2. Suppose now that it admits a perturbative expansion, allowing us to use the tools of Feynman diagrams. If we were considering hadrons, for example, this role could be played by an effective theory such as χPT. The $\phi_1\phi_2$ elastic scattering amplitude is given by the sum of all amputated $\phi_1\phi_2 \to \phi_1\phi_2$ diagrams.

A key ingredient for calculations using Feynman diagrams is the momentum-space dressed propagator, which takes the form

$$\Delta_{x,i\epsilon}(k) = \frac{i}{k^2 - M_x^2 - \Pi_x(k^2) + i\epsilon}\,, \tag{2.16}$$

for the two particle types $x \in \{1, 2\}$. We require the self-energy $\Pi_x(k^2)$ to satisfy $\Pi_x(M_x^2) = \Pi'_x(M_x^2) = 0$, where the prime indicates a derivative. Consequently, the residue of the single-particle pole has unit magnitude and M_x is the physical (pole) mass.

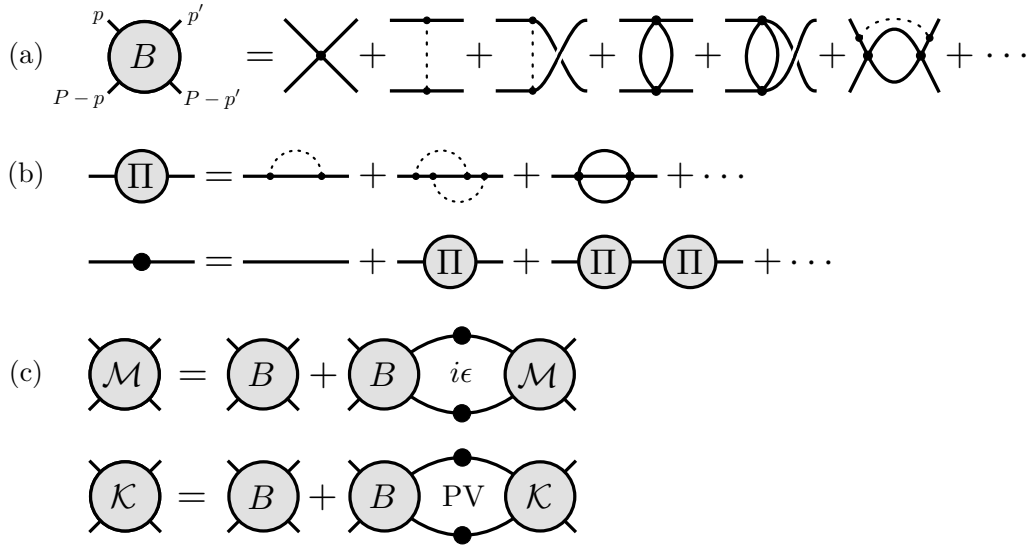

Figure 2.1 *(a) Diagrammatic representation of the Bethe-Salpeter kernel $B(P, p, p')$, built from all diagrams that are two-particle irreducible in the s-channel. This is shown here for identical particles, with the dashed lines representing exchanges of other particle types. (b) Diagrammatic representation of the self-energy $\Pi_x(p^2)$ and of the dressed propagator. (c) Representation of the infinite-volume integral equations: eqs.* (2.17) *and* (2.18) *of the main text.*

We now introduce the *Bethe-Salpeter kernel* $B(P,p,p')$, an object which will be central for the rest of this thesis. For the case of interest here, it is formally defined as the sum of all amputated $\phi_1\phi_2 \to \phi_1\phi_2$ diagrams that are two-particle irreducible with respect to cuts intersecting the flow of total energy and momentum, as shown in figure 2.1(a). The momentum labels have been assigned as in the previous section.

In terms of the fully-dressed propagator and the Bethe-Salpeter kernel, the scattering amplitude $\mathcal{M}$ and K-matrix $\mathcal{K}$ can be expressed, respectively, via the integral equations

$$\begin{aligned} i\mathcal{M}(P,p,p') &= iB(P,p,p') \\ &\quad + \sigma \int \frac{d^4k}{(2\pi)^4} iB(P,p,k)\Delta_{1,i\epsilon}(k)\Delta_{2,i\epsilon}(P-k)i\mathcal{M}(P,k,p')\,, \end{aligned} \tag{2.17}$$

$$\begin{aligned} i\mathcal{K}(P,p,p') &= iB(P,p,p') \\ &\quad + \sigma\ \mathrm{PV}\int \frac{d^3\boldsymbol{k}}{(2\pi)^3}\left[\int \frac{dk^0}{2\pi} iB(P,p,k)\Delta_{1,i\epsilon}(k)\Delta_{2,i\epsilon}(P-k)i\mathcal{K}(P,k,p')\right]_{\epsilon\to 0^+}, \end{aligned} \tag{2.18}$$

where the label PV indicates the use of a Cauchy principal value prescription and σ is the symmetry factor defined in the previous section. In eq. (2.18) the $i\epsilon$ prescription is only required to evaluate the k^0 integral, as indicated. See figure 2.1(b) for a diagrammatic representation of these equations.

We can iteratively substitute $\mathcal{M}$ and $\mathcal{K}$ onto the right-hand sides of these equations, allowing us to write a series of nested integrals in terms of Bethe-Salpeter kernels. Introducing a compact notation, this can be written as a "geometric series":

$$i\mathcal{M} = iB + iB \circ_{i\epsilon} i\mathcal{M} = \sum_{n=0}^{\infty} iB\left[\circ_{i\epsilon} iB\right]^n, \tag{2.19}$$

$$i\mathcal{K} = iB + iB \circ_{\mathrm{PV}} i\mathcal{K} = \sum_{n=0}^{\infty} iB\left[\circ_{\mathrm{PV}} iB\right]^n, \tag{2.20}$$

where the $\circ$ indicates that the quantities are combined via a loop integral, for

example:

$$iB \circ_{i\epsilon} iB = \sigma \int \frac{d^4k}{(2\pi)^4} iB(P,p,k)\Delta_{1,i\epsilon}(k)\Delta_{2,i\epsilon}(P-k)iB(P,k,p')\,, \tag{2.21}$$

$$iB \circ_{\mathrm{PV}} iB = \sigma\,\mathrm{PV}\!\int \frac{d^3\boldsymbol{k}}{(2\pi)^3}\left[\int \frac{dk^0}{2\pi} iB(P,p,k)\Delta_{1,i\epsilon}(k)\Delta_{2,i\epsilon}(P-k)iB(P,k,p')\right]_{\epsilon\to 0^+}. \tag{2.22}$$

Using the Bethe-Salpeter kernel, we can derive the form of the amplitude shown in eq. (2.12). Restricting our attention to the elastic scattering region, we can show that

$$iB \circ_{i\epsilon} iB - iB \circ_{\mathrm{PV}} iB = \sigma \int \frac{d^3\boldsymbol{k}}{(2\pi)^3} iB(P,p,k) \frac{\pi\delta(E-\omega_1(\boldsymbol{k})-\omega_2(\boldsymbol{P}-\boldsymbol{k}))}{2\omega_1(\boldsymbol{k})2\omega_2(\boldsymbol{P}-\boldsymbol{k})} iB(P,k,p')\,, \tag{2.23}$$

with $k = (\omega_1(\boldsymbol{k}), \boldsymbol{k})$. This holds because, when the k^0 integral is evaluated via contour integration, various contributions cancel between the principal-value and $i\epsilon$ integrals. In particular, contributions that are analytic in $\boldsymbol{k}$ and do not require a pole prescription will be identical between the two integrals. The exception is the contribution arising from the two-particle pole at $E = \omega_1(\boldsymbol{k}) + \omega_2(\boldsymbol{P}-\boldsymbol{k}) - i\epsilon$, for which only the imaginary part of the $i\epsilon$ contribution survives.

We can project the left-hand side of eq. (2.23) to definite angular momentum, e.g. for $iB \circ_{i\epsilon} iB$ let us define the projection as

$$\left[i\widetilde{B} \circ_{i\epsilon} i\widetilde{B}\right]_{\ell m,\ell' m'} \equiv \frac{1}{|\boldsymbol{p}^\star|^\ell |\boldsymbol{p}'^\star|^{\ell'}} \int \frac{d\Omega_{\hat{\boldsymbol{p}}^\star}}{4\pi} \int \frac{d\Omega_{\hat{\boldsymbol{p}}'^\star}}{4\pi}\, Y_{\ell m}(\hat{\boldsymbol{p}}^\star)\,(iB \circ_{i\epsilon} iB)\, Y^*_{\ell' m'}(\hat{\boldsymbol{p}}'^\star)\,, \tag{2.24}$$

where the $Y_{\ell m}$ are standard spherical harmonics and $d\Omega_{\hat{\boldsymbol{n}}}$ is the solid angle element in the direction of $\hat{\boldsymbol{n}}$. We have also divided out factors of $|\boldsymbol{p}^\star|^\ell |\boldsymbol{p}'^\star|^{\ell'}$ and use the tilde notation to indicate this rescaling. Doing so cancels out the leading-order momentum dependence, such that the projected elements approach a constant as $|\boldsymbol{p}^\star|, |\boldsymbol{p}'^\star| \to 0$. We can perform the same projection on the kernels on the right-hand side of eq. (2.23).

From this, it follows that

$$\left[i\widetilde{B} \circ_{i\epsilon} i\widetilde{B} - i\widetilde{B} \circ_{\mathrm{PV}} i\widetilde{B}\right]_{\ell m,\ell' m'} = \left[i\widetilde{B}\, \widetilde{\rho}\, i\widetilde{B}\right]_{\ell m,\ell' m'} , \tag{2.25}$$

where each of the three objects on the right-hand side is interpreted as a diagonal matrix in angular momentum index space. In particular,

$$\widetilde{\rho}_{\ell m,\ell' m'}(s) = 2\sigma\pi (k^\star_{\mathrm{os}})^{\ell+\ell'} \int \frac{d^3\boldsymbol{k}}{(2\pi)^3} Y_{\ell m}(\hat{\boldsymbol{k}}^\star) \frac{\pi\delta(E-\omega_1(\boldsymbol{k})-\omega_2(\boldsymbol{P}-\boldsymbol{k}))}{2\omega_1(\boldsymbol{k})2\omega_2(\boldsymbol{P}-\boldsymbol{k})} Y^*_{\ell' m'}(\hat{\boldsymbol{k}}^\star) , \tag{2.26}$$

$$= \delta_{\ell\ell'}\delta_{mm'}(k^\star_{\mathrm{os}})^{2\ell}\rho(s) , \tag{2.27}$$

with $\rho(s)$ being the phase space factor defined in eq. (2.11). The matrices $\widetilde{B}$ in the right-hand side have components $\widetilde{B}_{\ell m,\ell' m'}(s)$, corresponding to spherical-harmonic projections of the kernel with $|\boldsymbol{p}^\star| = |\boldsymbol{p}'^\star| = k^\star_{\mathrm{os}}$. A subtle point is that these matrices no longer depend on the CM magnitude of the integrated momentum $\boldsymbol{k}^\star$. This follows from re-expressing quantities in eq. (2.23) in terms of $\boldsymbol{k}^\star = |\boldsymbol{k}^\star|\hat{\boldsymbol{k}}^\star$ and subsequently using the Dirac delta function to set $|\boldsymbol{k}^\star| = k^\star_{\mathrm{os}}$, while the directional degrees of freedom are decomposed into the spherical harmonics.

Equation (2.25) holds for any factors on either side of $\circ_{i\epsilon}$ and $\circ_{\mathrm{PV}}$ and can be interpreted as an identity relating the pole prescriptions: $\circ_{i\epsilon} = \circ_{\mathrm{PV}} + i\widetilde{\rho}$. Combining it with eqs. (2.19) and (2.20) allows one to relate the scattering amplitude and the K-matrix through

$$i\widetilde{\mathcal{M}} = \sum_{n=0}^{\infty} i\widetilde{B}\left[(\circ_{\mathrm{PV}} + \widetilde{\rho})\, i\widetilde{B}\right]^n , \tag{2.28}$$

$$= \sum_{n=0}^{\infty} i\widetilde{\mathcal{K}}\left[\widetilde{\rho}\, i\widetilde{\mathcal{K}}\right]^n , \tag{2.29}$$

where the entries of $\widetilde{\mathcal{M}}$ and $\widetilde{\mathcal{K}}$ are given by

$$\widetilde{\mathcal{M}}_{\ell m,\ell' m'}(s) = \delta_{\ell\ell'}\delta_{mm'}(k^\star_{\mathrm{os}})^{-2\ell}\, \mathcal{M}^{(\ell)}(s) , \tag{2.30}$$

$$\widetilde{\mathcal{K}}_{\ell m,\ell' m'}(s) = \delta_{\ell\ell'}\delta_{mm'}(k^\star_{\mathrm{os}})^{-2\ell}\, \mathcal{K}^{(\ell)}(s) . \tag{2.31}$$

The geometric series in eq. (2.29) can be summed to obtain

$$\widetilde{\mathcal{M}} = \frac{1}{\widetilde{\mathcal{K}}^{-1} - i\widetilde{\rho}}\,, \tag{2.32}$$

which can be seen as a matrix version of eq. (2.12).

2.2 Finite-volume scattering formalism

Consider the field theory of two spinless particles introduced in the previous section, but place it now within a cubic finite spatial volume with periodic boundary conditions. We denote the spatial extent of the finite volume by L. This setup is, effectively, the continuum limit of a lattice spacetime with a large temporal extent ($T \to \infty$). In what follows, we will employ a more familiar Minkowski signature instead of a Euclidean signature because the final result is independent of which metric is used.

Placing the theory in a periodic finite volume has the effect of discretising the spectrum of the theory. The discrete energy levels, which we write $E_j(\boldsymbol{P}, L)$ ($j = 0, 1, ...$), depend on the value of total spatial momentum $\boldsymbol{P}$ and the length L. The relation derived by Lüscher in [3], called the *Lüscher quantisation condition*, can be written as

$$\det_{\ell m}\left[\widetilde{\mathcal{K}}(P_j) + \widetilde{F}(P_j, L)^{-1}\right] = 0\,, \tag{2.33}$$

for $P_j \equiv (E_j(\boldsymbol{P}, L), \boldsymbol{P})$. Here, $\widetilde{\mathcal{K}}$ is the diagonal matrix defined in the previous section, while $\widetilde{F}$ is a non-diagonal matrix of known functions, whose explicit definition will be given later in this section. Both are matrices in angular momentum index space $\ell m, \ell' m'$, with the determinant being performed over these indices, as reflected in the notation above. This condition links finite- and infinite-volume quantities, enabling us to compute the values of the infinite-volume K-matrix $\widetilde{\mathcal{K}}$ at the finite-volume energies. These can subsequently be used to obtain the scattering amplitude and phase shifts.

We now sketch a derivation of eq. (2.33), loosely following that given in [7]. We will not go too much into technical detail here, as this derivation is revisited in some depth in Chapter 3. In this chapter, we simply seek to introduce a few key concepts.

We start by introducing a finite-volume correlator

$$C_L(P) \equiv \int dx^0 \int_L d^3\boldsymbol{x}\, e^{iEx^0} e^{-i\boldsymbol{P}\cdot\boldsymbol{x}} \langle \hat{\mathcal{A}}(x)\hat{\mathcal{A}}(0)^\dagger \rangle_L \,, \tag{2.34}$$

where we use the notation $x \equiv (x^0, \boldsymbol{x})$ and $P \equiv (E, \boldsymbol{P})$. The operators $\hat{\mathcal{A}}(x)$ and $\hat{\mathcal{A}}(x)^\dagger$ are annihilation and creation operators, respectively, carrying the quantum numbers of an $\phi_1\phi_2$ state. We use the subscript L to emphasise the role of the finite volume: the integration $\int_L$ is performed over the cubic volume, while the matrix element $\langle\cdot\rangle_L$ is evaluated in the finite-volume theory.

This definition is similar to the lattice correlation function introduced in eq. (1.76). As done in section 1.3.3, we can perform a spectral decomposition of $C_L(P)$ and hence show that it has poles at the finite-volume energy levels of the system (see e.g. refs. [3, 7]):

$$C_L(P) = L^3 \sum_n \frac{2E_n \left|\langle 0|\hat{\mathcal{A}}(0)|E_n, \boldsymbol{P}\rangle\right|^2}{E^2 - E_n(\boldsymbol{P}, L)^2} \,. \tag{2.35}$$

As with the scattering amplitude and the K-matrix in the infinite-volume case, $C_L(P)$ admits a diagrammatic representation that we organize into a *skeleton expansion*, shown in figure 2.2. The expansion employs the building blocks introduced in the infinite-volume context of section 2.1, namely the fully-dressed propagator and the Bethe-Salpeter kernel. We denote these by $\Delta_{x,L}(p)$ (x standing for particle types ϕ_1, ϕ_2) and $B_L(P, p, p')$, respectively, in the finite-volume theory. The only new ingredients we need are the endcap "blobs", which represent functions in momentum-space resulting from the creation and annihilation operators. We write these as $\mathcal{A}_L^*(P, p)$ and $\mathcal{A}_L(P, p)$, respectively. As is well known (e.g. from refs. [3, 7]), this representation is useful because it allows us to identify the power-like L-dependence of $C_L(P)$ in the elastic regime, as we describe below.

The periodic boundary conditions discretise the spatial momenta to $\boldsymbol{k} = 2\pi\boldsymbol{n}/L$ with $\boldsymbol{n} \in \mathbb{Z}^3$. Therefore, in loops appearing in the diagrammatic representations of $\Delta_{x,L}(p)$, $B_L(P, p, p')$ or $C_L(P)$ itself, we replace the integrals over continuous spatial momentum with sums over the allowed discretised values:

$$\int \frac{d^4k}{(2\pi)^4} \;\longrightarrow\; \int \frac{dk^0}{2\pi} \frac{1}{L^3} \sum_{\boldsymbol{k} \in \frac{2\pi}{L}\mathbb{Z}^3} \,, \tag{2.36}$$

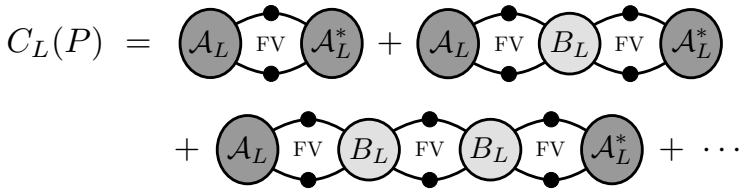

Figure 2.2 *Skeleton expansion for the finite-volume correlator $C_L(P)$, built from Bethe-Salpeter kernels $B_L(P,p,p')$, endcap functions $\mathcal{A}_L(P,p)$ and $\mathcal{A}_L^*(P,p)$ and fully-dressed nucleon propagators. Here we include the subscript L on all quantities to indicate that these are volume-dependent, albeit with exponentially suppressed scaling in the elastic regime. The finite-volume two-particle loops are denoted* FV*. Depending on the details of the operators used in $C_L(P)$, one may also have a contribution from a term with no intermediate two-particle states, which we omit here.*

where we use $k = (k^0, \boldsymbol{k})$. This is the key difference between finite- and infinite-volume diagrams, which we exploit below.

In analogy to what we did in the infinite-volume with the notations $\circ_{i\epsilon}$ and $\circ_{\mathrm{PV}}$ used in eqs. (2.21) and (2.22), we can introduce $\circ_{\mathrm{FV}}$ as a shorthand for the corresponding finite-volume operations:

$$iB_L \circ_{\mathrm{FV}} iB_L = \sigma \int \frac{dk^0}{2\pi} \frac{1}{L^3} \sum_{\boldsymbol{k}} iB_L(P,p,k)\Delta_{1,L}(k)\Delta_{2,L}(P-k)iB_L(P,k,p')\,. \quad (2.37)$$

Following the diagrammatic expansion of figure 2.2, the finite-volume correlator can be expressed as

$$C_L(P) = C_L^{(0)}(P) + \sum_{n=0}^{\infty} \mathcal{A}_L \circ_{\mathrm{FV}} \left[iB_L \circ_{\mathrm{FV}}\right]^n \mathcal{A}_L^*\,, \quad (2.38)$$

where $C_L^{(0)}(P)$ is a potential extra contribution with no $\phi_1\phi_2$ intermediate states (not shown explicitly in the skeleton expansion). This expression is useful for identifying the types of volume dependence present in the contributions to the correlator. The strategy for identifying power-like or exponentially-suppressed volume effects will be discussed in more detail in section 3.2.2 in the next chapter. For now, it suffices to say that power-like effects in the skeleton expansion (2.38) arise exclusively due to two-particle intermediate states, as shown in refs. [3, 7, 68]. Qualitatively, this

is because only $\phi_1\phi_2$ intermediate states are able to go on shell (i.e. realise the condition $E = \omega_1(\boldsymbol{k}) + \omega_2(\boldsymbol{P} - \boldsymbol{k})$ for some real $\boldsymbol{k}$) for energies in the elastic regime, dominating over contributions from off-shell states in loop integrals.

In the skeleton expansion, these $\phi_1\phi_2$ intermediate states appear exclusively through the dressed propagator pairs connecting kernels and end-caps, i.e. through the $\circ_{\mathrm{FV}}$ operation in eq. (2.38). All other building blocks (the Bethe-Salpeter kernels, endcaps and self-energy contributions to dressed propagators) will carry exponentially-suppressed $\mathcal{O}\left(e^{-\mu L}\right)$ effects instead, where μ is typically the mass of the lightest particle in the theory – corresponding to the pion in an effective theory of QCD. We may neglect these corrections provided $L \gg \mu^{-1}$, which we assume in the following. As such, we replace $B_L \to B$, $\Delta_{x,L} \to \Delta_{x,i\epsilon}$, $\mathcal{A}_L \to \mathcal{A}$ and $\mathcal{A}_L^* \to \mathcal{A}^*$ up to neglected $\mathcal{O}\left(e^{-\mu L}\right)$ corrections.

Let us look at a loop between two Bethe-Salpeter kernels in the skeleton expansion and consider the difference $D_L(P)$ between the finite- and infinite-volume versions of this loop:

$$D_L(P) \equiv iB_L \circ_{\mathrm{FV}} iB_L - iB \circ_{\mathrm{PV}} iB\,, \tag{2.39}$$

$$= iB \circ_{\mathrm{FV}} iB - iB \circ_{\mathrm{PV}} iB + \mathcal{O}\left(e^{-\mu L}\right)\,. \tag{2.40}$$

Labelling the loop momentum $k = (k^0, \boldsymbol{k})$, we can perform the k^0 integral to get

$$D_L(P) = \sigma\left[\frac{1}{L^3}\sum_{\boldsymbol{k}} - \mathrm{PV}\int\frac{d^3\boldsymbol{k}}{(2\pi)^3}\right]\frac{i\big[iB(P,p,k)iB(P,k,p')\big]_{k^0=\omega_1(\boldsymbol{k})}}{2\omega_1(\boldsymbol{k})\big[(E-\omega_1(\boldsymbol{k}))^2 - \omega_2(\boldsymbol{P}-\boldsymbol{k})^2\big]} + \mathcal{O}\left(e^{-\mu L}\right)\,, \tag{2.41}$$

$$= \sigma\left[\frac{1}{L^3}\sum_{\boldsymbol{k}} - \mathrm{PV}\int\frac{d^3\boldsymbol{k}}{(2\pi)^3}\right]\frac{i\big[iB(P,p,k)iB(P,k,p')\big]_{k^0=\omega_1(\boldsymbol{k}),|\boldsymbol{k}^\star|=k^\star_{\mathrm{os}}}}{4\omega_1(\boldsymbol{k})\big[(k^\star_{\mathrm{os}})^2 - (\boldsymbol{k}^\star)^2\big]} + \mathcal{O}\left(e^{-\mu L}\right)\,. \tag{2.42}$$

Note that we keep explicit only contributions with to power-like volume effects, arising from the two-particle pole at $E = \omega_1(\boldsymbol{k}) + \omega_2(\boldsymbol{P} - \boldsymbol{k})$, or equivalently $|\boldsymbol{k}^\star| = k^\star_{\mathrm{os}}$, corresponding to the intermediate state on-shell condition. In the second line, we use the fact that the value of the numerator at the pole will dominate the sum-integral difference to set the kernels to the on-shell spatial momentum $|\boldsymbol{k}^\star| = k^\star_{\mathrm{os}}$. The term encoding the difference between off- and on-shell kernels is exponentially suppressed and thus dropped from the main term.

As in last section, we can project the expressions above to definite angular momentum to give

$$\Big[\widetilde{D}_L\Big]_{\ell m,\ell' m'} = \Big[i\widetilde{B}\, i\widetilde{F}\, i\widetilde{B}\Big]_{\ell m,\ell' m'} + \mathcal{O}\left(e^{-\mu L}\right) , \tag{2.43}$$

with each block on the right-hand side denoting a matrix in the angular momentum index space. The entries of $\widetilde{F}$ are given by

$$\widetilde{F}_{\ell m,\ell' m'}(P,L) = \sigma \left[\frac{1}{L^3}\sum_{\boldsymbol{k}} - \mathrm{PV}\int \frac{d^3\boldsymbol{k}}{(2\pi)^3}\right] \frac{4\pi |\boldsymbol{k}^\star|^{\ell+\ell'} Y_{\ell m}(\hat{\boldsymbol{k}}^\star) Y^*_{\ell' m'}(\hat{\boldsymbol{k}}^\star)}{2\omega_1(\boldsymbol{k})\big[(E-\omega_1(\boldsymbol{k}))^2 - \omega_2(\boldsymbol{P}-\boldsymbol{k})^2\big]} . \tag{2.44}$$

This function is related to the finite-volume function defined by Kim, Sachrajda, and Sharpe (KSS) in ref. [7] according to $\widetilde{F}_{\ell m,\ell' m'} = (k^\star_{\mathrm{os}})^{\ell+\ell'} \mathrm{Re}(iF^{\mathrm{KSS}}_{\ell m,\ell' m'}/2)$, where we have added the superscript KSS to distinguish the earlier definition.

From this analysis, we get an effective identity for the finite-volume loops, which we can write as $\circ_{\mathrm{FV}} = \circ_{\mathrm{PV}} + i\widetilde{F}$. Note the similarity between this and the infinite-volume identity derived in the previous section, $\circ_{i\epsilon} = \circ_{\mathrm{PV}} + i\widetilde{\rho}$. This is not accidental, the underlying reason being that two-particle intermediate states can go on shell in the elastic regime and produce the pole at $E = \omega_1(\boldsymbol{k}) + \omega_2(\boldsymbol{P}-\boldsymbol{k})$. In infinite volume, the integral over spatial momentum then generates an imaginary contribution, while the corresponding sum in finite volume gives rise to power-like volume dependence.

We can now apply the loop identity above to the full correlator to obtain:

$$C_L(P) = C^{(0)}(P) + \sum_{n=0}^{\infty} \widetilde{\mathcal{A}}\Big[\circ_{\mathrm{PV}} + i\widetilde{F}\Big]\Big(i\widetilde{B}\Big[\circ_{\mathrm{PV}} + i\widetilde{F}\Big]\Big)^n \widetilde{\mathcal{A}}^\dagger + \mathcal{O}\left(e^{-\mu L}\right) , \tag{2.45}$$

where we have also replaced $C^{(0)}_L(P) \to C^{(0)}(P)$ since, by definition, this term contains no intermediate $\phi_1\phi_2$ states and will only receive exponentially suppressed corrections. Re-organising the series by grouping infinite-volume terms together and using the K-matrix expression of eq. (2.20), we obtain

$$C_L(P) = C_{\mathrm{PV}}(P) + \sum_{n=0}^{\infty} \widetilde{A}(P)\, i\widetilde{F}(P,L)\Big[i\widetilde{\mathcal{K}}(P)\, i\widetilde{F}(P,L)\Big]^n \widetilde{A}(P)^\dagger + \mathcal{O}\left(e^{-\mu L}\right) , \tag{2.46}$$

$$= C_{\mathrm{PV}}(P) + \widetilde{A}(P)\, \frac{i}{\widetilde{\mathcal{K}}(P) + \widetilde{F}(P,L)^{-1}} \widetilde{A}(P)^\dagger + \mathcal{O}\left(e^{-\mu L}\right) , \tag{2.47}$$

where we make the dependence on P and L explicit. We have introduced $C_{\mathrm{PV}}(P)$, the infinite-volume version of the correlator, computed using principal value prescriptions. We have also defined new endcap objects $\widetilde{A}(P)$ and $\widetilde{A}(P)^\dagger$ through the sums

$$\widetilde{A} \equiv \sum_{n=0}^{\infty} \widetilde{\mathcal{A}} \left[\circ_{\mathrm{PV}} i\widetilde{B} \right]^n , \qquad \widetilde{A}^\dagger \equiv \sum_{n=0}^{\infty} \left[i\widetilde{B} \circ_{\mathrm{PV}} \right]^n \widetilde{\mathcal{A}}^\dagger , \tag{2.48}$$

which are row and column vectors in the angular momentum index space, respectively. In the second line of eq. (2.47), we have summed the geometric series.

We know $C_L(P)$ contains poles at the finite-volume energies, as we have seen in eq. (2.35), and thus the expression above must diverge at these energies. This is is only possible if the matrix $\widetilde{\mathcal{K}}(P) + \widetilde{F}(P,L)^{-1}$ becomes singular, leading to the Lüscher quantisation condition (2.33), which we repeat here:

$$\det_{\ell m} \left[\widetilde{\mathcal{K}}(P_j) + \widetilde{F}(P_j, L)^{-1} \right] = 0 ,$$

at the finite-volume levels $P_j = (E_j(\boldsymbol{P}, L), \boldsymbol{P})$. Note that there are several equivalent ways of rewriting this condition and we choose the form above for its relevance in the next chapter. To obtain the partial-wave amplitudes, we can then use the relation of eq. (2.32).

2.2.1 Partial-wave truncation and finite-volume symmetry

The quantisation condition (2.33) involves formally infinite matrices since the set of angular momentum quantum numbers is infinite. To apply the condition in practice, we must therefore truncate the matrices to $\ell \leq \ell_{\mathrm{max}}$ for some choice of ℓ_{max}. Such a truncation is validated by the fact that contributions to the amplitude at higher angular momenta are expected to be numerically suppressed due to angular momentum conservation. In fact, it can be shown that the partial-wave amplitudes have $\mathcal{M}^{(\ell)}(s) \sim (k^\star_{\mathrm{os}})^{2\ell}$ near the two-particle threshold (i.e. for small $k^\star_{\mathrm{os}}$).

The simplest choice is truncation to S-wave, with $\ell_{\mathrm{max}} = 0$, keeping only the lowest-order partial wave. In this case, condition (2.33) reduces to the scalar equation

$$\mathcal{K}^{(0)}(s) = -\widetilde{F}_{00,00}(P, L)^{-1} , \tag{2.49}$$

which we can use to obtain the S-wave K-matrix at the finite-volume energies. In terms of the S-wave phase shift, we have

$$k^\star_{\text{os}} \cot \delta_0(k^\star_{\text{os}}) = -\frac{1}{\sigma} 8\pi\sqrt{s}\widetilde{F}_{00,00}(P, L)\,. \tag{2.50}$$

This relation gives us the S-wave phase shifts at the finite-volume energies and we can perform a fit using a physically-motivated models. For low energies, we can use the leading terms of the ERE (see eq. (2.15)) to describe the phase shift in terms of the scattering length a and effective range r of the interaction:

$$k^\star_{\text{os}} \cot \delta_0(k^\star_{\text{os}}) = -\frac{1}{a} + \frac{1}{2} r (k^\star_{\text{os}})^2 + \mathcal{O}\left((k^\star_{\text{os}})^4\right)\,. \tag{2.51}$$

Another common fit function is a Breit-Wigner, used to describe resonances:

$$\cot \delta_0(k^\star_{\text{os}}) = \frac{M_\Gamma^2 - s}{\sqrt{s}\,\Gamma(s)}\,, \qquad \text{with } \Gamma(s) = \frac{g_\Gamma^2 M_\Gamma^2 k^\star_{\text{os}}}{6\pi s}\,, \tag{2.52}$$

where M_Γ is the resonance mass and $\Gamma(s)$ is its energy-dependent width, dictated by the coupling g_Γ.

Another important aspect to take into account is the symmetry of the finite volume. The matrix $\widetilde{F}(P, L)$ is non-diagonal, meaning that there is mixing between different values of angular momenta. This is because the cubic finite volume breaks the $SO(3)$ rotational symmetry of the infinite volume to a subgroup, and thus angular momentum is no longer a good quantum number. In the rest frame ($\boldsymbol{P} = 0$), the leftover symmetries are simply the symmetries of the cube, the *octahedral group* O_h. For a moving frame ($\boldsymbol{P} \neq 0$), this is reduced further to the subgroup of O_h under which $\boldsymbol{P}$ is invariant, called the *little group* (i.e. the stabiliser of $\boldsymbol{P}$ under O_h).

The residual symmetry groups can be decomposed into a finite number of irreducible representations (irreps). We label these by Λ and the components ("rows") within each irrep by ρ, which play similar roles to ℓ and m in the infinite-volume $SO(3)$ symmetry, respectively. These labels provide good quantum numbers for the finite-volume eigenstates and we can separate the finite-volume spectrum into the spectra arising from each irrep.

We can take advantage of this structure by projecting the quantisation condition to specific irreps, employing projection operators $\mathbb{P}^\Lambda$. When cast in the basis $\Lambda\rho$, the matrix $\widetilde{F}(P, L)$ becomes block-diagonal, each block corresponding to an individual

irrep. This is because different irreps cannot mix but the rows within each can. As a result, the quantisation condition (2.33) can be factorised block-by-block, where the product runs over all irreps Λ and the determinants are taken over each block. Each determinant effectively gives us a separate quantisation condition for each Λ, which applies to the spectrum of that irrep.

Several values of ℓ are projected (*subduced*) into each irrep. For example, for two identical spinless bosons in the rest frame, we have three relevant irreps of the cubic group, labelled A_1^+, E^+ and T_2^+ (+ label denoting parity). A_1^+ has a leading contribution from S-wave ($\ell = 0$), while E^+ and T_2^+ have leading contributions from D-wave ($\ell = 2$), all three getting also contributions from the $\ell = 4, 6, 8, ...$ partial waves. The leading contribution is often assumed to dominate over the higher-ℓ corrections, although this will depend on the particular system considered.

2.3 Particles with spin

In this section, we look at the generalisation to two identical spin-half fermions ψ with physical mass M_ψ [14]. Most of the discussion carries over from the spin-zero case without major adjustments. The appropriate form of the dressed propagator for use in infinite-volume diagrammatic expansions is now

$$\Delta^{\alpha\beta}_{\psi,i\epsilon}(k) = \left[\frac{i}{A(k^2)\not{k} - B(k^2) + i\epsilon}\right]^{\alpha\beta}, \tag{2.53}$$

where α and β are Dirac indices. We have two self-energy functions $A(k^2)$ and $B(k^2)$, which are constrained by the on-shell renormalisation conditions to ensure that M_ψ is the pole mass. An expansion about the pole position gives

$$\Delta^{\alpha\beta}_{\psi,i\epsilon}(k) = \left[\frac{i(\not{k} + M_\psi)}{k^2 - M_\psi^2 + i\epsilon}\right]^{\alpha\beta} + \mathcal{O}\left(\left(k^2 - M_\psi^2\right)^0\right). \tag{2.54}$$

With the exception of eq. (2.23) for which an explanation is given below, eqs. (2.17)–(2.32) hold as written with the caveat that B, $\mathcal{K}$ and $\mathcal{M}$ all carry implicit indices that are contracted between adjacent factors. As an example, eq. (2.21) can be

written more explicitly as

$$[iB \circ_{i\epsilon} iB]^{\sigma\delta,\sigma'\delta'} = \frac{1}{2}\int \frac{d^4k}{(2\pi)^4} iB^{\sigma\delta,\alpha\beta}(P,p,k)\Delta^{\alpha\alpha'}_{\psi,i\epsilon}(k)\Delta^{\beta\beta'}_{\psi,i\epsilon}(P-k)iB^{\alpha'\beta',\sigma'\delta'}(P,k,p')\,, \tag{2.55}$$

where we have set the symmetry factor to 1/2 because we are considering identical particles. The key relation of eq. (2.23) does require some modification. The result with intrinsic spin takes the form

$$\begin{aligned}&\big[iB \circ_{i\epsilon} iB - iB \circ_{\mathrm{PV}} iB\big]_{tv,t'v'} = \\ &\quad\frac{1}{2}\int \frac{d^3\boldsymbol{k}}{(2\pi)^3} iB_{tv,rs}(P,p,k)\frac{\pi\delta(E-\omega_\psi(\boldsymbol{k})-\omega_\psi(\boldsymbol{P}-\boldsymbol{k}))\,\delta_{rr'}\delta_{ss'}}{2\omega_\psi(\boldsymbol{k})2\omega_\psi(\boldsymbol{P}-\boldsymbol{k})} iB_{r's',t'v'}(P,k,p')\,,\end{aligned} \tag{2.56}$$

where $\omega_\psi(\boldsymbol{p}) \equiv \sqrt{\boldsymbol{p}^2 + M_\psi^2}$ and

$$B_{tv,rs}(P,p,k) = \overline{u}^\sigma_t(\boldsymbol{p})\overline{u}^\delta_v(\boldsymbol{P}-\boldsymbol{p})B^{\sigma\delta,\alpha\beta}(P,p,k)u^\alpha_r(\boldsymbol{k})u^\beta_s(\boldsymbol{P}-\boldsymbol{k})\,, \tag{2.57}$$

are spin-projected versions of the Bethe-Salpeter kernels. To define these we have introduced the standard four-component Dirac spinors $\bar{u}^\alpha_r(\boldsymbol{k})$ and $u^\alpha_r(\boldsymbol{k})$, which satisfy the relation

$$[\not{k} + M_\psi]^{\alpha\beta} = \sum_{r=\pm} u^\alpha_r(\boldsymbol{k})\bar{u}^\beta_r(\boldsymbol{k})\,, \tag{2.58}$$

provided that on-shell momentum $k = (\omega_\psi(\boldsymbol{k}), \boldsymbol{k})$ is used on the left-hand side. The sum runs over the two possible spin states, labelled by the sign of the spin magnetic quantum number $r = \pm\frac{1}{2}$.

The spin-state indices appear through the Kronecker deltas in eq. (2.56), leading to a modification of the phase-space factor:

$$\rho_{rs,r's'}(s) = \frac{k^\star_{\mathrm{os}}}{16\pi\sqrt{s}}\,\delta_{rr'}\delta_{ss'}\,. \tag{2.59}$$

Completing the derivation of section 2.2, we get:

$$\widetilde{\mathcal{M}} = \frac{1}{\widetilde{\mathcal{K}}^{-1} - i\widetilde{\rho}}\,, \tag{2.60}$$

matching eq. (2.32) exactly. However, the objects in this equation are now matrices in the combined orbital angular momentum and spin index space, whose elements

are given by

$$\widetilde{\rho}_{\ell mrs,\ell' m' r' s'}(s) = \delta_{\ell\ell'}\delta_{mm'}(k^\star_{\rm os})^{2\ell}\rho_{rs,r's'}(s)\,, \tag{2.61}$$

$$\widetilde{\mathcal{K}}_{\ell mrs,\ell' m' r' s'}(s) = (k^\star_{\rm os})^{\ell+\ell'}\,\mathcal{K}_{\ell mrs,\ell' m' r' s'}(s)\,, \tag{2.62}$$

$$\widetilde{\mathcal{M}}_{\ell mrs,\ell' m' r' s'}(s) = (k^\star_{\rm os})^{\ell+\ell'}\,\mathcal{M}_{\ell mrs,\ell' m' r' s'}(s)\,. \tag{2.63}$$

Unlike the spinless case, we now need two sets of indices in the K-matrix and scattering amplitude since orbital angular momentum and spin are not individually conserved and may change between the incoming and outgoing states.

The entries $\mathcal{M}_{\ell mrs,\ell' m' r' s'}$ are projections of the amplitude to definite incoming and outgoing orbital angular momentum and single-particle spin states. We can write this projection as

$$\mathcal{M}_{\ell mrs,\ell' m' r' s'} = \big(\langle \ell' m'| \otimes \langle s_1 r', s_2 s'|\,\big)\,\mathcal{M}\,\big(\,|\ell m\rangle \otimes |s_1 r, s_2 s\rangle\big)\,, \tag{2.64}$$

where $|\ell m\rangle$ is a state of definite orbital angular momentum and $|s_1 r, s_2 s\rangle$ (with $s_1 = s_2 = \frac{1}{2}$ for the fermions ψ) encodes the two-particle spin states. We can arrive at a more useful set of indices by subsequent changes of basis, for example to definite total spin $\ell m S m_S, \ell' m' S' m'_S$ via

$$|\ell m, S m_S\rangle \equiv |\ell m\rangle \otimes |S m_S, s_1 s_2\rangle \tag{2.65}$$

$$= \sum_{r,s} \big(\,|\ell m\rangle \otimes |s_1 r, s_2 s\rangle\big)\langle s_1 r, s_2 s|S m_S, s_1 s_2\rangle\,, \tag{2.66}$$

where $\langle s_1 r, s_2 s|s_1 s_2, S m_S\rangle$ are the Clebsch-Gordon coefficients for the addition of the spins. One can combine these indices further and label the amplitude in terms of total angular momentum J, making use of the relation

$$|J m_J, \ell S\rangle = \sum_{m, m_S} |\ell m, S m_S\rangle\langle \ell m, S m_S|J m_J, \ell S\rangle\,. \tag{2.67}$$

The advantage is that total angular momentum is conserved and thus the amplitude is diagonal in J, m_J. The standard expressions for the K-matrix and amplitude in terms of the phase shift can be used with little alteration:

$$\mathcal{K}_{J m_J \ell S, J' m'_J \ell' S'} = \delta_{JJ'}\delta_{m_J m'_J}\mathcal{K}^{(J)}_{\ell S,\ell' S'} = \delta_{JJ'}\delta_{m_J m'_J}\,16\pi\sqrt{s}\,\frac{\tan\delta^{(J)}_{\ell S,\ell' S'}(k^\star_{\rm os})}{k^\star_{\rm os}}\,, \tag{2.68}$$

and

$$\mathcal{M}_{Jm_J\ell S,J'm'_J\ell'S'} = \delta_{JJ'}\delta_{m_Jm'_J}\mathcal{M}^{(J)}_{\ell S,\ell'S'} = \delta_{JJ'}\delta_{m_Jm'_J}\frac{16\pi\sqrt{s}}{k^\star_{\rm os}\cot\delta^{(J)}_{\ell S,\ell'S'}(k^\star_{\rm os}) - ik^\star_{\rm os}}\,, \quad (2.69)$$

where the phase shifts $\delta^{(J)}_{\ell S,\ell'S'}$ are labelled by the total angular momentum and total incoming and outgoing orbital angular momentum and spin. For a more detailed discussion on the inclusion of spin, see for example refs. [14, 114].

Let us now turn to a finite and periodic spatial volume and the derivation of a quantisation condition tying the finite-volume spectrum to the $\psi\psi$ elastic scattering amplitude. The arguments outlined in section 2.1 are broadly the same, taking into account the fact that all ingredients of the diagrammatic skeleton expansion now carry spinor indices, e.g. eq. (2.37) is changed to

$$\begin{aligned}&[iB_L \circ_{\rm FV} iB_L]^{\sigma\delta,\sigma'\delta'} = \\ &\quad\frac{1}{2}\int\frac{dk^0}{2\pi}\frac{1}{L^3}\sum_{\boldsymbol{k}} iB_L^{\sigma\delta,\alpha\beta}(P,p,k)\Delta^{\alpha\alpha'}_{\psi,L}(k)\Delta^{\beta\beta'}_{\psi,L}(P-k)iB_L^{\alpha'\beta',\sigma'\delta'}(P,k,p')\,. \quad (2.70)\end{aligned}$$

The difference between the finite- and infinite-volume loops analysed in eqs. (2.40)-(2.42) is modified to:

$$\begin{aligned}D_L^{\sigma\delta,\sigma'\delta'}(P) = \frac{1}{2}&\left[\frac{1}{L^3}\sum_{\boldsymbol{k}} - \mathrm{PV}\int\frac{d^3\boldsymbol{k}}{(2\pi)^3}\right]\frac{i}{4\omega_\psi(\boldsymbol{k})\left[(k^\star_{\rm os})^2-(\boldsymbol{k}^\star)^2\right]}\\ &\times\Big[iB^{\sigma\delta,\alpha\beta}(P,p,k)(\not{k}+M_\psi)^{\alpha\alpha'}\\ &\qquad(\not{P}-\not{k}+M_\psi)^{\beta\beta'}iB^{\alpha'\beta',\sigma'\delta'}(P,k,p')\Big]_{k^0=\omega_\psi(\boldsymbol{k}),|\boldsymbol{k}^\star|=k^\star_{\rm os}}\\ &+\mathcal{O}\left(e^{-\mu L}\right)\,. \quad (2.71)\end{aligned}$$

We can use the spin sum relations for on-shell momenta (2.58) to decompose the momentum-space Dirac matrices:

$$(\not{k}+M_\psi)^{\alpha\alpha'}\Big|_{k^0=\omega_\psi(\boldsymbol{k}),|\boldsymbol{k}^\star|=k^\star_{\rm os}} = \sum_{r=\pm}u^\alpha_r(\boldsymbol{k}_{\rm os})\bar{u}^{\alpha'}_r(\boldsymbol{k}_{\rm os})\,, \quad (2.72)$$

where $u^\alpha_r(\boldsymbol{k}_{\rm os})$ and $\bar{u}^{\alpha'}_r(\boldsymbol{k}_{\rm os})$ are the Dirac spinors describing a free ψ state with definite spin, with spin-up and down states labelled by $r=\pm$. These are evaluated at momenta $\boldsymbol{k}_{\rm os}$ obtained from boosting the CM on-shell momentum $\boldsymbol{k}^\star_{\rm os}\equiv k^\star_{\rm os}\hat{\boldsymbol{k}}^\star$,

back to the finite-volume frame, with boost velocity $\boldsymbol{\beta} = \boldsymbol{P}/E$.

We use eq. (2.57) to obtain kernels projected to states of definite spin and project to definite orbital angular momentum, as done in section 2.2. This yields a result with the same form but with extra spin indices:

$$\left[\widetilde{D}_L\right]_{rs\ell m,r's'\ell'm'} = \left[i\widetilde{B}\, i\widetilde{F}\, i\widetilde{B}\right]_{rs\ell m,r's'\ell'm'} + \mathcal{O}\left(e^{-\mu L}\right) , \tag{2.73}$$

with each matrix on the right-hand side carrying this same index set. The entries of $\widetilde{F}$ are given by

$$\widetilde{F}_{rs\ell m,r's'\ell'm'}(P,L) = \\ \frac{1}{2}\left[\frac{1}{L^3}\sum_{\boldsymbol{k}} - \mathrm{PV}\int\frac{d^3\boldsymbol{k}}{(2\pi)^3}\right]\frac{4\pi\delta_{rr'}\delta_{ss'}|\boldsymbol{k}^\star|^{\ell+\ell'}Y_{\ell m}(\hat{\boldsymbol{k}}^\star)Y^*_{\ell'm'}(\hat{\boldsymbol{k}}^\star)}{2\omega_\psi(\boldsymbol{k})\left[(E-\omega_\psi(\boldsymbol{k}))^2-\omega_\psi(\boldsymbol{P}-\boldsymbol{k})^2\right]} . \tag{2.74}$$

The derivation follows the same arguments as before, leading to the virtually identical quantisation condition:

$$\det_{rs\ell m}\left[\widetilde{\mathcal{K}}(P_j) + \widetilde{F}(P_j,L)^{-1}\right] = 0 , \tag{2.75}$$

at the finite-volume levels $P_j = (E_j(\boldsymbol{P},L),\boldsymbol{P})$. The spin state and orbital angular momentum basis is usually not the most advantageous, and we might prefer to change to the total angular momentum basis $Jm_J\ell S$ introduced above, using (2.66) and (2.67).

Having extensively reviewed the necessary background on infinite-volume scattering and the Lüscher formalism, we will now address the central topic of this thesis, the incorporation of the left-hand cut into this framework, in the following chapter.

Chapter 3

Extension of finite-volume formalism to the left-hand cut: identical particles

As we have discussed at length in the previous chapter, the method introduced by Lüscher [3] and subsequently developed in [4–14] can be used to constrain the infinite-volume hadronic two-body scattering amplitudes from the knowledge of the two-particle finite-volume spectrum. The following chapter concerns the "left-hand cut issue" arising in this formalism, discussed already in the Introduction. The results detailed here have been presented in [1, 2] and we follow the latter work closely.

We have seen that, for elastic nucleon-nucleon (NN) scattering, the standard formalism has a region of validity restricted to [14]:

$$(2M_N)^2 - M_\pi^2 < E_n(L, \boldsymbol{P})^2 - \boldsymbol{P}^2 < (2M_N + M_\pi)^2 \,, \tag{3.1}$$

where M_N is the nucleon mass. The upper bound here is simply the lowest-lying inelastic threshold and the lower bound is due to a left-hand cut from single-pion exchange and is the focus of this work. Although we focus on elastic nucleon-nucleon (NN) scattering throughout, the results derived in this chapter apply to any single-channel two-to-two system with identical scattering particles.

As already pointed out in ref. [15], the simplest way to see that the formalism breaks down is to note that the latter always predicts a real-valued scattering amplitude

for $s < (2M_N)^2$ whereas, for $s < (2M_N)^2 - M_\pi^2$, it is known that the angular-momentum-projected amplitude must be complex. The realness of the scattering amplitude is a symptom of the problem but does not directly reveal the underlying reason. As we discuss in detail in section 3.2, the fundamental issue is subtle. In short, the relation between finite-volume energies and infinite-volume scattering amplitudes is derived by studying an all-order diagrammatic expansion of a finite-volume correlation function. At various steps, sub-diagrams with four external legs are identified and, because these are inside a larger diagram, the momenta they carry take on all values and do not satisfy the on-shell condition $k^2 = M_N^2$. However, at a particular step in the derivation, one can show that the replacement $k^2 \to M_N^2$ is valid and only leads to neglected L-dependence of the form $e^{-\mu(s)L}$ for some (possibly energy-dependent) characteristic scale $\mu(s)$.

For $s < (2M_N)^2 - M_\pi^2$, however, this on-shell replacement is invalid. Here, we resolve the issue by separating out the pion exchanges in all diagrams and avoiding the problematic step for these contributions. The result is a generalized formalism that relates finite-volume energies to scattering amplitudes in an extended region:

$$(2M_N)^2 - (2M_\pi)^2 < E_n(L, \boldsymbol{P})^2 - \boldsymbol{P}^2 < (2M_N + M_\pi)^2 \,, \tag{3.2}$$

where the new lower limit arises from two-pion exchanges, such as that shown in figure 1(b). These are not treated in our generalization.

We further comment that the inequality (3.1) does not define strict boundaries of validity. As one approaches the inelastic threshold at $s = (2M_N + M_\pi)^2$ from below, $\mu(s)$ tends to zero so that the neglected $e^{-\mu(s)L}$ terms become enhanced. In this work, we find that the same breakdown occurs as one approaches the lower limit of $s = (2M_N)^2 - M_\pi^2$ from above. Thus, it is prudent to apply the formulas derived here, even for finite-volume energies above the branch point, to study the effect of potential enhancement of neglected exponentials. An analogous issue is that, for infinite-volume scattering amplitudes, the convergence of the partial-wave expansion becomes arbitrarily bad as one approaches $s = (2M_N)^2 - M_\pi^2$. This is also addressed with the formalism presented in this work since partial-wave projection is only required for an intermediate infinite-volume quantity in which the offending cut is absent.

Earlier work, of relevance for the left-hand cut in the finite-volume context, includes ref. [115], concerning exponentially suppressed corrections to finite-volume scattering

formula for $NN \to NN$, as well as ref. [116], which makes use of a plane-wave basis for the quantization condition. The latter is discussed in section 3.3.4.

The remainder of this chapter is organized as follows. Firstly, we examine the analytic continuation of the amplitude and the relations discussed in section 2.1 to the sub-threshold region. Then, in section 3.2, we turn to the finite-volume system. We detail the breakdown in the usual derivation and provide a resolution, summarized in section 3.2.8. As we explain there, this depends on an intermediate quantity that is related to the scattering amplitude via integral equations, which will be the topic of Chapter 5. Finally, in section 3.3, we explore the result in various ways, e.g. by recovering the standard formalism in the limiting case when the $NN\pi$ coupling vanishes.

3.1 Left-hand cuts in infinite volume

Without loss of generality, we will consider a generic relativistic quantum field theory with a heavy spinless particle, with mass M_N, and one light spinless particle, with mass M_π, such that $M_\pi \ll M_N$. Refer to the light particle as a pion (with associated quantities labelled π) and the heavy particle as a nucleon (with associated quantities labelled N). We further require that the nucleon is charged under a $U(1)$ symmetry such that the single-particle states can be written $|N, \boldsymbol{p}, \pm\rangle$ where the second label is spatial momentum and the third is charge. This conserved charge plays the part of baryon number, which arises from the vector $U(1)_V$ symmetry of QCD. In this setup, we consider a single flavor of pion, corresponding to the π^0 in nature. The field is neutral under the $U(1)$ charge, i.e. has baryon number zero.

The infinite-volume single-particle states are normalized as

$$\langle N, \boldsymbol{p}', q' | N, \boldsymbol{p}, q\rangle = \delta_{q'q} 2\omega_N(\boldsymbol{p})(2\pi)^3\delta^3(\boldsymbol{p}' - \boldsymbol{p})\,, \tag{3.3}$$

$$\langle \pi, \boldsymbol{p}' | \pi, \boldsymbol{p}\rangle = 2\omega_\pi(\boldsymbol{p})(2\pi)^3\delta^3(\boldsymbol{p}' - \boldsymbol{p})\,, \tag{3.4}$$

where

$$\omega_N(\boldsymbol{p}) = \sqrt{\boldsymbol{p}^2 + M_N^2}\,, \qquad \omega_\pi(\boldsymbol{p}) = \sqrt{\boldsymbol{p}^2 + M_\pi^2}\,. \tag{3.5}$$

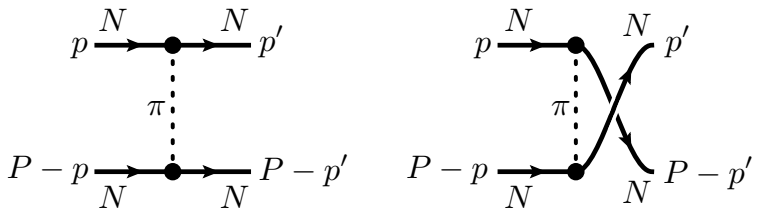

Figure 3.1 *Single-meson exchange contribution to the $NN \to NN$ scattering amplitude and K-matrix.*

We allow the theory to have generic interactions respecting the conservation of baryon number. In particular, we include $N \to N\pi$ couplings of the form

$$\mathcal{L}_{N^\dagger N\pi}(x) = N^\dagger(x)N(x)\mathcal{F}\big(\pi(x)\big)\,, \tag{3.6}$$

where $\mathcal{F}$ is a generic polynomial in the pion field, starting with a linear dependence on $\pi(x)$.

We can introduce the objects defined in section 2.1, e.g. the K-matrix, Bethe-Salpeter kernel and so on, in the context of NN scattering in this theory. As mentioned, the K-matrix is generally expected to be a meromorphic function in a region of the complex plane containing $(k^\star_{\rm os})^2 = 0$, corresponding to $s = (2M_N)^2$. As a result, one can expand $k\cot\delta_\ell(k)$ about this point as a series of polynomials and poles, as done in eq. (3.7), which we repeat here for convenience:

$$k\cot\delta_\ell(k) = -\frac{1}{a_\ell k^{2\ell}}\left[1 + \sum_{j=1}^{\infty} c_j k^{2j}\right] + \sum_i \sum_{j=0}^{\infty} \frac{A_{i,j}\,k^j}{k^2 - C_i}\,.$$

This expansion allows us to define a sub-threshold analytic continuation for the K-matrix.

In the case where interactions of the form $\pi(x)N^\dagger(x)N(x)$, $\pi(x)^2N^\dagger(x)N(x)$ are included, as in eq. (3.6), this expansion breaks down due to branch cuts, generically referred to as left-hand cuts, that run along the negative real axis of the complex s plane. The nearest cut starts at $s = 4M_N^2 - M_\pi^2$ and arises due to single pion exchanges.

To see this in more detail, we consider the tree-level t- and u-channel exchange diagrams shown in figure 3.1. First assuming a fully dressed pion propagator and

general vertex functions, these diagrams have the form

$$D_t(P,p,p') \equiv G(p,p')\ \Delta_{\pi,i\epsilon}(p'-p)\ G(P-p,P-p')\,, \tag{3.7}$$

$$D_u(P,p,p') \equiv G(p,P-p')\ \Delta_{\pi,i\epsilon}(P-p'-p)\ G(p,P-p')\,, \tag{3.8}$$

where the middle propagator factor in each expression was introduced in eq. (2.16). Here we have also introduced the form factor $G(p,p')$ defined as the amputated sum of all $N \to N\pi$ diagrams or, equivalently, via the matrix element

$$G(p,p') \equiv \Delta_{\pi,i\epsilon}(p'-p)^{-1}\langle N,\boldsymbol{p}',q'|\pi(0)|N,\boldsymbol{p},q\rangle\,. \tag{3.9}$$

Because our concern is the singularities in the diagrams $D_t(P,p,p')$ and $D_u(P,p,p')$, it will be convenient to identify simpler expressions that contain these relevant features but differ from the full diagram by analytic terms. To define these first note that, for the case where all fields have spin zero, $G(p,p')$ is a Lorentz scalar and only depends on Lorentz scalar momentum combinations. Further, noting that $p^2 = p'^2 = M_N^2$ in eq. (3.9), we see that the function in fact only depends on the momentum transfer. This allows us to define $\mathcal{G}$ as the same function of a single Lorentz invariant

$$\mathcal{G}\Big((p'-p)^2\Big) = G(p,p')\,. \tag{3.10}$$

We then define the coupling as

$$g \equiv \lim_{q^2\to M_\pi^2} \mathcal{G}(q^2)\,. \tag{3.11}$$

With this coupling defined, we now observe that the differences

$$\delta D_t(P,p,p') \equiv D_t(P,p,p') - ig^2\mathcal{T}(P,p,p')\,, \tag{3.12}$$

$$\delta D_u(P,p,p') \equiv D_u(P,p,p') - ig^2\mathcal{U}(P,p,p')\,, \tag{3.13}$$

are analytic in the vicinity of the pole, where

$$ig^2\mathcal{T}(P,p,p') \equiv -\frac{ig^2}{(p'-p)^2 - M_\pi^2 + i\epsilon} = -\frac{ig^2}{t - M_\pi^2 + i\epsilon}\ , \tag{3.14}$$

$$ig^2\mathcal{U}(P,p,p') \equiv -\frac{ig^2}{(P-p'-p)^2 - M_\pi^2 + i\epsilon} = -\frac{ig^2}{u - M_\pi^2 + i\epsilon}\ , \tag{3.15}$$

correspond precisely to the t- and u-channel exchange poles. Here we have also made use of the Mandelstam invariants t and u.

For the following section, it will be convenient to define versions of the exchanges of eqs. (3.14) and (3.15) in which the four-vectors p and p' are on shell and the corresponding three-momenta, as well as P, are expressed in the two-particle CM frame, e.g. for the t-channel exchange

$$\mathcal{T}(s, \boldsymbol{p}^\star, \boldsymbol{p}'^\star) \equiv \mathcal{T}(P, p, p')\Big|_{p^0=\omega_N(\boldsymbol{p}),\ p'^0=\omega_N(\boldsymbol{p}')} . \tag{3.16}$$

Here we abuse notation by letting the nature of the arguments distinguish the two functions. This can then be decomposed in partial waves as

$$\mathcal{T}(s, \boldsymbol{p}^\star, \boldsymbol{p}'^\star) = \sum_{\ell=0}^{\infty} \mathcal{T}_\ell(s, |\boldsymbol{p}^\star|, |\boldsymbol{p}'^\star|)\,(2\ell+1)\,P_\ell(\cos\theta^\star) . \tag{3.17}$$

The final step in reducing $\mathcal{T}_\ell(s, |\boldsymbol{p}^\star|, |\boldsymbol{p}'^\star|)$ is to note that, when the particles are scattering with physical back-to-back momenta, the magnitudes are constrained to satisfy $|\boldsymbol{p}^\star| = |\boldsymbol{p}'^\star| = k^\star_{\text{os}}$. For this reason, the partial-wave projected amplitude reduces to a single coordinate function that we denote by

$$\mathcal{T}^{\text{os}}_\ell(s) \equiv \mathcal{T}_\ell\big(s, k^\star_{\text{os}}, k^\star_{\text{os}}\big) . \tag{3.18}$$

Equivalent expressions hold for the u-channel exchange.

Combining eqs. (3.14) and (3.17) then gives

$$\mathcal{T}^{\text{os}}_\ell(s) = \frac{1}{2}\int_{-1}^{1} d(\cos\theta^\star)\,\frac{P_\ell(\cos\theta^\star)}{2(s/4-M_N^2)(1-\cos\theta^\star)+M_\pi^2-i\epsilon} , \tag{3.19}$$

$$\mathcal{U}^{\text{os}}_\ell(s) = \frac{1}{2}\int_{-1}^{1} d(\cos\theta^\star)\,\frac{P_\ell(\cos\theta^\star)}{2(s/4-M_N^2)(1+\cos\theta^\star)+M_\pi^2-i\epsilon} , \tag{3.20}$$

where we have used that $t = -2(s/4-M_N^2)(1-\cos\theta^\star)$. This integral is straightforward to evaluate for any fixed ℓ. For $\ell = 0$, for example, one finds

$$\mathcal{T}^{\text{os}}_0(s) = \frac{1}{s-4M_N^2}\log\left[1+\frac{s-4M_N^2}{M_\pi^2}-i\epsilon\right] . \tag{3.21}$$

The expression makes the logarithmic t-channel cut in the amplitude manifest. See figure 3.2 for a summary of this analytic structure. Note that the expression is

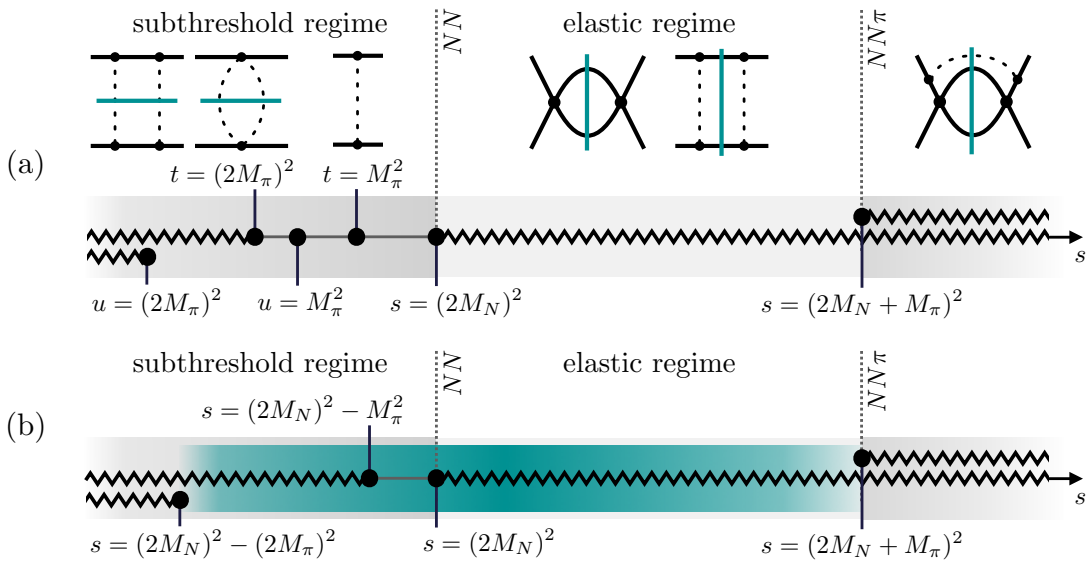

Figure 3.2 *Summary of the analytic structure of the $NN \to NN$ amplitude in the complex s plane: (a) at fixed CM scattering angle $\theta^\star$ and (b) angular-momentum projected to a given partial wave. In both cases, we have the usual s-channel cuts starting at the NN and $NN\pi$ thresholds (indicated as vertical dashed lines). Both poles and cuts, associated with the t-and u-channel exchanges, arise below threshold for the fixed $\theta^\star$ case of (a). These give rise to the left-hand cuts shown in (b). The formalism derived in this work holds for the region shown in cyan, i.e. for $(2M_N)^2 - (2M_\pi)^2 \lesssim s \lesssim (2M_N + M_\pi)^2$ where the limits are not sharp due to an enhancement of neglected exponentially suppressed terms near the branch points on either side.*

regular for $s = 4M_N^2$ with an expansion about that point giving

$$\mathcal{T}_0^{\text{os}}(s) = \frac{1}{M_\pi^2} - \frac{s - 4M_N^2}{2M_\pi^4} + \mathcal{O}\Big(\big(s - 4M_N^2\big)^2\Big) \ . \tag{3.22}$$

Note $\mathcal{U}_0^{\text{os}}(s)$ satisfies the same expansion.

We stress that the partial-wave expansion is expected to exhibit arbitrarily poor convergence near $t = M_\pi^2$ or $u = M_\pi^2$. This is intuitive because the expansion must reproduce an angular dependence that diverges at the pion exchange poles but is otherwise finite. In addition, the S-wave partial-wave-projected amplitudes diverge at the branch point $s = 4M_N^2 - M_\pi^2$, as can be seen from eq. (3.21). This generically does not match a divergence of the unprojected amplitude. In the following sections, we will circumvent these issues by introducing an intermediate quantity in which both the pole and the branch cut are removed. This is then related to the scattering amplitude via integral equations that recover the physical singularities as required.

3.2 Finite-volume analysis

In this section, we review the analysis of finite-volume correlation functions, originally worked out in refs. [3, 7], which leads to the quantization condition relating two-particle finite-volume energies to elastic scattering amplitudes. We then illustrate the problem with the derivation that arises in the case of a sub-threshold left-hand cut and derive a new formalism that can be applied for finite-volume energies extracted either near or on the cut. In sections 3.2.1- 3.2.4, we focus on energies in the above-threshold elastic regime, while commenting occasionally on what changes below threshold. We detail the issues that arise on the left-hand cut in sections 3.2.5 and 3.2.6. The derivation of the new quantization condition is presented in section 3.2.7 and the result is given in 3.2.8. Finally, the incorporation of intrinsic spin is explained in section 3.2.9.

3.2.1 Finite-volume correlator

Consider the system introduced in the previous section, now constrained to a finite, periodic volume with periodicity L in each of the three spatial directions. As done

in section 2.2 (eq. (2.34)), we define a time-ordered Minkowski correlator

$$C_L(P) \equiv \int dx^0 \int_L d^3\boldsymbol{x}\, e^{iEx^0} e^{-i\boldsymbol{P}\cdot\boldsymbol{x}} \langle \hat{\mathcal{A}}(x)\hat{\mathcal{A}}(0)^\dagger \rangle_L \ , \tag{3.23}$$

where we use the notation $x \equiv (x^0, \boldsymbol{x})$ for the spatial coordinate and $P \equiv (E, \boldsymbol{P})$ for the total four-momentum, as in the previous sections. The operators $\hat{\mathcal{A}}(x)$ and $\hat{\mathcal{A}}(x)^\dagger$ are annihilation and creation operators, respectively, carrying the quantum numbers of the NN states of interest.

Again, we expect $C_L(P)$ to contain poles at the finite-volume energy levels of the system. In a suitably defined infinite-volume ($L \to \infty$) limit, these poles will accumulate to form the s-channel branch cuts, matching the analytic structure of the amplitude shown in figure 3.2(a). However, the structure of the correlator below the (infinite-volume) elastic threshold, in both finite and infinite-volume versions, differs significantly from that of the amplitude: $C_L(P)$ contains no t- or u-channel poles or cuts. Particularly relevant for us later in this section is the fact that the single-meson-exchange cut described in section 3.1 is not present in the correlator, and only becomes an issue because of its presence in the two-to-two scattering amplitude.

We now employ a diagrammatic representation of the correlator that we organize into a skeleton expansion, identical to the one shown in figure 2.2. This expansion will include the finite-volume dressed nucleon propagator $\Delta_{N,L}(p)$ and Bethe-Salpeter kernel $B_L(P, p, p')$, as well as the endcap factors $\mathcal{A}_L^*(P, p)$ and $\mathcal{A}_L(P, p)$, derived from the creation and annihilation operators, respectively. As we review in section (3.2.2) based on the work of refs. [3, 7], these quantities have only exponentially suppressed volume dependence of all energies (including those on the left-hand cut). We will therefore drop the L subscripts in section 3.2.7, but keep them here to emphasize that the functions are defined in the finite-volume theory.

The n-loop contributions to the skeleton expansion of the correlator can be written

analytically as

$$C_L^{(1)}(P) = \frac{1}{2}\int \frac{dk_1^0}{(2\pi)}\frac{1}{L^3}\sum_{\boldsymbol{k}_1}\mathcal{A}_L(P,k_1)\,\Delta_{N,L}(k_1)\,\Delta_{N,L}(P-k_1)\mathcal{A}_L^*(P,k_1)\,, \tag{3.24}$$

$$\begin{aligned} C_L^{(n)}(P) = \frac{1}{2^n}\int \frac{dk_1^0\,dk_2^0\,...\,dk_n^0}{(2\pi)^n}\frac{1}{(L^3)^n}\sum_{\boldsymbol{k}_1,\boldsymbol{k}_2,...,\boldsymbol{k}_n}\mathcal{A}_L(P,k_1)\,\Delta_{N,L}(k_1)\,\Delta_{N,L}(P-k_1) \\ \times\prod_{j=2}^{n}\left[iB_L(P,k_{j-1},k_j)\,\Delta_{N,L}(k_j)\,\Delta_{N,L}(P-k_j)\right]\mathcal{A}_L^*(P,k_n) \qquad \text{for } n\geq 2\,. \end{aligned} \tag{3.25}$$

We can write this compactly by using the compact notation $\circ_{\mathrm{FV}}$ for the finite-volume loops, as introduced in section 2.2. The full correlation function can be expressed as

$$C_L(P) = C_L^{(0)}(P) + \sum_{n=0}^{\infty}\mathcal{A}_L\;\circ_{\mathrm{FV}}\left[iB_L\circ_{\mathrm{FV}}\right]^n\mathcal{A}_L^\dagger\,, \tag{3.26}$$

where $C_L^{(0)}(P)$ is a potential contribution with no NN intermediate states. This is simply eq. (2.38), which we repeat here for convenience.

In the following subsections, we illustrate the utility of this expression for identifying power-like volume dependence in the correlator. To do so, we first review the basic strategy for distinguishing power-like and exponentially suppressed volume effects.

3.2.2 Classifying finite-volume effects

, The prescription of summing over discretised momentum $\boldsymbol{k}\in(2\pi/L)\mathbb{Z}^3$ rather than integrating the spatial loop momenta is the only distinction between the finite- and infinite-volume Feynman rules. Thus, the relation between Feynman diagrams in the two contexts is conveniently understood by studying sum-integral differences.

A first key observation in this direction is as follows: if, for any direction of $\boldsymbol{k}$, a generic function, $f(\boldsymbol{k})$, has a strip of analyticity in the complex $|\boldsymbol{k}|$ plane then one can use the Poisson summation formula to show that

$$\left[\frac{1}{L^3}\sum_{\boldsymbol{k}} - \int\frac{d^3\boldsymbol{k}}{(2\pi)^3}\right]f(\boldsymbol{k}) = \mathcal{O}\left(e^{-\mu L}\right)\,, \tag{3.27}$$

for a characteristic scale μ, governed by the width of the strip. In words, the function has exponentially suppressed volume effects.[1] As is common to a large body of work quantifying finite-volume effects for scattering states, we will neglect such exponentially suppressed scaling throughout this work whenever $\mu \sim M_\pi$.

If, instead, one considers a function, $g(\boldsymbol{k})$, with a singularity on the real axis, then the difference has power-like scaling in L:

$$\left[\frac{1}{L^3}\sum_{\boldsymbol{k}} - \text{Presc.} \int \frac{d^3\boldsymbol{k}}{(2\pi)^3}\right] g(\boldsymbol{k}) = \mathcal{O}(L^{-n})\,, \tag{3.28}$$

for some integer n. This expression assumes that a suitable prescription has been used to make the integral of $g(\boldsymbol{k})$ well-defined, represented by the abbreviated "Presc." acting on the integral. In the case of a single pole, for example, both a principal-value and an $i\epsilon$ pole prescription may be used. In our analysis of Feynman diagrams, we will mainly use a principal value prescription, denoted by "PV" below. We stress that n can also be negative, in which case the sum-integral difference has a divergent infinite-volume limit.

Returning to the skeleton expansion of eq. (2.38), our task is to identify when summands are analytic and when these are singular with respect to the summed momentum coordinates $\boldsymbol{k}_i$. As has been shown in refs. [3, 7, 68], the singularity condition is related to the question of intermediate states going on shell. Whenever a set of internal propagators can go on shell (i.e. can carry the total external energy and momentum while satisfying $p^2 = M^2$ for each propagator, with M denoting the appropriate propagator mass), then singularities arise in the loop summands. By contrast, if a given propagator never appears in an on-shell set, then the summand has a strip of analyticity in the spatial loop momenta, and the sum can be replaced with an integral up to neglected $e^{-\mu L}$ effects.

As is discussed in refs. [20, 95], both based on the more general discussion in ref. [117], the statement of the on-shell condition can be made more precise via time-ordered perturbation theory (TOPT). TOPT is a method for generating expressions from Feynman diagrams with all k_i^0 integrals already performed. Figure 3.3 shows an example, with each ordering of the vertices corresponding to a distinct term. For a given time ordering, one identifies all cuts between consecutive vertices, and then

[1] An alternative condition is that if $f(\boldsymbol{k})$ is smooth, i.e. infinitely differentiable along the real axis, then the sum-integral difference falls faster than any power of $1/L$.

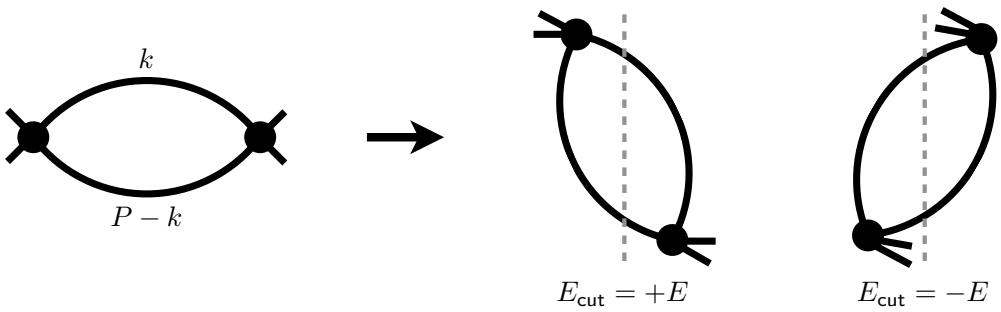

Figure 3.3 *Example application of time-ordered perturbation theory (TOPT) to a simple diagram. This can represent a contribution to $C_L(P)$ (in which the vertices are generated by the operators $\mathcal{A}(x)$ and $\mathcal{A}^\dagger(x)$) or a contribution to the finite-volume amplitude introduced in section 5.1 of Chapter 5. The diagram on the left has two possible time orderings of the vertices, shown on the right. The cuts between consecutive vertices are shown in blue. Defining the total energy flowing into the left diagram in a given frame as $E = P^0$, we note that the energy flowing across the cuts is $E_{\mathrm{cut}} = +E$ and $E_{\mathrm{cut}} = -E$ for the first and second diagram on the right, respectively. TOPT gives a framework to identify the singularities after k^0 integration. In the indicated case these occur at $E = \omega_N(\boldsymbol{k}) + \omega_N(\boldsymbol{P} - \boldsymbol{k})$ and $-E = \omega_N(\boldsymbol{k}) + \omega_N(\boldsymbol{P} - \boldsymbol{k})$.*

the TOPT rules generate a factor of

$$\frac{1}{E_{\text{cut}} - \sum_i \omega_{f(i)}(\boldsymbol{p}_i)}\,, \tag{3.29}$$

associated with each cut. Here E_{cut} is the total energy flow across the cut, defined as the sum of in-flowing p^0 components, from all external propagators, into all vertices to the left of (or "earlier than") the cut location. (See, for example, eq. (9.71) of ref. [117].) In the subtracted term, i labels the i propagator intersected by the cut; $\boldsymbol{p}_i$ is its corresponding momentum, and $f(i)$ is a flavor label. Note that $\sum_i \boldsymbol{p}_i = \boldsymbol{P}$ by total momentum conservation.

Provided $\hat{\mathcal{A}}(x)$ and $\hat{\mathcal{A}}(x)^\dagger$ are local in time, then any diagram contributing to $C_L(P)$ only has two vertices with external energy and momentum flow: $(E, \boldsymbol{P})$ flows in via $\hat{\mathcal{A}}(0)^\dagger$ and then back out via the Fourier transformed $\hat{\mathcal{A}}(x)$. Thus, $E_{\text{cut}} = \pm E$ or 0 for any cut in the diagram. In this way, the condition of an intermediate propagator set going on shell is simply reformulated as the condition that the TOPT pole is hit for some real-valued $\boldsymbol{p}_i$. If this is the case, then the summand is of the type of $g(\boldsymbol{k})$ in eq. (3.28), leading to power-like L scaling. If not, then the summand is like $f(\boldsymbol{k})$ in eq. (3.27) and the L dependence is neglected.

Restricting attention to the elastic scattering regime, $(2M_N)^2 < s < (2M_N + M_\pi)^2$, guarantees that only intermediate NN states can go on shell, implying that all sums arising in self-energy diagrams and Bethe-Salpeter kernels can be replaced by integrals. Thus, we can replace $B_L \to B$ and $\Delta_{N,L} \to \Delta_{N,i\epsilon}$, where the latter are understood as infinite-volume objects. Analogous replacements can also be made for the endcap factors. Conversely, power-like L dependence arises only from the sums over momenta in NN states and this is the motivation for the decomposition of eq. (2.38). We emphasize the parallel between $\circ_{\text{FV}}$ insertions leading to volume dependence in $C_L(P)$ and $\circ_{i\epsilon}$ insertions leading to imaginary contributions in the scattering amplitude. Both effects originate from poles in the spatial momentum dependence.

While these arguments guarantee that all contributions to $C_L(P)$ are safe, subtleties can arise when subdiagrams are considered in isolation. We come to this issue in section 3.2.6.

3.2.3 Reduction of the finite-volume two-particle loop

To continue the analysis of power-like L dependence in $C_L(P)$ for $(2M_N)^2 < s < (2M_N + M_\pi)^2$, we now analyze a single NN loop, arising at any location of any skeleton expansion term, as shown in figure 2.2. We introduce generic functions to the left and right of the loop, denoted $\mathcal{L}(P,k)$ and $\mathcal{R}^*(P,k)$ respectively.[2] These correspond to either endcap functions or Bethe-Salpeter kernels, and we omit other possible momentum arguments not relevant to the loop considered. The loop contribution can then be written as

$$\mathcal{L} \circ_{\mathrm{FV}} \mathcal{R}^\dagger = \frac{1}{2} \int \frac{dk^0}{2\pi} \frac{1}{L^3} \sum_{\boldsymbol{k}} \mathcal{L}(P,k)\, \Delta_{N,i\epsilon}(k)\, \Delta_{N,i\epsilon}(P-k)\, \mathcal{R}^*(P,k)\,. \tag{3.30}$$

The first step in simplifying the expression is to separate the propagator into the simple pole and a remainder

$$\Delta_{N,i\epsilon}(p) = \frac{i}{p^2 - M_N^2 + i\epsilon} + R_N(p)\,, \tag{3.31}$$

$$R_N(p) \equiv \frac{i}{p^2 - M_N^2 - \Pi_N(p^2) + i\epsilon} - \frac{i}{p^2 - M_N^2 + i\epsilon}\,. \tag{3.32}$$

The poles cancel in the second equation so that the remainder $R_N(p)$ is analytic in a neighbourhood around $p^2 = M_N^2$.[3]

Substituting this decomposition of each propagator, and denoting the sum of all terms containing at least one factor of R_N by $\mathcal{I}^{[1]}(P)$, we write

$$\mathcal{L} \circ_{\mathrm{FV}} \mathcal{R}^\dagger = \mathcal{I}^{[1]}(P) + \frac{1}{2} \int \frac{dk^0}{2\pi} \frac{1}{L^3} \sum_{\boldsymbol{k}} \frac{\mathcal{L}(P,k)\, i^2\, \mathcal{R}^*(P,k)}{[k^2 - M_N^2 + i\epsilon][(P-k)^2 - M_N^2 + i\epsilon]}\,. \tag{3.33}$$

The term $\mathcal{I}^{[1]}(P)$ is defined via summands that are analytic with respect to $|\boldsymbol{k}|$ in a strip including the real axis. Similar replacements will be made below and the superscript on $\mathcal{I}^{[i]}(P)$ will be incremented to indicate the change. In all cases, exponentially suppressed volume effects are being dropped.

[2] Here the * on $\mathcal{R}^*(P,k)$ indicates complex conjugation. This convention is useful when the functions represent the endcaps of a correlator constructed from an operator and its hermitian conjugate, as in eq. (2.34). In this case, $\mathcal{L}(P,k) = \mathcal{R}(P,k)$.

[3] This relies on the on-shell renormalisation scheme established after eq. (2.16) which sets M_N to be the pole mass and the residue to be unity.

Performing the integration over k^0 (closing the contour in the lower half of the complex plane) gives

$$\mathcal{L} \circ_{\mathrm{FV}} \mathcal{R}^\dagger = \mathcal{I}^{[2]}(P) + \sum_{\boldsymbol{k}} \frac{\mathcal{L}(P,k)\, i\, \mathcal{R}^*(P,k)}{2L^3 \cdot 2\omega_N(\boldsymbol{k})\big[(E-\omega_N(\boldsymbol{k}))^2 - \omega_N(\boldsymbol{P}-\boldsymbol{k})^2\big]}\bigg|_{k^0=\omega_N(\boldsymbol{k})} . \tag{3.34}$$

Note that, at this stage, k has been set on shell by $k^0 = \omega_N(\boldsymbol{k})$, but $P-k$ is itself not on shell, i.e. does not satisfy $(P-k)^2 = M_N^2$.

Additional contributions from the k^0 integral can be picked up from poles or branch cuts within $\mathcal{L}(P,k)$ and $\mathcal{R}^*(P,k)$, but these lead to analytic functions of $\boldsymbol{k}$ that can be absorbed into the remainder term via $\mathcal{I}^{[1]}(P) \to \mathcal{I}^{[2]}(P)$. This holds for all objects that can appear in place of $\mathcal{L}(P,k)$ and $\mathcal{R}^*(P,k)$, up to a caveat discussed in appendix B. The issue has to do with the distinction between t- and u-channel loops within kernels, defined according to the choice of momentum routing in the adjacent two-particle loops. The upshot is that it is always possible to find a routing for which $\mathcal{I}^{[2]}(P)$, $\mathcal{L}(P,k)$, and $\mathcal{R}^*(P,k)$ have the desired analyticity and exponentially suppressed volume dependence. This also holds for the t- and u-channel single-pion exchanges and for objects containing lower left-hand cuts and is demonstrated in section 3.2.6 below, together with appendix B.

Returning to eq. (3.34), we next decompose the functions $\mathcal{L}(P,k)$ and $\mathcal{R}^*(P,k)$, with on-shell $k = (\omega_N(\boldsymbol{k}), \boldsymbol{k})$, into spherical harmonics with respect to the direction of the three-momentum in the CM frame:

$$\mathcal{L}(P,k)\big|_{k^0=\omega_N(\boldsymbol{k})} \equiv \sqrt{4\pi}\, Y_{\ell m}(\hat{\boldsymbol{k}}^\star) |\boldsymbol{k}^\star|^\ell\, \widetilde{\mathcal{L}}_{\ell m}(P, |\boldsymbol{k}^\star|) , \tag{3.35}$$

$$\mathcal{R}^*(P,k)\big|_{k^0=\omega_N(\boldsymbol{k})} \equiv \sqrt{4\pi}\, Y^*_{\ell m}(\hat{\boldsymbol{k}}^\star) |\boldsymbol{k}^\star|^\ell\, \widetilde{\mathcal{R}}^*_{\ell m}(P, |\boldsymbol{k}^\star|) , \tag{3.36}$$

with sums over the indices ℓ, m left implicit. As before, the superscript $\star$ indicates the boost to the CM frame.

We include the factors of $|\boldsymbol{k}^\star|^\ell$ because $Y_{\ell m}(\hat{\boldsymbol{k}}^\star)$ without this factor is a singular function of $\boldsymbol{k}^\star$.[4] As the functions on the left-hand sides of eqs. (3.35) and

[4]For example

$$Y_{10}(\hat{\boldsymbol{k}}^\star) = \sqrt{\frac{3}{4\pi}}\, \frac{k_z^\star}{\sqrt{(k_x^\star)^2 + (k_y^\star)^2 + (k_z^\star)^2}} , \tag{3.37}$$

vanishes for $k_z^\star \to 0$ with fixed $(k_x^\star, k_y^\star)$ but can take on non-zero values if the origin is approached from a different direction.

(3.36) are non-singular, the coefficient of the spherical harmonic must vanish with the corresponding power of $|\boldsymbol{k}^\star|^\ell$. For the subsequent steps taken below, it is more convenient to separate out this scaling in our definition of $\widetilde{\mathcal{L}}_{\ell m}(P, |\boldsymbol{k}^\star|)$ and $\widetilde{\mathcal{R}}^*_{\ell m}(P, |\boldsymbol{k}^\star|)$ as we have done. The tilde notation denotes this rescaling, matching also the notation used in the last chapter.

It is also useful to introduce an index notation for the momenta. We find it more convenient to index with $\boldsymbol{k}^\star$ rather than $\boldsymbol{k}$. It is then understood that $\boldsymbol{k}^\star$ takes on a discrete set of allowed values inherited from $\boldsymbol{k} \in (2\pi/L)\mathbb{Z}^3$, via the boost of eq. (2.6). We write

$$\mathcal{L} \circ_{\mathrm{FV}} \mathcal{R}^\dagger = \mathcal{I}^{[3]}(P) + \widetilde{\mathcal{L}}_{\boldsymbol{k}^\star \ell m}(P)\, i S_{\boldsymbol{k}^\star \ell m, \boldsymbol{k}'^\star \ell' m'}(P, L)\, \widetilde{\mathcal{R}}^*_{\boldsymbol{k}'^\star \ell' m'}(P)\ , \tag{3.38}$$

where sums over all repeated indices (including momentum indices) are implied, and we have introduced the matrix

$$S_{\boldsymbol{k}^\star \ell m, \boldsymbol{k}'^\star \ell' m'}(P, L) = \frac{1}{2L^3} \frac{4\pi\, Y_{\ell m}(\hat{\boldsymbol{k}}^\star)\, Y^*_{\ell' m'}(\hat{\boldsymbol{k}}^\star)\, \delta_{\boldsymbol{k}^\star \boldsymbol{k}'^\star}\, |\boldsymbol{k}^\star|^{\ell+\ell'}\, H(\boldsymbol{k}^\star)}{4\omega_N(\boldsymbol{k}) \left[(k^\star_{\mathrm{os}})^2 - (\boldsymbol{k}^\star)^2\right]}\,. \tag{3.39}$$

A few manipulations are required to reach the form shown here from the preceding relations. These are detailed in appendix A.

We have also introduced a regulator function, $H(\boldsymbol{k}^\star)$, which must equal 1 whenever

$$(k^\star_{\mathrm{os}})^2 - (\boldsymbol{k}^\star)^2 = 0\,, \tag{3.40}$$

and should decay exponentially, with increasing $(\boldsymbol{k}^\star)^2$, to ensure that our final results are numerically tractable. The value of $1 - H(\boldsymbol{k}^\star)$ away from the pole (as well as a term resulting from the manipulations leading to eq. (3.39)) leads to a smooth summand that is absorbed by replacing $\mathcal{I}^{[2]}(P) \to \mathcal{I}^{[3]}(P)$, as shown.

One possible choice is the regulator used in ref. [7]

$$H(\boldsymbol{k}^\star) = \exp\Big(-\alpha\big[(\boldsymbol{k}^\star)^2 - (k^\star_{\mathrm{os}})^2\big]\Big)\,, \tag{3.41}$$

where $\alpha > 0$ should be chosen sufficiently small to not enhance the neglected volume dependence. Alternatively, one can make use of a piecewise definition of $H(\boldsymbol{k}^\star)$ that is identically zero above some cutoff, similar to that used in the relativistic field-theoretic three-particle quantization condition [20]. This type of function necessarily

has no strip of analyticity in the complex-$|\boldsymbol{k}^\star|$ plane and thus generically leads to neglected volume effects that are not exponentially suppressed, though still decaying faster than any power of $1/L$. In contrast to the three-particle formalism, in this application there is no reason to require the function to vanish identically, and we expect a function as in eq. (3.41) will be more useful. It may seem surprising here that $H(\boldsymbol{k}^\star) = 1$ is only required at $(\boldsymbol{k}^\star)^2 = (k^\star_{\text{os}})^2$ and not, for example, in the sub-threshold region where one encounters the t- and u-channel pion exchange poles. In a nutshell, this is valid because it leads to a correct representation of the singularities within $C_L(P)$ and the scattering amplitude.

Suppressing the indices, eq. (3.38) can be written in a compact matrix form

$$\mathcal{L} \circ_{\text{FV}} \mathcal{R}^\dagger = \mathcal{I}^{[3]}(P) + \widetilde{\mathcal{L}}(P)\, iS(P,L)\, \widetilde{\mathcal{R}}(P)^\dagger \,, \tag{3.42}$$

with $S(P,L)$ denoting the matrix with elements $S_{\boldsymbol{k}^\star \ell m; \boldsymbol{k}'^\star \ell' m'}(P,L)$, and $\widetilde{\mathcal{L}}(P)$ and $\widetilde{\mathcal{R}}(P)^\dagger$ denoting a row and column vector with components $\widetilde{\mathcal{L}}_{\boldsymbol{k}^\star \ell m}(P)$ and $\widetilde{\mathcal{R}}^*_{\boldsymbol{k}'^\star \ell' m'}(P)$, respectively. We also define the notation

$$\widetilde{\mathcal{L}} \circ_{\text{rm}} \widetilde{\mathcal{R}}^\dagger \equiv \mathcal{I}^{[3]}(P) \,, \tag{3.43}$$

for the remainder term, such that we can write the loop contribution as

$$\mathcal{L} \circ_{\text{FV}} \mathcal{R}^\dagger = \widetilde{\mathcal{L}} \left[\circ_{\text{rm}} + iS(P,L)\right] \widetilde{\mathcal{R}}^\dagger \,, \tag{3.44}$$

with $S(P,L)$ encoding the singular part of the summand and $\circ_{\text{rm}}$ the smooth part of the summand in the loop momentum sum. In a slight abuse of notation, we have dropped the arguments on $\widetilde{\mathcal{L}}(P)$ and $\mathcal{R}^\dagger(P)$ multiplying $S(P,L)$ so that we can group the remainder term, $\circ_{\text{rm}}$, with the singular factor as shown.

Our result for the contribution of a generic two-particle finite-volume loop can be applied to all loops in the skeleton expansion of eq. (3.44), provided that the momentum routing issue of appendix B is handled correctly. Note, however, that the factors multiplying $S(P,L)$ in eq. (3.44) still depend on off-shell values of $P - k$. In the next section, we discuss how to eliminate this issue. We highlight this intermediate result because partial off-shellness will be of great importance for treating the left-hand cuts, as detailed in sections 3.2.6 and 3.2.7.

3.2.4 On-shell intermediate states

In the elastic regime, $(2M_N)^2 < s < (2M_N + M_\pi)^2$, the singularity in the summand of the loop contribution, expressed compactly in eqs. (3.39) and (3.42), corresponds to the on-shell condition for the intermediate NN state. In terms of quantities in the finite-volume frame, this condition is $E = \omega_N(\boldsymbol{k}) + \omega_N(\boldsymbol{P} - \boldsymbol{k})$, and in the CM frame, this reduces to $|\boldsymbol{k}^\star| = k^\star_{\rm os}$. Due to the singularity, the L-dependence of $\widetilde{\mathcal{L}}(P)\, S(P,L)\, \widetilde{\mathcal{R}}(P)^\dagger$ is dominated by the left and right functions evaluated at these on-shell kinematics.

To express the on-shell-value dominance more explicitly, define

$$\widetilde{\mathcal{L}}^{\rm os}_{\ell m}(P) \equiv \widetilde{\mathcal{L}}_{\ell m}(P, k^\star_{\rm os})\,, \tag{3.45}$$

$$\widetilde{\mathcal{R}}^{{\rm os}*}_{\ell m}(P) \equiv \widetilde{\mathcal{R}}^*_{\ell m}(P, k^\star_{\rm os})\,, \tag{3.46}$$

and make the straightforward separation

$$\begin{aligned}\widetilde{\mathcal{L}}(P)\, S(P,L)\, \widetilde{\mathcal{R}}(P)^\dagger = \widetilde{\mathcal{L}}^{\rm os}(P)\, \xi\, S(P,L)\, \xi^\dagger\, \widetilde{\mathcal{R}}^{\rm os}(P)^\dagger \\ + \Big[\widetilde{\mathcal{L}}(P)\, S(P,L)\, \widetilde{\mathcal{R}}(P)^\dagger - \widetilde{\mathcal{L}}^{\rm os}(P)\, \xi\, S(P,L)\, \xi^\dagger\, \widetilde{\mathcal{R}}^{\rm os}(P)^\dagger\Big]\,.\end{aligned} \tag{3.47}$$

On the right-hand side we have introduced the trivial row vector ξ in the momentum index space, with elements $\xi_{\boldsymbol{k}^\star} = 1$, and the vectors $\mathcal{L}^{\rm os}(P)$ and $\mathcal{R}^{\rm os}(P)^\dagger$ in angular momentum index space, with components $\widetilde{\mathcal{L}}^{\rm os}_{\ell m}(P)$ and $\mathcal{R}^{{\rm os}*}_{\ell m}(P)$. The vectors ξ and $\xi^\dagger$ contract only with the momentum indices of $S(P,L)$, while $\widetilde{\mathcal{L}}^{\rm os}(P)$ and $\widetilde{\mathcal{R}}^{\rm os}(P)^\dagger$ contract with the angular momentum indices

$$\widetilde{\mathcal{L}}^{\rm os}(P)\, \xi\, S(P,L)\, \xi^\dagger \widetilde{\mathcal{R}}^{\rm os}(P)^\dagger = \widetilde{\mathcal{L}}^{\rm os}_{\ell m}(P)\, \xi_{\boldsymbol{k}^\star}\, S_{\boldsymbol{k}^\star \ell m; \boldsymbol{k}'^\star \ell' m'}(P,L)\, \xi_{\boldsymbol{k}'^\star} \widetilde{\mathcal{R}}^{{\rm os}*}_{\ell' m'}(P)\,, \tag{3.48}$$

$$= \widetilde{\mathcal{L}}^{\rm os}_{\ell m}(P) \Bigg(\sum_{\boldsymbol{k}^\star,\, \boldsymbol{k}'^\star} S_{\boldsymbol{k}^\star \ell m; \boldsymbol{k}'^\star \ell' m'}(P,L) \Bigg) \widetilde{\mathcal{R}}^{{\rm os}*}_{\ell' m'}(P)\,. \tag{3.49}$$

We note that the square-bracketed term in eq. (3.47) represents the sum over an analytic summand, with the singularities within $S(P,L)$ cancelling in the difference between terms. As a result, the sum can again be replaced with an integral up to exponentially suppressed terms, and the latter can be absorbed by replacing

$\mathcal{I}^{[3]}(P) \to \mathcal{I}^{[4]}(P)$. The loop contribution can thus be written as

$$\mathcal{L} \circ_{\mathrm{FV}} \mathcal{R}^\dagger = \mathcal{I}^{[4]}(P) + \widetilde{\mathcal{L}}^{\mathrm{os}}(P)\, \xi\, iS(P,L)\, \xi^\dagger\, \widetilde{\mathcal{R}}^{\mathrm{os}}(P)^\dagger \,. \tag{3.50}$$

Provided we are in the elastic regime, this expression is always valid up to exponentially suppressed L-dependence absorbed in $\mathcal{I}^{[4]}(P)$. However, in the case of a nearby left-hand cut present in the on-shell projected left and right functions, the scale μ in the $e^{-\mu L}$ scaling is set by the cut and can be significantly smaller than M_π such that the neglected volume effects can be numerically large. The situation is more dramatic in the sub-threshold regime where the on-shell projection can lead to neglected power-like effects, thus leading to a quantization condition that is no longer valid. In both cases the generalized quantization condition presented in section 3.2.8 is required.

In summary, on-shell dominance allows one to derive a simpler form for the loop with the L-dependence contained completely in $\xi\, S(P,L)\, \xi^\dagger$, provided the left and right functions can be safely put on-shell. We now consider the effect of analytically continuing below threshold, first on the $S(P,L)$ factor (in the next subsection) and then on the Bethe-Salpeter kernel (in section 3.2.6).

3.2.5 sub-threshold regime

The skeleton expansion for the correlator is applicable in the sub-threshold region $s < (2M_N)^2$, and employing the cutting rules of TOPT allows us to conclude that no intermediate states can go on-shell. Consequently, the summands of spatial loop momenta have the required strips of analyticity for all finite-volume effects to be exponentially suppressed:

$$C_L(P) - C_\infty(P) = \mathcal{O}(e^{-\mu L}) \,, \qquad \text{for } s < (2M_N)^2 \,, \tag{3.51}$$

for some, potentially s-dependent scale, μ. Here $C_\infty(P)$ is the correlator evaluated in infinite volume, defined through the same diagrammatic series as $C_L(P)$, but with integrated loops. Because the relation is given below threshold, no pole prescription is required. Alternatively, the definition is equivalent to the analytic continuation of the $i\epsilon$ prescription below threshold, on the physical Riemann sheet.

To make eq. (3.51) more concrete, we return to the partially off-shell loop decomposition of eq. (3.42). For $(2M_N)^2 < s < (2M_N + M_\pi)^2$, we have argued

that the terms generating $\mathcal{I}^{[3]}(P)$ have negligible exponentially suppressed scaling, while the second term, $\widetilde{\mathcal{L}}(P)\, S(P,L)\, \widetilde{\mathcal{R}}(P)^\dagger$, has power-like L dependence. Below threshold, the latter term is given by

$$\widetilde{\mathcal{L}}(P)\, S(P,L)\, \widetilde{\mathcal{R}}(P)^\dagger = \\ -\frac{1}{2}\frac{1}{L^3}\sum_{\boldsymbol{k}} \widetilde{\mathcal{L}}_{\ell m}(P,|\boldsymbol{k}^\star|)\frac{4\pi\, Y_{\ell m}(\hat{\boldsymbol{k}}^\star)Y^*_{\ell' m'}(\hat{\boldsymbol{k}}^\star)\,|\boldsymbol{k}^\star|^{\ell+\ell'} H(\boldsymbol{k}^\star)}{4\omega_N(\boldsymbol{k})\left[\kappa(s)^2+(\boldsymbol{k}^\star)^2\right]}\widetilde{\mathcal{R}}^*_{\ell m}(P,|\boldsymbol{k}^\star|)\,, \quad (3.52)$$

where we have introduced the sub-threshold binding momentum

$$\kappa(s) = \sqrt{M_N^2 - s/4}\,, \quad (3.53)$$

and the functions $\widetilde{\mathcal{L}}_{\ell m}(P,|\boldsymbol{k}^\star|)$ and $\widetilde{\mathcal{R}}^*_{\ell m}(P,|\boldsymbol{k}^\star|)$ are defined as analytic continuations in the energy of the above-threshold objects. In words, the above-threshold pole at $|\boldsymbol{k}^\star| = k^\star_{\text{os}}$ moves to the complex plane at $\pm i\kappa(s)$ and the function is analytic for $-\kappa(s) < \text{Im}(|\boldsymbol{k}^\star|) < \kappa(s)$. This leads to volume effects satisfying

$$\left[1 - \lim_{L\to\infty}\right]\widetilde{\mathcal{L}}(P)\, S(P,L)\, \widetilde{\mathcal{R}}(P)^\dagger = \mathcal{O}(e^{-\kappa(s)L})\,, \qquad \text{for } s < (2M_N)^2\,, \quad (3.54)$$

where we have used that the $L\to\infty$ limit is well-defined without a pole prescription for $s < (2M_N)^2$.

A key point for the derivation of the sub-threshold quantization condition below is that it is only well motivated if a hierarchy exists between the size of volume effects we include (within $\widetilde{\mathcal{L}}(P)\, S(P,L)\, \widetilde{\mathcal{R}}(P)^\dagger$) and those we neglect (within $\mathcal{I}^{[3]}(P)$). Roughly, this holds provided the binding momentum is below the pion mass: $\kappa(s) < M_\pi \implies e^{-M_\pi L} < e^{-\kappa(s)L}$.

The partially off-shell form of eq. (3.52) is valid, even for energies overlapping the left-hand cut. However, the subsequent step of $\widetilde{\mathcal{L}}_{\ell m}(P,k^\star_{\text{os}}) \to \widetilde{\mathcal{L}}^{\text{os}}_{\ell m}(P)$ and $\widetilde{\mathcal{R}}^*_{\ell m}(P,k^\star_{\text{os}}) \to \widetilde{\mathcal{R}}^{\text{os}*}_{\ell m}(P)$, described in section 3.2.4, fails in this region, as we now describe.

3.2.6 Analytic structure of the Bethe-Salpeter kernel

The infinite-volume Bethe-Salpeter kernel $B(P,p,p')$, which we defined in section 2.1.1 (see figure 2.1) as the sum of all amputated two-to-two diagrams that

are two-particle irreducible in the s-channel. In our analysis of the correlator $C_L(P)$ in sections 3.2.3–3.2.5, this kernel can appear as the left or right function of the finite-volume loops, in different versions with various on- and off-shell kinematics. This is of great importance as the nature and location of the t- and u-channel singularities depend on the specific configuration of these kernels.

We identify five different configurations of relevance:

1. **Most general case**: all external four-momenta p, $P-p$, p', $P-p'$ are off shell;

2. **Partially off-shell**: two of the external four-momenta, $p \equiv (p^0, \boldsymbol{p})$ and $p' \equiv (p'^0, \boldsymbol{p}')$, are placed on-shell, with $p^0 = \omega_N(\boldsymbol{p})$ and $p'^0 = \omega_N(\boldsymbol{p}')$ respectively, and the two remaining four-momenta are off-shell, leaving P, $\boldsymbol{p}$ and $\boldsymbol{p}'$ as the only free arguments;

3. **Fully on-shell**: as in Case 2, but with the remaining external four-momenta, $(P-p)$ and $(P-p')$, also on-shell, constraining the magnitude of CM momenta $|\boldsymbol{p}^\star| = |\boldsymbol{p}'^\star| = k^\star_{\text{os}}$ and leaving P, $\hat{\boldsymbol{p}}^\star$ and $\hat{\boldsymbol{p}}'^\star$ as free arguments;

4. **Partially off-shell, angular momentum projected**: Case 2 above, with $\hat{\boldsymbol{p}}^\star$ and $\hat{\boldsymbol{p}}'^\star$ integrated with spherical harmonics to derive projected components (labelled by $\ell m, \ell' m'$) which are functions of P, $|\boldsymbol{p}^\star|$ and $|\boldsymbol{p}'^\star|$;

5. **Fully on-shell, angular momentum projected**: Case 3, projected in the same way as Case 4. In this case the components (again labelled by $\ell m, \ell' m'$) are functions only of Mandelstam s.

The most general case (Case 1) appears in our expression for the correlator in eq. (2.38). The partially off-shell version (Case 2) then arises from performing the k^0 contour integration leading to eq. (3.34) while the angular momentum projection (Case 4) arises in eqs. (3.35) and (3.36). Finally, the fully on-shell and angular-momentum projected kernel (Case 5) arises from the separation discussed in subsection 3.2.4. Case 3, the on-shell but not-projected kernel, has not appeared in our analysis but is useful as an intermediate step in understanding the analytic structure of its angular-momentum-projected counterpart.

The analytic continuation of the on-shell kernel below threshold has common features with that of the full scattering amplitude, discussed in section 3.1 and

shown in figure 3.2(a). In particular, the single t- and u-channel pion exchanges are included in the kernel and give poles at $t = M_\pi^2$ and $u = M_\pi^2$. Similarly, multiple pion exchanges, also included in the kernel, lead to branch cuts.

It is instructive to study the on-shell kernel as a function of Mandelstam s at fixed CM scattering angle $\theta^\star$. The single exchange poles lie at

$$s = 4M_N^2 - \frac{M_\pi^2}{\sin^2(\theta^\star/2)} \qquad (t\text{-channel pole}), \tag{3.55}$$

$$s = 4M_N^2 - \frac{M_\pi^2}{\cos^2(\theta^\star/2)} \qquad (u\text{-channel pole}). \tag{3.56}$$

For both channels, the pole position varies between $s = -\infty$ and $s = 4M_N^2 - M_\pi^2$ as $\theta^\star$ is scanned from 0 to π. The integration required to project to definite angular momentum generates a branch cut along $s \in (-\infty,\ 4M_N^2 - M_\pi^2]$. The multiple meson exchanges lead to cuts in both the fixed $\theta^\star$ and the angular-momentum-projected Bethe-Salpeter kernel. For the latter, the corresponding branch points sit at $s = 4M_N^2 - (nM_\pi)^2$ for each $n \geq 2$.

The remainder of this subsection is dedicated to two important, but somewhat technical points. First, we argue that partially off-shell Bethe-Salpeter kernels (i.e. those with the kinematics of Cases 2 and 4) have no t-channel singularities. That is, provided that the spatial momenta $\boldsymbol{p}$ and $\boldsymbol{p}'$ are real, the partial off-shellness removes the t-channel branch cut. Second, we explain that the story is more subtle for the u-channel singularities, but can be addressed with a trick based on the invariance of Feynman diagrams under rerouting of internal loop momenta.

To understand the first point, consider the single-pion t-channel diagram in isolation. This is given in eq. (3.7) for the infinite-volume case, and the finite-volume analogue can be written as

$$D_{t,L}(P, p, p') \equiv G_L(p, p')\ \Delta_{\pi,L}(p' - p)\ G_L(P - p, P - p'), \tag{3.57}$$

where we have also introduced finite-volume versions of the $NN\pi$ form factors and the pion propagator. As discussed above, the L-dependence within $G_L(p, p')$ and $\Delta_{\pi,L}(p' - p)$ is exponentially suppressed as long as the energy and momentum flowing through the diagrams is below the lowest multi-particle threshold. We can then additionally separate out the singularity from a remainder, as in

eqs. (3.12) and (3.14), to write

$$ig^2\mathcal{T}(P,p,p') = -\frac{ig^2}{\big(\omega_N(\boldsymbol{p}) - \omega_N(\boldsymbol{p}')\big)^2 - (\boldsymbol{p}-\boldsymbol{p}')^2 - M_\pi^2 + i\epsilon} = -\frac{ig^2}{t - M_\pi^2 + i\epsilon}\,, \tag{3.58}$$

where we have already applied the partially off-shell kinematics of Case 2. As in the infinite-volume section, M_π is the physical pion mass and g is the residue of poles in the full scattering amplitude. This is the same residue as in the Bethe-Salpeter kernel as follows from the fact that the pole arises from the single-Bethe-Salpeter term of the skeleton expansion.

The first key observation for eq. (3.58) is that it simply has no s dependence, and therefore cannot generate any singularities in the complex s plane. In addition to this, the momenta entering the t-channel exchange here guarantee that $t < 0$ and thus that the singularity at $t = M_\pi^2$ is not encountered. This, in turn, implies that no power-like finite-volume effects arise in $C_L(P)$ due to this contribution. We will argue that this statement generalizes to any diagram that can be expressed as some number of t-channel exchanges.

We can also analyze the single t-channel exchange using TOPT. Following the rules described in ref. [117], we note that the diagram has two vertices and one internal propagator (see the left diagram of figure 3.1). For Case 2 kinematics, momentum $p - p' = \big(\omega_N(\boldsymbol{p}) - \omega_N(\boldsymbol{p}'), \boldsymbol{p} - \boldsymbol{p}'\big)$ flows into one vertex and out of the other. Thus, the energy flowing across the cut is given by $E_{\text{cut}} = \omega_N(\boldsymbol{p}) - \omega_N(\boldsymbol{p}')$ for one of the two time-orderings, and by $E_{\text{cut}} = -\omega_N(\boldsymbol{p}) + \omega_N(\boldsymbol{p}')$ for the other. Combining with the single pion propagator intersected by each cut, we expect the denominators $\omega_N(\boldsymbol{p}) - \omega_N(\boldsymbol{p}') - \omega_\pi(\boldsymbol{p} - \boldsymbol{p}')$ and $-\omega_N(\boldsymbol{p}) + \omega_N(\boldsymbol{p}') - \omega_\pi(\boldsymbol{p} - \boldsymbol{p}')$ to appear. These combine with other factors in the TOPT construction to reproduce eq. (3.58), which can be rewritten as

$$ig^2\mathcal{T}(P,p,p') = -\frac{ig^2}{2\omega_\pi(\boldsymbol{p}-\boldsymbol{p}')}\left[\frac{1}{\omega_N(\boldsymbol{p}) - \omega_N(\boldsymbol{p}') - \omega_\pi(\boldsymbol{p}-\boldsymbol{p}') + i\epsilon} + \frac{1}{-\omega_N(\boldsymbol{p}) + \omega_N(\boldsymbol{p}') - \omega_\pi(\boldsymbol{p}-\boldsymbol{p}') + i\epsilon}\right]. \tag{3.59}$$

More generally, for any diagram that contributes to the Bethe-Salpeter kernel, we can enumerate all time orderings and then identify the (possibly empty) set of cuts

for which $E_{\text{cut}} = \pm\big(\omega_N(\boldsymbol{p}) - \omega_N(\boldsymbol{p}')\big)$. Each will lead to a denominator of the form

$$E_{\text{cut}} - \sum_i \omega_{f(i)}(\boldsymbol{p}_i) = \pm\big(\omega_N(\boldsymbol{p}) - \omega_N(\boldsymbol{p}')\big) - \sum_i \omega_{f(i)}(\boldsymbol{p}_i)\,, \tag{3.60}$$

where the sum runs over all internal cut propagators, $f(i)$ is either N or π, and $\sum_i \boldsymbol{p}_i = \pm(\boldsymbol{p} - \boldsymbol{p}')$, with the sign matching that of E_{cut}. For these cases, no singularity is encountered for real three-momenta, since it would correspond to the decay of a nucleon into a multi-particle state, which is always forbidden either by kinematics or by the conserved quantum numbers.

Note the contrast of the discussion here to that in section 3.2.2 and refs. [20, 95]. If we are only interested in the singularities of the full correlator, $C_L(P)$, then the cuts always satisfy $E_{\text{cut}} = \pm E, 0$. However, if we are also concerned with singularities of the Bethe-Salpeter kernel itself, for various choices of external four-momenta, then it is necessary to revisit TOPT at the level of diagrams with four-external legs (as in figure 3.1). Then new energies can flow across the cuts, such as the case with $E_{\text{cut}} = \pm\big(\omega_N(\boldsymbol{p}) - \omega_N(\boldsymbol{p}')\big)$ considered above. If this were the only possibility, then the Bethe-Salpeter kernel would have no singularities on the real s-axis for $p = (\omega_N(\boldsymbol{p}), \boldsymbol{p})$ and $p' = (\omega_N(\boldsymbol{p}'), \boldsymbol{p}')$.

The second and final message of this section is that the u-channel exchanges, such as the right diagram in figure 3.1, are more subtle. Such diagrams have singularities when evaluated with Case 2 kinematics, i.e. with $k = (\omega_N(\boldsymbol{k}), \boldsymbol{k})$, but with $P - k$ off shell. These manifest in TOPT from orderings with the vertices that have inflowing p and outflowing $P - p'$ both appearing either to the left or to the right of a particular cut. Then one has $E_{\text{cut}} = \pm\big(\omega_N(\boldsymbol{p}) - E + \omega_N(\boldsymbol{p}')\big)$ and, as a result, the denominator has the form

$$E_{\text{cut}} - \sum_i \omega_{f(i)}(\boldsymbol{p}_i) = \pm\big(\omega_N(\boldsymbol{p}) - E + \omega_N(\boldsymbol{p}')\big) - \sum_i \omega_{f(i)}(\boldsymbol{p}_i)\,. \tag{3.61}$$

As we discuss in more detail in appendix B, this can lead to singularities in the partly off-shell Bethe-Salpeter kernel that do not correspond to singularities of $C_L(P)$. This is an artefact of the partial off-shellness and can be treated most easily by defining an auxiliary Bethe-Salpeter kernel, denoted by $B^{\mathbb{T}}(P, p, p')$, in which all u-channel exchanges are replaced by t-channel exchanges.

The explicit construction of this kernel is given in appendix B, so we do not provide the details here but only emphasize three key properties. Firstly, $B^{\mathbb{T}}(P, p, p')$, like

$\mathcal{T}(P,p,p')$ in eq. (3.58), has no singularities on the real s-axis when kinematics are assigned in the partially off-shell manner of Case 2 and Case 4 (the angular-momentum projected counterpart). This follows from the discussion for a generic t-channel diagram above and is detailed in appendix B. Second, $B^{\mathbb{T}}(P,p,p')$ does have singularities for fully on-shell (Case 5) kinematics, in the sub-threshold regime. For $(2M_N)^2-(2M_\pi)^2<s<(2M_N+M_\pi)^2$, these singularities are completely captured by $\mathcal{T}(P,p,p')$. Third, the auxiliary kernel is equal to the original Bethe-Salpeter kernel after symmetrisation:

$$B(P,p,p')=\frac{1}{2}\Big[B^{\mathbb{T}}(P,p,p')+B^{\mathbb{T}}(P,p,P-p')\Big]\,. \tag{3.62}$$

We now return to the loop-reduction equations, eqs. (3.42) and (3.50), recalling that while the first depends partially off-shell version: $\widetilde{\mathcal{L}}(P)S(P,L)\widetilde{\mathcal{R}}(P)^\dagger$, the second depends on the fully on-shell counterpart: $\widetilde{\mathcal{L}}^{\text{os}}(P)\xi S(P,L)\xi^\dagger\widetilde{\mathcal{R}}^{\text{os}}(P)^\dagger$. If the left or right function is taken to be a $B^{\mathbb{T}}$ insertion then we see the sub-threshold cut is absent from the first version it is present in the second, and therefore also present in the remainder term $\mathcal{I}^{[4]}(P)$. Neglecting this singularity in the remainder invalidates the subsequent steps in the standard derivation of a quantization condition.

To address the issue caused by $|\boldsymbol{k}^\star|\to k^\star_{\text{os}}$ on the cut, we introduce

$$\overline{B}^{\,\mathbb{T}}(P,p,p')\equiv B^{\mathbb{T}}(P,p,p')-2g^2\mathcal{T}(P,p,p')\,. \tag{3.63}$$

By construction, this does not contain single-exchange poles, and it is safe to perform the angular momentum projections and set the arguments on shell. Each partial-wave amplitude of this kernel is then a function of s with an analytic strip along the real axis for $s>(2M_N)^2-(2M_\pi)^2$. We cannot do the same for $\mathcal{T}(P,p,p')$ and thus reach a new quantization condition by keeping this party off-shell, as we explain in the next subsection.

Before turning to this, it is useful to define a subtracted version of the full Bethe-Salpeter kernel

$$\overline{B}(P,p,p')\equiv B(P,p,p')-g^2\mathcal{E}(P,p,p')\,, \tag{3.64}$$

where $\mathcal{E}(P,p,p')$ is the sum of the t- and u-channel single-pion exchanges

$$\mathcal{E}(P,p,p')\equiv\mathcal{T}(P,p,p')+\mathcal{U}(P,p,p')\,, \tag{3.65}$$

and $\mathcal{U}(P,p,p')$ is defined in eq. (3.15). A symmetrization relation holds between the subtracted kernels, directly inherited from the unsubtracted cases

$$\overline{B}(P,p,p') = \frac{1}{2}\Big[\overline{B}^{\,\mathbb{T}}(P,p,p') + \overline{B}^{\,\mathbb{T}}(P,p,P-p')\Big]\,. \tag{3.66}$$

3.2.7 Full decomposition of the finite-volume correlator

We are finally in a position to put together the results of the previous sections into the final derivation. Recalling the expression for the finite-volume correlator, eq. (2.38), and substituting the separation of the kernel introduced in eq. (3.64) above, we reach

$$C_L(P) = C^{(0)}(P) + \sum_{n=0}^{\infty} \mathcal{A} \circ_{\mathrm{FV}} \left[\left(i\overline{B} + ig^2\mathcal{E}\right) \circ_{\mathrm{FV}}\right]^n \mathcal{A}^\dagger\,, \tag{3.67}$$

$$= C^{(0)}(P) + \sum_{n=0}^{\infty} \mathcal{A} \circ_{\mathrm{FV}} \left[\left(i\overline{B}^{\,\mathbb{T}} + 2ig^2\mathcal{T}\right) \circ_{\mathrm{FV}}\right]^n \mathcal{A}^\dagger\,. \tag{3.68}$$

Here and in the following we drop the L subscripts of objects (such as $\mathcal{A}_L$) that are known to have exponentially suppressed volume dependence. Since the loops and the endcaps are exchange-symmetric, we have noted that both separations can be substituted for the Bethe-Salpeter kernel.

To further reduce this expression, consider a generic $\mathcal{T}$ factor with a finite-volume loop on both sides of it. In each loop, the contour integration leading to eq. (3.34) places one of the two momenta on shell. The resulting object is (cf. Case 2):

$$\mathcal{T}(P,p,p')\Big|_{\substack{p^0=\omega_N(\boldsymbol{p}),\\ p'^0=\omega_N(\boldsymbol{p}')}} = \frac{1}{2\omega_N(\boldsymbol{p}^\star)\omega_N(\boldsymbol{p}'^\star) - 2|\boldsymbol{p}^\star||\boldsymbol{p}'^\star|\cos\theta^\star - 2M_N^2 + M_\pi^2 - i\epsilon}\,. \tag{3.69}$$

This quantity has a strip of analyticity about the real-axis in the $|\boldsymbol{p}^\star|$ and $|\boldsymbol{p}'^\star|$ complex planes.[5] As a result, the loop separation identity of eq. (3.44), $\circ_{\mathrm{FV}} = \circ_{\mathrm{rm}} + iS(P,L)$, can be applied to two-particle loops involving $\mathcal{T}$ exchanges, and thus to all finite-volume loops appearing in (3.68). Note that there is a slight abuse of

[5] The contour integration also encircles the poles in $\mathcal{T}(P,p,p')$ itself, but this is not an issue as it simply leads to an $NN\pi$ intermediate state pole, which is above the elastic region, giving a smooth summand contribution that can be absorbed in the definition of $\mathcal{I}^{[2]}$ in eq. (3.34).

notation here and in the following pages, as the iS block is applied to harmonics-projected objects, while $\circ_{\rm rm}$ is not. Making the substitution, we reach

$$C_L(P) = C^{(0)}(P) + \sum_{n=0}^{\infty} \mathcal{A}\big[\circ_{\rm rm} + iS(P,L)\big]\Big[\big(i\overline{B}^{\,\mathbb{T}} + 2ig^2\mathcal{T}\big)\,\big[\circ_{\rm rm} + iS(P,L)\big]\Big]^n \mathcal{A}^\dagger\,. \tag{3.70}$$

Next, we rearrange the series by $S(P,L)$ insertions to find

$$C_L(P) = \mathcal{I}_C^{[1]}(P) + \sum_{n=0}^{\infty} A^{[1]}(P)\, iS(P,L)\Big[\big(i\overline{\mathcal{K}}^{[1]}(P) + 2ig^2\mathcal{T}(P)\big)\, iS(P,L)\Big]^n A^{[1]\dagger}(P)\,, \tag{3.71}$$

where all $\circ_{\rm rm}$ operations are absorbed into the four new L-independent quantities:

$$\mathcal{I}_C^{[1]}(P) = C^{(0)}(P) + \sum_{n=0}^{\infty} \mathcal{A} \circ_{\rm rm} \Big[\big(i\overline{B}^{\,\mathbb{T}} + 2ig^2\mathcal{T}\big) \circ_{\rm rm}\Big]^n \mathcal{A}^\dagger\,, \tag{3.72}$$

$$A^{[1]}(P) = \sum_{n=0}^{\infty} \mathcal{A}\Big[\circ_{\rm rm}\big(i\overline{B}^{\,\mathbb{T}} + 2ig^2\mathcal{T}\big)\Big]^n, \tag{3.73}$$

$$A^{[1]\dagger}(P) = \sum_{n=0}^{\infty} \Big[\big(i\overline{B}^{\,\mathbb{T}} + 2ig^2\mathcal{T}\big) \circ_{\rm rm}\Big]^n \mathcal{A}^\dagger\,, \tag{3.74}$$

$$i\overline{\mathcal{K}}^{[1]}(P) = \sum_{n=0}^{\infty} \Big[\big(i\overline{B}^{\,\mathbb{T}} + 2ig^2\mathcal{T}\big) \circ_{\rm rm}\Big]^n \big(i\overline{B}^{\,\mathbb{T}} + 2ig^2\mathcal{T}\big) - 2ig^2\mathcal{T}\,. \tag{3.75}$$

Here the $^{[1]}$ superscripts are used, as in section 3.2.3, to indicate intermediate quantities.

In contrast to eq. (3.70), in eq. (3.71) the integral operator does not appear explicitly. All factors are vectors or matrices on the $\boldsymbol{k}^\star\ell m$ space, multiplied with indices contracted in the usual way. In particular, $\mathcal{T}(P)$ is defined from the projection of $\mathcal{T}(P,p,p')$, as defined in eq. (3.69), to definite angular momentum [see also eq. (3.17)]:

$$\mathcal{T}(P,p,p')\Big|_{\substack{p^0=\omega_N(\boldsymbol{p}),\\ p'^0=\omega_N(\boldsymbol{p}')}} \equiv 4\pi\,|\boldsymbol{p}^\star|^\ell\, Y^*_{\ell m}(\hat{\boldsymbol{p}}^\star)\,\mathcal{T}_{\ell m,\ell' m'}(P,|\boldsymbol{p}^\star|,|\boldsymbol{p}'^\star|)\,|\boldsymbol{p}'^\star|^{\ell'}\, Y_{\ell' m'}(\hat{\boldsymbol{p}}'^\star)\,. \tag{3.76}$$

This leads us to define

$$\mathcal{T}_{\boldsymbol{k}^\star\ell m,\boldsymbol{k}'^\star\ell' m'}(P) = \mathcal{T}_{\ell m,\ell' m'}(P,|\boldsymbol{k}^\star|,|\boldsymbol{k}'^\star|)\,. \tag{3.77}$$

It is straightforward to work out expressions for particular angular-momentum components. The S-wave result, for example, is given by

$$\mathcal{T}_{\boldsymbol{k}^\star 00,\boldsymbol{k}'^\star 00}(P) = \frac{1}{4|\boldsymbol{k}^\star||\boldsymbol{k}'^\star|} \log\left(\frac{2\omega_N(\boldsymbol{k}^\star)\omega_N(\boldsymbol{k}'^\star) + 2|\boldsymbol{k}^\star||\boldsymbol{k}'^\star| - 2M_N^2 + M_\pi^2 - i\epsilon}{2\omega_N(\boldsymbol{k}^\star)\omega_N(\boldsymbol{k}'^\star) - 2|\boldsymbol{k}^\star||\boldsymbol{k}'^\star| - 2M_N^2 + M_\pi^2 - i\epsilon}\right), \tag{3.78}$$

which matches eq. (3.21) when we set $|\boldsymbol{k}^\star|$ and $|\boldsymbol{k}'^\star|$ to their complex, sub-threshold on-shell values.

The final step is to note that all insertions of $A^{[1]}(P)$, $\overline{\mathcal{K}}^{[1]}(P)$, and $A^{[1]\dagger}(P)$ can be set on shell, as described in sections 3.2.4 and 3.2.5. This requires a complicated set of redefinitions for the L-independent quantities, as detailed in appendix C. The resulting expression is

$$\begin{aligned} C_L(P) &= \mathcal{I}_C(P) \\ &+ \sum_{n=0}^{\infty} A^{\text{os}}(P)\,\xi\, iS(P,L)\left[\left(\xi^\dagger\, i\overline{\mathcal{K}}^{\text{os}}(P)\,\xi + 2ig^2\mathcal{T}(P)\right) iS(P,L)\right]^n \xi^\dagger\, A^{\text{os}}(P)^\dagger\,, \end{aligned} \tag{3.79}$$

where $\mathcal{I}_C(P)$, $A^{\text{os}}(P)$, $A^{\text{os}}(P)$, and $\overline{\mathcal{K}}^{\text{os}}(P)$, yet another set of infinite-volume quantities, are the final objects entering our decomposition of $C_L(P)$. Their detailed definitions are given in appendix C where we also prove eq. (3.79). Note that the definitions are not particularly relevant to the main derivation, since all quantities besides $\overline{\mathcal{K}}^{\text{os}}(P)$ do not appear in the final result. The latter is more usefully defined through its relation to the scattering amplitude, which we derive in Chapter 5. One crucial point, also addressed in appendix C, is that the asymmetry from $\overline{B}^{\,\mathbb{T}}$ is removed at this stage so that $\overline{\mathcal{K}}^{\text{os}}(P)$ is defined with the same exchange symmetry as the scattering amplitude.

Summing the geometric series in eq. (3.79), we finally obtain

$$C_L(P) = \mathcal{I}_C(P) + A^{\text{os}}(P)\xi \frac{i}{S(P,L)^{-1} + \xi^\dagger\,\overline{\mathcal{K}}^{\text{os}}(P)\,\xi + 2g^2\mathcal{T}(P)} \xi^\dagger A^{\text{os}}(P)^\dagger\,. \tag{3.80}$$

This is the main result of this subsection. Up to neglected exponentially suppressed contributions, the volume dependence of $C_L(P)$ is contained entirely in the second term, both through the explicit L dependence of $S(P,L)$ and the implicit dependence in the matrix multiplications, which involve sums over discretised spatial momenta.

3.2.8 Quantisation condition in $\boldsymbol{k}^\star \ell m$ space

For a given total spatial momentum $\boldsymbol{P}$ and volume L, let us denote the finite volume energy levels by $E_j(\boldsymbol{P}, L)$. Our main motivation for examining $C_L(P)$ was that it has poles at these energy levels and from eq. (3.80), we see that these poles arise at the values of the energy for which the matrix in the denominator has a vanishing eigenvalue. This gives us the following quantization condition:

$$\det_{\boldsymbol{k}^\star \ell m} \left[S(P_j, L)^{-1} + \xi^\dagger \, \overline{\mathcal{K}}^{\text{os}}(P_j) \, \xi + 2g^2 \mathcal{T}(P_j) \right] = 0 \,, \tag{3.81}$$

where $P_j = (E_j(\boldsymbol{P}, L), \boldsymbol{P})$ and the determinant is taken over the whole $\boldsymbol{k}^\star \ell m, \boldsymbol{k}'^\star \ell' m'$ index space, as indicated. This condition can be used to constrain $\overline{\mathcal{K}}^{\text{os}}(P)$, as well as the coupling g, via lattice-determined energies.[6]

To make this a stand-alone section, we collect all definitions required to numerically evaluate the quantization condition.

The matrix $\mathcal{T}(P)$, which encodes the angular-momentum projected t-channel exchange, has matrix elements given by

$$\begin{aligned} \mathcal{T}_{\boldsymbol{k}^\star \ell m, \boldsymbol{k}'^\star \ell' m'}(P) = \frac{1}{4\pi |\boldsymbol{k}^\star|^\ell |\boldsymbol{k}'^\star|^{\ell'}} \int d\Omega_{\hat{\boldsymbol{k}}^\star} d\Omega_{\hat{\boldsymbol{k}}'^\star} Y_{\ell m}(\hat{\boldsymbol{k}}^\star) \, Y^*_{\ell' m'}(\hat{\boldsymbol{k}}'^\star) \\ \times \left[\frac{1}{2\omega_N(\boldsymbol{k}^\star)\omega_N(\boldsymbol{k}'^\star) - 2|\boldsymbol{k}^\star||\boldsymbol{k}'^\star| \cos\theta^\star - 2M_N^2 + M_\pi^2 - i\epsilon} \right] , \end{aligned} \tag{3.82}$$

where $\cos\theta^\star = \hat{\boldsymbol{k}}^\star \cdot \hat{\boldsymbol{k}}'^\star$. This expression is reached by combining eqs. (3.69), (3.76) and (3.77) and using the orthogonality of spherical harmonics.

The matrix $S(P, L)$, which encodes the intermediate two-nucleon on-shell pole, was already defined in eq. (3.39). We repeat the expression here

$$S_{\boldsymbol{k}^\star \ell m, \boldsymbol{k}'^\star \ell' m'}(P, L) = \frac{1}{2L^3} \, \frac{4\pi \, Y_{\ell m}(\hat{\boldsymbol{k}}^\star) \, Y^*_{\ell' m'}(\hat{\boldsymbol{k}}^\star) \, \delta_{\boldsymbol{k}^\star \boldsymbol{k}'^\star} \, |\boldsymbol{k}^\star|^{\ell + \ell'} \, e^{-\alpha[(\boldsymbol{k}^\star)^2 - (k^\star_{\text{os}})^2]}}{4\omega_N(\boldsymbol{k}) \left[(k^\star_{\text{os}})^2 - (\boldsymbol{k}^\star)^2 \right]} \,, \tag{3.83}$$

where we have substituted the possible form for $H(\boldsymbol{k}^\star)$ from eq. (3.41). Recall that $\boldsymbol{k}^\star$ takes on all values reached by boosting $(\omega_N(\boldsymbol{k}), \boldsymbol{k})$ to the CM frame,

[6] We note that, in certain cases, it may be more feasible or practical to constrain g from fits to form factors, e.g. the nucleon axial form factor in the case of the physical NN system. In all cases, one must be certain that the extracted coupling satisfies the defining relation of being the residue of the physical scattering amplitude at the t- and u-channel poles.

where $\boldsymbol{k} \in (2\pi/L)\mathbb{Z}^3$ is a finite-volume momentum. Recall also the definition $k^\star_{\text{os}} = \sqrt{s/4 - M_N^2}$.

It remains to describe the middle term of eq. (3.81). First, $\overline{\mathcal{K}}^{\text{os}}(P)$ (the quantity one aims to determine from the spectrum) is a diagonal matrix in angular-momentum space so that we can write

$$\overline{\mathcal{K}}^{\text{os}}_{\ell m,\ell' m'}(P) = \delta_{\ell\ell'}\,\delta_{mm'}\,\overline{\mathcal{K}}^{\text{os}(\ell)}(s)\,, \tag{3.84}$$

where we have also used that each component is a Lorentz invariant, depending only on the CM energy, encoded here via the Mandelstam variable $s = P^2$. Unlike the standard K-matrix, this quantity is analytic in the extended energy range $(2M_N)^2 - (2M_\pi)^2 < s < (2M_N + M_\pi)^2$ and the usual parameterisations involving polynomials and poles can be used in this region. Finally, as introduced in section 3.2.4, ξ is a trivial vector with $\boldsymbol{k}^\star$ indices, defined as

$$\xi_{\boldsymbol{k}^\star} = 1\,, \tag{3.85}$$

used to promote $\mathcal{K}^{\text{os}}(P)$ from the ℓm space to the $\boldsymbol{k}^\star \ell m$ space.

This completes our discussion of the generalized quantization condition for spin-zero nucleons. In Chapter 5, we discuss how g and $\overline{\mathcal{K}}^{\text{os}}(P)$ can then be used to then obtain the $NN \to NN$ scattering amplitude. Before turning to this, we first discuss the extension to spinful particles.

3.2.9 Incorporating spin

Thus far, our finite-volume analysis has been restricted to particles without intrinsic spin. In this subsection, we describe how the derivation of (3.81) can be readily modified to accommodate spinful particles. We first present the extension to identical spin-half particles, relevant for physical two-nucleon systems, and then briefly comment on the generalization to arbitrary spin. These generalizations follows readily from the extension of the usual scattering formalism to include spin, as described in refs. [14, 114].

Consider a realistic, generic low-energy theory of QCD with Dirac spinors N representing nucleons and anti-nucleons coupled to pseudoscalar fields π representing

the spinless pions. The interactions in the Lagrangian are modified appropriately to contain all combinations of N, $\overline{N}$, and π with vacuum quantum numbers.

The dressed propagator of the nucleon in a finite volume can be written as

$$\Delta_{N,L}(k) = \frac{i(\not{k} + M_N)}{k^2 - M_N^2 + i\epsilon} + R_{N,L}(k) \ , \tag{3.86}$$

where $R_{N,L}(k)$ encodes the self-energy contributions. As above, we require M_N to be the physical pole mass and assume renormalisation such that the residue at the pole of $\Delta_{N,L}(k)$ is the same as that of the first term on the right-hand side. This has the consequence that $R_{N,L}(k)$ is analytic in a neighbourhood of the pole, up to the exponentially suppressed volume effects on the pole mass, which we neglect.

As in eq. (2.34), we define a correlator $C_L(P)$ of operators carrying the quantum numbers of an NN state with spin and consider the corresponding skeleton expansion. Following the steps of section 3.2.3, the contribution from a generic two-nucleon loop after k^0 integration is given by

$$\mathcal{L} \circ_{\mathrm{FV}} \mathcal{R}^\dagger = \mathcal{I}^{[1]}(P) \tag{3.87}$$

$$+ \sum_{\boldsymbol{k}} \frac{i}{2L^3} \frac{\mathcal{L}^{\alpha\beta}(P,k)(\not{k} + M_N)^{\alpha\alpha'}(\not{P} - \not{k} + M_N)^{\beta\beta'}\mathcal{R}^{\alpha'\beta'}(P,k)^*}{2\omega_N(\boldsymbol{k})\left[(E - \omega_N(\boldsymbol{k}))^2 - \omega_N(\boldsymbol{P} - \boldsymbol{k})^2\right]}\Bigg|_{k^0 = \omega_N(\boldsymbol{k})} \tag{3.88}$$

where we have absorbed the $R_{N,L}(k)$ dependent terms into $\mathcal{I}^{[1]}(P)$, since these only generate exponentially suppressed contributions. Here $\alpha, \beta, \alpha', \beta'$ are Dirac spinor indices and sums over repeated indices are implied.

Noting that k is on shell, we identify the spin sum relation

$$(\not{k} + M_N)^{\alpha\alpha'}\Big|_{k^0 = \omega_N(\boldsymbol{k})} = \sum_{r=\pm} u_r^\alpha(\boldsymbol{k})\bar{u}_r^{\alpha'}(\boldsymbol{k}) \ , \tag{3.89}$$

where $u_r^\alpha(\boldsymbol{k})$ and $\bar{u}_r^{\alpha'}(\boldsymbol{k})$ are the Dirac spinors describing a free N state with definite spin. The spin-up and down states are labelled by $r = \pm$. By contrast, the four-vector $(P-k)|_{k^0=\omega_N(\boldsymbol{k})} = (E - \omega_N(\boldsymbol{k}), \boldsymbol{P} - \boldsymbol{k})$ is not on-shell. To address this we

consider an on-shell vector $(P-k)_{\rm os} \equiv (\omega_N(\boldsymbol{P}-\boldsymbol{k}), \boldsymbol{P}-\boldsymbol{k})$ such that

$$(\not{P}-\not{k}+M_N)^{\beta\beta'} = \big((\not{P}-\not{k})_{\rm os}+M_N\big)^{\beta\beta'} + \big[(\not{P}-\not{k})-(\not{P}-\not{k})_{\rm os}\big]^{\beta\beta'} \ , \tag{3.90}$$

$$= \sum_{s=\pm} u_s^\beta(\boldsymbol{P}-\boldsymbol{k})\bar{u}_s^{\beta'}(\boldsymbol{P}-\boldsymbol{k}) + \left[E-\omega_N(\boldsymbol{k})-\omega_N(\boldsymbol{P}-\boldsymbol{k})\right](\gamma^0)^{\beta\beta'} \ , \tag{3.91}$$

where we have used the spin sum relation on $(P-k)_{\rm os}$. This intermediate step differs from the approach of refs. [14, 114] and discussed in section 2.3, more concretely in eq. (2.72) and the paragraphs below it. We adopt a different form here as it is more convenient for sub-threshold kinematics.

Substituting these expressions for $(\not{k}+M_N)^{\alpha\alpha'}$ and $(\not{P}-\not{k}+M_N)^{\beta\beta'}$ into (3.88), we see that the term $\left[E-\omega_N(\boldsymbol{k})-\omega_N(\boldsymbol{P}-\boldsymbol{k})\right](\gamma^0)^{\beta\beta'}$ in (3.91) leads to a cancellation of the pole, so we can include this contribution in the remainder term and obtain

$$\mathcal{L} \circ_{\rm FV} \mathcal{R}^\dagger = \mathcal{I}^{[2]}(P) + \sum_{\boldsymbol{k}} \frac{i}{2L^3} \frac{\mathcal{L}_{rs}(P,\boldsymbol{k}^\star)\,\delta_{rr'}\,\delta_{ss'}\,\mathcal{R}^*_{r's'}(P,\boldsymbol{k}^\star)}{2\omega_N(\boldsymbol{k})\left[(E-\omega_N(\boldsymbol{k}))^2-\omega_N(\boldsymbol{P}-\boldsymbol{k})^2\right]} \ , \tag{3.92}$$

where we have defined the objects

$$\begin{aligned} \mathcal{L}_{rs}(P,\boldsymbol{k}^\star) &\equiv \mathcal{L}^{\alpha\beta}(P,k)\big|_{k^0=\omega_N(\boldsymbol{k})}\, u_r^\alpha(\boldsymbol{k}) u_s^\beta(\boldsymbol{P}-\boldsymbol{k}) \ , \\ \mathcal{R}^*_{r's'}(P,\boldsymbol{k}^\star) &\equiv \bar{u}_{r'}^{\alpha'}(\boldsymbol{k})\bar{u}_{s'}^{\beta'}(\boldsymbol{P}-\boldsymbol{k})\,\mathcal{R}^{*\alpha'\beta'}(P,k)\big|_{k^0=\omega_N(\boldsymbol{k})} \ , \end{aligned} \tag{3.93}$$

which we choose to write as functions of the CM spatial loop momentum $\boldsymbol{k}^\star$.

We next decompose these functions into spherical harmonics

$$\begin{aligned} \mathcal{L}_{rs}(P,\boldsymbol{k}^\star) &\equiv \sqrt{4\pi}\,Y_{\ell m}(\hat{\boldsymbol{k}}^\star)\,|\boldsymbol{k}^\star|^\ell\,\widetilde{\mathcal{L}}_{rs,\ell m}(P,|\boldsymbol{k}^\star|) \ , \\ \mathcal{R}^*_{r's'}(P,\boldsymbol{k}^\star) &\equiv \sqrt{4\pi}\,Y^*_{\ell' m'}(\hat{\boldsymbol{k}}^\star)\,|\boldsymbol{k}^\star|^{\ell'}\,\widetilde{\mathcal{R}}^*_{r's',\ell' m'}(P,|\boldsymbol{k}^\star|) \ , \end{aligned} \tag{3.94}$$

and rearrange the pole term in eq. (3.92) to reach

$$\mathcal{L} \circ_{\rm FV} \mathcal{R}^\dagger = \mathcal{L} \circ_{\rm rm} \mathcal{R}^\dagger + \widetilde{\mathcal{L}}(P)\,iS(P,L)\,\widetilde{\mathcal{R}}(P)^\dagger \ , \tag{3.95}$$

where, as in the spin-zero case, we have absorbed extra terms in the in a redefinition of $\mathcal{I}^{[2]}(P) \to \mathcal{I}^{[3]}(P)$, and also introduced $\mathcal{I}^{[3]}(P) \equiv \mathcal{L} \circ_{\rm rm} \mathcal{R}^\dagger$. This result exactly matches eq. (3.44) above.

The objects $\widetilde{\mathcal{L}}(P)$ and $\widetilde{\mathcal{R}}(P)^\dagger$ are vectors in the combined space of spin, spatial loop

momentum, and angular momentum. The vector elements can be written explicitly as $\widetilde{\mathcal{L}}_{rs,\boldsymbol{k}^\star\ell m}(P)$ and $\widetilde{\mathcal{R}}^*_{r's',\boldsymbol{k}'^\star\ell'm'}(P)$, respectively. The matrix $S(P,L)$, in turn, has elements

$$S_{rs,\boldsymbol{k}^\star\ell m;\,r's',\boldsymbol{k}'^\star\ell'm'}(P,L) = \frac{1}{2L^3}\,\frac{4\pi\,Y_{\ell m}(\hat{\boldsymbol{k}}^\star)\,Y^*_{\ell'm'}(\hat{\boldsymbol{k}}^\star)\,\delta_{rr'}\,\delta_{ss'}\,\delta_{\boldsymbol{k}^\star\boldsymbol{k}'^\star}\,|\boldsymbol{k}^\star|^{\ell+\ell'}\,H(\boldsymbol{k}^\star)}{4\omega_N(\boldsymbol{k})\left[(k^\star_{\rm os})^2-(\boldsymbol{k}^\star)^2\right]}\,. \tag{3.96}$$

This matches eq. (3.39) up to the additional Kronecker deltas in the spin components.

To give the effect of spin on $\mathcal{T}$, the off-shell Bethe-Salpeter kernel is split into the contribution from the exchanges and a remainder, as before. The off-shell spin projection described above appears in this separation and leads to the following quantity:

$$\begin{aligned}\mathcal{T}_{rs,r's'}(P,\boldsymbol{p}^\star,\boldsymbol{p}'^\star) \equiv -\bar{u}^\alpha_r(\boldsymbol{p})\bar{u}^\beta_s(\boldsymbol{P}-\boldsymbol{p})\,\gamma_5^{\alpha\alpha'}\,\gamma_5^{\beta\beta'}\,u^{\alpha'}_{r'}(\boldsymbol{p}')u^{\beta'}_{s'}(\boldsymbol{P}-\boldsymbol{p}') \\ \times\ \mathcal{T}(P,p,p')\big|_{p^0=\omega_N(\boldsymbol{p}),\,p'^0=\omega_N(\boldsymbol{p}')}\,.\end{aligned} \tag{3.97}$$

Here we have also included the γ_5 factors that appear in the $NN\pi$ vertex, since the exchanged pion is a pseudoscalar. Projecting this to definite angular momentum, we reach a modified matrix of off-shell log functions, denoted by $\mathcal{T}$ as in the spin-zero case. The elements $\mathcal{T}_{rs,\boldsymbol{k}^\star\ell m;\,r's',\boldsymbol{k}'^\star\ell'm'}(P)$ of the matrix correspond to the projected functions.

In addition to S and $\mathcal{T}$, the matrix $\overline{\mathcal{K}}^{\rm os}$ is also modified and the elements with spin included are denoted by $\overline{\mathcal{K}}^{\rm os}_{rs,\ell m;\,r's',\ell'm'}$. The symmetry properties of this quantity match those of a physical two-to-two amplitude with an incoming spin state of orbital angular momentum ℓ',m' and spin components $r's'$ scattering to a state with ℓ,m and r,s. As with the usual two-to-two scattering formalism with spin, once a truncation in ℓ,ℓ' is set one can identify the non-zero components and their relations. Here it may be useful to work in the basis of total spin and total angular momentum J.

Having extended our results to spin-half particles, we now comment on the generalization to identical particles of arbitrary spin. If we take N to have spin S, the dressed propagator can be expanded about the on-shell point $k^2=M_N^2$ as

$$\Delta_{N,L}(k) = \frac{i\mathcal{P}_N(\boldsymbol{k})}{k^2-M_N^2+i\epsilon} + R_{N,L}(k)\ , \tag{3.98}$$

where $\mathcal{P}_N(\boldsymbol{k})$ is a volume-independent matrix carrying two sets of field indices A, A'. In the spin-half case, $\mathcal{P}_N(\boldsymbol{k})$ corresponds to $(\not{k}+M_N)|_{k^0=\omega_N(\boldsymbol{k})}$. As in the Dirac spinor case, this can be decomposed into projectors that relate the A, A' indices to the spin state indices r, r',

$$\mathcal{P}_N(\boldsymbol{k})^{AA'} = U_r^A(\boldsymbol{k})\,\delta_{rr'}\,\overline{U}_{r'}^{A'}(\boldsymbol{k})\,. \tag{3.99}$$

where r and r' are summed over the allowed values $r, r' = -S, -S+1, ..., S-1, S$, and the bar on $\overline{U}$ denotes the appropriate conjugation. Using eq. (3.99), we are left with the same form for the loop contribution as the spin-half case in eq. (3.92) above.

The details of the $\mathcal{T}$ factor will depend on how the light exchanged particle couples to the spin-S nucleon. For example, if we envision the case of a scalar (rather than a pseudoscalar) exchange particle coupled to two real vectors, we find

$$\begin{aligned}\mathcal{T}_{rs,r's'}(P,\boldsymbol{p}^\star,\boldsymbol{p}'^\star) \equiv \bar{\epsilon}_r^\alpha(\boldsymbol{p})\bar{\epsilon}_s^\beta(\boldsymbol{P}-\boldsymbol{p})\,\delta^{\alpha\alpha'}\,\delta^{\beta\beta'}\,\epsilon_{r'}^{\alpha'}(\boldsymbol{p}')\epsilon_{s'}^{\beta'}(\boldsymbol{P}-\boldsymbol{p}') \\ \times\ \mathcal{T}(P,p,p')\big|_{p^0=\omega_N(\boldsymbol{p}),\,p'^0=\omega_N(\boldsymbol{p}')}\,.\end{aligned} \tag{3.100}$$

3.3 Exploring the extended formalism

In this section, we study the new quantization condition and integral equations that we have derived. In section 3.3.1, we present an alternative form of the quantization condition that is superficially more similar to the standard formalism. Then, in section 3.3.2, we demonstrate that the standard Lüscher formalism is exactly recovered, also for $s < 4M_N^2 - M_\pi^2$, in the limit where the $NN\pi$ coupling is set to zero. Finally, in section 3.3.3, we give expressions in the case where all partial-wave components of $\overline{\mathcal{K}}^{\text{os}}$, besides the S-wave, are negligible.

3.3.1 Quantisation condition in ℓm space

An instructive rewriting of the quantization condition is reached by first noting that eq. (3.81) is satisfied whenever the following matrix has a divergent eigenvalue:

$$\Xi_L(P,L) = \frac{1}{1+\xi^\dagger\,\overline{\mathcal{K}}^{\text{os}}(P)\,\xi\big[S(P,L)^{-1}+2g^2\mathcal{T}(P)\big]^{-1}}\xi^\dagger\,\overline{\mathcal{K}}^{\text{os}}(P)\,\xi\,. \tag{3.101}$$

Expanding order by order and rearranging the factors of ξ, one finds that $\Xi_L(P,L)$ can be exactly rewritten as

$$\Xi_L(P,L) = \xi^\dagger \frac{1}{\overline{\mathcal{K}}^{\text{os}}(P)^{-1} + \xi\left[S(P,L)^{-1} + 2g^2\mathcal{T}(P)\right]^{-1}\xi^\dagger}\xi\,. \tag{3.102}$$

We thus reach the following alternative to eq. (3.81):

$$\det_{\ell m}\left[\overline{\mathcal{K}}^{\text{os}}(P_j)^{-1} + F^{\mathcal{T}}(P_j,L)\right] = 0\,, \tag{3.103}$$

where we have introduced

$$F^{\mathcal{T}}(P,L) = \xi S(P,L)\frac{1}{1+2g^2\mathcal{T}(P)S(P,L)}\xi^\dagger\,. \tag{3.104}$$

Crucially, this quantization condition is now defined as a determinant only on the orbital angular momentum, exactly as in refs. [3, 7]. We have included the ℓm subscript on the determinant to emphasize this point. One nice feature of this representation is that it allows one to use the standard technology for projection to irreps, discussed in section 2.2.1.

This rewriting also holds for the case of particles with intrinsic spin. The only adjustment is that the spin indices remain in the final determinant condition, directly inherited from the quantities introduced in section 3.2.9. We summarize this as

$$\det_{\ell m r s}\left[\overline{\mathcal{K}}^{\text{os}}(P_j)^{-1} + F^{\mathcal{T}}(P_j,L)\right] = \det_{J m_J \ell S}\left[\overline{\mathcal{K}}^{\text{os}}(P_j)^{-1} + F^{\mathcal{T}}(P_j,L)\right] = 0\,. \tag{3.105}$$

Here we have indicated two of the possible bases for particles with spin. In the first expression, the labels r and s refer to the components of individual particle spin, as in eq. (3.96). The second expression is labelled in terms of total angular momentum J as well as orbital angular momentum ℓ and total spin S.

Also common to the standard approach is the mixing of angular momenta due to the reduced symmetry of the finite-volume system. This means that, even after projection to a given irrep, the matrices entering the determinant are formally infinite-dimensional. As a result, numerical evaluation is only possible with truncation: one sets $\overline{\mathcal{K}}^{\text{os}}_{\ell m \ell' m'} = 0$ for $\ell, \ell' > \ell_{\text{max}}$ for some choice of ℓ_{max}. Having truncated $\overline{\mathcal{K}}^{\text{os}}$ in this way, one can do the same for $F^{\mathcal{T}}(P,L)$ without any additional

approximations. It is, however, an additional approximation to truncate $S(P,L)$ and $\mathcal{T}(P)$ within $F^{\mathcal{T}}(P,L)$, as we will examine in the following subsection.

3.3.2 Recovering the standard formalism

We now show that, in the case of vanishing trilinear coupling: $g = 0$, our modified quantization condition, eq. (3.81), is equivalent to the well-known Lüscher scattering formalism [3] and its extensions to nonzero spatial momentum in the finite-volume frame [4, 7]. To this end it is convenient to use the alternative form given in eq. (3.102). In the $g \to 0$ limit, the result becomes

$$\det_{\ell m} \left[\overline{\mathcal{K}}^{\text{os}}(P_j)^{-1} + \xi S(P_j, L) \xi^\dagger \right] = 0 \,, \tag{3.106}$$

where we have substituted $F^{\mathcal{T}}(P,L) \underset{g\to 0}{\longrightarrow} \xi S(P,L)\xi^\dagger$, as follows directly from eq. (3.104).

We next relate $\xi S(P,L)\xi^\dagger$ to a version of the Lüscher finite-volume function $\widetilde{F}(P,L)$, defined in eq. (2.44) in section 2.2.[7] The key distinction between $\xi S(P,L)\xi^\dagger$ and $\widetilde{F}(P,L)$ is simply that the latter is defined with a sum-integral difference while $\xi S(P,L)\xi^\dagger$ is defined only with a sum in isolation [see also eq. (3.49)]. Studying the definitions carefully, one finds that the relation takes the form

$$\xi S(P,L)\xi^\dagger = \widetilde{F}(P,L) + \widetilde{I}(P) \,, \tag{3.107}$$

where each of the quantities carries two sets of angular-momentum indices, and we have introduced

$$\widetilde{I}_{\ell m,\ell' m'}(P) \equiv \frac{1}{2} \,\text{PV} \int \frac{d^3\boldsymbol{k}}{(2\pi)^3} \, \frac{4\pi \, Y_{\ell m}(\hat{\boldsymbol{k}}^\star) \, Y^*_{\ell' m'}(\hat{\boldsymbol{k}}^\star) \, |\boldsymbol{k}^\star|^{\ell+\ell'} \, H(\boldsymbol{k}^\star)}{4\omega_N(\boldsymbol{k}) \left[(k^\star_{\text{os}})^2 - (\boldsymbol{k}^\star)^2 \right]} \,. \tag{3.108}$$

The final missing ingredient in recovering the standard scattering formalism from eq. (3.106) is the relation between $\overline{\mathcal{K}}^{\text{os}}(P)$ and the scattering amplitude. This can mostly easily be recovered from the integral equation, which we will give eq. (5.15) in section 5.2, which simplifies in three ways for $g = 0$. Firstly, the breaking of exchange symmetry in $\mathcal{M}^{\text{aux}}$ is removed so that this just directly becomes the scattering

[7] As above, the tilde here indicates rescaling by powers of $k^\star_{\text{os}}$. We do not use the tilde for $S(P,L)$ since this is a non-standard quantity anyway, as has been defined already with this rescaling.

amplitude. Secondly, the off-shell dependence of $\mathcal{M}^{\text{aux}}$ on $|\boldsymbol{k}^\star|$, which is inherited from $\mathcal{T}$, is removed when the coupling vanishes. Finally, we can replace $\mathcal{K}^{\mathcal{T}} \to \overline{\mathcal{K}}^{\text{os}}$ everywhere, since the difference between the two is proportional to g^2. We reach

$$\begin{aligned}\widetilde{\mathcal{M}}_{\ell m,\ell' m'}(P) &= \overline{\mathcal{K}}^{\text{os}}_{\ell m,\ell' m'}(P) \\ &\quad - \widetilde{\mathcal{M}}_{\ell m,\ell'' m''}(P)\,\frac{1}{2}\int_0^\infty \frac{d|\boldsymbol{k}^\star|}{(2\pi)^3}\frac{4\pi|\boldsymbol{k}^\star|^{2\ell''+2}H(\boldsymbol{k}^\star)}{4\omega_N(\boldsymbol{k}^\star)\big[(k^\star_{\text{os}})^2-(\boldsymbol{k}^\star)^2+i\epsilon\big]}\,\overline{\mathcal{K}}^{\text{os}}_{\ell'' m'',\ell' m'}(P)\,.\end{aligned} \tag{3.109}$$

Switching to a matrix notation to drop indices and multiplying both sides by $\mathcal{M}(P)^{-1}$ on the right and $\overline{\mathcal{K}}^{\text{os}}(P)^{-1}$ on the left, we find

$$\overline{\mathcal{K}}^{\text{os}}(P)^{-1} = \widetilde{\mathcal{M}}(P)^{-1} - \widetilde{I}^{i\epsilon}(P)\,, \tag{3.110}$$

where we have introduced

$$\widetilde{I}^{i\epsilon}_{\ell m,\ell' m'}(P) \equiv \delta_{\ell\ell'}\delta_{mm'}\frac{1}{2}\int_0^\infty \frac{d|\boldsymbol{k}^\star|}{(2\pi)^3}\frac{4\pi|\boldsymbol{k}^\star|^{2\ell+2}H(\boldsymbol{k}^\star)}{4\omega_N(\boldsymbol{k}^\star)\big[(k^\star_{\text{os}})^2-(\boldsymbol{k}^\star)^2+i\epsilon\big]}\,. \tag{3.111}$$

The notation for this quantity is well-chosen. As can be seen by evaluating the angular integrals in eq. (3.108), $\widetilde{I}(P)$ and $\widetilde{I}^{i\epsilon}(P)$ differ only in the pole prescription.

In particular, since the principal value defining $\widetilde{I}(P)$ is equivalent to the real part of the $i\epsilon$ prescription, the difference in integrals is just the imaginary part of $\widetilde{I}^{i\epsilon}(P)$:

$$\widetilde{I}^{i\epsilon}_{\ell m,\ell' m'}(P) - \widetilde{I}_{\ell m,\ell' m'}(P) = \delta_{\ell\ell'}\delta_{mm'}\frac{i}{2}\text{Im}\int_0^\infty \frac{d|\boldsymbol{k}^\star|}{(2\pi)^3}\frac{4\pi|\boldsymbol{k}^\star|^{2\ell+2}H(\boldsymbol{k}^\star)}{4\omega_N(\boldsymbol{k}^\star)\big[(k^\star_{\text{os}})^2-(\boldsymbol{k}^\star)^2+i\epsilon\big]}\,, \tag{3.112}$$

$$= -\delta_{\ell\ell'}\delta_{mm'}i\rho(s)(k^\star_{\text{os}})^{2\ell} = -i\widetilde{\rho}_{\ell m,\ell' m'}(s)\,, \tag{3.113}$$

where $\rho(s)$ is the usual phase space, defined in eq. (2.11), as is $\widetilde{\rho}_{\ell m,\ell' m'}(s)$ in eq. (2.27).

It is exactly this phase space factor that appears in the relation between the scattering amplitude $\widetilde{\mathcal{M}}$ and the standard two-particle K-matrix

$$\widetilde{\mathcal{K}}(P)^{-1} = \widetilde{\mathcal{M}}(P)^{-1} + i\widetilde{\rho}(P)\,. \tag{3.114}$$

For convenience, we give the relation to the scattering phase shift:

$$\widetilde{\mathcal{K}}_{\ell m,\ell' m'}(P) = \frac{1}{(k^\star_{\rm os})^{2\ell}} \delta_{\ell\ell'}\delta_{mm'} \frac{16\pi\sqrt{s}}{k^\star_{\rm os}} \tan\delta^{(\ell)}(k^\star_{\rm os})\,. \tag{3.115}$$

Finally, combining eqs. (3.110), (3.113) and (3.114), we deduce

$$\overline{\mathcal{K}}^{\rm os}(P)^{-1} = \widetilde{\mathcal{K}}(P)^{-1} - \widetilde{I}(P)\,. \tag{3.116}$$

Together with eq. (3.107), this is the second key identity of this subsection. Substituting the identities into eq. (3.106), one finally obtains

$$\det_{\ell m}\left[\widetilde{\mathcal{K}}(P_j)^{-1} - \widetilde{I}(P_j) + \widetilde{F}(P_j,L) + \widetilde{I}(P_j)\right] = \det_{\ell m}\left[\widetilde{\mathcal{K}}(P_j)^{-1} + \widetilde{F}(P_j,L)\right] = 0\,. \tag{3.117}$$

This is the standard quantization condition of Lüscher, generalized to nonzero momentum $\boldsymbol{P}$ in the finite-volume frame [3, 4, 7]. We have thus achieved the aim of this section.

Before concluding, we briefly return to the case of $g \neq 0$. If we restrict our attention to energies above the left-channel cut, i.e. with $s > (2M_N)^2 - M_\pi^2$, then we can ignore the presence of the latter in the on-shell Bethe-Salpeter kernel, up to exponentially suppressed L-dependence, albeit dependence that can be enhanced if we are too close to saturating the inequality. In this case, one can formally group the g dependent term into $\overline{B}^{\,\mathbb{T}}$ and apply an effective $g = 0$ analysis to again deduce the usual formulas. It would be instructive to analytically recover the standard formalism from our results in the above threshold regime and to quantify the neglected exponentially suppressed corrections. We leave this for future work.

As mentioned above, our perspective is that, in a numerical calculation, one should ensure that there are no statistically significant differences between the scattering predictions arising from the standard and the improved formalisms and, if there are, to use the latter.

3.3.3 S-wave dominance

In this section, we consider the form of the quantization condition and the integral equations in the case that only the S-wave component of $\overline{\mathcal{K}}^{\rm os}$ is non-zero. Beginning

with the quantization condition, eq. (3.103) becomes

$$\overline{\mathcal{K}}^{\mathrm{os}(0)}(P_j)^{-1} + F_0^{\mathcal{T}}(P_j, L) = 0\,, \tag{3.118}$$

where we have introduced the S-wave quantities

$$\overline{\mathcal{K}}^{\mathrm{os}(0)}(P_j) = \overline{\mathcal{K}}^{\mathrm{os}}_{00,00}(P_j)\,, \tag{3.119}$$

$$F_0^{\mathcal{T}}(P, L) = Z(P, L) - V^\dagger(P, L)\frac{1}{1 + 2g^2\mathcal{T}(P)S(P, L)}2g^2\mathcal{T}(P)V(P, L)\,, \tag{3.120}$$

with the latter expressed in terms of two new building blocks, a scalar function $Z(P, L)$ and a vector function $V(P, L)$:

$$Z(P, L) \equiv [\xi S(P, L)\xi^\dagger]_{00,00} = \frac{1}{2L^3}\sum_{\boldsymbol{k}} \frac{e^{-\alpha[(\boldsymbol{k}^\star)^2 - (k^\star_{\mathrm{os}})^2]}}{4\omega_N(\boldsymbol{k})\left[(k^\star_{\mathrm{os}})^2 - (\boldsymbol{k}^\star)^2\right]}\,, \tag{3.121}$$

$$V^\dagger_{\boldsymbol{k}'^\star\ell'm'}(P, L) \equiv \xi_{\boldsymbol{k}^\star} S_{\boldsymbol{k}^\star 00, \boldsymbol{k}'^\star\ell'm'}(P, L) = \frac{1}{2L^3}\frac{\sqrt{4\pi}\, Y^*_{\ell'm'}(\hat{\boldsymbol{k}'}^\star)\, |\boldsymbol{k}'^\star|^{\ell'}\, e^{-\alpha[(\boldsymbol{k}'^\star)^2 - (k^\star_{\mathrm{os}})^2]}}{4\omega_N(\boldsymbol{k}')\left[(k^\star_{\mathrm{os}})^2 - (\boldsymbol{k}'^\star)^2\right]}\,. \tag{3.122}$$

The key observation here is that $V(P, L)$ is still populated with all angular momentum components, even though $F^{\mathcal{T}}(P, L)$ has been truncated to the S-wave. This is because the exchanges, encoded in $\mathcal{T}(P)$, depend on all partial waves, and the truncation of this object is logically separate from the truncation of the quantization condition. In practice, the approach is to evaluate $F_0^{\mathcal{T}}(P, L)$ for various truncations of $\mathcal{T}(P)$ and look for saturation. The convergence will depend on the values of g, P, L. Further investigation is needed to understand this in detail.

To give one explicit example, we consider the case of zero total momentum and the trivial irrep of the finite-volume symmetry group, called A_1^+. Then the lowest-lying contaminating partial wave is $\ell = 4$ and the m component is removed by irrep projection such that one can define a two-dimensional angular momentum space.

The resulting building blocks for $F_0^{\mathcal{T}}(P,L)$ are then given by

$$V_{\boldsymbol{k}}^{\dagger}(P,L) = \frac{1}{2L^3}\,\frac{e^{-\alpha[(\boldsymbol{k})^2-(k_{\rm os})^2]}}{4\omega_N(\boldsymbol{k})\left[(k_{\rm os})^2-(\boldsymbol{k})^2\right]}\Big(1 \qquad \mathcal{Y}_4^{A_1^+}(\boldsymbol{k})\Big)\,, \tag{3.123}$$

$$\mathcal{T}_{\boldsymbol{k},\boldsymbol{k}'}(P) = \begin{pmatrix} \mathcal{T}_{\boldsymbol{k},\boldsymbol{k}'}^{(\ell=0),A_1^+}(P) & 0 \\ 0 & \mathcal{T}_{\boldsymbol{k},\boldsymbol{k}'}^{(\ell=4),A_1^+}(P) \end{pmatrix}\,, \tag{3.124}$$

$$S_{\boldsymbol{k},\boldsymbol{k}'}(P,L) = \frac{1}{2L^3}\,\frac{\delta_{\boldsymbol{k}\boldsymbol{k}'}\,e^{-\alpha[(\boldsymbol{k})^2-(k_{\rm os})^2]}}{4\omega_N(\boldsymbol{k})\left[(k_{\rm os})^2-(\boldsymbol{k})^2\right]}\begin{pmatrix} 1 \\ \mathcal{Y}_4^{A_1^+}(\boldsymbol{k}) \end{pmatrix}\Big(1 \qquad \mathcal{Y}_4^{A_1^+}(\boldsymbol{k})\Big)\,, \tag{3.125}$$

where we have introduced the S-wave projected G-wave spherical harmonic:

$$\mathcal{Y}_4^{A_1^+}(\boldsymbol{k}) = \frac{\sqrt{21}}{4}\Big(5(k_x^4+k_y^4+k_z^4)-3(\boldsymbol{k}^2)^2\Big)\,. \tag{3.126}$$

This is also used to define the G-wave component of $\mathcal{T}(P)$, which is given explicitly by

$$\begin{aligned}\mathcal{T}_{\boldsymbol{k},\boldsymbol{k}'}^{(\ell=4),A_1^+}(P) = \frac{21}{16(4\pi)^2|\boldsymbol{k}|^4|\boldsymbol{k}'|^4}\int d\Omega_{\hat{\boldsymbol{n}}}\int d\Omega'_{\hat{\boldsymbol{n}}} \\ \times\,\frac{\big(5(\hat{n}_x^4+\hat{n}_y^4+\hat{n}_z^4)-3\big)\big(5(\hat{n}_x'^4+\hat{n}_y'^4+\hat{n}_z'^4)-3\big)}{2\omega_N(\boldsymbol{k})\omega_N(\boldsymbol{k}')-2|\boldsymbol{k}||\boldsymbol{k}'|\hat{\boldsymbol{n}}\cdot\hat{\boldsymbol{n}}'-2M_N^2+M_\pi^2-i\epsilon}\,,\end{aligned} \tag{3.127}$$

where $\hat{\boldsymbol{n}} = (\sin\theta\cos\phi, \sin\theta\sin\phi, \cos\theta)$ and similar with primed coordinates. One can evaluate the integral to find

$$\mathcal{T}_{\boldsymbol{k},\boldsymbol{k}'}^{(\ell=4),A_1^+}(P) = \frac{\mathcal{G}\Big(|\boldsymbol{k}|/M_N, |\boldsymbol{k}'|/M_N\Big)}{M_N^{10}}\,, \tag{3.128}$$

where we have introduced

$$\begin{aligned}\mathcal{G}(x,y) = \frac{5F(x,y)(-21F(x,y)^2+44x^2y^2)}{384x^8y^8} \\ +\,\frac{35F(x,y)^4-120x^2y^2F(x,y)^2+48x^4y^4}{512x^9y^9}\log\left[\frac{F(x,y)-xy}{F(x,y)+xy}\right]\,,\end{aligned} \tag{3.129}$$

$$F(x,y) = -2\sqrt{1+x^2}\sqrt{1+y^2}+2-(M_\pi/M_N)^2+i\epsilon\,. \tag{3.130}$$

The second function also allows us to express the S-wave component in eq. (3.78)

in a more compact form:

$$\mathcal{T}_{\boldsymbol{k},\boldsymbol{k}'}^{(\ell=0),A_1^+}(P) = \frac{1}{M_N^2}\frac{1}{4xy}\log\left[\frac{F(x,y)-xy}{F(x,y)+xy}\right] . \tag{3.131}$$

These expressions can be readily extended to higher dimensions, simply by working out the trivial irrep harmonics and the integrals of the latter entering $\mathcal{T}(P)$. In this way one can reliably estimate $F_0^{\mathcal{T}}(P,L)$ and thereby determine the relation between $\overline{\mathcal{K}}_0^{\text{os}}(P)$, in a given parametrization, and the finite-volume energies on the left-hand cut.

The second step of the procedure is then using the S-wave determined $\overline{\mathcal{K}}_0^{\text{os}}(P)$ together with g to solve for scattering amplitude. The strategies presented in refs. [118] will clearly be useful here. We leave a detailed numerical exploration to future work.

3.3.4 Exchanges in plane-wave basis

The formulation of the quantisation condition in the pure angular momentum ℓm basis, given in eq. (3.102), introduces the object $F^{\mathcal{T}}(P,L)$, defined through eq. (3.104) in terms of $S(P,L)$ and the off-shell exchange matrix $\mathcal{T}(P)$. Convergence in the numerical evaluation of $F^{\mathcal{T}}(P,L)$ as a function of the necessary truncations of its building blocks is not a trivial issue and further numerical studies are necessary.

This is partly related to the expected issues with convergence for partial-wave and spherical-harmonic expansions of the pion exchanges. Some recent approaches to the left-hand cut issue have avoided projecting the exchanges altogether, as the presence of the exchange pole will spoil convergence. Namely, in [], the authors advocate instead for the use of a pure plane-wave basis. In the present work, concretely in section 3.2.6, we argue that this is not present an issue if we work with a nonsingular partially off-shell form of the exchange (3.69), which becomes the matrix $\mathcal{T}(P)$ in the subsequent derivation of the quantisation conditions (3.81) and (3.102).

In the formulation of the condition in the mixed momentum and angular momentum $\boldsymbol{k}^\star \ell m$ basis, given in eq. (3.81), we have full separation of the building blocks into $\overline{\mathcal{K}}^{\text{os}}(P)$, $S(P,L)$, and $\mathcal{T}(P)$. $\overline{\mathcal{K}}^{\text{os}}(P)$ is a generic analytic function and requires parameterisation to extract scattering predictions from finite-volume energies. In

that sense, this is the most challenging input and the one for which partial-wave convergence is most important. For this reason it is important that the single-exchange left-hand cut is removed from $\overline{\mathcal{K}}^{\text{os}}(P)$, such that this object does not suffer the associated partial-wave convergence problems. By contrast, while the convergence for $S(P,L)$ and $\mathcal{T}(P)$ is less obvious, no new free parameters are introduced if one varies the size of these quantities. One can thus envision cases where only the S-wave component of $\overline{\mathcal{K}}^{\text{os}}(P)$ is kept but we keep many more components of the other factors. This will still lead to an $(n+1)$-parameter description of the finite-volume energies, with n being the number of free parameters used in the S component of $\overline{\mathcal{K}}^{\text{os}}(P)$. Nevertheless, we do recognise that the off-shell exchange (3.69) does still contain singularities off the real axis in the momentum magnitudes $|\boldsymbol{p}^\star|, |\boldsymbol{p}'^\star|$, which might still restrict the radius of convergence of a partial-wave expansion.

The formulation in ℓm space, eq. (3.102), is more flexible in this case, as the truncation in the overall angular momentum index space of the quantisation condition is clearly independent of the truncation in the $\boldsymbol{k}^\star \ell m$ space within $F^{\mathcal{T}}(P,L)$, as remarked at the end of 3.3.1. This also allows us to express $F^{\mathcal{T}}(P,L)$ in a way that does not make use of projections of the pion exchanges, such that we may use the exact pole form.

To see this, let us first re-expand $F^{\mathcal{T}}(P,L)$ as a geometric series:

$$F^{\mathcal{T}}(P,L) = \sum_{n=0}^{\infty} \xi S(P,L) \left[-2g^2 \mathcal{T}(P) S(P,L)\right]^n \xi^\dagger \,. \tag{3.132}$$

We now define two matrices, $\mathsf{S}(P,L)$ and $\mathsf{T}(P,L)$, with elements given by:

$$\mathsf{S}_{\boldsymbol{k}^\star \boldsymbol{k}'^\star}(P,L) \equiv \frac{\delta_{\boldsymbol{k}^\star \boldsymbol{k}'^\star}\, H(\boldsymbol{k}^\star)}{4\omega(\boldsymbol{k})\left[(k^\star_{\text{os}})^2 - (\boldsymbol{k}^\star)^2 + i\epsilon\right]} \,, \tag{3.133}$$

$$\mathsf{T}_{\boldsymbol{k}^\star \boldsymbol{k}'^\star}(P,L) \equiv -\frac{1}{\left(\omega_N(\boldsymbol{k}^\star) - \omega_N(\boldsymbol{k}'^\star)\right)^2 - (\boldsymbol{k}^\star - \boldsymbol{k}'^\star)^2 - M_\pi^2 + i\epsilon} \,, \tag{3.134}$$

$$= \frac{1}{2\omega_N(\boldsymbol{k}^\star)\omega_N(\boldsymbol{k}'^\star) - 2\boldsymbol{k}^\star \cdot \boldsymbol{k}'^\star - 2M_N^2 + M_\pi^2 - i\epsilon} \,. \tag{3.135}$$

These matrices are in effect versions of $S(P,L)$ and $\mathcal{T}(P,L)$ indexed only by the spatial momenta $\boldsymbol{k}^\star$. Note that, unlike the elements of $\mathcal{T}(P,L)$, the elements of $\mathsf{T}(P,L)$ do depend on the direction of the momentum indices, and not only on their direction.

The relations between these objects is given by

$$S_{\boldsymbol{k}^\star \ell m,\, \boldsymbol{k}'^\star \ell' m'}(P,L) = 4\pi |\boldsymbol{k}^\star|^\ell |\boldsymbol{k}'^\star|^{\ell'} \, Y_{\ell m}(\hat{\boldsymbol{k}}^\star)\, \mathsf{S}_{\boldsymbol{k}^\star \boldsymbol{k}'^\star}(P,L)\, Y^*_{\ell' m'}(\hat{\boldsymbol{k}}'^\star)\,, \tag{3.136}$$

$$\mathsf{T}_{\boldsymbol{k}^\star \boldsymbol{k}'^\star}(P) = 4\pi |\boldsymbol{k}^\star|^\ell |\boldsymbol{k}'^\star|^{\ell'} \, Y^*_{\ell m}(\hat{\boldsymbol{k}}^\star)\, \mathcal{T}_{\boldsymbol{k}^\star \ell m,\, \boldsymbol{k}'^\star \ell' m'}(P)\, Y_{\ell' m'}(\hat{\boldsymbol{k}}'^\star)\,. \tag{3.137}$$

In the second line, we sum over the repeated ℓm, $\ell' m'$ indices, reversing the spherical harmonic decomposition of the elements of $\mathcal{T}(P)$. By shuffling around spherical harmonics and barrier factors and applying these relations, we can rewrite the elements of $F^{\mathcal{T}}(P,L)$ as

$$F^{\mathcal{T}}_{\ell m, \ell' m'}(P,L) = \sum_{n=0}^{\infty} \mathsf{Y}_{\ell m}\, \mathsf{S}(P,L) \left[-2g^2 \mathsf{T}(P,L)\, \mathsf{S}(P,L)\right]^n \mathsf{Y}^\dagger_{\ell' m'}\,, \tag{3.138}$$

$$= \mathsf{Y}_{\ell m}\, \mathsf{S}(P,L) \frac{1}{1 + 2g^2 \mathsf{T}(P,L)\, \mathsf{S}(P,L)} \mathsf{Y}^\dagger_{\ell' m'}\,. \tag{3.139}$$

Here, we have introduced the notation

$$(\mathsf{Y}_{\ell m})_{\boldsymbol{k}^\star} \equiv \xi_{\boldsymbol{k}^\star} \sqrt{4\pi}\, |\boldsymbol{k}^\star|^\ell \, Y_{\ell m}(\hat{\boldsymbol{k}}^\star) = \sqrt{4\pi}\, |\boldsymbol{k}^\star|^\ell \, Y_{\ell m}(\hat{\boldsymbol{k}}^\star)\,. \tag{3.140}$$

Using this form of $F^{\mathcal{T}}(P,L)$ allows us to use the exact form of the t-channel pole. It is still necessary to truncate in the momentum indices, but convergence is helped by the suppression provided by the regulator functions $H(\boldsymbol{k}^\star)$ present in the $\mathsf{S}(P,L)$ matrices.

Chapter 4

Extension of finite-volume formalism to the left-hand cut: non-degenerate particles

We look now at extending the discussion of the previous chapter to the case of non-identical and non-degenerate particles. As mentioned already in the Introduction, this extension is relevant for systems such as DD^* scattering at heavier-than-physical pion mass, for which the vector meson D^* is stable, and BB^* scattering. In this work, we focused only on a simplified, but generic, scalar model of these systems.

The discussion in this chapter closely mirrors that of Chapter 3 and is structured as follows: In the next section, we detail the most relevant changes to the infinite-volume scattering setup given in section 3.1. In section 4.2, we give a summary of the necessary modifications to the steps outlined in section 3.2. This chapter is mostly comprised of as-of-yet unpublished material.

4.1 Infinite-volume details

Consider two complex spin-zero fields φ_1, φ_2 with physical masses M_1 and M_2, and a lighter real spin-zero particle π, with mass M_π, such that $M_\pi \ll M_2 \leq M_1$. We further require that $M_1 - M_2 < M_\pi$, so that φ_1 is stable (cannot decay via $\varphi_1 \to \varphi_2\pi$). Single-particle states can be written $|\varphi_1, \boldsymbol{p}, q\rangle$, $|\varphi_2, \boldsymbol{p}, q\rangle$ and $|\pi, \boldsymbol{p}\rangle$,

$q = \pm$ denotes $U(1)$ charges associated to these complex fields. As before, we have the usual relativistic normalisations:

$$\langle \varphi_{i'}, \boldsymbol{p}', q' | \varphi_i, \boldsymbol{p}, q \rangle = \delta_{i'i}\, \delta_{q'q}\, 2\omega_i(\boldsymbol{p})\, (2\pi)^3\, \delta^3(\boldsymbol{p}' - \boldsymbol{p}) \quad (i, i' = 1, 2)\,, \tag{4.1}$$

$$\langle \pi, \boldsymbol{p}' | \pi, \boldsymbol{p} \rangle = 2\omega_\pi(\boldsymbol{p})\, (2\pi)^3\, \delta^3(\boldsymbol{p}' - \boldsymbol{p})\,, \tag{4.2}$$

with

$$\omega_x(\boldsymbol{p}) \equiv \sqrt{\boldsymbol{p}^2 + M_x^2}\,, \qquad\qquad x \in \{1, 2, \pi\}\,. \tag{4.3}$$

The discussion of the scattering amplitude, K-matrix and Bethe-Salpeter kernel in Chapter 2 (section 2.1) naturally applies here to the elastic process $\varphi_1\varphi_2 \to \varphi_1\varphi_2$. The sub-threshold structure of the amplitude and K-matrix will of course depend on the specific nature of the interactions considered. We assume there is a term of the form

$$\mathcal{L}_{\varphi_1\varphi_2\pi} = \pi(x)\big[\varphi_1^\dagger(x)\varphi_2(x) + \varphi_2^\dagger(x)\varphi_1(x)\big] \tag{4.4}$$

in the effective Lagrangian. These terms give rise to t- and u-channel pion exchanges, which generate left-hand cuts. The nearest cut to threshold has a branch point $s = 2M_1^2 + 2M_2^2 - M_\pi^2$ and arises due to a single u-channel exchange. In the next subsection, we analyse this u-channel exchange in more detail. These particular choices again seek to model the DD^* (or BB^*) system, where the nearest left-hand cut comes about due to a u-channel single pion exchange, as discussed in []. Note that there is an overall $U(1)$ charge that is conserved by the interaction terms above, which would correspond to the conservation of charm quantum number in DD^*.

4.1.1 Single u-channel exchange

In the following, we take all momentum assignments as in the previous chapters. Similarly to what was done in section 3.1, the fully-dressed single u-channel π exchange can be written as

$$D_u(P, p, p') \equiv G(p, P - p')\Delta_{\pi,i\epsilon}(P - p' - p)G(P - p, p')\,, \tag{4.5}$$

where we use the $\varphi_1\varphi_2\pi$ form factor $G(k, k')$, defined as

$$G(k, k') \equiv \Delta_{\pi,i\epsilon}(k' - k)^{-1}\langle \varphi_2, \boldsymbol{k}', q' | \pi(0) | \varphi_1, \boldsymbol{k}, q \rangle\,. \tag{4.6}$$

We want to isolate the pole contribution in this exchange. Noting that $G(k,k')$ depends only on the Lorentz invariant $(k'-k)^2$, i.e. $G(k,k') = \mathcal{G}((k'-k)^2)$ for some function $\mathcal{G}$, we first define the effective coupling:

$$g \equiv \lim_{p^2 \to M_\pi^2} \mathcal{G}(p^2)\,. \tag{4.7}$$

The difference

$$\delta D_u(P,p,p') \equiv D_u(P,p,p') - ig^2\mathcal{U}(P,p,p')\,, \tag{4.8}$$

is then analytic near the u-channel pole at $(P-p'-p)^2 = M_\pi^2$, where we introduced

$$ig^2\mathcal{U}(P,p,p') \equiv -\frac{ig^2}{(P-p'-p)^2 - M_\pi^2 + i\epsilon} = -\frac{ig^2}{u - M_\pi^2 + i\epsilon}\,, \tag{4.9}$$

corresponding to the u-channel pole and the corresponding residue.

We also consider the fully on-shell object as a function of Mandelstam s and the centre-of-mass scattering angle $\theta^\star$, as it is this object that subsequently produces the left-hand cut of concern here. It is given by

$$\mathcal{U}^{\rm os}(s,\theta^\star) = \frac{1}{2(k^\star_{\rm os})^2(1+\cos\theta^\star) - (M_1^2-M_2^2)^2/s + M_\pi^2 - i\epsilon}\,, \tag{4.10}$$

where we have used that $u = (P-p'-p)^2 = (M_1^2-M_2^2)^2/s - 2(k^\star_{\rm os})^2(1+\cos\theta^\star)$ when all momenta are on shell. Here $k^\star_{\rm os}$ is again the magnitude of the CM frame spatial momentum of the two scatterers, which is given already in 2.7 but we repeat it here for convenience:

$$k^\star_{\rm os} = \frac{1}{2}\sqrt{s - 2(M_1^2+M_2^2) + (M_1^2-M_2^2)^2/s}\,. \tag{4.11}$$

We project to partial waves in the usual way, via

$$\mathcal{U}^{\rm os}_\ell(s) = \frac{1}{2}\int_{-1}^{1} d(\cos\theta^\star)\,\frac{P_\ell(\cos\theta^\star)}{2(k^\star_{\rm os})^2(1+\cos\theta^\star) - (M_1^2-M_2^2)^2/s + M_\pi^2 - i\epsilon}\,. \tag{4.12}$$

This integral is straightforward to evaluate for any fixed ℓ. For $\ell = 0$, we obtain

$$\mathcal{U}^{\rm os}_0(s) = \frac{1}{2(k^\star_{\rm os})^2}\log\left[\frac{s - 2M_1^2 - 2M_2^2 + M_\pi^2}{M_\pi^2 - (M_1^2-M_2^2)^2/s} - i\epsilon\right], \tag{4.13}$$

$$= \frac{1}{2(k^\star_{\rm os})^2}\log\left[1 + \frac{4(k^\star_{\rm os})^2}{M_\pi^2 - (M_1^2-M_2^2)^2/s} - i\epsilon\right]. \tag{4.14}$$

From the first line, it is possible to identify the logarithmic u-channel branch point at $s = 2M_1^2 + 2M_2^2 - M_\pi^2 = (M_1 + M_2)^2 - M_\pi^2 + (M_1 - M_2)^2$. However, because the scatterer masses are different, the cut now splits into two, with additional branch points appearing at $s = 0$ and $s = (M_1^2 - M_2^2)^2/M_\pi^2$ where the logarithm also diverges. Thus, there is a lower cut going from $s = -\infty$ to $s = 0$ and another cut from $s = (M_1^2 - M_2^2)^2/M_\pi^2$ to $s = 2M_1^2 + 2M_2^2 - M_\pi^2$. The latter is the nearest cut to the two-particle threshold and is the one we will focus on.

4.2 Finite-volume analysis

In this section, we retrace the steps of the derivation outlined throughout section 3.2 in the last chapter and comment on the necessary alterations to take into account non-degenerate particles.

As done there, we introduce a finite-volume correlator $C_L(P)$, which can be represented diagrammatically through a skeleton expansion (see fig. 2.2). The analysis of sections 3.2.1 and 3.2.2 then follows through with little modification: power-like dependence emerges from $\varphi_1\varphi_2$ intermediate states in this expansion and the remaining elements (Bethe-Salpeter kernels, endcap factors and self-energies) carry only exponentially suppressed effects.

4.2.1 Finite-volume loop

We can then proceed to examine a two-particle loop in the skeleton expansion:

$$\mathcal{L} \circ_{\mathrm{FV}} \mathcal{R}^\dagger \equiv \int_{k^0} \frac{1}{L^3} \sum_{\boldsymbol{k}} \mathcal{L}(P,k)\Delta_{1,i\epsilon}(k)\Delta_{2,i\epsilon}(P-k)\mathcal{R}^*(P,k)\,. \tag{4.15}$$

where $\mathcal{L}(P,k)$ and $\mathcal{R}^*(P,k)$ denote generic functions on the left and right of the loop. The dressed propagators can be split into the simple pole and remainder terms:

$$\Delta_{j,i\epsilon}(p) = \frac{i}{p^2 - M_j^2 + i\epsilon} + R_j(p)\,, \tag{4.16}$$

$$R_j(p) \equiv \frac{i}{p^2 - M_j^2 - \Pi_j(p^2) + i\epsilon} - \frac{i}{p^2 - M_j^2 + i\epsilon}\,, \tag{4.17}$$

with $j \in \{1, 2\}$ denoting each of the two particle types and $\Pi_j(p^2)$ the corresponding self-energies. The remainder terms contain exclusively multi-particle state poles and are analytic in the neighbourhood of the corresponding single-particle poles $p^2 = M_j^2$, thus leading only to neglected exponential corrections in the volume.

We can follow section 3.2.3 closely, performing the integration over k^0 to obtain

$$\mathcal{L} \circ_{\mathrm{FV}} \mathcal{R}^\dagger = \mathcal{I}^{[2]}(P) + \frac{1}{L^3} \sum_{\boldsymbol{k}} \frac{\mathcal{L}(P,k)\, i\, \mathcal{R}^*(P,k)}{2\omega_1(\boldsymbol{k}) \left[(E - \omega_1(\boldsymbol{k}))^2 - \omega_2(\boldsymbol{P} - \boldsymbol{k})^2\right]} \Bigg|_{k^0 = \omega_1(\boldsymbol{k})}, \tag{4.18}$$

$$= \mathcal{I}^{[2']}(P) + \frac{1}{L^3} \sum_{\boldsymbol{k}} \frac{2E}{2\omega_1(\boldsymbol{k}) 2\omega_2(\boldsymbol{P} - \boldsymbol{k})} \times \frac{\mathcal{L}(P,k)\, i\, \mathcal{R}^*(P,k)}{(E^\star)^2 - (\omega_1(\boldsymbol{k}^\star) + \omega_2(\boldsymbol{k}^\star))^2} \Bigg|_{k^0 = \omega_1(\boldsymbol{k})}, \tag{4.19}$$

$$= \mathcal{I}^{[2'']}(P) + \sum_{\boldsymbol{k}} \frac{\gamma}{L^3} \frac{\omega_1(\boldsymbol{k}^\star)}{\omega_1(\boldsymbol{k})} \frac{\omega_2(\boldsymbol{k}^\star)}{\omega_2(\boldsymbol{P} - \boldsymbol{k})} \frac{\mathcal{L}(P,k)\, i\, \mathcal{R}^*(P,k)}{E^\star \left[(k^\star_{\mathrm{os}})^2 - (\boldsymbol{k}^\star)^2\right]} \Bigg|_{k^0 = \omega_1(\boldsymbol{k})}, \tag{4.20}$$

where $\gamma = E/E^\star$ is the Lorentz factor for the boost from the finite-volume frame to the CM frame. The first line above mirrors the result of eq. (3.34) closely. The next two lines, in turn, show two ways of rewriting the pole, which differ by terms that are analytic in the loop momentum $\boldsymbol{k}$. These lead to exponentially suppressed volume dependence and the corresponding differences are absorbed into the remainder term (denoted by the primes). Other forms for the pole are of course possible and we chose to show two expressions for which the summand (excluding the left and right function factors) is symmetric in the particle masses $M_1 \leftrightarrow M_2$. As noted after eq. (3.34) in section 3.2.3, k has been set on shell by $k^0 = \omega_1(\boldsymbol{k})$ in all expressions above, but $P - k$ is itself not on shell (i.e. does not satisfy $(P - k)^2 = M_2^2$).

We can decompose $\mathcal{L}(P,k)$ and $\mathcal{R}^*(P,k)$ into spherical harmonics in the usual way:

$$\mathcal{L}(P,k)\big|_{k^0 = \omega_1(\boldsymbol{k})} = \sqrt{4\pi}\, Y_{\ell m}(\hat{\boldsymbol{k}}^\star) |\boldsymbol{k}^\star|^\ell\, \widetilde{\mathcal{L}}_{\ell m}(P, |\boldsymbol{k}^\star|)\,, \tag{4.21}$$

$$\mathcal{R}^*(P,k)\big|_{k^0 = \omega_1(\boldsymbol{k})} = \sqrt{4\pi}\, Y^*_{\ell m}(\hat{\boldsymbol{k}}^\star) |\boldsymbol{k}^\star|^\ell\, \widetilde{\mathcal{R}}^*_{\ell m}(P, |\boldsymbol{k}^\star|)\,, \tag{4.22}$$

with sums over the indices ℓ, m implicit. Later, we will have cause to switch which argument is on shell in the left function $\mathcal{L}(P,k)$. We achieve this by making the replacement $\mathcal{L}(P,k)|_{k^0 = \omega_1(\boldsymbol{k})} \to \mathcal{L}(P,k)|_{k^0 = E - \omega_2(\boldsymbol{P} - \boldsymbol{k})}$, up to a smooth difference absorbed into the remainder term. In this case, the left function decomposition

is adjusted to

$$\mathcal{L}(P,k)\big|_{k^0=E-\omega_2(\boldsymbol{P}-\boldsymbol{k})} = \sqrt{4\pi}\, Y_{\ell m}(\hat{\boldsymbol{k}}^\star)|\boldsymbol{k}^\star|^\ell\, \widetilde{\mathcal{L}}_{\ell m}(P,|\boldsymbol{k}^\star|)\,, \tag{4.23}$$

with all else proceeding as usual.

Writing the loop momentum dependence as an extra index, the loop contribution can be cast in the same form as in eq. (3.38):

$$\mathcal{L} \circ_{\mathrm{FV}} \mathcal{R}^\dagger = \mathcal{I}^{[3]}(P) + \widetilde{\mathcal{L}}_{\boldsymbol{k}^\star\ell m}(P)\, iS_{\boldsymbol{k}^\star\ell m,\boldsymbol{k}'^\star\ell' m'}(P,L)\, \widetilde{\mathcal{R}}^*_{\boldsymbol{k}'^\star\ell' m'}(P)\,, \tag{4.24}$$

with the summand matrix

$$S_{\boldsymbol{k}^\star\ell m,\boldsymbol{k}'^\star\ell' m'}(P,L) = \delta_{\boldsymbol{k}^\star\boldsymbol{k}'^\star}\frac{\gamma}{L^3}\frac{\omega_1(\boldsymbol{k}^\star)}{\omega_1(\boldsymbol{k})}\frac{\omega_2(\boldsymbol{k}^\star)}{\omega_2(\boldsymbol{P}-\boldsymbol{k})}\frac{4\pi\, Y_{\ell m}(\hat{\boldsymbol{k}}^\star)Y^*_{\ell' m'}(\hat{\boldsymbol{k}}^\star)|\boldsymbol{k}^\star|^{\ell+\ell'}H(\boldsymbol{k}^\star)}{E^\star\left[(k^\star_{\mathrm{os}})^2-(\boldsymbol{k}^\star)^2\right]}\,. \tag{4.25}$$

As mentioned above, many specific forms for this matrix are possible, this particular form following from eq. (4.20). The regulator function $H(\boldsymbol{k}^\star)$ is also included here and must equal 1 when $(\boldsymbol{k}^\star)^2 = (k^\star_{\mathrm{os}})^2$ and decay exponentially as $(\boldsymbol{k}^\star)^2 \to \infty$.

Eq. (4.24) can be given in matrix form

$$\mathcal{L} \circ_{\mathrm{FV}} \mathcal{R}^\dagger = \mathcal{I}^{[3]}(P) + \widetilde{\mathcal{L}}(P)\, iS(P,L)\, \widetilde{\mathcal{R}}(P)^\dagger\,, \tag{4.26}$$

with $S(P,L)$ denoting the matrix with elements $S_{\boldsymbol{k}^\star\ell m,\boldsymbol{k}'^\star\ell' m'}(P,L)$, and $\widetilde{\mathcal{L}}(P)$ and $\widetilde{\mathcal{R}}(P)^\dagger$ denoting a row and column vector with components $\widetilde{\mathcal{L}}_{\boldsymbol{k}^\star\ell m}(P)$ and $\widetilde{\mathcal{R}}^*_{\boldsymbol{k}'^\star\ell' m'}(P)$.

The discussion of section 3.2.4 relating to the dominance of the value of the left and right functions at the two-particle intermediate state pole in the elastic regime, i.e. $s > (M_1+M_2)^2$ and below any inelastic thresholds. If this applies to the left and right functions, the loop contribution can be written as

$$\mathcal{L} \circ_{\mathrm{FV}} \mathcal{R}^\dagger = \mathcal{I}^{[4]}(P) + \widetilde{\mathcal{L}}^{\mathrm{os}}(P)\, \xi\, iS(P,L)\, \xi^\dagger\, \widetilde{\mathcal{R}}^{\mathrm{os}}(P)^\dagger\,, \tag{4.27}$$

where $\mathcal{I}^{[4]}(P)$ is the remainder term with negligible volume dependence, the on-shell

left and right functions are defined through

$$\widetilde{\mathcal{L}}^{\text{os}}_{\ell m}(P) \equiv \widetilde{\mathcal{L}}_{\ell m}(P, k^{\star}_{\text{os}})\,, \tag{4.28}$$

$$\widetilde{\mathcal{R}}^{\text{os}*}_{\ell m}(P) \equiv \widetilde{\mathcal{R}}^{*}_{\ell m}(P, k^{\star}_{\text{os}})\,, \tag{4.29}$$

and the $\xi, \xi^{\dagger}$ are trivial vectors with components $\xi_{\boldsymbol{k}^{\star}} = 1$, as before.

Below threshold $s < (M_1 + M_2)^2$, our discussion follows section 3.2.5. We have only exponentially suppressed volume corrections and no power-like dependence in the correlator since no intermediate two-particle states can go on shell in this region, as in eq. (3.51). The loop contribution given in eq. (4.20) can be expressed here as

$$\begin{aligned}\widetilde{\mathcal{L}}(P) S(P,L) \widetilde{\mathcal{R}}(P)^{\dagger} = -\sum_{\boldsymbol{k}} \widetilde{\mathcal{L}}_{\ell m}(P, |\boldsymbol{k}^{\star}|) \frac{\gamma}{L^3} \frac{\omega_1(\boldsymbol{k}^{\star})}{\omega_1(\boldsymbol{k})} \frac{\omega_2(\boldsymbol{k}^{\star})}{\omega_2(\boldsymbol{P}-\boldsymbol{k})} \\ \times \frac{4\pi\, Y_{\ell m}(\hat{\boldsymbol{k}}^{\star}) Y^{*}_{\ell' m'}(\hat{\boldsymbol{k}}^{\star})\, |\boldsymbol{k}^{\star}|^{\ell+\ell'} H(\boldsymbol{k}^{\star})}{\sqrt{s}\big[\kappa(s)^2 + (\boldsymbol{k}^{\star})^2\big]} \widetilde{\mathcal{R}}^{*}_{\ell m}(P, |\boldsymbol{k}^{\star}|)\,,\end{aligned} \tag{4.30}$$

where $\kappa(s)$ is a sub-threshold binding momentum

$$\kappa(s) = \frac{1}{2\sqrt{s}} \sqrt{[(M_1+M_2)^2 - s][s - (M_1 - M_2)^2]}\,. \tag{4.31}$$

The difference between the infinite- and finite-volume loop will satisfy

$$\Big[1 - \lim_{L\to\infty}\Big]\, \widetilde{\mathcal{L}}(P)\, S(P,L)\, \widetilde{\mathcal{R}}(P)^{\dagger} = \mathcal{O}(e^{-\kappa(s)L})\,, \qquad \text{for } s < (M_1+M_2)^2\,. \tag{4.32}$$

With these results for generic two-particle finite-volume loops in hand, we can apply them to the skeleton expansion loops and hence obtain expressions for the correlator.

4.2.2 Structure of the Bethe-Salpeter kernel

The Bethe-Salpeter kernel for $\varphi_1\varphi_2$ elastic scattering $B(P, p, p')$ will appear in several configurations when we apply the loop analysis of the previous section to the skeleton expansion. These are identical to the five cases given in section 3.2.6 (with appropriate adjustments taking into account the different masses). We briefly recap here: *1.) general case* – all momentum arguments are off-shell; *2.) partially off shell* – momenta p, p' individually on shell and $P - p, P - p'$ off shell; *3.) fully*

on shell – all momenta placed on shell; *4.)* case 2 projected to spherical harmonics; *5.)* case 3 projected to spherical harmonics.

The kernel has a pole at $u = M_\pi^2$ resulting from the single u-channel π exchange. Applying fully on-shell kinematics (Case 3 in the classification of section 3.2.6) will place this pole on the real axis in the complex-s plane, somewhere below the two-particle threshold, with position specified by the CM scattering angle $\theta^\star$. Recalling the discussion in the last chapter, corresponding to $M_1 = M_2$, the pole position varies between $s = 4M_1^2 - M_\pi^2$ and $s = -\infty$ as we vary $\theta^\star$ from 0 to π. Partial-wave projection of the on-shell kernel (Case 5) then leads to a branch cut for $s \in (-\infty,\ 4M_1^2 - M_\pi^2]$. Considering now $M_1 \neq M_2$, this branch cut splits into two cuts, with extra branch points at $s = 0$ and $s = (M_1^2 - M_2^2)^2/M_\pi^2$: a lower cut going from $s = -\infty$ to $s = 0$ and another, going from $s = (M_1^2 - M_2^2)^2/M_\pi^2$ to $s = 2M_1^2 + 2M_2^2 - M_\pi^2 = (M_1 + M_2)^2 - M_\pi^2 + (M_1 - M_2)^2$.

Cuts in both the fixed-$\theta^\star$ and projected kernel arise due to multiple π exchanges in the t and u channels, corresponding to $t, u = (nM_\pi)^2$ for integers $n \geq 2$. The positions of the nearest branch points in the projected kernel are given explicitly by

$$\begin{aligned} s &= M_1^2 + M_2^2 - \frac{1}{2}(nM_\pi)^2 + \frac{1}{2}\sqrt{\left((2M_1)^2 - (nM_\pi)^2\right)\left((2M_2)^2 - (nM_\pi)^2\right)}\,, \\ &= \frac{1}{4}\left[\sqrt{(2M_1)^2 - (nM_\pi)^2} + \sqrt{(2M_2)^2 - (nM_\pi)^2}\right]^2, \qquad (4.33) \\ s &= 2M_1^2 + 2M_2^2 - (nM_\pi)^2\,, \\ &= (M_1 + M_2)^2 + (M_1 - M_2)^2 - (nM_\pi)^2\,. \qquad (4.34) \end{aligned}$$

Case 2 refers to a partially on-shell configuration, where p and p' are individually on shell, i.e. we have $p^0 = \omega_1(\boldsymbol{p})$ and $p'^0 = \omega_1(\boldsymbol{p}')$, which we will refer to below as case 2(i). As mentioned in the last section, we will also be considering an alternative configuration with p and $(P - p')$ individually on shell, i.e. with $p^0 = \omega_1(\boldsymbol{p})$ and $(P - p')^0 = \omega_2(\boldsymbol{P} - \boldsymbol{p}')$ (note that here $p'^0 = E - \omega_2(\boldsymbol{P} - \boldsymbol{p}')$, so p' is itself not on shell). The alternative form, which we will call case 2(ii), is reached by the substitution $\omega_1(\boldsymbol{p}') \to E - \omega_2(\boldsymbol{P} - \boldsymbol{p}')$. The two forms will coincide when put fully on shell (Case 3), as the momenta will obey $E = \omega_1(\boldsymbol{p}') + \omega_2(\boldsymbol{P} - \boldsymbol{p}')$.

The two versions of Case 2 kinematics are useful due to the restrictions they place on Mandelstam t and u. If p' is on shell and $P - p'$ is not, we have $t = (p' - p)^2 \leq 0$, while $u = (P - p' - p)^2$ can take any real value for real spatial momenta due to

its explicit dependence on E. Conversely, if $(P - p')$ is on shell and p' is not, u is constrained by $u \leq (M_1 - M_2)^2$, while t can take any real value.

Therefore, sticking to one of the two versions for all kernel contributions may put us at risk of hitting t- or u-channel singularities, respectively. By making judicious use of the two versions at our disposal, we can achieve this as follows. Suppose we identify and separate the t- and u-dependent contributions from a particular diagram within the Bethe-Salpeter kernel. We can keep the t-dependent contributions with p' on shell and adjust the form of the u-dependent contributions to put $(P - p')$ on shell instead.

This same issue arises in the case of identical particles, as examined in section 3.2.6. There, we introduced a new kernel $B^{\mathbb{T}}(P, p, p')$, whose construction is given in appendix B, and where all u-channel exchanges have been converted to t-channel exchanges. Here, we cannot use the same procedure now as we have different and need an alternative approach.

To simplify the complicated picture of the overall kernel, let us consider the diagrams contained in it individually. Firstly, we look at the single u-channel exchange (which gives rise to the $u = M_\pi^2$ pole) and then extend the arguments to arbitrary diagrams within the kernel. This dressed single π exchange corresponds to

$$D_{u,L}(P, p, p') \equiv G_L(p, P - p')\Delta_{\pi,L}(P - p' - p)G_L(P - p, p')\,, \tag{4.35}$$

the finite-volume version of eq. (4.5). As in section 3.2.6, we can separate out the pole contribution to this exchange, $ig^2\mathcal{U}(P, p, p')$, as defined in eq. (4.9). All other contributions will lead to exponentially suppressed volume corrections, which we neglect.

Applying the two partially on-shell configurations of Case 2 to $\mathcal{U}(P, p, p')$ gives

$$\mathcal{U}(P, p, p')\Big|_{\substack{p^0=\omega_1(\boldsymbol{p}),\\ p'^0=\omega_1(\boldsymbol{p}')}} = -\frac{1}{\big(E - \omega_1(\boldsymbol{p}') - \omega_1(\boldsymbol{p})\big)^2 - \omega_\pi(\boldsymbol{P} - \boldsymbol{p}' - \boldsymbol{p})^2 + i\epsilon}\,, \tag{4.36}$$

$$\mathcal{U}(P, p, p')\Big|_{\substack{p^0=\omega_1(\boldsymbol{p}),\\ (P-p')^0=\omega_2(\boldsymbol{P}-\boldsymbol{p}')}} = -\frac{1}{\big(\omega_2(\boldsymbol{P} - \boldsymbol{p}') - \omega_1(\boldsymbol{p})\big)^2 - \omega_\pi(\boldsymbol{P} - \boldsymbol{p}' - \boldsymbol{p})^2 + i\epsilon}\,, \tag{4.37}$$

The first line, corresponding to the configuration with p' on shell, has explicit E dependence, and we can hit the pole for some value of real $\boldsymbol{p}$, $\boldsymbol{p}'$. The second line, on the other hand, corresponds to the case with $P - p'$ on shell and contains no explicit E dependence. Since $u \leq (M_1 - M_2)^2 < M_\pi^2$ for this kinematic configuration, it is safe (i.e. non-singular) for all energies relevant for us. Therefore, we see that the second form of the exchange is safe with the kinematics of Case 2, and consequently Case 4.

Consider now other diagrams contained in the kernel and apply the kinematics of Case 2(i), with p' on shell. We may use TOPT to identify the contributions from this diagram which give rise to t- and u-channel cuts. This is described in detail in appendix B. In short, we identify the possible time orderings of the vertices and then identify, if they exist, cuts for which $E_{\text{cut}} = \pm\big(\omega_1(\boldsymbol{p}) - \omega_1(\boldsymbol{p}')\big)$ or $E_{\text{cut}} = \pm\big(\omega_1(\boldsymbol{p}) - E + \omega_1(\boldsymbol{p}')\big)$. These will produce multiple-exchange t- and u-channel cuts, respectively.

The former (t-channel) type will lead to a denominator of the form

$$E_{\text{cut}} - \sum_i \omega_{f(i)}(\boldsymbol{k}_i) = \pm\big(\omega_1(\boldsymbol{p}) - \omega_1(\boldsymbol{p}')\big) - \sum_i \omega_{f(i)}(\boldsymbol{k}_i)\,, \tag{4.38}$$

where the sum runs over all internal cut propagators (indexed by i), $f(i)$ is a flavor label taking the values φ_1, φ_2 or π, and the sum of all propagator momenta $\sum_i \boldsymbol{k}_i = \pm(\boldsymbol{p} - \boldsymbol{p}')$, with the sign matching that of E_{cut}. For these cases, no singularity is encountered for real three-momenta, as we use the kinematic setup for which $t \leq 0$.

The latter (u-channel) type will produce a denominator of the form

$$E_{\text{cut}} - \sum_i \omega_{f(i)}(\boldsymbol{k}_i) = \pm\big(\omega_1(\boldsymbol{p}) - E + \omega_1(\boldsymbol{p}')\big) - \sum_i \omega_{f(i)}(\boldsymbol{k}_i)\,, \tag{4.39}$$

with total momenta of the cut propagators $\sum_i \boldsymbol{k}_i = \pm(\boldsymbol{P} - \boldsymbol{p}' - \boldsymbol{p})$. As described above, this singularity can actually be hit for real values of the momenta. Switching the on-shell argument from p' to $P - p'$ by replacing $\omega_1(\boldsymbol{p}') \to E - \omega_2(\boldsymbol{P} - \boldsymbol{p}')$, as described above, we obtain instead

$$E_{\text{cut}} - \sum_i \omega_{f(i)}(\boldsymbol{p}_i) = \pm\big(\omega_1(\boldsymbol{p}) - \omega_2(\boldsymbol{P} - \boldsymbol{p}')\big) - \sum_i \omega_{f(i)}(\boldsymbol{p}_i)\,. \tag{4.40}$$

This is now safe because the singularity cannot be hit.

The proposed strategy is to first split the contributions from diagrams in the kernel into "t-channel-like", "u-channel-like" and a safe category which can be divided evenly between the two previous groups. This separation can be achieved using TOPT to identify each dependence, as described above and explained in more detail in appendix B. We denote the two resulting groupings $B^T(P,p,p')$ and $B^U(P,p,p')$, respectively, with

$$B(P,p,p') = B^T(P,p,p') + B^U(P,p,p')\,. \tag{4.41}$$

In the identical particle case, we would be able to identify $B^T(P,p,p') = \frac{1}{2}B^{\mathbb{T}}(P,p,p')$ and $B^U(P,p,p') = \frac{1}{2}B^{\mathbb{T}}(P,p,P-p')$, reproducing eq. (3.62).

When going through the finite-volume loop analysis shown in the last section, we assume the left or right functions (or both) to be a kernel $B(P,p,p')$ insertion. Performing the contour integration leading to eq. (4.20) enforces Case 2(i) kinematics on the kernels:

$$B(P,p,p') \to B(P,p,p')\Big|_{\substack{p^0=\omega_1(\boldsymbol{p}),\\ p'^0=\omega_1(\boldsymbol{p}')}}\,.$$

At this point, we can split the kernel as in eq. (4.41) and observe that B^T is safe (no t-channel singularities can be hit), while B^U is not (we can encounter u-channel singularities). We can perform the switch from case 2(i) to case 2(ii) kinematics, as described above, only on the object B^U:

$$B^U(P,p,p')\Big|_{\substack{p^0=\omega_1(\boldsymbol{p}),\\ p'^0=\omega_1(\boldsymbol{p}')}} \to B^U(P,p,p')\Big|_{\substack{p^0=\omega_1(\boldsymbol{p}),\\ (P-p')^0=\omega_2(\boldsymbol{P}-\boldsymbol{p}')}}\,,$$

The difference between the two objects is absorbed into the remainder term as it cancels the two-particle intermediate pole. We can reassemble the full kernel using this form of B^U:

$$B'(P,\boldsymbol{p},\boldsymbol{p}') \equiv B^T(P,p,p')\Big|_{\substack{p^0=\omega_1(\boldsymbol{p}),\\ p'^0=\omega_1(\boldsymbol{p}')}} + B^U(P,p,p')\Big|_{\substack{p^0=\omega_1(\boldsymbol{p}),\\ (P-p')^0=\omega_2(\boldsymbol{P}-\boldsymbol{p}')}}\,, \tag{4.42}$$

which now is fully safe on the real line in the complex-s plane for real momenta $\boldsymbol{p},\boldsymbol{p}'$. Note that, although the kernels B and B' are different in general, they coincide when put fully on shell, by setting $|\boldsymbol{p}^\star| = |\boldsymbol{p}'^\star| = k^\star_{\text{os}}$ (Case 3 kinematics).

Provided we have replaced

$$B(P,p,p')\Big|_{\substack{p^0=\omega_1(\boldsymbol{p}),\\ p'^0=\omega_1(\boldsymbol{p}')}} \to B'(P,\boldsymbol{p},\boldsymbol{p}')$$

at this stage, we can proceed with the rest of the analysis, reaching the two versions of the loop-reduction equation, (4.26) and (4.27). One encounters the kinematics of Case 4 in $\widetilde{\mathcal{L}}(P)S(P,L)\widetilde{\mathcal{R}}(P)^\dagger$ within eq. (4.26) and that of Case 5 in $\widetilde{\mathcal{L}}^{\text{os}}(P)\xi S(P,L)\xi^\dagger\widetilde{\mathcal{R}}^{\text{os}}(P)^\dagger$ within eq. (4.27). Since B' will contain the u-channel exchange $\mathcal{U}$, we see that the associated left-hand cut is absent from the first version but it is present in the second, and must therefore also be present in the remainder term $\mathcal{I}^{[4]}(P)$. Neglecting this singularity in the remainder would invalidate the subsequent steps in the standard derivation of a quantization condition. This point is almost identical to the discussion at the end of section 3.2.6.

To address the issue caused by the on-shell placement $|\boldsymbol{k}^\star| \to k^\star_{\text{os}}$ on the cut, we introduce the subtracted kernel, as done in 3.2.6:

$$\overline{B}(P,p,p') \equiv B(P,p,p') - g^2\mathcal{U}(P,p,p')\,, \tag{4.43}$$

and the equivalent for B':

$$\overline{B}'(P,\boldsymbol{p},\boldsymbol{p}') \equiv B'(P,\boldsymbol{p},\boldsymbol{p}') - g^2\mathcal{U}(P,p,p')\Big|_{\substack{p^0=\omega_1(\boldsymbol{p}),\\ (P-p')^0=\omega_2(\boldsymbol{P}-\boldsymbol{p}')}}\,. \tag{4.44}$$

By construction, these will not contain the u-channel pole and we can project to definite angular momentum and set the arguments on shell. Partial-wave-projections of the subtracted kernel are functions of s with an analytic strip along the real axis above the next-nearest left-hand cut (due to multiple π exchanges).

4.2.3 Rearrangement of the correlator and quantisation condition

Recalling the expression for the finite-volume correlator given in eq. (2.38), we can proceed roughly as described in the last section

$$C_L(P) = C^{(0)}(P) + \sum_{n=0}^{\infty} \mathcal{A} \circ_{\text{FV}} \left[iB \circ_{\text{FV}}\right]^n \mathcal{A}^\dagger\,, \tag{4.45}$$

$$= C^{(0)}(P) + \sum_{n=0}^{\infty} \mathcal{A} \circ_{\text{FV}} \left[\left(i\overline{B} + ig^2\mathcal{U}\right)\circ_{\text{FV}}\right]^n \mathcal{A}^\dagger\,. \tag{4.46}$$

We drop any L subscripts in endcaps and kernels, as we know these lead to exponentially suppressed volume dependence.

A generic $\mathcal{U}$ insertion between loops can be analysed as described in the previous sections, so that we get this exchange with Case 2(ii) kinematics, as in eq. (4.37). A $\overline{B}$ insertion is handled also as explained in the last section, through the replacement by $\overline{B}'$. The rearrangement of the correlator proceeds identically to the derivation outlined in section 3.2.7, with $\overline{B}'$ and $g^2\mathcal{U}$ taking the place of $\overline{B}^{\,\mathbb{T}}$ and $2g^2\mathcal{T}$. Following that section and the re-definitions given in appendix C, we can obtain the correlator in the form

$$C_L(P) = \mathcal{I}_C(P) + A^{\text{os}}(P)\xi \frac{i}{S(P,L)^{-1} + \xi^\dagger\, \overline{\mathcal{K}}^{\text{os}}(P)\, \xi + g^2\mathcal{U}(P)} \xi^\dagger A^{\text{os}}(P)^\dagger \,. \tag{4.47}$$

This is quite similar to the result of eq. (3.80). Again, $\overline{\mathcal{K}}^{\text{os}}(P)$ is a volume-independent matrix in angular momentum index space. The matrix $\mathcal{U}(P)$, which encodes the angular-momentum projected u-channel exchange, has matrix elements given by

$$\begin{aligned}\mathcal{U}_{\boldsymbol{k}^\star \ell m, \boldsymbol{k}'^\star \ell' m'}(P) = \frac{1}{4\pi |\boldsymbol{k}^\star|^\ell |\boldsymbol{k}'^\star|^{\ell'}} \int d\Omega_{\hat{\boldsymbol{k}}^\star} d\Omega_{\hat{\boldsymbol{k}}'^\star} Y_{\ell m}(\hat{\boldsymbol{k}}^\star)\, Y^*_{\ell' m'}(\hat{\boldsymbol{k}}'^\star) \\ \times \left[\frac{1}{2\omega_1(\boldsymbol{k}^\star)\omega_2(\boldsymbol{k}'^\star) + 2|\boldsymbol{k}^\star||\boldsymbol{k}'^\star| \cos\theta^\star - M_1^2 - M_2^2 + M_\pi^2 - i\epsilon} \right],\end{aligned} \tag{4.48}$$

where $\cos\theta^\star = \hat{\boldsymbol{k}}^\star \cdot \hat{\boldsymbol{k}}'^\star$. The matrix $S(P,L)$, which encodes the intermediate two-nucleon on-shell pole, is already defined in eq. (4.25). The other elements include the $\mathcal{I}_C(P)$, a volume-independent remainder (up to neglected exponentially suppressed corrections), and $A^{\text{os}}(P)$ and $A^{\text{os}}(P)^\dagger$, derived from the endcap factors.

At the finite-volume energy levels $E_j(\boldsymbol{P}, L)$, we can obtain the quantisation condition

$$\det_{\boldsymbol{k}^\star \ell m} \left[S(P_j, L)^{-1} + \xi^\dagger\, \overline{\mathcal{K}}^{\text{os}}(P_j)\, \xi + g^2 \mathcal{U}(P_j) \right] = 0 \,, \tag{4.49}$$

where $P_j = (E_j(\boldsymbol{P}, L), \boldsymbol{P})$ and the determinant is taken over the whole $\boldsymbol{k}^\star \ell m, \boldsymbol{k}'^\star \ell' m'$ index space. A rewriting like that of section 3.3.1 gives a quantisation condition in the angular momentum index space:

$$\det_{\ell m} \left[\overline{\mathcal{K}}^{\text{os}}(P_j)^{-1} + F^{\mathcal{U}}(P_j, L) \right] = 0 \,, \tag{4.50}$$

where we have introduced

$$F^{\mathcal{U}}(P,L) = \xi S(P,L)\frac{1}{1+g^2\mathcal{U}(P)S(P,L)}\xi^\dagger\,. \tag{4.51}$$

The form of both quantisation conditions and the definition of the finite-volume function $F^{\mathcal{U}}(P,L)$ is essentially the same as those given in Chapter 3 – concretely, eqs. (3.81), (3.102) and (3.104). The main practical difference arising here is the absence of a symmetry factor of 2 in front of the single-particle exchanges. This factor comes about in the identical-particle case because we can have both t- and u-channel exchanges and we trade the latter for the former, doubling the t-channel contribution. Its absence makes intuitive sense here since we have contributions from single u-channel exchanges exclusively.

The derivation of the above conditions concludes our discussion of the extension of the formalism introduced in Chapter 3 to non-degenerate particles. The inclusion of spin is not considered here and is left to upcoming work, although it is expected that it should follow the arguments laid out in section 3.2.9 closely.

Chapter 5

Recovering scattering amplitudes

The work detailed in Chapters 3 and 4 served to derive generalisations of the standard Lüscher quantisation condition to the nearest sub-threshold left-hand cuts, which arise from single-particle exchanges. These extended conditions – given by eqs. (3.81) and (3.102) for identical particles, and by eqs. (4.49) and (4.50) for non-degenerate particles – allow one to constrain the volume-independent object $\overline{\mathcal{K}}^{\text{os}}(P)$ using the finite-volume spectrum. As emphasised, this quantity differs from the standard K-matrix, for example, due to its dependence on the cutoff function $H(\boldsymbol{k}^\star)$, appearing in the definition of $S(P, L)$.

In the present chapter, we show how the scheme-independent $\overline{\mathcal{K}}^{\text{os}}(P)$ is related to the corresponding infinite-volume scattering amplitude, denoted $\mathcal{M}(P, p, p')$ and thus also to more standard K-matrix definitions. Similar procedures have been employed in the context of three-particle relativistic formalism, for example in refs. [21, 81, 87, 89]. This chapter is mostly composed of the work presented already in section 5 of [2], including also some unpublished material. The discussion will focus on the case of identical particles, but the generalisation to non-degenerate particles is straightforward.

5.1 Finite-volume amplitude

We begin by introducing a finite-volume quantity $\mathcal{M}_L(P, p, p')$, which we loosely refer to as a "*finite-volume amplitude*". We definite it diagrammatically as the sum of all amputated two-to-two diagrams but with all diagrams evaluated in a finite volume

and with external arguments not necessarily set on shell. This quantity is useful because we can formally recover the physical amplitude from it by introducing an $i\epsilon$ prescription on the propagators and taking an ordered double limit: first $L \to \infty$ at fixed ϵ, leading to the spatial loop momentum sums to converge to the usual $i\epsilon$-prescription Feynman integrals, followed by $\epsilon \to 0$ and the on-shell limit, to reach the standard scattering amplitude.

Using the notation introduced in the previous chapter, we can write this object as

$$i\mathcal{M}_L = \sum_{n=0}^{\infty} \left[iB \circ_{\mathrm{FV}}\right]^n iB + i\Delta\mathcal{M}_L \,, \tag{5.1}$$

where we omit the dependence on total four-momentum P and external momentum arguments p and p' for simplicity. Here, we have introduced $\Delta\mathcal{M}_L$ as an additional volume-dependent term that vanishes when the external momenta are set on shell. This represents an additional freedom we have in the definition of $\mathcal{M}_L$ since any quantity that vanishes in the on-shell limit will be irrelevant to the value of the extracted amplitude. Below we make a particular choice of $\Delta\mathcal{M}_L$ that simplifies the relation between $\mathcal{M}_L$ and $\overline{\mathcal{K}}^{\mathrm{os}}$.

For the case of identical particles, one can express $\mathcal{M}_L$ in terms of the t-exchange modified kernel $B^{\mathbb{T}}$, which can then be separated into the subtracted part $\overline{B}^{\,\mathbb{T}}$ and the exchange term $2g^2\mathcal{T}$, as shown in section 3.2.7. In contrast to $C_L(P)$, however, the lack of exchange symmetry within $B^{\mathbb{T}}$ will affect the amplitude constructed from it. To handle this, we define a finite-volume auxiliary amplitude $\mathcal{M}_L^{\mathrm{aux}}(P,p,p')$, as follows:

$$i\mathcal{M}_L^{\mathrm{aux}} \equiv \sum_{n=0}^{\infty} \left[iB^{\mathbb{T}} \circ_{\mathrm{FV}}\right]^n iB^{\mathbb{T}} + i\Delta\mathcal{M}_L^{\mathrm{aux}} \,, \tag{5.2}$$

$$= \sum_{n=0}^{\infty} \left[\left(i\overline{B}^{\,\mathbb{T}} + 2ig^2\mathcal{T}\right) \circ_{\mathrm{FV}} \right]^n \left(i\overline{B}^{\,\mathbb{T}} + 2ig^2\mathcal{T}\right) + i\Delta\mathcal{M}_L^{\mathrm{aux}} \,. \tag{5.3}$$

We additionally define the infinite-volume counterpart of $\mathcal{M}_L^{\mathrm{aux}}$ via

$$i\mathcal{M}^{\mathrm{aux}} = \sum_{n=0}^{\infty} \left[iB^{\mathbb{T}} \circ_{i\epsilon}\right]^n iB^{\mathbb{T}} + i\Delta\mathcal{M}^{\mathrm{aux}} \,, \tag{5.4}$$

and observe this satisfies the ordered double limit described in the first paragraph

of this subsection

$$i\mathcal{M}^{\text{aux}} = \lim_{\epsilon\to 0}\lim_{L\to\infty} i\mathcal{M}_L^{\text{aux}}\Big|_{E\to E+i\epsilon}\,. \tag{5.5}$$

To recover the standard amplitude from the auxiliary amplitude, one simply symmetrises under the exchange $p' \leftrightarrow (P-p')$:

$$\mathcal{M}(P,p,p') = \frac{1}{2}\left[\mathcal{M}^{\text{aux}}(P,p,p') + \mathcal{M}^{\text{aux}}(P,p,P-p')\right] \qquad \text{for bosons}\,, \tag{5.6}$$

with the corresponding result for fermions as required by the total spin state.

In the remainder of this chapter, we make extensive use of the angular momentum-projected versions of these amplitudes. The relations between $\mathcal{M}$ and $\mathcal{M}^{\text{aux}}$ and their spherical harmonic projections are given in the usual way:

$$\mathcal{M}(P,p,p') = 4\pi\,|\boldsymbol{p}^\star|^\ell|\boldsymbol{p}'^\star|^{\ell'}\,Y^*_{\ell m}(\hat{\boldsymbol{p}}^\star)\,\widetilde{\mathcal{M}}_{\ell m,\ell' m'}(P,|\boldsymbol{p}^\star|,|\boldsymbol{p}'^\star|)\,Y_{\ell' m'}(\hat{\boldsymbol{p}}'^\star)\,, \tag{5.7}$$

$$\mathcal{M}^{\text{aux}}(P,p,p') = 4\pi\,|\boldsymbol{p}^\star|^\ell|\boldsymbol{p}'^\star|^{\ell'}\,Y^*_{\ell m}(\hat{\boldsymbol{p}}^\star)\,\widetilde{\mathcal{M}}^{\text{aux}}_{\ell m,\ell' m'}(P,|\boldsymbol{p}^\star|,|\boldsymbol{p}'^\star|)\,Y_{\ell' m'}(\hat{\boldsymbol{p}}'^\star)\,. \tag{5.8}$$

These projections have a straightforward relation to the partial wave expansion coefficients, which we denote again by an (ℓ) superscript:

$$\widetilde{\mathcal{M}}_{\ell m,\ell' m'}(P,|\boldsymbol{p}^\star|,|\boldsymbol{p}'^\star|) = \delta_{\ell\ell'}\delta_{mm'}\frac{1}{|\boldsymbol{p}^\star|^\ell|\boldsymbol{p}'^\star|^\ell}\,\mathcal{M}^{(\ell)}(P,|\boldsymbol{p}^\star|,|\boldsymbol{p}'^\star|)\,, \tag{5.9}$$

$$\widetilde{\mathcal{M}}^{\text{aux}}_{\ell m,\ell' m'}(P,|\boldsymbol{p}^\star|,|\boldsymbol{p}'^\star|) = \delta_{\ell\ell'}\delta_{mm'}\frac{1}{|\boldsymbol{p}^\star|^\ell|\boldsymbol{p}'^\star|^\ell}\,\mathcal{M}^{\text{aux}(\ell)}(P,|\boldsymbol{p}^\star|,|\boldsymbol{p}'^\star|)\,. \tag{5.10}$$

The symmetry properties of the amplitude under momentum exchanges, mentioned above, allow us to derive the following relations for identical bosons:

$$\mathcal{M}^{(\ell)}(P,|\boldsymbol{p}^\star|,|\boldsymbol{p}'^\star|) = \mathcal{M}^{\text{aux}(\ell)}(P,|\boldsymbol{p}^\star|,|\boldsymbol{p}'^\star|)\,, \qquad \text{for even } \ell\,, \tag{5.11}$$

$$\mathcal{M}^{(\ell)}(P,|\boldsymbol{p}^\star|,|\boldsymbol{p}'^\star|) = 0\,, \qquad \text{for odd } \ell\,. \tag{5.12}$$

with the corresponding results for fermions again as required by the total spin state.

The series given in eq. (5.3) can be manipulated in much the same way as the correlator series of eq. (3.26). All steps detailed in section 3.2 can be applied in a

straightforward manner and one obtains

$$i\mathcal{M}_L^{\text{aux}}(P) \equiv \sum_{n=0}^{\infty} \Big[\left(\xi^\dagger \, i\overline{\mathcal{K}}^{\text{os}}(P)\, \xi + 2ig^2\mathcal{T}(P)\right) iS(P,L) \Big]^n \left(\xi^\dagger \, i\overline{\mathcal{K}}^{\text{os}}(P)\, \xi + 2ig^2\mathcal{T}(P)\right) . \quad (5.13)$$

As with other similarly notated quantities and with a slight abuse of notation, $\mathcal{M}_L^{\text{aux}}(P)$ denotes the matrix with elements $\mathcal{M}^{\text{aux}}_{L,\boldsymbol{p}^\star\ell m;\boldsymbol{p}'^\star\ell' m'}(P)$ and not the auxiliary amplitude $\mathcal{M}_L^{\text{aux}}(P,p,p')$, which should be clear from context. Note that the $\boldsymbol{p}^\star$ and $\boldsymbol{p}'^\star$ labels of the elements $\mathcal{M}^{\text{aux}}_{L,\boldsymbol{p}^\star\ell m;\boldsymbol{p}'^\star\ell' m'}(P)$ may be misleading since the quantity actually only depends on the magnitudes of these vectors and the directional dependence has been removed by angular-momentum projection.[1]

A somewhat subtle point, explained in more detail in appendix C, is that the right-hand side of eq. (5.13) and the first term in eq. (5.3) differ by terms that vanish when all external momenta are set on shell. These are the terms collected in $\Delta\mathcal{M}_L^{\text{aux}}$ and, in this sense, it is actually eq. (5.13) that provides the precise definition of $\mathcal{M}_L^{\text{aux}}(P)$. Since the final step in our approach requires setting external legs on shell anyway, this distinction is irrelevant to the scattering amplitude predicted. $\Delta\mathcal{M}_L^{\text{aux}}$ is defined by taking the difference between eqs. (5.3) and (5.13) and $\Delta\mathcal{M}_L$ is from it by symmetrisation, i.e. by applying eq. (5.6).

To see why this is necessary, consider the $n = 0$ terms of eqs. (5.3) and (5.13) in turn. For eq. (5.3) this includes the off-shell parts of $\overline{B}^{\,\mathbb{T}}$ while in (5.13) this same object appears inside $\overline{\mathcal{K}}^{\text{os}}$ and is therefore defined with all momenta on the mass shell. The difference between the two terms is an example of the contributions collected in $\Delta\mathcal{M}_L$.

5.2 Integral equations

We now derive an integral equation relating $\overline{\mathcal{K}}^{\text{os}}(P)$ to the auxiliary amplitude $\mathcal{M}^{\text{aux}}(P,p,p')$, using the finite-volume amplitude $\mathcal{M}_L^{\text{aux}}$ to do so. We begin by

[1] A subtlety arises from the fact that the momentum indices in $\mathcal{M}_L^{\text{aux}}(P)$ are in the set of allowed finite-volume momenta. Consequently, one does not have the continuous rotational symmetry for the angular momentum projection. This is resolved by noting that the dependence in fact only appears in infinite-volume quantities after the reduction to eq. (5.13), and thus the extension of $\mathcal{M}_L^{\text{aux}}(P)$ to the continuous infinite-volume set of momenta is straightforward. See also the discussion above eq. (35) of ref. [21].

removing the infinite sum of eq. (5.13) by substituting this equation into itself, yielding

$$i\mathcal{M}_L^{\text{aux}}(P) = \left(\xi^\dagger\, i\overline{\mathcal{K}}^{\text{os}}(P)\,\xi + 2ig^2\mathcal{T}(P)\right) + i\mathcal{M}_L^{\text{aux}}(P)\, iS(P,L)\left(\xi^\dagger\, i\overline{\mathcal{K}}^{\text{os}}(P)\,\xi + 2ig^2\mathcal{T}(P)\right) . \quad (5.14)$$

Starting from this equation, we replace the energy as $E \to E + i\epsilon$ in the matrix $S(P,L)$, thereby introducing the $i\epsilon$ prescription to the relevant two-particle intermediate state pole, and take the infinite-volume limit $L \to \infty$. These steps lead to the following integral equation:

$$\widetilde{\mathcal{M}}^{\text{aux}}_{\ell m,\ell' m'}(P,|\boldsymbol{p}^\star|,|\boldsymbol{p}'^\star|) = \mathcal{K}^{\mathcal{T}}_{\ell m,\ell' m'}(P,|\boldsymbol{p}^\star|,|\boldsymbol{p}'^\star|) - \frac{1}{2}\int_0^\infty \frac{d|\boldsymbol{k}^\star|}{(2\pi)^3} \frac{\widetilde{\mathcal{M}}^{\text{aux}}_{\ell m,\ell'' m''}(P,|\boldsymbol{p}^\star|,|\boldsymbol{k}^\star|)\, 4\pi|\boldsymbol{k}^\star|^{2\ell''+2} H(\boldsymbol{k}^\star)\, \mathcal{K}^{\mathcal{T}}_{\ell'' m'',\ell' m'}(P,|\boldsymbol{k}^\star|,|\boldsymbol{p}'^\star|)}{4\omega_N(\boldsymbol{k}^\star)\left[(k^\star_{\text{os}})^2 - (\boldsymbol{k}^\star)^2 + i\epsilon\right]} , \quad (5.15)$$

where we have introduced

$$\mathcal{K}^{\mathcal{T}}_{\ell m,\ell' m'}(P,|\boldsymbol{p}^\star|,|\boldsymbol{p}'^\star|) \equiv \overline{\mathcal{K}}^{\text{os}}_{\ell m,\ell' m'}(P) + 2g^2\mathcal{T}_{\ell m,\ell' m'}(P,|\boldsymbol{p}^\star|,|\boldsymbol{p}'^\star|) . \quad (5.16)$$

Note that the $L \to \infty$ limit is performed with fixed external momentum, requiring an extension allowing these to be outside the set of discretised finite-volume momenta for a given L (see footnote 1 and the reference indicated for further discussion). Observe also that no L dependence appears in eq. (5.15) and that we have replaced the indices indicating discrete CM spatial momenta with continuous arguments. To reach this expression, we have also performed the angular integral resulting from the infinite-volume limit applied to the sums over $S(P,L)$.

As indicated at various points above, both $\overline{\mathcal{K}}^{\text{os}}$ and $\mathcal{M}^{\text{aux}}$ can be represented either as matrices with angular-momentum indices or as single functions of the scattering momenta. The two forms are connected in the usual way, already seen for $\mathcal{M}^{\text{aux}}$ in eq. (5.8). For $\overline{\mathcal{K}}^{\text{os}}$, this is simply

$$\overline{\mathcal{K}}^{\text{os}}(P,p,p') = 4\pi\,|\boldsymbol{p}^\star|^\ell |\boldsymbol{p}'^\star|^{\ell'}\, Y^*_{\ell m}(\hat{\boldsymbol{p}}^\star)\, \overline{\mathcal{K}}^{\text{os}}_{\ell m,\ell' m'}(P)\, Y_{\ell' m'}(\hat{\boldsymbol{p}}'^\star) , \quad (5.17)$$

Combining these relations with eq. (5.15), we obtain a second type of integral

equation, directly for the unprojected auxiliary amplitude:

$$\mathcal{M}^{\text{aux}}(P,p,p') = \mathcal{K}^{\mathcal{T}}(P,p,p') - \frac{1}{2}\int \frac{d^3\boldsymbol{k}^\star}{(2\pi)^3} \frac{\mathcal{M}^{\text{aux}}(P,p,k)\, H(\boldsymbol{k}^\star)\, \mathcal{K}^{\mathcal{T}}(P,k,p')}{4\omega_N(\boldsymbol{k}^\star)\big[(k^\star_{\text{os}})^2 - (\boldsymbol{k}^\star)^2 + i\epsilon\big]}\,, \quad (5.18)$$

where

$$\mathcal{K}^{\mathcal{T}}(P,p,p') = \overline{\mathcal{K}}^{\text{os}}(P,p,p') + 2g^2\mathcal{T}(P,p,p')\,, \quad (5.19)$$

and where the four-momentum arguments p, p', k are all taken to be on shell.

Though the relations given here completely solve the task of relating $\overline{\mathcal{K}}^{\text{os}}$ to $\mathcal{M}^{\text{aux}}$ in principle, the singularities within $\mathcal{M}^{\text{aux}}$ and $\mathcal{T}$ could well make numerical evaluation very difficult. For this reason, we can consider an alternative, based on a divergence-free intermediate quantity.

5.2.1 Divergence-free amplitude

To find the physical scattering amplitude, $\mathcal{M}(P,p,p')$, from the intermediate quantity, $\overline{\mathcal{K}}^{\text{os}}(P,p,p')$, one needs to set all external four-momenta, p, $P-p$, p', $P-p'$, to their on-shell values. This, in turn, requires setting the momenta within the auxiliary amplitude, $\mathcal{M}^{\text{aux}}(P,p,p')$, on shell. However, this may lead to an unstable numerical evaluation, associated with the fact that the angular-momentum components of the auxiliary amplitude contain a branch point at $s = 4M_N^2 - M_\pi^2$, and the unprojected amplitude contains a pole at $t = M_\pi^2$. Since both of these singularities only arise for on-shell momenta, extrapolating or interpolating to physical kinematics could be challenging.

Moreover, the partial-wave expansion of $\mathcal{M}^{\text{aux}}(P,p,p')$ is expected to be slowly converging in the vicinity of the t-channel pole and, for this reason, an order-by-order determination of the partial-wave components through eq. (5.15) will not be useful near $t = M_\pi^2$. This is partly addressed with the unprojected integral equation, eq. (5.18). An alternative solution, again taking inspiration from refs. [20, 119], is to instead introduce a divergence-free scattering amplitude, defined as follows:

$$\mathcal{M}^{\text{df}}(P,p,p') \equiv \mathcal{M}^{\text{aux}}(P,p,p') - 2g^2\mathcal{T}(P,p,p')\,. \quad (5.20)$$

Projecting this quantity to spherical harmonics as in eq. (5.8) gives a faster converging series, down to the neighbourhood of the second left-hand cut, i.e. for

$s \gtrsim (2M_N)^2 - (2M_\pi)^2$. We can substitute the divergence-free amplitude into eq. (5.18) to find

$$\mathcal{M}^{\mathrm{df}}(P,p,p') = \overline{\mathcal{K}}^{\mathrm{os}}(P,p,p') - \frac{1}{2}\int \frac{d^3\boldsymbol{k}}{(2\pi)^3} \frac{H(\boldsymbol{k}^\star)\big[\mathcal{M}^{\mathrm{df}}(P,p,k) + 2g^2\mathcal{T}(P,p,k)\big]\mathcal{K}^{\mathcal{T}}(P,k,p')}{4\omega_N(\boldsymbol{k})\big[(k^\star_{\mathrm{os}})^2 - (\boldsymbol{k}^\star)^2 + i\epsilon\big]}\,. \quad (5.21)$$

The two terms in the numerator on the right-hand side (in square brackets) should be treated in practice as two separate integrals. The $\mathcal{T}$-dependent integral can be calculated numerically given knowledge of $\overline{\mathcal{K}}^{\mathrm{os}}(P,p,p')$ and g. We can then for $\mathcal{M}^{\mathrm{df}}(P,p,p')$ using standard integral-equation techniques, with the $\mathcal{T}$-dependent integral and $\overline{\mathcal{K}}^{\mathrm{os}}$ forming the driving term.

Having obtained $\mathcal{M}^{\mathrm{df}}(P,p,p')$, one can recover the amplitude $\mathcal{M}(P,p,p')$ by combining eqs. (5.6) and (5.20)

$$\mathcal{M}(P,p,p') = \frac{1}{2}\left[\mathcal{M}^{\mathrm{df}}(P,p,p') + \mathcal{M}^{\mathrm{df}}(P,p,P-p')\right] + g^2\mathcal{E}(P,p,p')\,. \quad (5.22)$$

We can see that, when putting external arguments on shell, the $\mathcal{E}(P,p,p')$ term (as defined in eq. (3.65)) is responsible for generating the t- and u-channel π exchange poles present in the amplitude, and the divergence-free auxiliary amplitudes does not carry any singular behaviour until one reaches the two-pion-exchange cut.

5.2.2 Analytic continuation

Evaluating the on-shell scattering amplitude below threshold requires analytically continuing the external momenta to be complex, such that $|\boldsymbol{p}^\star| = |\boldsymbol{p}'^\star| = i\sqrt{M_N^2 - s/4}$. One method to achieve this is to first solve the integral equation (5.21) for real external momenta, hence obtaining the amplitude, and then compute

the sub-threshold on-shell values using the relation

$$\begin{aligned}\mathcal{M}(P,p,p') = \overline{\mathcal{K}}^{\text{os}}(P,p,p') + ig^2\mathcal{E}(P,p,p') \\ + \frac{1}{2}\int\frac{d^3\boldsymbol{k}}{(2\pi)^3}\frac{H(\boldsymbol{k}^\star)\,\mathcal{K}^{\mathcal{T}}(P,p,k)\big[\overline{\mathcal{K}}^{\text{os}}(P,k,p') + ig^2\mathcal{E}(P,k,p')\big]}{4\omega_N(\boldsymbol{k})\big[(k^\star_{\text{os}})^2 - (\boldsymbol{k}^\star)^2 + i\epsilon\big]} \\ - \frac{1}{4}\int\frac{d^3\boldsymbol{k}}{(2\pi)^3}\int\frac{d^3\boldsymbol{k}'}{(2\pi)^3}\frac{H(\boldsymbol{k}^\star)\,\mathcal{K}^{\mathcal{T}}(P,p,k)\,\mathcal{M}(P,k,k')}{4\omega_N(\boldsymbol{k})\big[(k^\star_{\text{os}})^2 - (\boldsymbol{k}^\star)^2 + i\epsilon\big]} \\ \times\ \frac{H(\boldsymbol{k}'^\star)\mathcal{K}^{\mathcal{T}}(P,k',p')}{4\omega_N(\boldsymbol{k}')\big[(k'^\star_{\text{os}})^2 - (\boldsymbol{k}'^\star)^2 + i\epsilon\big]}\,.\end{aligned} \tag{5.23}$$

The momenta p, p', $P-p$ and $P-p'$ can be put on shell and taken below threshold here. The key point is that the amplitude on the right-hand side is nested between two loops and thus its arguments are always real. Knowledge of $\mathcal{M}$ for real momenta can thus be exploited to obtain its sub-threshold on-shell value. These methods can similarly be applied to continue the amplitude into the complex plane.

5.2.3 Reduction of the integral equations

In the paper, we define the auxiliary (i.e. unsymmetrised) finite-volume amplitude $\mathcal{M}_L^{\text{aux}}(P)$ as the series

$$i\mathcal{M}_L^{\text{aux}}(P) \equiv \sum_{n=0}^{\infty}\Big(\big[\xi^\dagger\, i\overline{\mathcal{K}}^{\text{os}}(P)\,\xi + 2ig^2\mathcal{T}(P)\big]\,iS(P,L)\Big)^n\,\big[\xi^\dagger\, i\overline{\mathcal{K}}^{\text{os}}(P)\,\xi + 2ig^2\mathcal{T}(P)\big]\,. \tag{5.24}$$

This can be rewritten as a matrix equation for $\mathcal{M}_L^{\text{aux}}(P)$:

$$\begin{aligned}i\mathcal{M}_L^{\text{aux}}(P) = \big[\xi^\dagger\, i\overline{\mathcal{K}}^{\text{os}}(P)\,\xi + 2ig^2\mathcal{T}(P)\big] + \\ \big[\xi^\dagger\, i\overline{\mathcal{K}}^{\text{os}}(P)\,\xi + 2ig^2\mathcal{T}(P)\big]\,iS(P,L)\,i\mathcal{M}_L^{\text{aux}}(P)\,.\end{aligned} \tag{5.25}$$

Replacing $E \to E + i\epsilon$ and taking the limit $L \to \infty$, we obtain the integral equations for the infinite-volume auxiliary amplitude $\mathcal{M}^{\text{aux}}(P)$. If, instead, one replaces $E \to E + i\epsilon$ and takes the real part of the pole before taking the infinite-volume limit, we can obtain an integral equation for an auxiliary K-matrix, from which we can get the actual K-matrix after symmetrisation and placement of the momentum arguments on shell.

As an alternative to the integral equations, it is possible to relate the $\overline{\mathcal{K}}^{\text{os}}(P)$ matrix directly to the K-matrix algebraically. Let us first define a ladder quantity $\mathcal{D}_L(P)$,

given by

$$i\mathcal{D}_L(P) = 2ig^2\mathcal{T}(P) + 2ig^2\mathcal{T}(P)\, iS(P,L)\, i\mathcal{D}_L(P)\,, \tag{5.26}$$

$$= \sum_{n=0}^{\infty} 2ig^2\mathcal{T}(P)\big[iS(P,L)\, 2ig^2\mathcal{T}(P)\big]^n\,. \tag{5.27}$$

We can re-express $F_L^{\mathcal{T}}(P)$ in terms of this quantity:

$$iF_L^{\mathcal{T}}(P) = \xi\, iS(P,L)\,[1 + i\mathcal{D}_L(P)\, iS(P,L)]\,\xi^\dagger\,, \tag{5.28}$$

and also define the objects

$$iF_L^{\mathcal{T},\text{left}}(P) = [1 + i\mathcal{D}_L(P)\, iS(P,L)]\,\xi^\dagger\,, \tag{5.29}$$

$$iF_L^{\mathcal{T},\text{right}}(P) = \xi\,[1 + iS(P,L)\, i\mathcal{D}_L(P)]\,. \tag{5.30}$$

$F_L^{\mathcal{T}}(P)$ is a matrix in angular momentum index space $\ell m, \ell' m'$, while $F_L^{\mathcal{T},\text{left}}(P)$ is a matrix indexed by $\boldsymbol{k}^\star \ell m, \ell' m'$ and $F_L^{\mathcal{T},\text{right}}(P)$ is a matrix indexed by $\ell m, \boldsymbol{k}'^\star \ell' m'$. Making use of these objects, we can rewrite the finite-volume amplitude series as

$$i\mathcal{M}_L^{\text{aux}}(P) = i\mathcal{D}_L(P) + \sum_{n=0}^{\infty} iF_L^{\mathcal{T},\text{left}}(P)\, i\overline{\mathcal{K}}^{\text{os}}(P)\big[iF_L^{\mathcal{T}}(P)\, i\overline{\mathcal{K}}^{\text{os}}(P)\big]^n\, iF_L^{\mathcal{T},\text{right}}(P)\,, \tag{5.31}$$

$$= i\mathcal{D}_L(P) + iF_L^{\mathcal{T},\text{left}}(P)\,\frac{i}{\overline{\mathcal{K}}^{\text{os}}(P)^{-1} + F_L^{\mathcal{T}}(P)}\, iF_L^{\mathcal{T},\text{right}}(P)\,. \tag{5.32}$$

Suppose now that we fix the external spatial momentum arguments, say $\boldsymbol{k} = \boldsymbol{p}$, $\boldsymbol{k}' = \boldsymbol{p}'$, and denote it as an argument:

$$i\mathcal{M}_L^{\text{aux}}(P,\boldsymbol{p},\boldsymbol{p}') = i\mathcal{D}_L(P,\boldsymbol{p},\boldsymbol{p}') + iF_L^{\mathcal{T},\text{left}}(P,\boldsymbol{p})\,\frac{i}{\overline{\mathcal{K}}^{\text{os}}(P)^{-1} + F_L^{\mathcal{T}}(P)}\, iF_L^{\mathcal{T},\text{right}}(P,\boldsymbol{p}')\,. \tag{5.33}$$

All the matrices involved are in angular momentum index space now. Replacing

$E \to E + i\epsilon$ and taking the infinite-volume limit, we can get

$$i\mathcal{K}^{\text{aux}}(P, |\boldsymbol{p}^\star|, |\boldsymbol{p}'^\star|) = i\mathcal{D}_\infty(P, |\boldsymbol{p}^\star|, |\boldsymbol{p}'^\star|) + iF_\infty^{\mathcal{T},\text{left}}(P, |\boldsymbol{p}^\star|)\, \frac{i}{\overline{\mathcal{K}}^{\text{os}}(P)^{-1} + F_\infty^{\mathcal{T}}(P)}\, iF_\infty^{\mathcal{T},\text{right}}(P, |\boldsymbol{p}'^\star|)\,. \quad (5.34)$$

Here, all the infinite-volume loops inside the definitions of these matrices are taken using principal value prescriptions. Note that, in the infinite-volume limit, the matrices can only depend on the magnitude of the centre-of-mass spatial momentum arguments.

We can then place the auxiliary K-matrix on shell and symmetrise in the outgoing momenta to obtain a relation between the physical K-matrix and the K-bar matrix:

$$\mathcal{K}^{\text{os}}(s) = \mathcal{D}_\infty^{\text{os}}(P) - F_\infty^{\mathcal{T},\text{left, os}}(P)\, \frac{1}{\overline{\mathcal{K}}^{\text{os}}(P)^{-1} + F_\infty^{\mathcal{T}}(P)}\, F_\infty^{\mathcal{T},\text{right, os}}(P)\,. \quad (5.35)$$

Note that the unprojected K-matrix $\mathcal{K}(P, p, p')$ and the ladder $\mathcal{D}_\infty(P, p, p')$, with arguments on shell, contain the t-channel exchange pole. Therefore, partial-wave expansions of these objects might converge slowly near and on the resulting left-hand cut. This should not be a problem for the combination $(\mathcal{K}(P, p, p') - \mathcal{D}_\infty(P, p, p'))$.

The unprojected function $\mathcal{D}_\infty(P, p, p')$, with p and p' on shell, obeys the integral equation

$$\mathcal{D}_\infty(P, p, p') = 2g^2\mathcal{T}(P, p, p') - \frac{1}{2}\int \frac{d^3\boldsymbol{k}^\star}{(2\pi)^3} \frac{H(\boldsymbol{k}^\star)\, 2g^2\mathcal{T}(P, p, k)\, \mathcal{D}_\infty(P, k, p')}{4\omega(\boldsymbol{k}^\star)\left[(k_{\text{os}}^\star)^2 - (\boldsymbol{k}^\star)^2 + i\epsilon\right]}\,. \quad (5.36)$$

One can solve this equation and hence compute the on-shell matrix $\mathcal{D}_\infty^{\text{os}}(P)$, as well as the matrices $F_\infty^{\mathcal{T}}(P)$, $F_\infty^{\mathcal{T},\text{left, os}}(P)$ and $F_\infty^{\mathcal{T},\text{right, os}}(P)$, which obey infinite-volume relations analogous to their finite-volume versions.

Conclusions and Outlook

In this thesis, we investigated the issues arising in applications of the Lüscher scattering formalism [3] and its many extensions [4–14] to sub-threshold energies that coincide with a left-hand branch cut in the partial-wave scattering amplitudes of the system considered, which is generated by a single light meson exchange.

This was first highlighted as a practical problem in lattice calculations in [15], a calculation of baryon-baryon scattering in the H-dibaryon sector at the $SU(3)$-flavor-symmetric point. In that work, finite-volume energies were extracted on top of the cut and could not be used to extract scattering observables due to the breakdown of the standard formalism. More recently, the same problem was also pointed out in calculations of DD^* scattering, relevant for lattice studies of the doubly-charmed tetraquark $T_{cc}(3875)^+$ [18, 19, 120, 121].

To circumvent the issues posed by the presence of the left-hand cut, we presented alternative forms of the Lüscher method which have an extended region of validity and allow the computation of the physical amplitude near and on the cut.

In Chapter 3, we presented the derivation of two alternative quantisation conditions, eqs. (3.81) and (3.102) in the context of elastic NN scattering, where a lighter pion π can be exchanged. These conditions are distinguished by the underlying index space used and are valid both in the elastic regime and at subthreshold energies down to the nearest two-particle exchange cut. Although framed in terms of NN scattering, the discussion applies without modification to any single-channel elastic scattering process with identical particles (and arbitrary intrinsic spins).

This was followed, in Chapter 4, by the derivation of quantisation conditions, eqs. (4.49) and (4.50), that apply to nonidentical spinless particles that can exchange a lighter spinless particle in the u-channel, which can be seen as a scalar model of DD^*.

The quantisation conditions derived in this work allow us to extract an intermediate infinite-volume quantity, which we call $\overline{\mathcal{K}}^{\text{os}}$, from the finite-volume energy levels. These quantities are related, in a subsequent step, to the physical scattering amplitude. This is achieved through the use of integral equations, as derived in Chapter 5.

Immediate formal developments of the work presented here are underway, namely the conclusion of the extension to non-degenerate particles and the further extension to multi-channel processes, relevant for processes such as coupled-channel DD^*-D^*D^* scattering [122]. Numerical work seeking to test and cross-check the formalism with results obtained from the three-particle formalism [93, 123, 124] is also ongoing.

Longer-term goals would involve the treatment of lower left-hand cuts, generated by multi-particle exchanges. This would extend the range of validity of the formalism to lower energies but involves addressing a few technical challenges. Given the increased interest in DD^* systems in recent years, there is now a wealth of lattice data on which the formalism developed here can be applied with little modification. Therefore, implementation and applications to real lattice can also be considered.

Besides the plane-wave approach already mentioned in the text [19, 116, 125, 126], other approaches have since been proposed, including the direct use of the relativistic three-particle formalism [127] and a NREFT-based method [128]. Clarifying the relations between these proposals will be an interesting future prospect.

Appendix A

Manipulating the finite-volume S-function

In this appendix, we describe the steps required to go from eq. (3.34) to eqs. (3.38) and (3.39) in Chapter 3. Recalling the definitions, the task is to show that

$$\mathcal{L} \circ_{\mathsf{fv}} \mathcal{R}^\dagger = \mathcal{I}^{[2]}(P) + \sum_{\boldsymbol{k}} \frac{\mathcal{L}(P,k)\, i\, \mathcal{R}^*(P,k)}{2L^3 \cdot 2\omega_N(\boldsymbol{k}) \left[(E-\omega_N(\boldsymbol{k}))^2 - \omega_N(\boldsymbol{P}-\boldsymbol{k})^2\right]} \Bigg|_{k^0=\omega_N(\boldsymbol{k})},$$

can be rewritten as

$$\begin{aligned}\mathcal{L} \circ_{\mathsf{fv}} \mathcal{R}^\dagger &= \mathcal{I}^{[3]}(P) \\ &\quad + \widetilde{\mathcal{L}}_{\boldsymbol{k}^\star \ell m}(P)\, \frac{1}{2L^3}\, \frac{i4\pi\, Y_{\ell m}(\hat{\boldsymbol{k}}^\star)\, Y^*_{\ell' m'}(\hat{\boldsymbol{k}}^\star)\, \delta_{\boldsymbol{k}^\star \boldsymbol{k}'^\star}\, |\boldsymbol{k}^\star|^{\ell+\ell'}\, H(\boldsymbol{k}^\star)}{4\omega_N(\boldsymbol{k}) \left[(k^\star_{\mathrm{os}})^2 - (\boldsymbol{k}^\star)^2\right]}\, \widetilde{\mathcal{R}}^*_{\boldsymbol{k}'^\star \ell' m'}(P)\,, \end{aligned} \quad \text{(A.1)}$$

where we have combined eqs. (3.38) and (3.39) to reach eq. (A.1).

Taking the difference of these two results and using the definitions of $\widetilde{\mathcal{L}}_{\ell m}(P, |\boldsymbol{k}^\star|)$ and $\widetilde{\mathcal{R}}_{\ell m}(P, |\boldsymbol{k}^\star|)$, eqs. (3.35) and (3.36), it remains to show

$$\begin{aligned}\mathcal{I}^{[2]}(P) - \mathcal{I}^{[3]}(P) = \frac{i}{2L^3} \sum_{\boldsymbol{k}} \frac{1}{2\omega_N(\boldsymbol{k})} \mathcal{L}(P,k)\, \mathcal{R}^*(P,k) \\ \times \left[\frac{1}{(E-\omega_N(\boldsymbol{k}))^2 - \omega_N(\boldsymbol{P}-\boldsymbol{k})^2} - \frac{H(\boldsymbol{k}^\star)/2}{(k^\star_{\mathrm{os}})^2 - (\boldsymbol{k}^\star)^2}\right]\Bigg|_{k^0=\omega_N(\boldsymbol{k})}, \end{aligned} \quad \text{(A.2)}$$

with the key claim being that $\mathcal{I}^{[2]}(P) - \mathcal{I}^{[3]}(P)$ only has exponentially suppressed L dependence. This follows from the Poisson summation formula, provided that

the summand on the right-hand side has a horizontal strip of analyticity in the complex-$|\boldsymbol{k}|$ plane, which includes the real axis. Here we abuse notation by thinking of $z = |\boldsymbol{k}|$ as a complex variable.

For $P^2 = s < (2M_N + M_\pi)^2$, the analyticity holds for $\mathcal{L}(P,k)\,\mathcal{R}^*(P,k)$ by construction, and also for $\omega_N(\boldsymbol{k})$, which is analytic for $|\mathrm{Im}[|\boldsymbol{k}|]| < M_N$. The non-trivial step is to show the same for the difference of the two terms in square brackets. To demonstrate this we define the quantity in question via

$$Q(P,\boldsymbol{k}) = \frac{1}{(E-\omega_N(\boldsymbol{k}))^2 - \omega_N(\boldsymbol{P}-\boldsymbol{k})^2} - \frac{H(\boldsymbol{k}^\star)/2}{(k^\star_{\mathrm{os}})^2 - (\boldsymbol{k}^\star)^2}\,. \tag{A.3}$$

We then observe that

$$(E-\omega_N(\boldsymbol{k}))^2 - \omega_N(\boldsymbol{P}-\boldsymbol{k})^2 = (P-k)^2 - M_N^2 = (E^\star - \omega_N(\boldsymbol{k}^\star))^2 - \omega_N(\boldsymbol{k}^\star)^2\,, \tag{A.4}$$

where we have used $P^\mu = (E,\boldsymbol{P})^\mu$ and $k^\mu = (\omega_N(\boldsymbol{k}),\boldsymbol{k})^\mu$ in the middle step. This makes manifest that the combination is a Lorentz scalar and can be written in the CM frame, as we have done.

Further algebraic manipulations then yield

$$(E-\omega_N(\boldsymbol{k}))^2 - \omega_N(\boldsymbol{P}-\boldsymbol{k})^2 = \frac{E^\star}{E^\star + 2\omega_N(\boldsymbol{k}^\star)}\left[E^{\star 2} - 4\omega_N(\boldsymbol{k}^\star)^2\right]. \tag{A.5}$$

Substituting $(k^\star_{\mathrm{os}})^2 = E^{\star 2}/4 - M_N^2$ and then substituting back for $Q(P,\boldsymbol{k})$, we finally deduce

$$Q(P,\boldsymbol{k}) = \left[\frac{E^\star + 2\omega_N(\boldsymbol{k}^\star)}{4E^\star} - \frac{H(\boldsymbol{k}^\star)}{2}\right]\frac{1}{(k^\star_{\mathrm{os}})^2 - (\boldsymbol{k}^\star)^2}\,. \tag{A.6}$$

Note that the factor in square brackets scales as $[(k^\star_{\mathrm{os}})^2 - (\boldsymbol{k}^\star)^2]$ as $(\boldsymbol{k}^\star)^2 \to (k^\star_{\mathrm{os}})^2$, and therefore cancels the pole. This holds because

$$\left[\frac{E^\star + 2\omega_N(\boldsymbol{k}^\star)}{4E^\star} - \frac{H(\boldsymbol{k}^\star)}{2}\right]\Bigg|_{(\boldsymbol{k}^\star)^2=(k^\star_{\mathrm{os}})^2} = 0\,, \tag{A.7}$$

together with the fact that all functions are analytic for $(\boldsymbol{k}^\star)^2 > -M_N^2$. We thus conclude a non-zero strip of analyticity for $Q(P,\boldsymbol{k})$.

The manipulations needed to reach the corresponding expressions for the loop contributions and $S(P,L)$ for non-degenerate particles – such as those given in

eqs. (4.18)-(4.20) and (4.25) of Chapter 4 – are very similar to those outlined above, with the appropriate modifications to accommodate non-degenerate masses.

Appendix B

Analyticity of the Bethe-Salpeter kernel

In this appendix, we give additional details concerning the conditions under which the Bethe-Salpeter kernel is an analytic function of E with exponentially suppressed volume effects in its finite-volume analogue.

The discussion is broken into two subsections. Firstly, we analyse the diagram shown in figure B.1(a) from various perspectives to illustrate an important and subtle point about diagrams with u-channel-like momentum routing. We show that, in our energy range of interest: $(2M_N)^2 - (2M_\pi)^2 < s < (2M_N + M_\pi)^2$, this diagram has no singularities besides that associated with the two-particle s-channel cut. At the same time, we find that applying the analysis of section 3.2.3 to this diagram does lead to neglected singularities inside the term denoted $\mathcal{I}^{[2]}(P)$, together with spurious singularities in the terms that are kept explicit. This is an artefact of the partially off-shell kinematics and is removed once all external legs of the Bethe-Salpeter kernel are set on shell. The issue must nonetheless be addressed since the derivation uses properties of the partially off-shell Bethe-Salpeter kernel to reach the final result.

After demonstrating the issue in detail for the diagram of figure B.1(a), we explain how the result generalises to all contributions to the Bethe-Salpeter kernel. The basic insight is that a diagram with a u-channel sub-diagram is invariant under the replacement $k \to P - k$, which converts it to a t-channel sub-diagram. In this sense, the distinction between u- and t-channel is artificial and relies on the particular

choice of internal momentum routing. This ultimately leads to the definition of $B^{\mathbb{T}}$, an intermediate quantity that resolves the issue. When the partially off-shell kinematics are projected fully on shell, $B^{\mathbb{T}}$ can be safely symmetrised to the usual kernel. As a result, our final expressions are not affected by these issues.

B.1 The u-channel loop

We begin by using time-ordered perturbation theory (TOPT) to directly identify the singularities that arise in the full diagram shown in figure B.1(a). For concreteness, we envision evaluating the diagram in a finite volume, such that all spatial loop momenta are summed. The corresponding infinite-volume behaviour can be inferred by replacing the sums at any stage with an integral, together with a pole prescription. The external kinematics of the diagram are evaluated with p on shell: $p^0 = \omega_N(\boldsymbol{p})$, but with $P - p = (E - \omega_N(\boldsymbol{p}), \boldsymbol{P} - \boldsymbol{p})$ generally off shell.

As is shown in figure B.1(b), six time-orderings contribute. The corresponding singularities are given by multiplying factors of $[E_{\text{cut}} - \sum_i \omega_i]^{-1}$, one for each vertical cut, before summing over time orderings. Here E_{cut} is the energy flowing across the cut and $\sum_i \omega_i$ the sum of on-shell energies for the internal propagators that intersect the cut. Following ref. [117], E_{cut} is defined as the sum of inflowing p^0 components into all vertices appearing to the left of the cut. So, for example, when only vertex B appears to the left, then $E_{\text{cut}} = E - \omega_N(\boldsymbol{p})$.

Studying B.1(b), we note that only two of the six time-orderings have the $E - \omega_N(\boldsymbol{k}) - \omega_N(\boldsymbol{P} - \boldsymbol{k})$ singularity leading to the relevant two-particle pole. These are the first two diagrams, labelled ABC and BAC, respectively. The full singularity structure of the two orderings is

$$[ABC] = \frac{1}{\omega_N(\boldsymbol{p}) - \omega_N(\boldsymbol{P} - \boldsymbol{k}) - \omega_\pi(\boldsymbol{P} - \boldsymbol{p} - \boldsymbol{k} - \boldsymbol{\ell}) - \omega_\pi(\boldsymbol{\ell})} \frac{1}{E - \omega_N(\boldsymbol{k}) - \omega_N(\boldsymbol{P} - \boldsymbol{k})}, \tag{B.1}$$

$$[BAC] = \frac{1}{E - \omega_N(\boldsymbol{p}) - \omega_N(\boldsymbol{k}) - \omega_\pi(\boldsymbol{P} - \boldsymbol{p} - \boldsymbol{k} - \boldsymbol{\ell}) - \omega_\pi(\boldsymbol{\ell})} \frac{1}{E - \omega_N(\boldsymbol{k}) - \omega_N(\boldsymbol{P} - \boldsymbol{k})}, \tag{B.2}$$

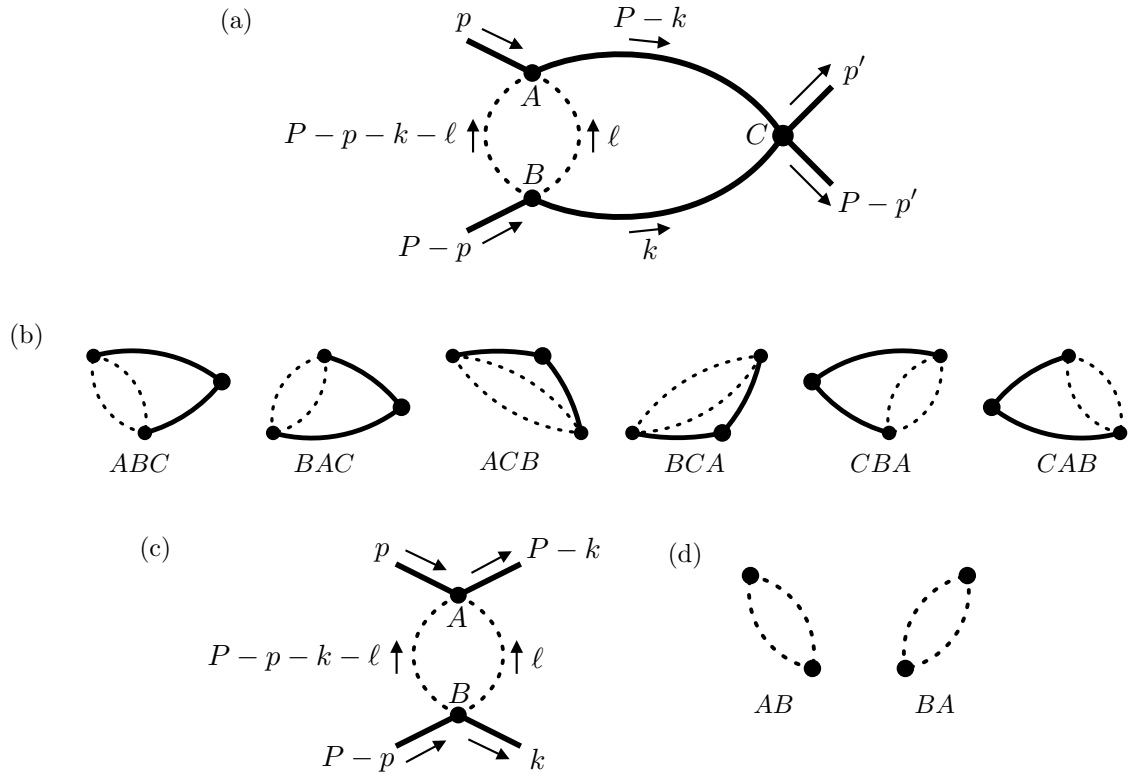

Figure B.1 *(a) u-channel-loop diagram with momentum routing that causes problems in the standard analysis of section 3.2.3; (b) the time-ordered perturbation theory (TOPT) contributions to the diagram of (b); (c) the u-channel contribution to the Bethe-Salpeter kernel in isolation; (d) TOPT contributions corresponding to (c).*

where we have introduced $[ABC]$, etc. as a shorthand, representing the poles generated by a given vertex ordering.

Crucially, both the $[ABC]$ and $[BAC]$ have no singularities in the relevant kinematic range, besides that at $E = \omega_N(\boldsymbol{k}) + \omega_N(\boldsymbol{P} - \boldsymbol{k})$. However, if we consider the simple u-channel loop of figure B.1(c) and the corresponding time orderings of figure B.1(d) in isolation, we instead get the following contributions:

$$[AB] = \frac{1}{\omega_N(\boldsymbol{p}) - E + \omega_N(\boldsymbol{k}) - \omega_\pi(\boldsymbol{P} - \boldsymbol{p} - \boldsymbol{k} - \boldsymbol{\ell}) - \omega_\pi(\boldsymbol{\ell})}\,, \tag{B.3}$$

$$[BA] = \frac{1}{E - \omega_N(\boldsymbol{p}) - \omega_N(\boldsymbol{k}) - \omega_\pi(\boldsymbol{P} - \boldsymbol{p} - \boldsymbol{k} - \boldsymbol{\ell}) - \omega_\pi(\boldsymbol{\ell})}\,. \tag{B.4}$$

In these one-loop diagrams, the notion of external momentum has changed. For example, vertex A now has the external momenta $p - P + k$ flowing into it. As a result, the cut in $[AB]$ has $E_{\text{cut}} = \omega_N(\boldsymbol{p}) - E + \omega_N(\boldsymbol{k})$. We see that, while $[BA]$ exactly matches the factor appearing within $[BAC]$, the $[AB]$ contribution differs. The reason this matters is that the $[AB]$ form is what appears after k^0 integration is applied to the general two-particle loop in section 3.2.3. See, in particular, eq. (3.34), which is repeated in the paragraph after next.

The first factor in $[ABC]$ can be converted to $[AB]$ via the replacement $\omega_N(\boldsymbol{P}-\boldsymbol{k}) \to E - \omega_N(\boldsymbol{k})$. Thus, the difference between the two is something that vanishes whenever $E = \omega_N(\boldsymbol{k}) + \omega_N(\boldsymbol{P} - \boldsymbol{k})$. Such replacements are often valid in deriving finite-volume relations since they amount to neglecting a difference with exponentially suppressed L dependence. In this case, the replacement is invalid, since the form of $[AB]$ in isolation has unphysical singularities. For example, in the case where $\boldsymbol{P} = \boldsymbol{0}$ and $\boldsymbol{p} = -\boldsymbol{k}$, the $[AB]$ factor has a pole at $E = 2\omega_N(\boldsymbol{p}) - 2\omega_\pi(\boldsymbol{\ell})$. There is no pole in the original diagram at this location; the singularity is only an artefact of setting the Bethe-Salpeter kernel to partially off-shell kinematics.

An alternative way to identify the same complication is to track what goes wrong in the derivation of section 3.2.3, for this type of diagram. The problem is the step going from eq. (3.33),

$$\mathcal{L} \circ_{\text{FV}} \mathcal{R}^\dagger = \mathcal{I}^{[1]}(P) + \frac{1}{2} \int \frac{dk^0}{2\pi} \frac{1}{L^3} \sum_{\boldsymbol{k}} \frac{\mathcal{L}(P,k)\, i^2\, \mathcal{R}^*(P,k)}{[k^2 - M_N^2 + i\epsilon][(P-k)^2 - M_N^2 + i\epsilon]}\,,$$

to eq. (3.34),

$$\mathcal{L} \circ_{\mathrm{FV}} \mathcal{R}^\dagger = \mathcal{I}^{[2]}(P) + \sum_{\boldsymbol{k}} \frac{\mathcal{L}(P,k)\, i\, \mathcal{R}^*(P,k)}{2L^3 \cdot 2\omega_N(\boldsymbol{k}) \big[(E - \omega_N(\boldsymbol{k}))^2 - \omega_N(\boldsymbol{P}-\boldsymbol{k})^2 \big]} \bigg|_{k^0 = \omega_N(\boldsymbol{k})} ,$$

(both repeated here for convenience). As we now show, the k^0 integration has contributions other than the $k^0 = \omega_N(\boldsymbol{k})$ part and these generate singularities in $\mathcal{I}^{[2]}(P)$, which thus carries power-like L dependence. Simultaneously, singularities and associated power-like L dependence are hidden within $\mathcal{L}(P,k)$ in eq. (3.34). The poles cancel and are also both removed when all external legs are set on shell.

To avoid clutter of notation, we demonstrate the problem explicitly for slightly simplified three-vector kinematics. In particular, we take $\boldsymbol{P} = \boldsymbol{0}$ and $\boldsymbol{p} = \boldsymbol{k}$ (aligned rather than anti-aligned as above). For these values, the pion energies are distinct: $\omega_\pi(\boldsymbol{\ell})$ and $\omega_\pi(2\boldsymbol{p}+\boldsymbol{\ell})$ while all on-shell nucleons carry $\omega_N(\boldsymbol{p})$. The relevant singularities are then captured by the function

$$\begin{aligned} \mathcal{F}(\boldsymbol{p},\boldsymbol{\ell}) \equiv \int \frac{dk^0}{2\pi} \int \frac{d\ell^0}{2\pi} & \frac{1}{\ell^0 - \omega_\pi(\boldsymbol{\ell}) + i\epsilon} \frac{1}{\ell^0 + \omega_\pi(\boldsymbol{\ell}) - i\epsilon} \\ & \frac{1}{k^0 + \ell^0 + \omega_N(\boldsymbol{p}) - E - \omega_\pi(2\boldsymbol{p}+\boldsymbol{\ell}) + i\epsilon} \\ & \frac{1}{k^0 + \ell^0 + \omega_N(\boldsymbol{p}) - E + \omega_\pi(2\boldsymbol{p}+\boldsymbol{\ell}) - i\epsilon} \\ & \frac{1}{k^0 - \omega_N(\boldsymbol{p}) + i\epsilon} \frac{1}{k^0 + \omega_N(\boldsymbol{p}) - i\epsilon} \\ & \frac{1}{k^0 - E - \omega_N(\boldsymbol{p}) + i\epsilon} \frac{1}{k^0 - E + \omega_N(\boldsymbol{p}) - i\epsilon} , \end{aligned} \tag{B.5}$$

which follows from simply factorizing the four covariant propagators.

Beginning with the ℓ^0 integral (which is internal to $\mathcal{L}(P,k)$ in the general construction), and closing the contour in the lower half of the complex ℓ^0 plane, we note that two terms arise from encircling the poles at $\ell^0 = \omega_\pi(\boldsymbol{\ell}) - i\epsilon$ and

$\ell^0 = -k^0 - \omega_N(\boldsymbol{p}) + E + \omega_\pi(2\boldsymbol{p}+\boldsymbol{\ell}) - i\epsilon$. The result reads

$$\begin{aligned}\mathcal{F}(\boldsymbol{p},\boldsymbol{\ell}) \equiv (-i)\frac{1}{2\omega_\pi(\boldsymbol{\ell})}\int\frac{dk^0}{2\pi}\,&\frac{1}{k^0+\omega_\pi(\boldsymbol{\ell})+\omega_N(\boldsymbol{p})-E-\omega_\pi(2\boldsymbol{p}+\boldsymbol{\ell})+i\epsilon}\\ &\frac{1}{k^0+\omega_\pi(\boldsymbol{\ell})+\omega_N(\boldsymbol{p})-E+\omega_\pi(2\boldsymbol{p}+\boldsymbol{\ell})-i\epsilon}\\ &\frac{1}{k^0-\omega_N(\boldsymbol{p})+i\epsilon}\frac{1}{k^0+\omega_N(\boldsymbol{p})-i\epsilon}\\ &\frac{1}{k^0-E-\omega_N(\boldsymbol{p})+i\epsilon}\frac{1}{k^0-E+\omega_N(\boldsymbol{p})-i\epsilon}\\ +(-i)\frac{1}{2\omega_\pi(2\boldsymbol{p}+\boldsymbol{\ell})}\int\frac{dk^0}{2\pi}\,&\frac{1}{-k^0-\omega_N(\boldsymbol{p})+E+\omega_\pi(2\boldsymbol{p}+\boldsymbol{\ell})-\omega_\pi(\boldsymbol{\ell})+i\epsilon}\\ &\frac{1}{-k^0-\omega_N(\boldsymbol{p})+E+\omega_\pi(2\boldsymbol{p}+\boldsymbol{\ell})+\omega_\pi(\boldsymbol{\ell})-i\epsilon}\\ &\frac{1}{k^0-\omega_N(\boldsymbol{p})+i\epsilon}\frac{1}{k^0+\omega_N(\boldsymbol{p})-i\epsilon}\\ &\frac{1}{k^0-E-\omega_N(\boldsymbol{p})+i\epsilon}\frac{1}{k^0-E+\omega_N(\boldsymbol{p})-i\epsilon}\,.\end{aligned} \tag{B.6}$$

When we then subsequently evaluate the k^0 integral, each of these two terms generates three, for a total of six terms in the final result. But the paradigm reviewed in the main text only keeps the $k^0 = \omega_N(\boldsymbol{k})$ contributions explicit with all others buried inside $\mathcal{I}^{[2]}(P)$. However, if we consider the $k^0 = -\omega_N(\boldsymbol{p}) + E + \omega_\pi(2\boldsymbol{p}+\boldsymbol{\ell}) + \omega_\pi(\boldsymbol{\ell}) - i\epsilon$ contribution within the second term above, we identify a contribution of the form

$$\begin{aligned}\mathcal{F}(\boldsymbol{p},\boldsymbol{\ell}) \supset -(-i)^2\frac{1}{2\omega_\pi(\boldsymbol{\ell})}\frac{1}{2\omega_\pi(2\boldsymbol{p}+\boldsymbol{\ell})}\Bigg[&\frac{1}{E-2\omega_N(\boldsymbol{p})+\omega_\pi(2\boldsymbol{p}+\boldsymbol{\ell})+\omega_\pi(\boldsymbol{\ell})}\\ &\frac{1}{E+\omega_\pi(2\boldsymbol{p}+\boldsymbol{\ell})+\omega_\pi(\boldsymbol{\ell})}\\ &\frac{1}{\omega_\pi(2\boldsymbol{p}+\boldsymbol{\ell})+\omega_\pi(\boldsymbol{\ell})-2\omega_N(\boldsymbol{p})}\\ &\frac{1}{\omega_\pi(2\boldsymbol{p}+\boldsymbol{\ell})+\omega_\pi(\boldsymbol{\ell})}\Bigg],\end{aligned} \tag{B.7}$$

which includes a singularity at $E = 2\omega_N(\boldsymbol{p}) - \omega_\pi(\boldsymbol{\ell}) - \omega_\pi(2\boldsymbol{p}+\boldsymbol{\ell})$.

In the construction of section 3.2.3, this singularity is included in $\mathcal{I}^{[2]}(P)$. Similarly, keeping the $k^0 = \omega_N(\boldsymbol{p})$ result leads to a contribution to $\mathcal{L}(P,k)$ with the same pole,

the one identified in the TOPT analysis of figure B.1(c) above. These poles cancel in the full expression for the diagram, but they formally disrupt the smoothness assumptions for both $\mathcal{I}^{[2]}(P)$ and $\mathcal{L}(P,k)$.

B.2 Shuffling t- and u-type subdiagrams

Having discussed the problem of u-channel-like Bethe-Salpeter contributions in the context of a particular example, we now turn to the solution, first for the specific case considered and then for all contributions to the Bethe-Salpeter kernel.

For the example of the single u-channel loop, the problem is solved by simply replacing $\mathcal{L}(P,k) \to \mathcal{L}(P,P-k)$ before k^0 integration. Since the expression is invariant under $k \to P-k$, this does not change the value of the full diagram, but it does change the definition (and indeed the basic properties) of particular contributions such as $\mathcal{I}^{[2]}(P)$. In particular, the TOPT contributions identified above are transformed to

$$[ABC] = \frac{1}{\omega_N(\boldsymbol{p}) - \omega_N(\boldsymbol{k}) - \omega_\pi(\boldsymbol{k}-\boldsymbol{p}-\boldsymbol{\ell}) - \omega_\pi(\boldsymbol{\ell})} \frac{1}{E - \omega_N(\boldsymbol{k}) - \omega_N(\boldsymbol{P}-\boldsymbol{k})}\,, \tag{B.8}$$

$$[BAC] = \frac{1}{E - \omega_N(\boldsymbol{p}) - \omega_N(\boldsymbol{P}-\boldsymbol{k}) - \omega_\pi(\boldsymbol{k}-\boldsymbol{p}-\boldsymbol{\ell}) - \omega_\pi(\boldsymbol{\ell})} \frac{1}{E - \omega_N(\boldsymbol{k}) - \omega_N(\boldsymbol{P}-\boldsymbol{k})}\,, \tag{B.9}$$

$$[AB] = \frac{1}{\omega_N(\boldsymbol{p}) - \omega_N(\boldsymbol{k}) - \omega_\pi(\boldsymbol{k}-\boldsymbol{p}-\boldsymbol{\ell}) - \omega_\pi(\boldsymbol{\ell})}\,, \tag{B.10}$$

$$[BA] = \frac{1}{-\omega_N(\boldsymbol{p}) + \omega_N(\boldsymbol{k}) - \omega_\pi(\boldsymbol{k}-\boldsymbol{p}-\boldsymbol{\ell}) - \omega_\pi(\boldsymbol{\ell})}\,. \tag{B.11}$$

In this case, we find that the $[AB]$ and $[BA]$ terms faithfully represent the true singularities, without adding any spurious poles. For $[AB]$, the expression for the sub-diagram matches the full diagram exactly, while for $[BA]$ it is related by the replacement $E - \omega_N(\boldsymbol{P}-k) \to \omega_N(\boldsymbol{k})$. In contrast to the situation of the preceding subsection, here the replacement does not generate spurious poles and leads to an E-independent expression for the sub-diagram. (To see that $[AB]$ and $[BA]$ are safe note that either denominator vanishing would correspond to the kinematics of an on-shell $N \to N\pi\pi$ decay, which is not possible.)

It remains to show how the replacement $\mathcal{L}(P,k) \to \mathcal{L}(P,P-k)$ is generalised to all diagrams. The guiding principle is to replace u-channel-like momentum routing with t-channel-like routing. However, this is ambiguous since certain diagrams, like those shown in figure B.2(a), have both u- and t-channel-like behaviour. Such ambiguities are resolved by performing all internal ℓ^0 integrals in a given Bethe-Salpeter contribution before applying the momentum reassignments.

This leads to a diagrammatic definition of the modified Bethe-Salpeter kernel $B^{\mathbb{T}}(P,p,p')$:

1. For a generic diagram contributing to the Bethe-Salpeter kernel, label the four vertices connected to propagators in the adjacent two-particle loops as A_{L}, B_{L}, A_{R}, and B_{R}, where L and R stand for left and right, respectively. [See figure B.2(b).]

2. If A_{L} and B_{L} or A_{R} and B_{R} are the same vertex, (if $[(A_{\mathsf{L}} = B_{\mathsf{L}})$ or $(A_{\mathsf{R}} = B_{\mathsf{R}})]$ is true), then the diagram is a contribution to $B^{\mathbb{T}}(P,p,p')$ without any further modification.

3. If A_{L} and B_{L} are distinct from each other, and also A_{R} and B_{R} are distinct, then evaluate the TOPT contributions to the diagram by enumerating all orderings of A_{L}, B_{L}, A_{R}, and B_{R}, as well as the set of all vertices not attached to neighbouring loops. Note, it can still be the case that $A_{\mathsf{L}} = A_{\mathsf{R}}$ or $B_{\mathsf{L}} = B_{\mathsf{R}}$ (or else $A_{\mathsf{L}} = B_{\mathsf{R}}$ or $B_{\mathsf{L}} = A_{\mathsf{R}}$) as with the single u-channel loop.

4. For concreteness, define the momentum flowing into each vertex from the neighbouring loops as follows: k into A_{L}, $P-k$ into B_{L}, k' into A_{R}, $P-k'$ into B_{R}. [Again see figure B.2(b).] Then all time-orderings contribute to $B^{\mathbb{T}}(P,p,p')$ without modification, except for the following orderings of the external vertices, also shown in figure B.2(c):

   $A_{\mathsf{L}} \cdots B_{\mathsf{R}} \cdots A_{\mathsf{R}} \cdots B_{\mathsf{L}}$,

   $A_{\mathsf{L}} \cdots B_{\mathsf{R}} \cdots B_{\mathsf{L}} \cdots A_{\mathsf{R}}$,

   $B_{\mathsf{R}} \cdots A_{\mathsf{L}} \cdots A_{\mathsf{R}} \cdots B_{\mathsf{L}}$,

   $B_{\mathsf{R}} \cdots A_{\mathsf{L}} \cdots B_{\mathsf{L}} \cdots A_{\mathsf{R}}$,

   where the ellipses represent other internal vertices and cuts that can appear in the ordering. (For our u-channel loop, both orderings are of this type.)

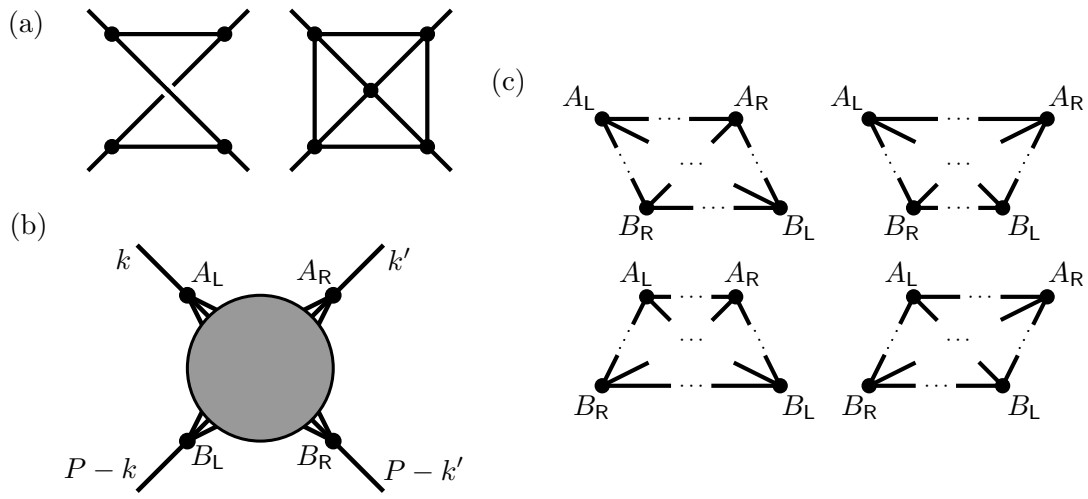

Figure B.2 *(a) Examples of diagrams for which the notion of u-channel-like and t-channel like is ambiguous. (b) Scheme for labelling vertices in a generic diagram. (c) Summary of orderings for which a momentum rerouting is required.*

5. For all orderings given above, dangerous cuts appear between the middle two vertices (i.e. in the central ellipses). The energy flowing across these cuts is u-channel like, of the form $\omega_N(\boldsymbol{k}) - E + \omega_N(\boldsymbol{k'})$, and this leads to the spurious singularities discussed above. Therefore, for all such orderings we replace $\boldsymbol{k}$ with $\boldsymbol{P} - \boldsymbol{k}$ and $\omega_N(\boldsymbol{k})$ with $E - \omega_N(\boldsymbol{k})$. This replaced definition yields the contribution of this diagram to $B^{\mathbb{T}}(P, p, p')$. For all other time orderings the contribution to $B^{\mathbb{T}}(P, p, p')$ is unmodified. This completes our construction of the modified Bethe-Salpeter kernel.

This modified kernel is useful because it allows us to follow the procedure of section 3.2.3 without encountering spurious singularities. In particular, the k^0 integration of eq. (3.33) is now valid. The ordering of vertices guarantees that the only energies that can flow across the cuts in the TOPT approach are E and $\pm[\omega_N(\boldsymbol{k}) - \omega_N(\boldsymbol{k'})]$. Thus, in the case where no single meson exchange occurs, $B^{\mathbb{T}}(P, p, p')$ is analytic in s and has exponentially suppressed volume effects for $4M_N^2 - 4M_\pi^2 < s < (2M_N + M_\pi)^2$. This is the same range of validity that holds for the subtracted kernel $\overline{B}^{\mathbb{T}}(P, p, p')$ in theories with a single meson exchange.

Appendix C

Rearrangement of the correlator

In this appendix, we discuss the manipulations required to go from eq. (3.71):

$$C_L(P) = \mathcal{I}_C^{[1]}(P) + \sum_{n=0}^{\infty} A^{[1]}(P)\, iS(P,L) \left[\left(i\overline{\mathcal{K}}^{[1]}(P) + 2ig^2 \mathcal{T}(P) \right) iS(P,L) \right]^n A^{[1]\dagger}(P)\,,$$

to eq. (3.79):

$$C_L(P) = \mathcal{I}_C(P) + \sum_{n=0}^{\infty} A^{\mathrm{os}}(P)\, \xi\, iS(P,L) \left[\left(\xi^\dagger\, i\overline{\mathcal{K}}^{\mathrm{os}}(P)\, \xi + 2ig^2 \mathcal{T}(P) \right) iS(P,L) \right]^n \xi^\dagger\, A^{\mathrm{os}}(P)^\dagger\,,$$

where we have repeated both results here for convenience.

The basic idea is that the initial four infinite-volume quantities ($\mathcal{I}_C^{[1]}(P)$, $\overline{\mathcal{K}}^{[1]}(P)$, $A^{[1]}(P)$, and $A^{[1]\dagger}(P)$) are modified to alternatives ($\mathcal{I}_C(P)$, $\overline{\mathcal{K}}^{\mathrm{os}}(P)$, $A^{\mathrm{os}}(P)$, and $A^{\mathrm{os}}(P)^\dagger$) with ℓm indices in place of $\boldsymbol{k}^\star \ell m$ everywhere, i.e. the $\boldsymbol{k}^\star$ index is removed in quantities labelled by os, which stands for *on shell*. This is possible because, if both nucleons in a given two-nucleon state are on shell, then the state is completely specified by energy and angular momentum and the $\boldsymbol{k}^\star$ index is redundant. This is not true for the quantities labelled by [1] as these are off-shell and the magnitude of $\boldsymbol{k}^\star$ can be freely varied.

The simplest instance of replacing off-shell with on-shell quantities is given by the

relation

$$\mathcal{I}_C^{[1]}(P)+A^{[1]}(P)iS(P,L)A^{[1]\dagger}(P) = \widetilde{\mathcal{I}}_C^{[1]}(P)+A^{[1]\text{os}}(P)\,\xi\,iS(P,L)\,\xi^\dagger\,A^{[1]\text{os}}(P)^\dagger\,, \quad \text{(C.1)}$$

which trivially follows from the definition

$$\widetilde{\mathcal{I}}_C^{[1]}(P) = \mathcal{I}_C^{[1]}(P) + A^{[1]}(P)iS(P,L)A^{[1]\dagger}(P) - A^{[1]\text{os}}(P)\,\xi\,iS(P,L)\,\xi^\dagger\,A^{[1]\text{os}}(P)^\dagger\,, \quad \text{(C.2)}$$

where $A_{\ell m}^{[1]\text{os}}(P) = A_{\boldsymbol{k}^\star \ell m}^{[1]}(P)\Big|_{|\boldsymbol{k}^\star|=k_{\text{os}}^\star}$ and similar for the conjugated factor. This replacement is valid because $A_{\ell m}^{[1]\text{os}}(P)$ does not have a left-hand cut and the singularity of $S(P,L)$ cancels between the last two terms of eq. (C.2). Thus the sum, implicit in the second two terms, can be replaced with an integral up to exponentially suppressed terms that we neglect.

In this appendix, we will describe a series of such replacements that have the effect of converting eq. (3.71) to eq. (3.79). The guiding principles of the replacements are as follows:

1. In quantities without a left-hand cut in the region that we control ($4M_N^2 - 4M_\pi^2 < s$), one can safely set $|\boldsymbol{k}^\star|$ to $k_{\text{os}}^\star$ up to differences that cancel neighbouring $S(P,L)$ poles.

2. The cancellation of $S(P,L)$ poles, in turn, allows one to replace sums with integrals and the integrated terms are absorbed in redefinitions of infinite-volume quantities, such as in eq. (C.2).

3. An iterative process then emerges. This is because the resulting integrals create new quantities for which the replacement $|\boldsymbol{k}^\star| \to k_{\text{os}}^\star$ can safely be performed.

To explain in detail, it will be useful to introduce a more compact notation. We use bold symbols to represent the building blocks compactly and suppress all arguments, factors of i and g^2, and overlines. We then define the $(n+1)$th or $(n'+1)$th term

in our starting and target sums, respectively, as

$$C_L^{[1],(n)}(P) = \mathbf{A}^{[1]}\,\mathbf{S}\left[\left(\mathbf{K}^{[1]}+\mathbf{T}\right)\mathbf{S}\right]^{n-1}\mathbf{A}^{[1]\dagger}\,, \tag{C.3}$$

$$C_L^{[\mathrm{os}],(n')}(P) = \mathbf{A}^{\mathrm{os}}\,\xi\,\mathbf{S}\left[\left(\xi^\dagger\,\mathbf{K}^{\mathrm{os}}\,\xi+\mathbf{T}\right)\mathbf{S}\right]^{n'-1}\xi^\dagger\,\mathbf{A}^{\mathrm{os}\dagger}\,, \tag{C.4}$$

with $n=0$ corresponding to the $\mathbf{S}$-independent quantity in each case, i.e. $\mathcal{I}_C^{[1]}(P)$ or $\mathcal{I}_C(P)$.

The key claim is that, for any non-negative integer n, $C_L^{[1],(n)}$ generates a series of contributions to $C_L^{[\mathrm{os}],(n')}(P)$ for all $n' \leq n$. We now sketch the argument for $n=0,1,2,3$, since new features emerge at each of these orders. We then give the all-order construction.

For $n=0$ it is straightforward; we simply note that $\mathcal{I}_C^{[1]}(P)$ is one of the terms entering the definition of $\mathcal{I}_C(P)$. In addition, we have already addressed $n=1$ above in our motivating example. In our more compact notation, we begin with

$$C_L^{[1],(1)}(P) = \mathbf{A}^{[1]}\,\mathbf{S}\,\mathbf{A}^{[1]\dagger}\,. \tag{C.5}$$

The on-shell projection is then exactly shown in eq. (C.1). We generate contributions to $n'=0$ and $n'=1$, i.e. to

$$C_L^{[\mathrm{os}],(0)}(P) = \mathcal{I}_C(P)\,, \qquad C_L^{[\mathrm{os}],(1)}(P) = \mathbf{A}^{\mathrm{os}}\,\xi\,\mathbf{S}\,\xi^\dagger\,\mathbf{A}^{\mathrm{os}\dagger}\,. \tag{C.6}$$

Before moving to higher n, we introduce some additional notation and show how this applies to the $n=1$ case. In particular, we define

$$\delta^\dagger\mathbf{A}^{[1]\,\mathrm{os}\,\dagger} = \mathbf{A}^{[1]\,\dagger} - \xi^\dagger\mathbf{A}^{[1]\,\mathrm{os}\,\dagger}\,, \qquad \mathbf{A}^{[1]\,\mathrm{os}}\delta = \mathbf{A}^{[1]} - \mathbf{A}^{[1]\,\mathrm{os}}\,\xi\,, \tag{C.7}$$

and write

$$C_L^{[1],(1)}(P) = \mathbf{A}^{[1]}\,\mathbf{S}\,\mathbf{A}^{[1]\dagger} = \mathbf{A}^{[1]\,\mathrm{os}}\,(\xi+\delta)\,\mathbf{S}\,(\xi^\dagger+\delta^\dagger)\,\mathbf{A}^{[1]\,\mathrm{os}\,\dagger}\,. \tag{C.8}$$

Note that the quantities with a δ are not truly on shell as the label implies. We nonetheless use this notation so that ξ and δ can be compactly grouped as shown. We next use the rule that, whenever one or more δ factors appear next to an $\mathbf{S}$, the singularity cancels and the sum is replaced with an integral.[1] In this way, of the

[1]It should be emphasised that similar tricks were used heavily in addressing singularities and

four terms generated by multiplying out the $(\xi + \delta)$ and $(\xi^\dagger + \delta^\dagger)$ binomials, three contribute to $C_L^{[\mathrm{os}],(0)}(P)$, as claimed.

We are now ready to turn to $n = 2$, where a new and subtle aspect of the derivation arises. We write out the expression as

$$C_L^{[1],(2)}(P) = \mathbf{A}^{[1]}\,\mathbf{S}\,\mathbf{K}^{[1]}\,\mathbf{S}\,\mathbf{A}^{[1]\dagger} + \mathbf{A}^{[1]}\,\mathbf{S}\,\mathbf{T}\,\mathbf{S}\,\mathbf{A}^{[1]\dagger}\,, \tag{C.9}$$

$$\begin{aligned} &= \mathbf{A}^{[1]\,\mathrm{os}}\,(\xi+\delta)\,\mathbf{S}\,(\xi^\dagger+\delta^\dagger)\,\mathbf{K}^{[1]\,\mathrm{os}}\,(\xi+\delta)\,\mathbf{S}\,(\xi^\dagger+\delta^\dagger)\,\mathbf{A}^{[1]\,\mathrm{os}\,\dagger} \\ &\qquad + \mathbf{A}^{[1]\,\mathrm{os}}\,(\xi+\delta)\,\mathbf{S}\,\mathbf{T}\,\mathbf{S}\,(\xi^\dagger+\delta^\dagger)\,\mathbf{A}^{[1]\,\mathrm{os}\,\dagger}\,, \end{aligned} \tag{C.10}$$

where in the second equality we have applied the $\xi + \delta$ decomposition to both $\mathbf{A}^{[1]}$ and $\mathbf{K}^{[1]}$.

First consider the $2^4 = 16$ terms generated by expanding all binomials in the first term of eq. (C.10). Using the usual rule that a δ always annihilates a neighbouring $\mathbf{S}$ we see that all terms can be identified as contributions to $C_L^{[\mathrm{os}],(\mathrm{n}')}(P)$ with $n' \leq 2$.

More effort is required for the second term of (C.10). Of the $2^2 = 4$ terms, the term with ξ and $\xi^\dagger$ has a straightforward match in the $\mathbf{A}^{\mathrm{os}}\,\xi\,\mathbf{S}\,\mathbf{T}\,\mathbf{S}\,\xi^\dagger\,\mathbf{A}^{\mathrm{os}\dagger}$ part of $C_L^{[\mathrm{os}],(1)}(P)$. Also, the term with δ and $\delta^\dagger$ is clear, since all singularities are cancelled and one reaches a fully integrated contribution to $C_L^{[\mathrm{os}],(0)}(P)$. The challenge is the remaining contributions with a single factor of either δ or $\delta^\dagger$.

Consider, for concreteness, $\mathbf{A}^{[1]\,\mathrm{os}}\,\delta\,\mathbf{S}\,\mathbf{T}\,\mathbf{S}\,\xi^\dagger\,\mathbf{A}^{[1]\,\mathrm{os}\,\dagger}$. The issue is that $\mathbf{T}$ cannot be placed on shell but, at the same time, the δ cancelling the pole in $\mathbf{S}$ will lead to an integral combining the off-shell $\mathbf{T}$ into the left endcap. We require a final piece of notation to reflect this:

$$\mathbf{A}^{[k+1]} = \mathbf{A}^{[k]\,\mathrm{os}}\,\delta\,\mathbf{S}\,\mathbf{T}\,. \tag{C.11}$$

Of which the special case relevant here is simply $\mathbf{A}^{[2]} = \mathbf{A}^{[1]\,\mathrm{os}}\,\delta\,\mathbf{S}\,\mathbf{T}$. So we find that $\mathbf{T}$ can convert an on-shell contribution back to an off-shell contribution. In other words, $\mathbf{A}^{[2]}$ is dependent on $\boldsymbol{k}^\star$ within $\boldsymbol{k}^\star \ell m$, and is thus not defined on the desired index space.

Having articulated the extra complication, the resolution follows from an imitation of what we have already done. The terms that we have to address are of the form

redefinitions for the three-to-three finite-volume formalism [20] and in the study of two-to-two processes with an external current [119].

$\mathbf{A}^{[2]}\,\mathbf{S}\,\xi^\dagger\,\mathbf{A}^{[1]\,\mathrm{os}\,\dagger}$ and $\mathbf{A}^{[1]\,\mathrm{os}}\,\xi\,\mathbf{S}\,\mathbf{A}^{[2]\,\dagger}$. But, now that the $\mathbf{T}$ factors within $\mathbf{A}^{[2]}$ have integrated momenta, these no longer have cuts when set on shell. It follows that the on-shell projections of $\mathbf{A}^{[2]}$ and $\mathbf{A}^{[2]\,\dagger}$ are safe, and we can write

$$\mathbf{A}^{[2]}\,\mathbf{S}\,\xi^\dagger\,\mathbf{A}^{[1]\,\mathrm{os}\,\dagger} = \mathbf{A}^{[2]\,\mathrm{os}}\,(\xi+\delta)\,\mathbf{S}\,\xi^\dagger\,\mathbf{A}^{[1]\,\mathrm{os}\,\dagger}\,, \tag{C.12}$$

$$\mathbf{A}^{[1]\,\mathrm{os}}\,\xi\,\mathbf{S}\,\mathbf{A}^{[2]\,\dagger} = \mathbf{A}^{[1]\,\mathrm{os}}\,\xi\,\mathbf{S}\,(\xi^\dagger+\delta^\dagger)\,\mathbf{A}^{[2]\,\mathrm{os}\,\dagger}\,. \tag{C.13}$$

At this stage, the δ-dependent terms are absorbed into $C_L^{[\mathrm{os}],(0)}(P)$ and the remaining terms are absorbed into the part of $C_L^{[\mathrm{os}],(1)}(P)$ that is linear in $\mathbf{S}$.

The last claim above relies on the definition for the full on-shell matrix element

$$\mathbf{A}^{\mathrm{os}} = \sum_{k=1}^{\infty}\mathbf{A}^{[k]\,\mathrm{os}}\,, \qquad \mathbf{A}^{\mathrm{os}\,\dagger} = \sum_{k=1}^{\infty}\mathbf{A}^{[k]\,\mathrm{os}\,\dagger}\,. \tag{C.14}$$

These definitions indicate that the final endcap factors are built from an infinite set of $\mathbf{T}$ factors, attached with integrals to a neighbouring factor of $\mathbf{S}$ in which the pole has been cancelled. In all such cases, the factor of $\mathbf{T}$ is not evaluated at $|\boldsymbol{k}^\star| = k^\star_{\mathrm{os}}$ until after integration. In this way, one avoids introducing spurious left-hand cuts in the finite-volume correlator.

A final new feature arises within $C_L^{[1],(3)}$, defined as

$$C_L^{[1],(3)}(P) = \mathbf{A}^{[1]}\,\mathbf{S}\,\big(\mathbf{K}^{[1]}+\mathbf{T}\big)\,\mathbf{S}\,\big(\mathbf{K}^{[1]}+\mathbf{T}\big)\,\mathbf{S}\,\mathbf{A}^{[1]\dagger}\,, \tag{C.15}$$

namely that factors of $\mathbf{T}$ must also be absorbed into a redefinition of the K matrix.

At this stage, we think it more pedagogical to explain this partly in words, without introducing additional heavy notation to represent the absorptions. When one inserts the $(\xi+\delta)$ decomposition for all $\mathbf{A}^{[1]}$, $\mathbf{A}^{[1]\dagger}$ and $\mathbf{K}^{[1]}$ in eq. (C.15), a term arises with the left $\mathbf{K}^{[1]}$ replaced by $\xi^\dagger\mathbf{K}^{[1]\,\mathrm{os}}\delta$, leading to combinations such as the following:

$$C_L^{[1],(3)}(P) \supset \mathbf{A}^{[1]\,\mathrm{os}}\,\xi\,\mathbf{S}\,\xi^\dagger\Big(\mathbf{K}^{[1]\,\mathrm{os}}\,\delta\,\mathbf{S}\,\mathbf{T}\Big)\mathbf{S}\,\xi^\dagger\,\mathbf{A}^{[1]\,\mathrm{os}\,\dagger}\,, \tag{C.16}$$

where the $\supset$ symbol indicates we have only kept one term. Observe that the factor in parentheses here is analogous to $\mathbf{A}^{[2]}$ defined in eq. (C.11) above. Any number of $\mathbf{T}$ factors can be attached on either side of $\mathbf{K}$ in this way. After such an attachment, the function no longer has a cut in the region of interest and can be set on shell. The sum over all such on-shell, $\mathbf{T}$-absorbing factors defines the final K-matrix denoted by $\mathbf{K}^{\mathrm{os}}$.

Fortunately, we do not have to make use of this definition, since the relation of $\mathbf{K}^{\text{os}}$ to the finite-volume correlation function provides an alternative definition in terms of the two-to-two scattering amplitude. Here the situation is analogous to the three-particle formalism of refs. [20]. Also in that work, a not-so-elegant iterative definition of a K-matrix was provided but never used, favouring instead an alternative derivation of a more direct relation to the scattering amplitude [21].

At this stage, we have presented all features that arise in expressing $C_L^{[1],(n)}(P)$ in terms of $C_L^{[\text{os}],(n')}(P)$ for $n' \leq n$. We summarise the general construction as follows:

1. For a given $C_L^{[1],(n)}(P)$ insert all allowed factors of $\xi + \delta$ and $\xi^\dagger + \delta^\dagger$. A total of $2n$ such binomials arise, 2 from the endcaps and the remaining $(2n-2)$ from the $n-1$ insertions of $\mathbf{K}^{[1]}$.

2. Multiplying out the terms yields 2^{2n} combinations, with various sequences of ξ, $\xi^\dagger$, δ and $\delta^\dagger$.

3. All contributions are immediately identified within $C_L^{[\text{os}],(n')}(P)$, except for those where an off-shell $\mathbf{T}$ is attached to either an endcap or a K-matrix.

4. These remaining terms correspond to a contribution within $C_L^{[1],(n-j)}(P)$ for some $j \geq 1$. That is, they match a factor with fewer explicit $\mathbf{T}$s since some are absorbed into $\mathbf{A}^{[k]}$, $\mathbf{A}^{[k]\dagger}$ or the corresponding K matrix.

5. For these remaining terms, new $\xi + \delta$ insertions arise and are processed as above.

6. The iterative procedure always either generates terms that match those in $C_L^{[\text{os}],(n')}(P)$ or else reduces the explicit $\mathbf{T}$ factors in the remaining, unmatched terms.

7. It follows that, after n such iterations on $C_L^{[1],(n)}(P)$, the process terminates and the matching to the desired expression is complete.

Thus, we have achieved our aim to show the equivalence of eqs. (3.71) and (3.79) (the first two equations of this appendix). We emphasise that the result requires a sequence of redefinitions that is analogous to the three-particle finite-volume

scattering formalism of refs. [20, 21]. These parallels are expected since the same underlying $NN\pi$ state is leading to the left-hand cut addressed here.

We close this appendix with two comments. First, we consider the analogous equivalence arising for $\mathcal{M}_L^{\mathsf{aux}}$. For this quantity, the starting point is eq. (5.3), which can be recast as

$$i\mathcal{M}_L^{\mathsf{aux}}(P) = \sum_{n=0}^{\infty} \Big[\big(i\overline{B}^{\mathfrak{T}} + 2ig^2\mathcal{T}\big) \big[\circ_{\mathsf{rm}} + iS(P,L)\big] \Big]^n \big(i\overline{B}^{\mathfrak{T}} + 2ig^2\mathcal{T}\big) + i\Delta\mathcal{M}_L^{\mathsf{aux}} \,. \quad \text{(C.17)}$$

Then, following the same steps as with $C_L(P)$, this can first be rewritten as

$$i\mathcal{M}_L^{\mathsf{aux}}(P) = \sum_{n=0}^{\infty} \Big[\big(i\overline{\mathcal{K}}^{[1]}(P) + 2ig^2\mathcal{T}(P)\big)\, iS(P,L) \Big]^n \big(i\overline{\mathcal{K}}^{[1]}(P) + 2ig^2\mathcal{T}(P)\big) + i\Delta\mathcal{M}_L^{\mathsf{aux}} \,, \quad \text{(C.18)}$$

where $\overline{\mathcal{K}}^{[1]}(P)$ is defined in eq. (3.75). The aim is then to show that this can be rewritten as eq. (5.13), repeated here for convenience

$$i\mathcal{M}_L^{\mathsf{aux}}(P) \equiv \sum_{n=0}^{\infty} \Big[\big(\xi^\dagger\, i\overline{\mathcal{K}}^{\mathrm{os}}(P)\,\xi + 2ig^2\mathcal{T}(P)\big)\, iS(P,L) \Big]^n \big(\xi^\dagger\, i\overline{\mathcal{K}}^{\mathrm{os}}(P)\,\xi + 2ig^2\mathcal{T}(P)\big) \,.$$

The argument follows the pattern used for $C_L(P)$, with the additional feature that any quantities that vanish when external legs are on shell are absorbed into $\Delta\mathcal{M}_L^{\mathsf{aux}}$. For example, the $n = 1$ term includes contributions with a difference between on- and off-shell $\overline{\mathcal{K}}^{[1]}(P)$. This cancels the singularity in $S(P,L)$ and can be absorbed as an $n = 0$ contribution. Also, order by order, contributions with off-shell external kinematics can be set on-shell with the difference absorbed in $\Delta\mathcal{M}_L^{\mathsf{aux}}$. We do not spell out the steps in more detail here as they are very repetitive to those given above.

Finally, we briefly address the exchange symmetry and Lorentz invariance of $\overline{\mathcal{K}}^{\mathrm{os}}(P)$. Note that $\overline{\mathcal{K}}^{[1]}(P)$ is neither exchange nor Lorentz invariant since it is defined with $\overline{B}^{\,\mathbb{T}}$, for which both of these properties are broken due to the separation of t- and u-channel-like diagrams at the level of TOPT. However, invariance is recovered for $\overline{\mathcal{K}}^{\mathrm{os}}(P)$ when its external momenta are set on-shell, also because any non-symmetric part does not contribute to $C_L(P)$. For example, in any given diagram, when the outermost factors of $\overline{\mathcal{K}}^{\mathrm{os}}(P)$ are combined with the exchange-symmetric endcaps, any antisymmetric component is annihilated in the sum. This effectively symmetrises the outermost insertions and a recursive argument can be used to see that all factors

of $\overline{\mathcal{K}}^{\mathrm{os}}(P)$ are symmetrised. In practice, this means that only even partial waves of $\overline{\mathcal{K}}^{\mathrm{os}}(P)$ are nonzero for indistinguishable particles. The symmetrisation of $\overline{\mathcal{K}}^{\mathrm{os}}(P)$ also leads to the same for $\overline{B}^{\,\mathbb{T}}$ and this has the consequence that Lorentz invariance is recovered for $\overline{\mathcal{K}}^{\mathrm{os}}(P)$. The Lorentz invariance can also be seen from the relation between $\overline{\mathcal{K}}^{\mathrm{os}}(P)$ and the scattering amplitude, which is manifestly Lorentz invariant.

Bibliography

[1] André Baião Raposo and Maxwell T. Hansen. The Lüscher scattering formalism on the t-channel cut. *PoS*, LATTICE2022:051, 2023.

[2] André Baião Raposo and Maxwell T. Hansen. Finite-volume scattering on the left-hand cut. *JHEP*, 08:075, 2024.

[3] M. Luscher. Volume Dependence of the Energy Spectrum in Massive Quantum Field Theories. 2. Scattering States. *Commun. Math. Phys.*, 105:153–188, 1986.

[4] K. Rummukainen and Steven A. Gottlieb. Resonance scattering phase shifts on a nonrest frame lattice. *Nucl. Phys. B*, 450:397–436, 1995.

[5] Song He, Xu Feng, and Chuan Liu. Two particle states and the S-matrix elements in multi-channel scattering. *JHEP*, 07:011, 2005.

[6] Norman H. Christ, Changhoan Kim, and Takeshi Yamazaki. Finite volume corrections to the two-particle decay of states with non-zero momentum. *Phys. Rev.*, D72:114506, 2005.

[7] C. h. Kim, C. T. Sachrajda, and Stephen R. Sharpe. Finite-volume effects for two-hadron states in moving frames. *Nucl. Phys. B*, 727:218–243, 2005.

[8] Michael Lage, Ulf-G. Meißner, and Akaki Rusetsky. A Method to measure the antikaon-nucleon scattering length in lattice QCD. *Phys. Lett.*, B681:439–443, 2009.

[9] V. Bernard, M. Lage, U. G. Meissner, and A. Rusetsky. Scalar mesons in a finite volume. *JHEP*, 01:019, 2011.

[10] Ziwen Fu. Rummukainen-Gottlieb's formula on two-particle system with different mass. *Phys. Rev.*, D85:014506, 2012.

[11] Raul A. Briceno and Zohreh Davoudi. Moving multichannel systems in a finite volume with application to proton-proton fusion. *Phys. Rev. D*, 88(9):094507, 2013.

[12] Maxwell T. Hansen and Stephen R. Sharpe. Multiple-channel generalization of Lellouch-Luscher formula. *Phys. Rev. D*, 86:016007, 2012.

[13] Peng Guo, Jozef Dudek, Robert Edwards, and Adam P. Szczepaniak. Coupled-channel scattering on a torus. *Phys. Rev.*, D88(1):014501, 2013.

[14] Raul A. Briceno. Two-particle multichannel systems in a finite volume with arbitrary spin. *Phys. Rev. D*, 89(7):074507, 2014.

[15] Jeremy R. Green, Andrew D. Hanlon, Parikshit M. Junnarkar, and Hartmut Wittig. Weakly bound H dibaryon from SU(3)-flavor-symmetric QCD. *Phys. Rev. Lett.*, 127(24):242003, 2021.

[16] Roel Aaij et al. Observation of an exotic narrow doubly charmed tetraquark. *Nature Phys.*, 18(7):751–754, 2022.

[17] Roel Aaij et al. Study of the doubly charmed tetraquark T_{cc}^{+}. *Nature Commun.*, 13(1):3351, 2022.

[18] M. Padmanath and S. Prelovsek. Signature of a Doubly Charm Tetraquark Pole in DD* Scattering on the Lattice. *Phys. Rev. Lett.*, 129(3):032002, 2022.

[19] Meng-Lin Du, Arseniy Filin, Vadim Baru, Xiang-Kun Dong, Evgeny Epelbaum, Feng-Kun Guo, Christoph Hanhart, Alexey Nefediev, Juan Nieves, and Qian Wang. Role of Left-Hand Cut Contributions on Pole Extractions from Lattice Data: Case Study for Tcc(3875)+. *Phys. Rev. Lett.*, 131(13):131903, 2023.

[20] Maxwell T. Hansen and Stephen R. Sharpe. Relativistic, model-independent, three-particle quantization condition. *Phys. Rev. D*, 90(11):116003, 2014.

[21] Maxwell T. Hansen and Stephen R. Sharpe. Expressing the three-particle finite-volume spectrum in terms of the three-to-three scattering amplitude. *Phys. Rev. D*, 92(11):114509, 2015.

[22] R. L. Workman et al. Review of Particle Physics. *PTEP*, 2022:083C01, 2022.

[23] Murray Gell-Mann. A Schematic Model of Baryons and Mesons. *Phys. Lett.*, 8:214–215, 1964.

[24] G. Zweig. *An SU(3) model for strong interaction symmetry and its breaking. Version 2*, pages 22–101. 2 1964.

[25] M. Y. Han and Yoichiro Nambu. Three Triplet Model with Double SU(3) Symmetry. *Phys. Rev.*, 139:B1006–B1010, 1965.

[26] Chen-Ning Yang and Robert L. Mills. Conservation of Isotopic Spin and Isotopic Gauge Invariance. *Phys. Rev.*, 96:191–195, 1954.

[27] H. Fritzsch, Murray Gell-Mann, and H. Leutwyler. Advantages of the Color Octet Gluon Picture. *Phys. Lett. B*, 47:365–368, 1973.

[28] David J. Gross and Frank Wilczek. Ultraviolet Behavior of Nonabelian Gauge Theories. *Phys. Rev. Lett.*, 30:1343–1346, 1973.

[29] H. David Politzer. Reliable Perturbative Results for Strong Interactions? *Phys. Rev. Lett.*, 30:1346–1349, 1973.

[30] M. Tanabashi et al. Review of Particle Physics. *Phys. Rev. D*, 98(3):030001, 2018.

[31] Emmy Noether. Invariant Variation Problems. *Gott. Nachr.*, 1918:235–257, 1918.

[32] Stephen L. Adler. Axial-vector vertex in spinor electrodynamics. *Phys. Rev.*, 177:2426–2438, Jan 1969.

[33] J. S. Bell and R. Jackiw. A PCAC puzzle: $\pi^0 \to \gamma\gamma$ in the σ model. *Nuovo Cim. A*, 60:47–61, 1969.

[34] William A. Bardeen. Anomalous Ward identities in spinor field theories. *Phys. Rev.*, 184:1848–1857, 1969.

[35] Y. Aoki et al. FLAG Review 2021. *Eur. Phys. J. C*, 82(10):869, 2022.

[36] J. Goldstone. Field Theories with Superconductor Solutions. *Nuovo Cim.*, 19:154–164, 1961.

[37] Jeffrey Goldstone, Abdus Salam, and Steven Weinberg. Broken Symmetries. *Phys. Rev.*, 127:965–970, 1962.

[38] Gerard 't Hooft. How Instantons Solve the U(1) Problem. *Phys. Rept.*, 142:357–387, 1986.

[39] E. Witten. Global Aspects of Current Algebra. *Nucl. Phys. B*, 223:422–432, 1983.

[40] G. Veneziano. U(1) Without Instantons. *Nucl. Phys. B*, 159:213–224, 1979.

[41] L. David Roper. Evidence for a P-11 Pion-Nucleon Resonance at 556 MeV. *Phys. Rev. Lett.*, 12:340–342, 1964.

[42] Volker D. Burkert and Craig D. Roberts. Colloquium : Roper resonance: Toward a solution to the fifty year puzzle. *Rev. Mod. Phys.*, 91(1):011003, 2019.

[43] P.A. Zyla et al. Review of Particle Physics. *PTEP*, 2020(8):083C01, 2020.

[44] Nora Brambilla, Simon Eidelman, Christoph Hanhart, Alexey Nefediev, Cheng-Ping Shen, Christopher E. Thomas, Antonio Vairo, and Chang-Zheng Yuan. The XYZ states: experimental and theoretical status and perspectives. *Phys. Rept.*, 873:1–154, 2020.

[45] Steven Weinberg. Phenomenological Lagrangians. *Physica*, A96(1-2):327–340, 1979.

[46] Steven Weinberg. Pion scattering lengths. *Phys. Rev. Lett.*, 17:616–621, 1966.

[47] J. Gasser and H. Leutwyler. Chiral Perturbation Theory to One Loop. *Annals Phys.*, 158:142, 1984.

[48] H. Leutwyler. On the foundations of chiral perturbation theory. *Annals Phys.*, 235:165–203, 1994.

[49] G. Ecker. Chiral perturbation theory. *Prog. Part. Nucl. Phys.*, 35:1–80, 1995.

[50] Stefan Scherer. Introduction to chiral perturbation theory. *Adv. Nucl. Phys.*, 27:277, 2003.

[51] Nathan Isgur and Mark B. Wise. Weak Decays of Heavy Mesons in the Static Quark Approximation. *Phys. Lett. B*, 232:113–117, 1989.

[52] Estia Eichten and Brian Russell Hill. An Effective Field Theory for the Calculation of Matrix Elements Involving Heavy Quarks. *Phys. Lett. B*, 234:511–516, 1990.

[53] Howard Georgi. An Effective Field Theory for Heavy Quarks at Low-energies. *Phys. Lett. B*, 240:447–450, 1990.

[54] J. Wess and B. Zumino. Consequences of anomalous Ward identities. *Phys. Lett. B*, 37:95–97, 1971.

[55] J. L. Manes. Differential Geometric Construction of the Gauged Wess-Zumino Action. *Nucl. Phys. B*, 250:369–384, 1985.

[56] J. Bijnens. Chiral perturbation theory and anomalous processes. *Int. J. Mod. Phys. A*, 8:3045–3105, 1993.

[57] J. Gasser, M. E. Sainio, and A. Svarc. Nucleons with chiral loops. *Nucl. Phys. B*, 307:779–853, 1988.

[58] A. Krause. Baryon Matrix Elements of the Vector Current in Chiral Perturbation Theory. *Helv. Phys. Acta*, 63:3–70, 1990.

[59] Elizabeth Ellen Jenkins and Aneesh V. Manohar. Baryon chiral perturbation theory using a heavy fermion Lagrangian. *Phys. Lett. B*, 255:558–562, 1991.

[60] S. R. Beane, Paulo F. Bedaque, M. J. Savage, and U. van Kolck. Towards a perturbative theory of nuclear forces. *Nucl. Phys. A*, 700:377–402, 2002.

[61] Kenneth G. Wilson. Confinement of Quarks. *Phys. Rev. D*, 10:2445–2459, 1974.

[62] Holger Bech Nielsen and M. Ninomiya. Absence of Neutrinos on a Lattice. 1. Proof by Homotopy Theory. *Nucl. Phys. B*, 185:20, 1981. [Erratum: Nucl.Phys.B 195, 541 (1982)].

[63] Holger Bech Nielsen and M. Ninomiya. Absence of Neutrinos on a Lattice. 2. Intuitive Topological Proof. *Nucl. Phys. B*, 193:173–194, 1981.

[64] John B. Kogut and Leonard Susskind. Hamiltonian Formulation of Wilson's Lattice Gauge Theories. *Phys. Rev. D*, 11:395–408, 1975.

[65] Herbert Neuberger. Exactly massless quarks on the lattice. *Phys. Lett. B*, 417:141–144, 1998.

[66] K. Symanzik. Continuum Limit and Improved Action in Lattice Theories. 1. Principles and φ^4 Theory. *Nucl. Phys. B*, 226:187–204, 1983.

[67] K. Symanzik. Continuum Limit and Improved Action in Lattice Theories. 2. O(N) Nonlinear Sigma Model in Perturbation Theory. *Nucl. Phys. B*, 226:205–227, 1983.

[68] M. Lüscher. Volume Dependence of the Energy Spectrum in Massive Quantum Field Theories. 1. Stable Particle States. *Commun. Math. Phys.*, 104:177, 1986.

[69] B. Sheikholeslami and R. Wohlert. Improved Continuum Limit Lattice Action for QCD with Wilson Fermions. *Nucl. Phys. B*, 259:572, 1985.

[70] S. Duane, A. D. Kennedy, B. J. Pendleton, and D. Roweth. Hybrid Monte Carlo. *Phys. Lett. B*, 195:216–222, 1987.

[71] Benoit Blossier, Michele Della Morte, Georg von Hippel, Tereza Mendes, and Rainer Sommer. On the generalized eigenvalue method for energies and matrix elements in lattice field theory. *JHEP*, 04:094, 2009.

[72] Martin Lüscher and Ulli Wolff. How to Calculate the Elastic Scattering Matrix in Two-dimensional Quantum Field Theories by Numerical Simulation. *Nucl. Phys. B*, 339:222–252, 1990.

[73] H. Lehmann, K. Symanzik, and W. Zimmermann. On the formulation of quantized field theories. *Nuovo Cim.*, 1:205–225, 1955.

[74] Martin Hansen, Alessandro Lupo, and Nazario Tantalo. Extraction of spectral densities from lattice correlators. *Phys. Rev. D*, 99(9):094508, 2019.

[75] John Bulava and Maxwell T. Hansen. Scattering amplitudes from finite-volume spectral functions. *Phys. Rev. D*, 100(3):034521, 2019.

[76] John Bulava, Maxwell T. Hansen, Michael W. Hansen, Agostino Patella, and Nazario Tantalo. Inclusive rates from smeared spectral densities in the two-dimensional O(3) non-linear σ-model. *JHEP*, 07:034, 2022.

[77] John Bulava. The spectral reconstruction of inclusive rates. *PoS*, LATTICE2022:231, 2023.

[78] Agostino Patella and Nazario Tantalo. Scattering Amplitudes from Euclidean Correlators: Haag-Ruelle theory and approximation formulae. 7 2024.

[79] Raul A. Briceno, Jozef J. Dudek, and Ross D. Young. Scattering processes and resonances from lattice QCD. *Rev. Mod. Phys.*, 90(2):025001, 2018.

[80] K. Polejaeva and A. Rusetsky. Three particles in a finite volume. *Eur. Phys. J. A*, 48:67, 2012.

[81] Raúl A. Briceño, Maxwell T. Hansen, and Stephen R. Sharpe. Relating the finite-volume spectrum and the two-and-three-particle S matrix for relativistic systems of identical scalar particles. *Phys. Rev. D*, 95(7):074510, 2017.

[82] Peng Guo and Vladimir Gasparian. A solvable three-body model in finite volume. *Phys. Lett. B*, 774:441–445, 2017.

[83] Hans-Werner Hammer, Jin-Yi Pang, and A. Rusetsky. Three-particle quantization condition in a finite volume: 1. The role of the three-particle force. *JHEP*, 09:109, 2017.

[84] H. W. Hammer, J. Y. Pang, and A. Rusetsky. Three particle quantization condition in a finite volume: 2. general formalism and the analysis of data. *JHEP*, 10:115, 2017.

[85] M. Mai and M. Döring. Three-body Unitarity in the Finite Volume. *Eur. Phys. J. A*, 53(12):240, 2017.

[86] M. Döring, H. W. Hammer, M. Mai, J. Y. Pang, § A. Rusetsky, and J. Wu. Three-body spectrum in a finite volume: the role of cubic symmetry. *Phys. Rev. D*, 97(11):114508, 2018.

[87] Raúl A. Briceño, Maxwell T. Hansen, and Stephen R. Sharpe. Numerical study of the relativistic three-body quantization condition in the isotropic approximation. *Phys. Rev. D*, 98(1):014506, 2018.

[88] P. Klos, S. König, H. W. Hammer, J. E. Lynn, and A. Schwenk. Signatures of few-body resonances in finite volume. *Phys. Rev. C*, 98(3):034004, 2018.

[89] Raúl A. Briceño, Maxwell T. Hansen, and Stephen R. Sharpe. Three-particle systems with resonant subprocesses in a finite volume. *Phys. Rev. D*, 99(1):014516, 2019.

[90] Peng Guo, Michael Döring, and Adam P. Szczepaniak. Variational approach to N-body interactions in finite volume. *Phys. Rev. D*, 98(9):094502, 2018.

[91] Tyler D. Blanton, Fernando Romero-López, and Stephen R. Sharpe. Implementing the three-particle quantization condition including higher partial waves. *JHEP*, 03:106, 2019.

[92] Jin-Yi Pang, Jia-Jun Wu, H. W. Hammer, Ulf-G. Meißner, and Akaki Rusetsky. Energy shift of the three-particle system in a finite volume. *Phys. Rev. D*, 99(7):074513, 2019.

[93] Fernando Romero-López, Stephen R. Sharpe, Tyler D. Blanton, Raúl A. Briceño, and Maxwell T. Hansen. Numerical exploration of three relativistic particles in a finite volume including two-particle resonances and bound states. *JHEP*, 10:007, 2019.

[94] Maxwell T. Hansen, Fernando Romero-López, and Stephen R. Sharpe. Generalizing the relativistic quantization condition to include all three-pion isospin channels. *JHEP*, 07:047, 2020.

[95] Tyler D. Blanton and Stephen R. Sharpe. Alternative derivation of the relativistic three-particle quantization condition. *Phys. Rev. D*, 102(5):054520, 2020.

[96] Tyler D. Blanton and Stephen R. Sharpe. Equivalence of relativistic three-particle quantization conditions. *Phys. Rev. D*, 102(5):054515, 7 2020.

[97] Peng Guo. Modeling few-body resonances in finite volume. *Phys. Rev. D*, 102(5):054514, 2020.

[98] Jin-Yi Pang, Jia-Jun Wu, and Li-Sheng Geng. DDK system in finite volume. *Phys. Rev. D*, 102(11):114515, 2020.

[99] Fernando Romero-López, Akaki Rusetsky, Nikolas Schlage, and Carsten Urbach. Relativistic N-particle energy shift in finite volume. *JHEP*, 02:060, 2021.

[100] Tyler D. Blanton and Stephen R. Sharpe. Relativistic three-particle quantization condition for nondegenerate scalars. *Phys. Rev. D*, 103(5):054503, 11 2021.

[101] Fabian Müller, Tiansu Yu, and Akaki Rusetsky. Finite-volume energy shift of the three-pion ground state. *Phys. Rev. D*, 103(5):054506, 2021.

[102] Fabian Müller and Akaki Rusetsky. On the three-particle analog of the Lellouch-Lüscher formula. *JHEP*, 03:152, 2021.

[103] Maxwell T. Hansen, Fernando Romero-López, and Stephen R. Sharpe. Decay amplitudes to three hadrons from finite-volume matrix elements. *JHEP*, 04:113, 2021.

[104] Tyler D. Blanton and Stephen R. Sharpe. Three-particle finite-volume formalism for $\pi+\pi+\mathrm{K}+$ and related systems. *Phys. Rev. D*, 104(3):034509, 2021.

[105] Fabian Müller, Jin-Yi Pang, Akaki Rusetsky, and Jia-Jun Wu. Relativistic-invariant formulation of the NREFT three-particle quantization condition. *JHEP*, 02:158, 2022.

[106] Tyler D. Blanton, Fernando Romero-López, and Stephen R. Sharpe. Implementing the three-particle quantization condition for $\pi^+\pi^+\mathrm{K}^+$ and related systems. *JHEP*, 02:098, 2022.

[107] Fabian Müller, Jin-Yi Pang, Akaki Rusetsky, and Jia-Jun Wu. Three-particle Lellouch-Lüscher formalism in moving frames. *JHEP*, 02:214, 2023.

[108] Andrew W. Jackura, Raúl A. Briceño, and Maxwell T. Hansen. Three-pion effects in $K^0 - \bar{K}^0$ mixing. *PoS*, LATTICE2022:062, 2023.

[109] Daniel Severt, Maxim Mai, and Ulf-G. Meißner. Particle-dimer approach for the Roper resonance in a finite volume. *JHEP*, 04:100, 2023.

[110] Jorge Baeza-Ballesteros, Johan Bijnens, Tomáš Husek, Fernando Romero-López, Stephen R. Sharpe, and Mattias Sjö. The isospin-3 three-particle K-matrix at NLO in ChPT. *JHEP*, 05:187, 2023.

[111] Zachary T. Draper, Maxwell T. Hansen, Fernando Romero-López, and Stephen R. Sharpe. Three relativistic neutrons in a finite volume. *JHEP*, 07:226, 2023.

[112] Rishabh Bubna, Fabian Müller, and Akaki Rusetsky. Finite-volume energy shift of the three-nucleon ground state. *Phys. Rev. D*, 108(1):014518, 2023.

[113] Zachary T. Draper and Stephen R. Sharpe. Three-particle formalism for multiple channels: the $\eta\pi\pi + K\overline{K}\pi$ system in isosymmetric QCD. *JHEP*, 07:083, 2024.

[114] Raúl A. Briceño and Maxwell T. Hansen. Multichannel $0 \to 2$ and $1 \to 2$ transition amplitudes for arbitrary spin particles in a finite volume. *Phys. Rev. D*, 92(7):074509, 2015.

[115] Ikuro Sato and Paulo F. Bedaque. Fitting two nucleons inside a box: Exponentially suppressed corrections to the Luscher's formula. *Phys. Rev. D*, 76:034502, 2007.

[116] Lu Meng and E. Epelbaum. Two-particle scattering from finite-volume quantization conditions using the plane wave basis. *JHEP*, 10:051, 2021.

[117] George Sterman. *An Introduction to Quantum Field Theory.* Cambridge University Press, 1993.

[118] Sebastian M. Dawid, Md Habib E. Islam, Raul A. Briceno, and Andrew W. Jackura. Evolution of Efimov states. *Phys. Rev. A*, 109(4):043325, 2024.

[119] Raúl A. Briceño and Maxwell T. Hansen. Relativistic, model-independent, multichannel $2 \to 2$ transition amplitudes in a finite volume. *Phys. Rev. D*, 94(1):013008, 2016.

[120] Yan Lyu, Sinya Aoki, Takumi Doi, Tetsuo Hatsuda, Yoichi Ikeda, and Jie Meng. Doubly Charmed Tetraquark Tcc+ from Lattice QCD near Physical Point. *Phys. Rev. Lett.*, 131(16):161901, 2023.

[121] Sara Collins, Alexey Nefediev, M. Padmanath, and Sasa Prelovsek. Toward the quark mass dependence of Tcc+ from lattice QCD. *Phys. Rev. D*, 109(9):094509, 2024.

[122] Travis Whyte, David J. Wilson, and Christopher E. Thomas. Near-threshold states in coupled $DD^* - D^*D^*$ scattering from lattice QCD. 5 2024.

[123] Andrew W. Jackura, Raúl A. Briceño, Sebastian M. Dawid, Md Habib E. Islam, and Connor McCarty. Solving relativistic three-body integral equations in the presence of bound states. *Phys. Rev. D*, 104(1):014507, 2021.

[124] Sebastian M. Dawid, Md Habib E. Islam, and Raúl A. Briceño. Analytic continuation of the relativistic three-particle scattering amplitudes. *Phys. Rev. D*, 108(3):034016, 2023.

[125] Lu Meng and Evgeny Epelbaum. Quantization conditions in the finite volume within the plane wave basis expansion. *PoS*, LATTICE2021:361, 2022.

[126] Lu Meng and Evgeny Epelbaum. Finite volume NN systems using plane wave expansion and eigenvector continuation. *PoS*, LATTICE2022:201, 2023.

[127] Maxwell T. Hansen, Fernando Romero-López, and Stephen R. Sharpe. Incorporating DDπ effects and left-hand cuts in lattice QCD studies of the $\mathrm{T}_{cc}(3875)^+$. *JHEP*, 06:051, 2024.

[128] Rishabh Bubna, Hans-Werner Hammer, Fabian Müller, Jin-Yi Pang, Akaki Rusetsky, and Jia-Jun Wu. Lüscher equation with long-range forces. *JHEP*, 05:168, 2024.